

The Combustion of Titanium Powder in Air and Iron Oxide

by Robert Alexander Brown, BEng

**Thesis submitted to the University of Nottingham for the degree of
Doctor of Philosophy, October 2000**

BEST COPY AVAILABLE.

VARIABLE PRINT QUALITY

Contents

1. INTRODUCTION	1
2. LITERATURE SURVEY – BACKGROUND INFORMATION.....	4
2.1 HISTORICAL PERSPECTIVE.....	4
2.2 BASIC PRINCIPLES	5
2.3 PRACTICAL ADVANTAGES TO THE SHS PROCESS.....	9
2.4 LIMITATIONS OF THE SHS PROCESS	17
2.5 THERMOCHEMICAL THEORY.....	18
2.6 SHS REACTION MECHANISMS.....	20
2.6.1 <i>Solid – Gas</i>	20
2.6.2 <i>Solid – Solid</i>	22
2.6.3 <i>Solid – Liquid</i>	22
2.6.3.1 <i>The Ti + C + Metal Reaction</i>	26
2.6.4 <i>Liquid – Liquid</i>	27
2.7 COMBUSTION WAVE CHARACTERISTICS	28
2.7.1 <i>Maximum Reaction Temperature</i>	30
2.8 PROCESS PARAMETERS.....	30
2.8.1 <i>Powder Diameter and Morphology</i>	31
2.8.2 <i>Pellet Density</i>	32
2.9 FIGURES.....	34
3. LITERATURE SURVEY – DETAILED LITERATURE.....	36
3.1 TITANIUM OXIDES AND ALLOYS.....	36
3.1.1 <i>Titanium and Titanium Oxides</i>	36

3.1.2 Titanium and Iron Alloys.....	38
3.2 IRON AND IRON OXIDES	39
3.3 REACTIONS BETWEEN BULK TITANIUM AND AIR	41
3.3.1 Isothermal Oxidation	41
3.3.2 Anisothermal Oxidation	46
3.3.3 Burning.....	52
3.4 REACTIONS BETWEEN POWDERED TITANIUM AND AIR	56
3.5 REACTIONS BETWEEN TITANIUM AND Al_2O_3	63
3.6 REACTIONS BETWEEN TITANIUM AND Fe_2O_3	63
3.7 SUMMARY	65
3.8 FIGURES.....	69
4. EXPERIMENTAL PROCEDURE	79
4.1 INTRODUCTION	79
4.2 MATERIALS USED	79
4.3 SAMPLE PREPARATION	82
4.3.1 Weighing, Mixing and Pressing	82
4.4 COMBUSTION METHODS	84
4.4.1 Radiant Heat, Box Furnace (Ambient Atmosphere).....	84
4.4.1.1 Deducing the Reaction Time	84
4.4.2 Radiant Heat, Tube Furnace (Argon Atmosphere)	85
4.4.3 Tungsten Filament (Argon Atmosphere)	85
4.5 DATA RECORDING	86
4.5.1 Temperature Measurements.....	86
4.6 MICROSTRUCTURAL EXAMINATION.....	87
4.6.1 Sample Preparation	87
4.6.1.1 Mounted and Polished Samples	87
4.6.1.2 SEM Samples	88

4.6.1.3 XRD samples.....	88
4.6.2 Optical Microscopy.....	88
4.6.3 Scanning Electron Microscopy (SEM)	88
4.6.3.1 JOEL 6400.....	89
4.6.3.2 Philips FEG-ESEM.....	89
4.6.4 X-Ray Diffraction Analysis (XRD).....	90
4.7 FIGURES.....	91

5. THE REACTION BETWEEN TITANIUM AND AIR , AND TITANIUM AND IRON (II) OXIDE, HEATED IN THE THERMAL EXPLOSION MODE.....	97
5.1 INTRODUCTION.....	97
5.2 EXPERIMENTS.....	98
5.2.1 Series 1: Titanium Powder Compacts Heated in Air	98
5.2.2 Series 2: Titanium Powder + Al ₂ O ₃ Compacts Heated in Air and Argon.....	102
5.2.3 Series 3: Titanium Powder + Fe ₂ O ₃ Compacts Heated in Air and Argon	103
5.2.4 Series 4: Bulk Titanium and Fe ₂ O ₃ Reactions.....	104
5.3 RESULTS.....	105
5.3.1 Series 1 : Titanium Powder Pellets Heated in Air.....	105
5.3.1.1 Series 1A : Titanium Powder Pellets Held in a Pre Heated Furnace in Air.....	105
5.3.1.2 Series 1B : Titanium Powder Pellets Heated at 10°C / Min in Air	109
5.3.2 Series 2 : Titanium Powder + Al ₂ O ₃ Pellets Heated in Air and Argon.....	110
5.3.3 Series 3 : Titanium Powder + Fe ₂ O ₃ Pellets Heated in Air and Argon	112
5.3.3.1 'Sintered' Compacts Heated in Air.....	114
5.3.3.2 'Sintered' Compacts Heated in Argon	116
5.3.4 Series 4 : Bulk Titanium and Fe ₂ O ₃ Reactions.....	117
5.4 DISCUSSION.....	119
5.4.1 Series 1: Titanium Powder Pellets Heated in Air.....	119
5.4.1.1 The Effect of the Pellet Size and Density	120

5.4.1.2 The Effect of the Titanium Powder Diameter	121
5.4.1.3 The Effect of the Heating Rate	122
5.4.1.4 Oxidation Characteristics of the Pellet.....	123
5.4.2 Series 2 : Titanium Powder + Al ₂ O ₃ Pellets Heated in Air and Argon	128
5.4.3 Series 3 : Titanium Powder and Fe ₂ O ₃ Pellets Heated in Air and Argon	130
5.4.3.1 Reactions In Air.....	131
5.4.3.2 'Sintered' Samples Heated in Air	133
5.4.3.3 Reactions in Argon	135
5.4.3.4 'Sintered' Samples Heated in Argon.....	135
5.4.4 Series 4 : Bulk Titanium and Fe ₂ O ₃ Reactions.....	137
5.5 SUMMARY	138
5.6 CONCLUSIONS.....	139
5.7 FIGURES.....	141

6. NUMERICAL CALCULATIONS FOR THE OXIDATION REACTION OF

TITANIUM IN AIR OR TITANIUM IN Fe₂O₃.....	161
6.1 INTRODUCTION.....	161
6.2 BASIC CALCULATION AND ASSUMPTIONS	161
6.3 ASSUMPTIONS AND CONSTANTS	163
6.4 CALCULATIONS	164
6.4.1 Reaction Energy Calculation for the Formation of TiO ₂ by Fe ₂ O ₃	164
6.4.2 Reaction Energy Calculation for the Formation of TiO by Fe ₂ O ₃	164
6.4.3 Reaction Energy Calculation for the Formation of TiO ₂ or TiO by Gaseous Oxygen (Air).....	165
6.4.4 Powder Calculations.....	165
6.4.5 Calculation of Energy Released when the Reaction Layer is TiO ₂	166
6.4.6 Calculation of Energy Released when the Reaction Layer is TiO.....	166
6.4.7 Calculation of the Energy Required to Melt the Titanium Powder Particle	167

6.5 RESULTS	167
6.6 DISCUSSION	168
6.7 CONCLUSIONS.....	170
7. NUMERICAL MODEL TO PREDICT THE BEHAVIOUR OF A TITANIUM POWDER PELLET HEATED IN AIR.....	171
7.1 INTRODUCTION	171
7.2 MODEL OUTLINE	172
7.3 DEFINING THE PELLET	173
7.3.1 Pellet Dimensions.....	174
7.3.2 Titanium Powder Data.....	175
7.3.3 Pellet Data	176
7.4 OXIDATION	178
7.4.1 Temperature Increase Due to Oxidation.....	182
7.5 HEATING AND COOLING OF THE PELLET.....	183
7.6 PELLET TEMPERATURE CHANGES.....	186
7.7 PELLET IGNITION	187
7.8 RESULTS FROM RUNNING THE PROGRAMME.....	190
7.8.1 Introduction.....	190
7.8.2 Standard Input Variables	190
7.8.3 Graphical Outputs.....	191
7.8.3.1 The Effect of the Pellet Parameters.....	191
7.8.3.2 The Effect of the Furnace Parameters.....	192
7.9 EXPERIMENTAL VERIFICATION OF PROGRAMME RESULTS	192
7.9.1 Introduction.....	192
7.9.2 Experimental	193
7.9.3 Results	193
7.9.4 Discussion	194

7.10 DISCUSSION	195
7.10.1 <i>The Effect of the Pellet Parameters</i>	195
7.10.1.1 The Variation in Pellet Diameter and Size	195
7.10.1.1.1 Experimental Verification	198
7.10.1.2 The Variation of Powder Diameter	198
7.10.1.2.1 Experimental Verification	201
7.10.1.3 The Combined Effect of Pellet Size and Powder Diameter	202
7.10.1.4 The Effect of the Oxide Layer on the Pellet Ignition	202
7.10.1.4.1 Experimental Verification	204
7.10.1.5 The Variation in Active Factor	204
7.10.1.5.1 Experimental Verification	205
7.10.2 <i>The Effect of the Furnace Parameters</i>	205
7.10.2.1.1 Experimental Verification	207
7.11 CONCLUSIONS	207
7.12 FIGURES	209

8. THE EFFECT OF THE INITIAL POWDER COMPOSITION AND THE ADDITION OF AN IRON POWDER DILUENT ON THE PRODUCTS OF THE SHS REACTION BETWEEN Fe_2O_3 AND TITANIUM	229
8.1 INTRODUCTION	229
8.2 EXPERIMENTS	229
8.3 RESULTS	231
8.3.1 <i>Product Morphology</i>	232
8.3.2 <i>The $Fe_2O_3 + 3Ti$ Reaction</i>	233
8.3.3 <i>Partial Reactions</i>	234
8.4 DISCUSSION	236
8.4.1 <i>Product Oxide Composition</i>	236
8.4.2 <i>Reaction Temperature</i>	237

8.4.3 <i>The Effect of Iron Diluent</i>	239
8.4.3.1 Reaction Temperature Profiles.....	241
8.4.4 <i>The Fe₂O₃ + 3Ti Reaction</i>	242
8.4.5 <i>Morphology Control and the 'Ideal' Morphology</i>	243
8.4.6 <i>Reaction Mechanism</i>	244
8.5 CONCLUSIONS.....	247
8.6 FIGURES.....	248
9. CONCLUSIONS AND FUTURE WORK	259
9.1 CONCLUSIONS.....	259
9.2 FUTURE WORK	260
10. ACKNOWLEDGEMENTS	262
11. BIBLIOGRAPHY	263
12. APPENDICIES	276
A. FIGURE 7.2 - FLOWCHART FOR THE TITANIUM OXIDATION COMPUTER PROGRAMME....	276
B. WALK THROUGH OF THE COMPUTER PROGRAMME - TI_BURN.BAS.....	277
C. COMPUTER PROGRAMME - TI_BURN.BAS	288
D. COMPUTER PROGRAMME - POWDER.BAS.....	298

Abstract

The quest for ever stronger and tougher steels has led to an interest in the 'Acicular Ferrite' microstructure, its chaotic and disordered morphology imparting a high degree of toughness to the steel. To date, only complex and expensive materials and manufacturing processes have formed acicular ferrite within bulk cast steel. As such, the thrust of this research is to produce a cheap steel addition, an iron - titanium oxide metal-ceramic composite, that will facilitate the formation of acicular ferrite in conventionally manufactured bulk cast steels.

The Self-propagating High-temperature Synthesis (SHS) process has been utilised to manufacture the iron - titanium oxide material from compacts pressed from $\text{Fe}_2\text{O}_3 + \text{Ti}$ powders. The fundamental reactions that occur as titanium powder and $\text{Fe}_2\text{O}_3 + \text{Ti}$ powder compacts are heated in air and argon atmospheres have been investigated. The process's ^{PROCESSES} involved are reported and have been modelled mathematically. A computer simulation of the reaction process has been developed and tested against experimental evidence.

The effect of various compact parameters, the starting compact stoichiometry and other processing variables have been examined with respect to the composition of the products and their morphology.

Chapter 1

Introduction

Chemical reactions can be classed as endothermic or exothermic. Simply put, endothermic reactions absorb heat and exothermic reactions release heat. A simple exothermic reaction is the 'reduction – oxidation' reaction between Al and Fe_2O_3 . This is commonly called the 'Thermite' reaction. During the reaction, the Al is oxidised and the Fe_2O_3 reduced, producing the products Al_2O_3 and Fe. The reaction is sufficiently exothermic to melt both products. Over the past 25 years the use of exothermic reactions to form useful products has been investigated. The term given to these reactions is 'combustion synthesis' or 'Self-propagating High-temperature Synthesis' (SHS). The process provides a simple and energy efficient way of manufacturing a variety of ceramics, intermetallics and mixed metal-ceramic composites (MMC's). Notable examples of products that are successfully manufactured by the SHS process are TiC, TiB_2 and TiN (Moore and Feng 1995b).

Whilst titanium carbide, borides and nitrides have many uses in their pure forms - tool inserts and coatings to name a few – they can also act as significant reinforcement when added to steels. To this end, the last 8 years has seen an increased interest in the application of the SHS process to form MMC's. The formation of the ceramic component dispersed within the metallic binder bypasses some of the problems of wettability and ceramic oxidation that are encountered by conventional composite production processes.

The addition of certain ceramic particles to steel may also promote the formation of the desirable microstructure 'Acicular Ferrite'. The microstructure is produced when Bainite nucleates from ceramic inclusions within the grain, rather than the grain boundaries, forming a disordered chaotic structure. Significant improvements in the toughness of the steel are produced as a result. Recent research has highlighted the high potency of titanium oxide bearing inclusions in acting as nucleation sites for the acicular ferrite (Gregg and Bhadeshia 1994a and Gregg and Bhadeshia 1994b). To this end, the general thrust of this research was to understand the SHS reaction processes that result in an iron based MMC, containing titanium oxide based ceramic particles. The reaction to produce this product was based around the starting components of Fe_2O_3 and titanium.

The SHS process has been researched at both fundamental and applied levels over the last 25 years. Whilst there has been significant successes with the application of the technology, the fundamentals that govern them are not so well understood. This is due to the complex nature of the reactions; they occur at very high temperatures with large temperature gradients and cooling rates resulting in reaction conditions that are far from equilibrium. Thus the first step in this research was to understand the fundamentals that govern the reaction between Fe_2O_3 and titanium.

Initial investigations into the general oxidation characteristics of titanium were followed by an investigation into the reaction between Fe_2O_3 and titanium. This area has received little attention in the literature and required a detailed

study of the fundamentals. Knowledge gained in this work was useful in understanding the processes involved in the SHS reaction between powdered Fe_2O_3 and titanium. The stoichiometry of the reaction was investigated as it was known that the product of the SHS reaction is dependent on the starting composition.

The experimental knowledge gained was used to write a simple computer programme that models the thermal history of a titanium powder pellet being heated in air. This model was tested against experimental results to determine its accuracy and viability.

Chapter 2

Literature Survey – Background Information

2.1 Historical Perspective.

The 'combustion synthesis' reaction is not new. As early as 1825 investigations into this process were being conducted (McCauley 1990). From then, sporadic investigations in Europe and America produced a wide variety of compounds, ranging from nitrides, borides and carbides to phosphates, arsenides and silicides. However, it was not until 1967, at the Russian Institute for Structural Macrokinetics, that a systematic investigation into combustion synthesis occurred. It was here that Borovinskaya, Skhiro and Merzhanov realised the full potential of the process for synthesising ceramic and metal materials in a cost and energy efficient manner (McCauley 1990). They not only looked at the variety of materials that could be synthesised but also at the physical parameters that occurred before, during and after the reaction. This area of interest was coined 'Structural Macrokinetics'. It describes the evolution of structure in the course of chemical transformations taking into account heat and mass transfer processes (Merzhanov and Rogachev 1992). A schematic of the principle concept of structural macrokinetics is shown in figure 2.1. During the research, the team produced a variety of different materials. Some of their commercial successes include titanium carbide for 'KT' polishing paste and Ni-Ti shape memory alloys for medical applications.

Since the mid 1980's investigations into combustion synthesis reactions have occurred all over the world, but most extensively in the U.S.A, Japan and Russia. The early work was concerned with the variety of products that could be formed by the process, however, recently there has been an interest in the mechanisms of the many types of SHS processes - the area of 'Structural Macrokinetics'. Many of the recent papers examining SHS processes use the $Ti + C \Rightarrow TiC$ reaction and consequently this is now fairly well understood. The other emerging trend in SHS research is the application of the SHS process to other technologies – Functionally Graded Materials (FGM's), nanoparticles and composite pipes etc., and the application of other technologies to the SHS process. An example of this is the application of an electric current to a powder compact (Gedevanishvili and Munir 1994, Feng and Munir 1994 and Shon and Munir 1995). The generated electric field interacts with the compact to produce heat and thus enables reactions with a low degree of exothermicity to combust in the SHS mode (Feng and Munir 1996). Other parameters such as the product particle size are also seen to be affected by the field (Munir 1996).

Whilst interest is increasing, the study of the SHS process is still in its infancy. The basics are understood, but the complexity of the process means that each new reaction still has to be investigated from its fundamentals upwards.

2.2 Basic Principles

Self-Propagating High-Temperature Synthesis (SHS) is the name given to the process of using self sustaining chemical reactions to produce desirable

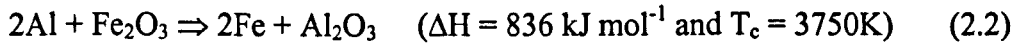
products; ceramics, intermetallics and metal-ceramic composites. SHS reactions are usually initiated in a compact of mixed reactant powders (e.g. $\text{Ti}_{(s)} + \text{C}_{(s)}$) under inert conditions, or a compact of metal powders in a reactant atmosphere (e.g. $\text{Ti}_{(s)} + \text{N}_{2(g)}$). The self sustaining nature of the SHS process means that once the reaction has been started it will propagate through the entire reactant mixture without any additional heat input. There are two modes in which the reaction can be initiated; locally (SHS) or globally (thermal explosion). In the former case, a compact is ignited by a localised heat source such as an electrical resistance heated tungsten filament. Spontaneous global ignition characteristic of the 'thermal explosion' mode is typically achieved by heating the whole compact in a furnace.

The temperature at which the compact ignites (i.e. becomes self sustaining) is termed the 'ignition temperature', T_{ig} . Once ignited, the reaction temperature increases to the adiabatic combustion temperature, T_{ad} . This can be in excess of 5000 K (McCauley 1990). The adiabatic combustion temperature is the theoretical maximum combustion temperature that can be achieved in a system with no heat losses. It is often taken as the maximum reaction temperature, even though in practice the actual combustion temperature T_c , can be significantly lower (Yi and Moore 1990). Full definitions of the terms used in the understanding of the combustion synthesis process can be found in section 2.5 - Thermochemical Theory. A schematic of the process is shown in figure 2.2.

A typical reaction schematic is set out below:



An example of this is the '*thermite*' reaction:



For the reaction to be self sustaining, the heat energy released has to be sufficient to raise the temperature of the surrounding unreacted material above T_{ig} . For this to happen, it has been suggested that $T_{ad} > 1800 \text{ K}$ (Yi and Moore 1990 and Moore and Feng 1995). It is normal for reactions that are weakly exothermic ($T_{ad} < 1800 \text{ K}$) to be ignited in the thermal explosion mode, as the compact requires pre-heating to overcome the short fall in exothermic reaction energy. Highly exothermic reactions ($T_{ad} > 1800 \text{ K}$) are usually ignited in the energetically favourable SHS mode as they are self sustaining. SHS reactions can generally be classified as:

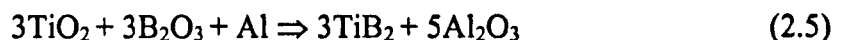
1. Thermite type: Oxidation-reduction reactions:



2. Compound formation: Reaction from elemental or compound constituents:



3. Mixed: Thermite and compound reactions:



A useful tool in the analysis of binary (two component) SHS reactions is the classifications first developed by Merzhanov (1983). The classifications are based on the adiabatic temperature and the melting and boiling points of the reactants as shown in table 2.1. Most SHS processes are based around compositions where at least one of the components is in the liquid state during the reaction, a liquid phase allowing far higher reaction rates than solid state or solid – gas reactions.

Table 2.1 Physiochemical classification of the SHS mechanisms in a binary system. Merzhanov (1983).

Relation between T_{ad} , T_m and T_b	Characteristics of the system	Examples
$T_{ad} < T_b^i$ $i = 1, 2$	Ideal gas free combustion occurs if $P(T_{ad}) / P_0 \Rightarrow 0$	$Ti + 2B = TiB_2$ $T_{ad} = 3200 \text{ K } (T_0 = 293 \text{ K})$ $P_{Ti}(3200 \text{ K}) = 8 \text{ k Pa}$ $P_B(3200 \text{ K}) = 0.4 \text{ k Pa}$ Gasless reaction only at high pressures
$T_m^i < T_{ad} < T_b^i$ $i = 1, 2$	Both components in the liquid state.	$Ni + Al = NiAl$ $T_{ad} = 1910 \text{ K}$ $T_m \text{ (K): Ni} = 1726, \text{ Al} = 933$ $T_b \text{ (K): Ni} = 3373, \text{ Al} = 2773$
$T_m^1 < T_{ad} < T_m^2$	Solid and liquid reaction. Highest propagation velocity.	$Ti + C = TiC$ $T_{ad} = 3210 \text{ K}$ $T_m^{Ti} = 1933 \text{ K}$ $T_m^C = 3973 \text{ K}$
$T_{ad} < T_m^i$ $i = 1, 2$	Both components in the solid state. Lowest combustion velocity.	$2Ta + C = Ta_2C$ $T_{ad} = 2600 \text{ K}$ $T_m^{Ta} = 3269 \text{ K}$
$T_b^1 < T_{ad} < T_b^2$	One component in the gas phase and the other in the condensed state.	Widely used process, formation of nitrides, sulphides, phosphides etc.
$T_{ad} > T_b^i$ $i = 1, 2$	Both reactants in the gas phase and solid product	Very few systems studied (Mg + S)

2.3 Practical Advantages to the SHS Process

Due to the self-sustaining nature of the SHS reaction, it is energetically efficient. Because of this, it has a distinct advantage over the traditional production routes for the manufacture of ceramics, intermetallics and metal-ceramic composites (Borovinskaya 1992 and Subrahmanyam and Vijayakumar 1992). The traditional manufacturing routes require the reactants to undergo long periods in high temperature furnaces or plasma reactors. The equipment required for traditional processing is both large and expensive. In contrast, the SHS process is very quick. For example, the *London and Scandinavian Metallurgical Company UK (L.S.M.)* are able to produce 30 kg of metal-ceramic composite in under 5 minutes. Additionally, the equipment required to enable SHS manufacturing is inexpensive, small and easy to scale up. An example of a manufacturing route with details of the equipment required is below:

1. Mix the reactant powders – ball mixer, tumbler.
2. Press (by hand or mechanically) the powders into a reaction chamber - usually a graphite or silica based crucible.
3. Ignite the powders – various methods including oxy-acetylene torch and chemical fuses.
4. Crush / process the product after the reaction has taken place -hammer crush, ball milling and sieve.

The SHS reaction can be initiated in a variety of ways (Barzykin 1992). Some examples are:

- Combustion Wave Ignition: Chemical fuses which are easy to ignite generating sufficient heat to ignite the main reaction. Examples of chemical fuses are mixtures of Al + Fe₂O₃. The benefits of the method are ease of use and availability of the chemical compounds. However, contamination of the product with the products of the fuse combustion may occur.
- Radiant Flux Ignition: A xenon bulb is focused to a small diameter (~10mmØ) on the top surface of the compact. It is controllable and there is no chemical contamination of the compact. However, the power density is lower than other ignition methods (~ 6 x10⁶ W m⁻²) and thus it is only suitable for small or highly exothermic compacts. A more standard approach is to use the heat flux generated by an electrically heated tungsten filament, situated close to the top of the compact.
- Laser Induced Ignition: Laser radiation is utilised to ignite a compact. Neodymium-doped glass, ruby and caesium bromide lasers have all been successfully used. Flux densities as high as ~ 10¹¹ W m⁻² are realised, which is sufficient to melt and vaporise components in the compact. The power and cleanliness of the ignition method are contrasted with its expense.
- Chemical Oven: The heat produced from highly exothermic chemical reactions is utilised promote another reaction of much lower exothermicity. This is different from ignition by the chemical fuse method as the two

reaction compounds are intermixed within the compact. An example of this is the highly exothermic $\text{Ti} + \text{C} \Rightarrow \text{TiC}$ reaction, which is used to produce tungsten carbides, WC, via the reaction $2\text{Ti} + \text{W} + 3\text{C} \Rightarrow 2\text{TiC} + \text{WC}$.

The effect of the heat source on the ignition of SHS reactions has been investigated by Kanuary and Hernandez-Guerrero (1995).

In contrast to conventionally produced materials, SHS products are often of higher purity and homogeneity. This is due to the high reaction temperature found in SHS processing, which results in volatile impurities such as S, Cl, Cu, Fe, Ca, Si, Mg and Al being removed from the product (Chang *et al.* 1995 and Shteinberg *et al.* 1995). Bloshenko *et al.* (1984a, 1985) also showed that SHS manufactured compounds can have a lower concentrations of impurity oxygen than their starting constituents.

The SHS process provides a way of creating unique products that can not be made in any other way; this applies in particular to metal-ceramic composites. L.S.M. UK are one of the first commercial suppliers of a SHS produced metal-ceramic composite with their Fe(W,TiC) casting addition. The product consists of W,TiC ceramic particles evenly distributed within an iron based matrix. The W,TiC particles refine the grain size and improve the wear characteristics of cast, rolled and heat treated steels (Wood *et al.* 1995). Saidi *et al.* (1994), Capaldi and Wood (1996) and Capaldi *et al.* (1997) have investigated the characteristics of the SHS reaction that produces Fe – TiC composites, whilst

Fan *et al.* (1997) specifically investigated the role of iron in the reaction. Ustundag *et al.* (1993) have researched Fe-Mn-O composites and Terry and Chinyamakobvu (1992b) assessed Fe-TiB₂ reactions. Investigations into TiC reinforced Ni based composites have been conducted by LaSalvia *et al.* (1992), LaSalvia and Meyers (1992), Bunin *et al.* (1993), Zhirkov *et al.* (1995) and Capaldi and Wood (1996). A comparison with conventionally produced (cast) Ni - TiC composites was presented in the work of Skolianos *et al.* (1994). Feng *et al.* (1994) expanded the simple systems and looked at the multiphase metal ceramic composites Al + Al₂O₃ + TiC and Al + Al₂O₃ + B₄C. Other novel SHS products are:

- Ceramic alloys: The chemical and mechanical properties of ceramics (toughness, thermal shock resistance, oxidation resistance etc.) can be improved by mixing them with other ceramic compounds. Some SHS produced ceramic alloys are; TiC + Al₂O₃, ZrB₂ + Al₂O₃ and ZrC + Al₂O₃ (Bowen *et al.* 1991, Bowen and Derby 1994), B₄C + Al₂O₃ (Wang *et al.* 1994a). Wang *et al.* (1994b) have also investigated the SHS production of B₄C fibres within a MgO ceramic. The physical and chemical properties of some interesting SHS produced ceramic alloys are presented in a paper by Levashov *et al.* (1996).
- Intermetallic / Ceramic alloys: Intermetallics are often brittle and hard, however, their high melting point, stiffness and resistance to oxidation and creep make them of interest to developers of aircraft and engine

components (Meier and Pettit 1992). Song *et al.* (1995) found that the SHS process could be manipulated to produce FeSi_2 with varying thermal conductivity and Deevi (1994) has investigated the characteristics of the Mo-Si SHS reaction. Ceramics or other intermetallics (Grake *et al.* 1992) dispersed within an intermetallic, offer the potential of increased toughness, wear resistance and greater high temperature strength. Misra (1990) found that TiC, ZrC, TiB_2 and Al_2O_3 were all thermodynamically stable reinforcement ceramics for inclusion into FeAl intermetallics. The high temperature stability of group IV, V and VI transition metal borides, carbides, nitrides and oxides has been assessed by Wiedemeier and Singh (1991). They found that V_3B_4 , HfC, HfN and Ti_3O_5 were the most stable materials in each class. TiAl / TiB_2 (Yamada and Miyamoto 1992), TiAl / TiC (Tomoshige and Matsushita 1996), Ti_2Cu / TiB_2 (Li *et al.* 1992) and reinforced shape memory NiTi / TiC (Mari and Dunand 1995) are examples of ceramic / intermetallic SHS composites, whilst MoSi_2 reinforced with WSi_2 (Subrahmanyam and Mohan Rao 1994) is an example of an intermetallic / intermetallic SHS composite.

- Nanocrystalline Powders: Nanocrystalline powders can have desirable mechanical, optical, electronic and magnetic properties. Venkatachari *et al.* (1995) reported that combustion synthesis could produce nanocrystalline yttria doped (stabilised) ZrO_2 powders. Kingsley *et al.* (1990) have produced fine metal aluminates for refractory applications via the SHS process whilst Wang *et al.* (1995) have researched SHS produced sub

micron MgO / B₄C composites and Lee *et al.* (1995) applied the technique to produce submicron Al₂O₃ / SiC particles.

- Functionally Graded Materials (FGM's): Whilst ceramic components have a variety of uses in the engineering world, they have a very low resistance to thermal gradients, strain and cracking (Askeland 1992). One solution to this problem is to coat a tough metal substrate with the hard and thermally resistant ceramic. However, this solution encounters problems in the weak bond between the two materials. FGM's have been employed as a method to solve the problems of ceramic / metal bonding by grading the transition between the materials e.g. multilayer coatings (Carbide substrate / TiC / Al₂O₃ / TiN) on machining tools (Kalpakjian 1992 and Eroglu and Gallois 1997). FGM's are composite materials that can be successfully manufactured by the SHS process. The FGM is built from a number of increasingly 'metallic' layers. The initial layer is purely ceramic, with subsequent layers containing an increasing amount of metal, and the final layer being pure metal. As porosity is a problem with the SHS process, the manufacture of the FGM's is often accompanied by either dynamic compaction or HIPing (Strangle and Miyamoto 1995). Examples of composites produced in this way are Cr₃C₂ / Ni (Tanihata *et al.* 1993 and Miyamoto and Ohyanagi 1993), Al₂O₃ / TiC / Ni and Al₂O₃ / Cr₃C₂ / Ni (Miyamoto *et al.* 1995a) and MoSi₂ / Al₂O₃ / Ni (Miyamoto *et al.* 1995b and Kang *et al.* 1995).

- Composite Pipes: Duan *et al.* (1996) have reported on the use of the SHS process in the manufacture of steel pipes that are coated on the inside with a corrosion / erosion resistant coating. A reactant mixture is put within a spinning pipe and ignited. The reactant mixtures investigated produced an Fe, Ni or Cr metallic phase with a Al_2O_3 slag. The metallic phase is more dense than the Al_2O_3 and thus bonds with the pipe under the imposed centrifugal forces. The Al_2O_3 slag remains on the inner surface and can be removed after processing but is usually left in place to act as an additional resistant coating (Vukhvid 1992). The centrifugal forces help to produce a relatively dense coating. Other workers (Odawara 1990 and Subrahmanyam and Vijayakumar 1992) have also researched the application of SHS technology to composite pipe manufacturing.

The high thermal gradients encountered during SHS reactions, created by rapid heating and cooling of the compact, can lead to the formation of products that are in a non-equilibrium state or have large defect concentrations. There may be benefits associated with both states. Non-equilibrium structures allow the compositional tailoring of the products e.g. in TiC-WC, the ceramic particle has a WC rich outer and a TiC rich inner core (Degnan 1995). High defect concentrations have been seen to increase the sintering ability of some ceramics (Ko *et al.* 1995).

The ease and effectiveness of the SHS process lends itself to experimentation. Over the years more than 500 different compounds have been successfully

synthesised, as seen in table 2.2. Table 2.3 lists the many commercial applications in which SHS produced materials have found a niche.

Table 2.2 A Selection of Materials Produced by the SHS Process. Moore and Feng (1995a).

Chemical Class	Typical SHS formed ceramics
Borides	CrB, HfB ₂ , NbB, TaB ₂ , TiB ₂ , LaB ₆ , MoB ₄ , WB, ZrB ₂ , VB ₂
Carbides	TiC, ZrC, HfC, NbC, SiC, Cr ₃ C ₂ , B ₄ C, WC, TaC, VC, Al ₄ C ₃ , Mo ₂ C
Nitrides	Mg ₃ N ₂ , BN, AlN, SiN, TiN, ZrN, HfN, VN, NbN, Ta ₂ N
Silicides	TiSi ₃ , ZrSi, MoSi ₂ , TaSi ₂ , NbSi ₂ , WSi ₂ , V ₅ Si ₃
Aluminides	NiAl, CoAl, NbAl ₃
Hydrides	TiH ₂ , ZrH ₂ , NbH ₂ , CsH ₂ , PrH ₂ , IH ₂
Intermetallics	NiAl, FeAl, NbGe, TiNi, CoTi, CuAl
Carbonitrides	TiC-TiN, NbC-NbN, TaC-TaN, ZrC-ZrN
Cemented Carbides	TiC-Ni, TiC-(Ni, Mo), WC-Co, Cr ₂ C ₃ -(Ni, Mo)
Binary Compounds	TiB ₂ -MoB ₂ , TiB ₂ -CrB ₂ , ZrB ₂ -CrB ₂ , TiC-WC, TiN-ZrN, MoS ₂ -NbS ₂ , WS ₂ -NbS ₂
Chalcogenides	MgS, NbSe ₂ , TaSe ₂ , MoS ₂ , MoSe ₂ , WS ₂ , WSe ₂
Composites	TiB ₂ -Al ₂ O ₃ , TiC-Al ₂ O ₃ , B ₄ C-Al ₂ O ₃ , TiN-Al ₂ O ₃ , TiC-TiB ₂ , MoSi ₂ -Al ₂ O ₃ , MoB-Al ₂ O ₃ , Cr ₂ C ₃ -Al ₂ O ₃ , 6VN-5Al ₂ O ₃ , ZrO ₂ -Al ₂ O ₃ -2Nb

Table 2.3 Typical Uses of SHS Produced Materials. Moore and Feng (1995a).

	Descriptions
1	Abrasives, cutting tools and polishing powders, e.g. TiC, cemented carbides.
2	Resistive heating elements, e.g. MoSi ₂ .
3	Shape memory alloys (SMA), e.g. TiNi.
4	High temperature intermetallic compounds, e.g. nickel aluminides
5	Steel processing additives, e.g. nitrided ferroalloys
6	Electrodes for electrolysis of corrosive media, e.g. TiN, TiB ₂ .
7	Coating for the containment of liquid metals and corrosive media.
8	Powders for further ceramic processing, e.g. Si ₃ N ₄ .
9	Thin films and coatings, e.g. MoSi ₂ , TiB ₂ .
10	Functionally-graded materials (FGM), e.g. TiC + Ni
11	Composite materials, e.g. TiC + Al ₂ O ₃ , TiC + Al + Al ₂ O ₃ .
12	Materials with specific magnetic, electrical or physical properties, e.g. BaTiO ₃ .

2.4 Limitations of the SHS Process

The major drawback to the SHS process is the high degree of porosity created within the products. Absorbed gases and moisture on the powders and within the green compact rapidly expand during the reaction. They violently escape and produce gas channels, voids and cracks (Chang *et al.* 1995 and Shteinberg *et al.* 1995). The escaping gases may also take molten compounds with them. It has been calculated that in some cases the pressure inside gas filled pores during the reaction can be as high as 1000 atm. (Moore and Feng 1995a). Additional porosity can be caused by the increased density of the products over their initial constituents. Due to the porosity, product densities can be as low. Halverson *et al.* (1993) measured some SHS produced TiC samples to be ~36% of theoretical maximum density. This is not always a problem. Indeed it can be a benefit, with an example being that it eases crushing of the product in the production of ceramic powders (Moore and Feng 1995b). However, for those applications that require a dense product there are various densification technologies available. The powder compact can be ignited under pressure (Maupin and Rawers 1993, Lee *et al.* 1996, Olevsky *et al.* 1996 and Dumez *et al.* 1996), reaction sintered (Murry and German 1992, Mughal and Plumb 1993, Chandran *et al.* 1995 and Royal *et al.* 1996), reaction HIPed (Shingu *et al.* 1990, Miyamoto *et al.* 1995a and Miyamoto *et al.* 1995b), simultaneously ignited and forged - dynamic densification (LaSalvia *et al.* 1994) or reaction hot pressed (Murray and German 1992, Vukhvid 1992 and Stolin *et al.* 1995). These processes can produce near net-shaped artefacts of greater than 95% of theoretical density (LaSalvia *et al.* 1994 and Moore and Feng 1995b).

2.5 Thermochemical Theory

In SHS systems the enthalpy change between the reactants and the products produces the high combustion temperatures. An understanding of the enthalpy of a reaction will indicate whether that reaction will be self sustaining or not. Generally, reactions require a high enthalpy of reaction to be self sustaining. Before we look at the calculation of the enthalpy of reaction it is worth noting the temperature points that are used in SHS research.

In any given SHS reaction there are four important temperature points which have an affect on the reaction and the final products:

1. The initial temperature, T_0 : The average temperature of the sample before the reaction is started. This temperature does not apply to those reactions that are initiated in the thermal explosion mode as the whole sample is at the ignition point, T_{ig} .
2. The ignition temperature, T_{ig} : The point at which the SHS reaction is activated and will continue to be self sustaining without any additional heat supply.
3. The adiabatic combustion temperature, T_{ad} : The maximum combustion temperature achieved under adiabatic conditions. This is generally the melting point or decomposition (boiling) point of the combustion products (Glassman and Papas 1994). Above the decomposition temperature the products cannot form and thus the reaction temperature is limited.

4. The actual combustion temperature, T_c : The measured (usually via thermocouple or optical pyrometer) combustion temperature, found under non-adiabatic conditions.

For a pellet undergoing a combustion reaction, the enthalpy of the reaction at temperature T_0 , is $\Delta H(r)_{T_0}$. The heat evolved is converted to an increase in temperature of the products from T_0 to T_{ad} . This is given by the heat balance condition:

$$\Delta H(r)_{T_0} = \int_{T_0}^{T_{ad}} C_p dT \quad (2.6)$$

where C_p is the combined heat capacity of the products. As the products of most combustion reactions undergo phase transformations below the adiabatic temperature, T_{ad} calculated in equation 2.6, the corresponding changes in the enthalpy and heat capacities have to be taken into account. T_{ad} then has to be calculated in a part wise manner. Typically the products are molten and thus the heat balance equation has to take this into account:

$$\Delta H(r)_{T_0} = \int_{T_0}^{T_1} C_p dT + L_1 + \int_{T_1}^{T_2} C_p dT + L_2 \dots\dots\dots + \int_{T_n}^{T_{ad}} C_p dT \quad (2.7)$$

where L is the enthalpy of the phase transformation of the products. In this equation it is assumed that the reaction occurs under adiabatic conditions. As

such T_{ad} is only a measure of the exothermicity of the reaction and defines the upper limits of the combustion system.

The relationship between heat generated by the reaction and heat lost to the environment governs the rate of reaction wave propagation, stability and temperature. As heat is lost to the environment, T_c is less than T_{ad} .

Another important parameter is the activation energy of the reaction. The activation energy gives a measure of the ease of ignition of the reaction. High activation energies are found in reactions with low exothermicities and vice versa. Low exothermic reactions are characterised by a high ignition temperature, the requirement of pre-heating and an unstable combustion wave. A knowledge of the activation energy can also illuminate the reaction mechanism. In the case of titanium nitration in gaseous nitrogen, the activation energy of the combustion reaction is similar to the activation energy of nitrogen diffusion into a layer of TiN, $\sim 350 \text{ kJ mol}^{-1}$ (Munir 1992b), thus indicating that the SHS reaction proceeds by a similar mechanism.

2.6 SHS Reaction Mechanisms

2.6.1 Solid – Gas

Solid – gas SHS reactions are predominately used to form hydrides, oxides and nitrides (Dunmead *et al.* 1989). During the reaction the products reach high combustion temperatures ($T_{ad} = 4900 \text{ K}$ for $\text{Ti} + \text{N}_2$). Theoretically, for the

product to form, the gas pressure during the reaction has to be higher than the dissociation pressure of the product. For the $\text{Ti} + \frac{1}{2}\text{N}$ reaction this would mean a gas pressure greater than 1000 atm. However, as has been mentioned previously, the adiabatic temperature is seldom reached due to heat losses and thus a gas pressure as low as 400 atm can achieve full compact conversion. However, solid - gas reactions at atmospheric pressure typically fail to achieve full reactant conversion (Munir 1992*b*).

The most distinctive feature of solid – gas reactions is the combustion process. Since the gas is primarily external to the solid compact, the reaction starts at the surface of the compact and moves inwards. As such, the availability of gas within the compact is the critical factor in the reaction. Gas pressure and compact porosity are the physical parameters which control this factor. Higher pressure and more porosity allow more gas into the compact and increase the combustion wave velocity and decrease the conversion ratio. The conversion ratio, the percentage of product formed, is related to the combustion wave velocity. A slower wave keeps the compact at a higher temperature for longer and thus allows a greater degree of conversion (Kudo and Odawara 1989). Solid – gas SHS reactions are diffusion limited. In the case of titanium powder in nitrogen, the reaction method is one of nitrogen diffusion into the titanium through a layer of TiN. This produces slow combustion wave velocities which are not seen to increase with nitrogen pressure (Munir 1992*b*). Zhou and Stangle (1995) have found that the rapid heating rates ($>10^3 - 10^5 \text{ K s}^{-1}$) found in solid – gas SHS type reactions may overcome the diffusional restrictions

attributed to the formation of a product layer on the reactant material. Solid – gas SHS type reactions with reference to the titanium – oxygen and titanium – nitrogen reactions are discussed in greater detail in Chapter 3.

2.6.2 Solid – Solid

In solid – solid reactions only slow solid state diffusional mechanisms can operate. Once a layer of product has formed around the reactant materials further reaction is governed by the rate of diffusion of the species (Terry and Chinyamakobvu 1992*b* and Akhtar *et al.* 1996). Typical of this type of reaction is Ta + C. It has a slow reaction rate and a combustion wave velocity between 0.32 – 0.62 cm s⁻¹ (Subrahmanyam and Vijayakumar 1992). In these types of systems it is important to use as fine a powder as possible, to increase the amount of active surface area in the compact. These types of reactions can be classed as ‘reactive sintering’ when the exothermicity of the reaction is so low as to require a substantial additional heat input. Solid-solid reactions often occur in powdered compacts prior to a self-propagating (solid – liquid) reaction (Javel *et al.* 1996).

2.6.3 Solid – Liquid

Solid – liquid reactions are common in the SHS manufacture of many carbides, borides and silicides. In the production of carbides and borides the metallic phase is liquid during the reaction, as in the case of the well studied Ti + C system. In the production of silicides, the silicon is the molten phase. A

classification of these compounds has been proposed, based on the ratio of the atomic radii of the constituent components, R_c / R_m where R_c is the radius of the non metallic atom and R_m is the radius of the metallic atom (Subrahmanyam and Vijayakumar 1992). If the ratio is <0.59 , as in carbides and borides, the crystal structure is simple (i.e. MeC) with non-metal atoms sited interstitially within the metal lattice. In this case, unstable combustion only leads to incomplete reaction of the constituent materials. If the ratio is >0.59 , as in silicides, complex crystal structures can form with many non-metal rich phases. Unstable combustion then leads to inhomogeneity and a variety of phases in the product.

In the Ti + C system it is the melting of the titanium that initiates the self-propagating combustion reaction (Lihrmann *et al.* 1991, Deevi 1991, Terry and Chinyamakobvu 1992, Halverson *et al.* 1993, Saidi *et al.* 1994, Makino *et al.* 1994, Choi and Rhee 1994, Choi and Rhee 1995, Halverson *et al.* 1995, Ko *et al.* 1995, Lihrmann *et al.* 1995, Lee and Chung 1995, Fan *et al.* 1996, Mishra *et al.* 1997, Fan *et al.* 1997, Capaldi *et al.* 1997). Below the melting point of the titanium there is a small degree of solid state reaction between the reactants that accounts for no more than 6% of the TiC formed (Vrel *et al.* 1994). Munir *et al.* (1990) classically outlined the mechanism of reaction between titanium and carbon in the self-propagating mode to be :

1. Heating of the sample to the melting point of titanium.
2. Capillary spreading of the liquid titanium over the carbon particles. Liquid titanium exothermically reacting with the solid carbon to form a saturated

Ti and C solution.

3. Precipitation of TiC particles out of the saturated solution.
4. Growth of the TiC particles.

Deevi (1991) postulated that after the initial melting of the titanium, TiC is formed on and surrounds the carbon particles, full conversion occurs with a diffusional reaction between liquid titanium and solid carbon through a layer of solid TiC. A different mechanism has been suggested by Fan *et al.* (1996) who suggested the mechanism of the self-propagating Ti + C reaction to consist of three different steps:

1. Initial heating of the compact promotes a solid state Ti + C reaction that forms a solid TiC layer around the titanium particle.
2. The exothermic energy of the solid state reaction causes the titanium to melt. It is confined within the TiC shell (experimentally recorded reaction temperatures are between 2000-3000 K, TiC melts at 3423 K).
3. Carbon diffuses into the molten titanium, through the TiC shell, and then precipitates as discrete TiC particles within it.

The different reaction mechanisms can be explained by the experimental procedures used by the authors. Fan *et al.* (1996) studied artificially quenched samples and Munir (1990) and Deevi (1991) studied reacted and part reacted

samples. The artificially quenched samples were held for a long time at a lower temperature (in effect sintered), whilst the part reacted samples had a reaction wave move through them, but have not fully transformed. The thermal history of the pellets thus influences the observations upon which the reaction mechanisms are based. Additionally, Lee and Chung (1995) proposed that the size of the carbon powder could influence the reaction mechanism. Carbon black ($\sim 0.01\mu\text{m}$) would react to form TiC shells, whilst graphite powder (< 325 mesh) would promote the capillary spreading reaction mechanism. A change in reaction mechanism according to the size of reactant powders in the compact was also seen by Vol'pe and Evstigneev (1993) in the Ti – Al – C system.

Various papers have been published that mathematically model the combustion process or aspects of it. Munir (1992a) initially produced a microstructural and mechanistic analyses of SHS systems. Armstrong (1992) furthered the work of Zenin *et al.* (1981) and investigated the stability of the combustion wave. Bhattacharya (1992) modelled the effect of porosity and particle size on the velocity of the reaction wave. This work was expanded upon by Cao and Varma (1994) and Viljoen and Puszynski (1994). Kanuany and Hernandez-Guerrero (1994) additionally derived equations to predict the length of heating required to ignite the compact. Yuranov *et al.* (1994) constructed a quasi-equilibrium model for the chemical processes that occur during SHS reactions. Zhirkov *et al.* (1995) and Vukhvid *et al.* (1997) numerically analysed the crystallisation process of SHS formed products.

2.6.3.1 The Ti + C + Metal Reaction

Including another metal in the $\text{Ti} + \text{C} \Rightarrow \text{TiC}$ reaction, e.g. :



leads to the formation of a ceramic / metallic composite. The extra metallic component is often called a 'binder' or diluent phase. The binder phase does not significantly react with the titanium or carbon and forms a product of TiC particles distributed through the metallic binder phase. The metallic binder has various effects on the combustion reaction and product.

The addition of Fe on the $\text{Ti} + \text{C}$ reaction has been studied by various researchers. Saidi *et al.* (1994) found that the ignition temperature of $\text{Ti} + \text{C}$ samples containing iron was dictated by the eutectic temperature of the Fe – Ti system. A solid-state reaction between titanium and iron was thought to occur during the heating cycle, to form the intermetallic FeTi_2 . This phase melts at 1085°C , which coincides with the recorded ignition temperature of the samples. As little as 2.7wt% iron added to a stoichiometric $\text{Ti} + \text{C}$ compact was sufficient to reduce the ignition temperature from $\sim 1550^\circ\text{C}$ to 1250°C . Capaldi and Wood (1996) saw that the addition of an iron diluent reduced the combustion temperature and reduced the wave velocity; however, complete combustion still occurred in compacts containing up to 60wt% Fe. The addition of the iron diluent also refined the TiC particle size.

Fan *et al.* (1997) disagreed with the above combustion initiation mechanism and suggested that carbon diffusion into the iron would cause premature

melting of the iron particle. The Fe – C system has a minimum melting point of 1147°C. This would be the initial liquid phase to form as interstitial carbon diffusion into iron (to form the Fe-C compound) would be orders of magnitude faster than solute titanium diffusion into iron (to form FeTi₂).

LaSalvia *et al.* (1995) and LaSalvia and Meyers (1995) investigated the addition of Ni to the Ti + C reaction. No one reaction mechanism could be identified as the ignition process because Ni / Ti reactions occurred alongside Ni / C and Ti / C reactions. It was, however, shown that the self-propagating reaction was initiated by the formation of a liquid phase.

In summary, it is the formation of a liquid phase that facilitates the self-propagating reaction to occur (Wang *et al.* 1995). Prior to this, solid-state reactions may occur between the compact constituents. The addition of a metallic diluent can reduce the ignition temperature by forming low melting point alloys with the other reactant powders.

2.6.4 Liquid – Liquid

Many intermetallics and aluminides are formed from a molten reaction phase. The SHS manufacture of Ni₃Al from Ni and Al powders has a recorded maximum reaction temperature of ~1400°C. Whilst nickel melts at ~1450°C, aluminium melts at 600°C and spreads over the solid nickel powders. The nickel dissolves into the aluminium and exothermically reacts to form various Ni - Al intermetallic phases. If the composition is stoichiometric it continues

until Ni_3Al is formed (Wenning *et al.* 1994). Garkol' *et al.* (1994) and Vol'pe *et al.* (1995) have used high speed pyrometry to analyse the phase changes and combustion methods that occur in Ni – Al combustion synthesis. As in the solid – liquid reactions, it is the formation of a liquid phase that promotes the self-propagating reaction.

2.7 Combustion Wave Characteristics

The combustion wave seen in SHS reactions is the area of the compact that is undergoing the primary exothermic chemical reaction. It has a velocity and an exothermicity that is dependent on many of the compact parameters – porosity, homogeneity, powder morphology, etc. (Shteinberg and Knyazik 1992 and Bhattacharya 1992). Three important parameters can be associated with this wave; temperature (T), degree of chemical conversion (η) and the rate of heat evolution (ϕ) (Dunmead and Munir 1992*a*). These parameters are shown with reference to an ideal reaction wave in figure 2.3. The schematic depicts a wave travelling from right to left. The reaction reaches completion ($T = T_c$, $\eta = 1$, $\phi = 0$) in a narrow reaction zone, δW . The schematic shows pre heating of the compact in front of the wave, where the temperature increases from T_0 to T_p . T_p is the point that product formation commences ($\eta > 0$) but is not necessarily the ignition point, T_{ig} . In the case of the Ti + C reaction, the pre heating zone initiates some solid state TiC formation prior to the arrival of the combustion wave (Vrel *et al.* 1994).

A more realistic schematic is shown in figure 2.4. The effects of the reactions kinetics (diffusion rates, powder morphology considerations etc.) means that not all the reactants are converted in the reaction wave. There is a degree of conversion, and thus exothermicity, after the wave has passed. This effect is termed the 'afterburn'. The kinetic effects of the reaction also increase the width of the reaction wave (Dunmead and Munir 1992*b*).

The reaction wave is said to be under steady-state conditions when it travels through the compact at a constant rate. This has been seen to be in the order of 1 to 150 mm s⁻¹ (Moore and Feng 1995*a*). In samples that are ignited from the top, a horizontal combustion wave is seen to travel at a constant velocity down the compact.

A non steady-state combustion mode is defined as the non-uniform velocity of the combustion wave as it travels through time and / or space. There are generally three types of non steady-state combustion; oscillating, spinning and repeated combustion. In oscillating combustion the wave is seen to stop and start as it moves through the compact. The product is often layered, the layers sometimes having different chemical compositions. Spin combustion is generally a surface related phenomena where only the outside of the compact reacts. The combustion wave is seen to spiral down the outside of the compact, leaving the bulk of the sample untouched. Repeat combustion primarily occurs in solid – gas reactions such as Ti + N₂. Typically a fast initial wave is seen to travel down over the sample. This wave generally effects the surface of the

pellet only. Then a secondary wider wave, travelling at a slower rate appears as the bulk of the sample reacts. A schematic of these combustion wave types is shown in figure 2.5.

2.7.1 Maximum Reaction Temperature

The maximum reaction temperature of a SHS reaction (T_{ad} or T_c) is not set. Pre heating the sample increases the temperature (Moore and Feng 1995), whilst diluting the reactants – usually achieved by adding quantities of the reactions products – lowers the temperature (Singh 1996). This flexibility has uses in post reaction processing of the compact. Dynamic compaction can be employed to press the compact just after it has reacted. The soft or liquid products will then be densified. To aid the process, pre heating of the sample increases the maximum reaction temperature, enabling the products to be workable for a longer period of time. The addition of a diluent is a useful tool in tailoring the products of a reaction. Kim *et al.* (1995) found that the product chemical composition could be changed by the addition of an inert diluent. The cooling effect of a diluent has applications in the production of near net shape artefacts where the production of large amounts of a liquid phase would not be beneficial.

2.8 Process Parameters

In a compact of fixed composition, the combustion characteristics are dependant on the reactant powder size, reactant powder morphology and the

compact density. These parameters have been investigated with reference to their influence on SHS reactions ignited in the thermal explosion mode and in the self-propagating mode. As the only difference between the combustion modes is the compact temperature at the point of ignition, both are affected in the same way by variance in the compact parameters. A compact heated in the thermal explosion mode is essentially undergoing the same process as the heated area of a self-propagating compact.

2.8.1 Powder Diameter and Morphology

Work on the $\text{Ti} + \text{C} \Rightarrow \text{TiC}$ reaction by Halverson *et al.* (1993) found that the powder size of the titanium had no effect on the final product density, but changed the product morphology. Finer titanium powders yielded a finer TiC morphology in the product, and vice versa. Vol'pe and Evstigneev (1993) found that the combustion temperature and wave velocity were higher in compacts with smaller titanium powders in the Ti – Al – C system. Saidi *et al.* (1994) found that the ignition temperature of Ti + C compacts decreased with decreasing titanium powder diameter.

The work by Halverson *et al.* (1993) also looked at the effect of the carbon powder on the $\text{Ti} + \text{C} \Rightarrow \text{TiC}$ reaction. The carbon powder was seen to have a very strong influence on the TiC product morphology. High surface area carbon powders produce a finer microstructure and vice versa. Lee and Chung (1995) investigated the same reaction and observed similar results. The ignition

temperature of the compact was lowered when finer carbon powders were used.

2.8.2 Pellet Density

The work of Halverson *et al.* (1993) on the $\text{Ti} + \text{C} \Rightarrow \text{TiC}$ reaction showed that a higher green compact density produces a higher product density. This is achieved by high compaction pressures and a small non-metallic powder diameter. The metallic powder generally yields under pressure and does not inhibit compaction, the non-metallic powder is generally brittle and thus determines the limits of compaction.

A lower and higher compaction limit (density) of the compact exists (Saidi *et al.* 1994); the pellet did not combust outside of the limits. At low compaction pressures (<2MPa) there is not a significant intimacy between the reactant materials and thus the rate of reaction is diminished, below that required to be self sustaining. Above the limit (>10MPa), the thermal diffusion of the compact ahead of the combustion front is so great as to slow the heating of the compact; thus sterilising solid TiC forms around the titanium powders. Under very high green densities, Halverson *et al.* (1993) found that the combustion kinetics were reduced and there was incomplete product formation. The limits are dependent on powder size, heating rate and compact dimensions (Deevi 1991). A maximum reaction wave velocity is found within the limits, attributed to the best case of thermal conductivity and thermal losses (Deevi 1991). The stoichiometry of the TiC product is dependant on the starting composition

(Choi and Rhee 1994 and Capaldi *et al.* 1997). In the region $\text{TiC}_{0.55} - \text{TiC}_{0.95}$ the product stoichiometry is the same as the starting stoichiometry.

In the thermal explosion mode the ignition temperature decreases and the combustion temperature increases with decreasing titanium powder diameter (Yi and Moore 1989a). This is attributed to the increased intimacy between the reactant powders, generating a higher rate of exothermic release (Capaldi *et al.* 1997). Increasing the heating rate of the compact also promoted ignition in compacts that did not ignite at lower heating rates. This is attributed to the effect of reduced heat conduction away from the compact. Yi and Moore (1989b) found that the ignition temperature decreased linearly with an increase in the heating rate.

With respect to the $\text{Ti} + \text{C}$ reaction, at low heating rates the exothermic energy has time to dissipate and thus only a solid state reaction occurs between the titanium and the carbon. A high heating rate is required ($\sim 350^\circ\text{C} / \text{min}$) to keep the period of solid state formation to a minimum before the titanium melts. If too much solid TiC forms around the titanium particles they become inert and thus the thermal explosion reaction cannot occur (Capaldi *et al.* 1997). This effect has also been seen in self-propagating reactions.

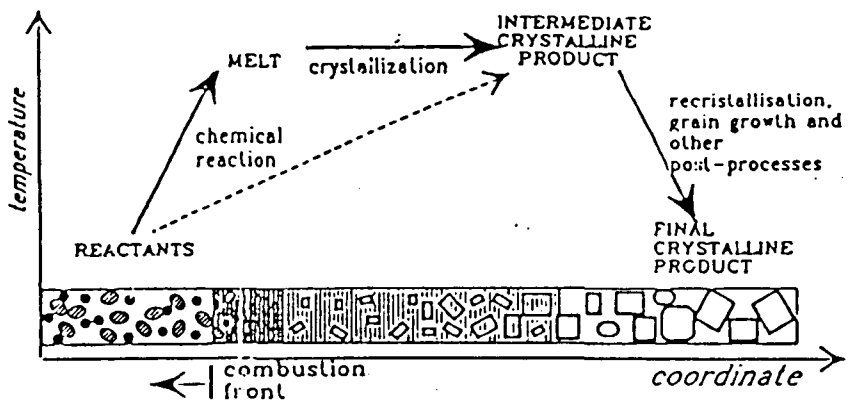


Figure 2.1 The Principle Concept of Structural Macrokinetics. Merzhanov and Rogachev (1992).

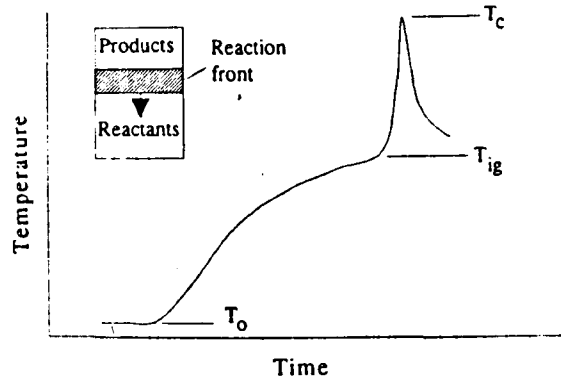


Figure 2.2 Schematic Representation of The Temperature-Time Curve During an SHS Reaction. T_0 = Initial Temperature, T_{ig} = Ignition Temperature, T_c = Maximum Reaction Temperature. Saidi (1995).

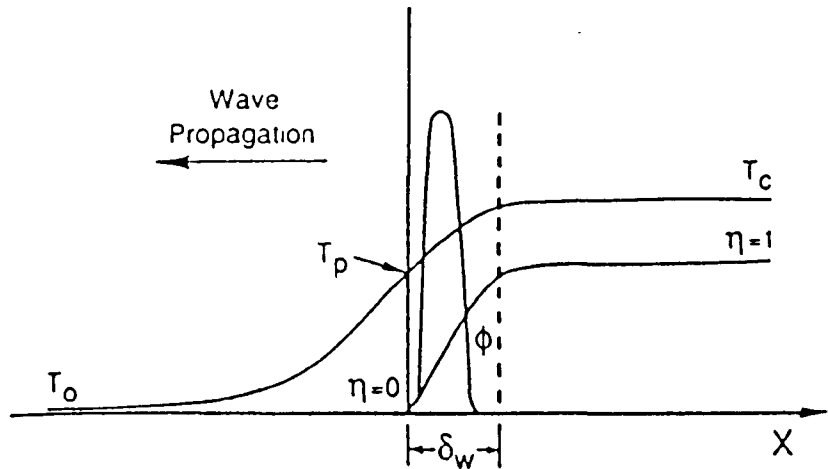


Figure 2.3 Schematic Representation of the Temperature (T), Degree of Conversion (η) and the Rate of Heat Generation (ϕ), in the Combustion Wave. T_0 = Initial Temperature, T_p = Ignition Temperature, T_c = Maximum Reaction Temperature, δ_w = Reaction Wave Width. Moore and Feng (1995b).

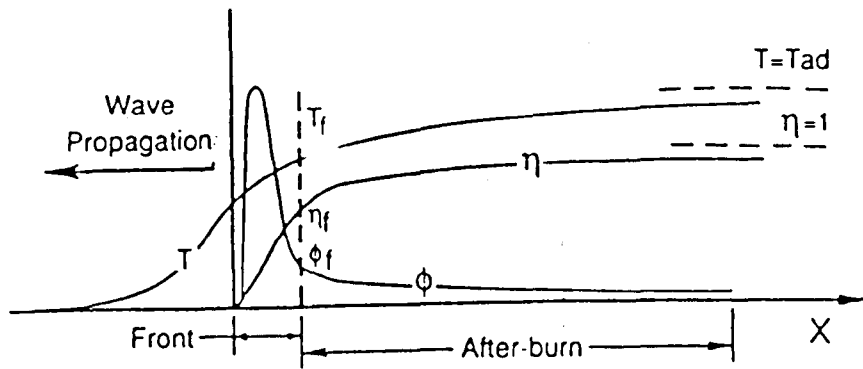


Figure 2.4 Schematic Representation of the Temperature (T), Degree of Conversion (η) and the Rate of Heat Generation (ϕ), in the Combustion Wave with Afterburn. Subscript f denotes the end of the reaction front. Subrahmanyam and Vijaykumar (1992).

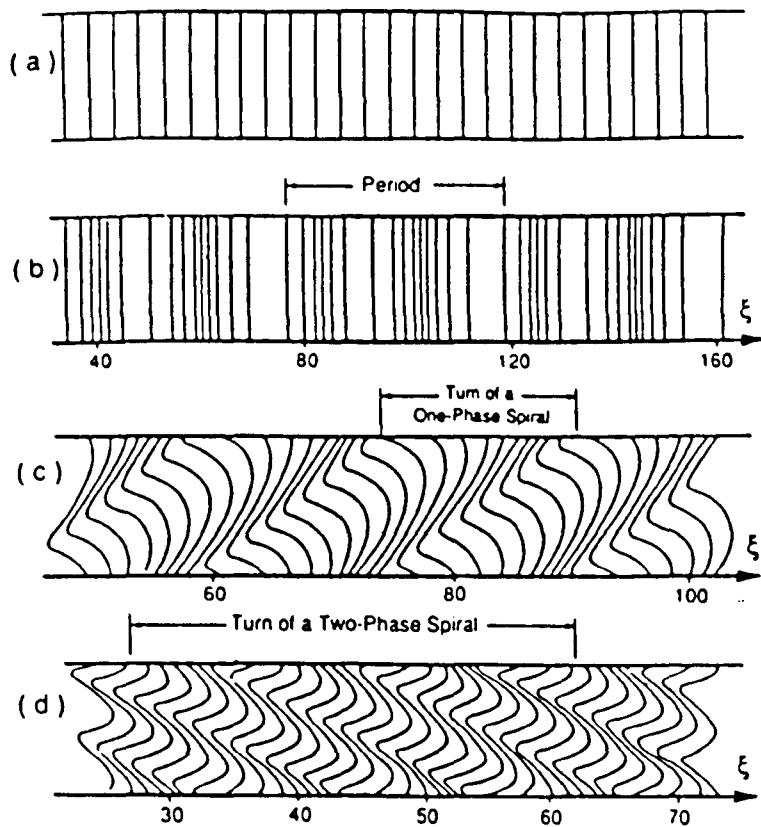


Figure 2.5 Schematic Representation of Combustion Modes: (a) Stable; (b) Pulsating; (c) Spin Combustion with One Reaction Centre; (d) Spin Combustion with Two Reaction Centres. Moore and Feng (1995b).

Chapter 3

Literature Survey – Detailed Literature

3.1 *Titanium Oxides and Alloys*

3.1.1 Titanium and Titanium Oxides

In bulk, titanium is a relatively light weight metal that provides excellent corrosion resistance, a high strength-to-weight ratio and good high-temperature properties. With a density of 4.505 Mg m^{-3} and strengths up to 1380 MPa, the material has excellent mechanical properties. An adherent, protective, TiO_2 film provides resistance to corrosion and contamination below $\sim 535^\circ\text{C}$. Above this, the protective nature of the oxide film decreases, and small atoms, such as carbon, nitrogen and hydrogen embrittle the titanium.

Titanium is allotropic, having a HCP (α) crystal structure at low temperature and a BCC (β) crystal structure above the transformation temperature of 882°C . Alloying elements provide solid solution strengthening and alter the allotropic transformation temperature (Askland 1992).

Elements such as aluminium, oxygen, carbon and nitrogen are classed as '*alpha stabilising*' elements. These elements increase the transformation temperature at which α transforms to β . For example, 15 at% oxygen dissolved in titanium raises the transformation temperature to $\sim 1750^\circ\text{C}$.

The opposite effect is seen with elements such as iron, manganese and chromium. The addition of these elements produce a eutectoid reaction, reducing the transformation temperature so that a mixed $\alpha+\beta$ titanium can be formed at room temperature. The physical properties of titanium metal area detailed in table 3.1

Table 3.1 The Physical Properties of Titanium Metal at 20°C	
<u>Property</u>	<u>Value</u>
Atomic Number	22
Crystal Structure	HCP
Lattice Parameter / nm	a = 0.29503 c = 0.46831
Atomic Mass / g mol ⁻¹	47.9
Atomic Radius / nm	0.1475
Valence	+4
Density / g cm ⁻³	4.507
Melting Temperature / °C	1668
Boiling Temperature / °C	3290

Titanium can dissolve oxygen interstitially, up to a composition of TiO_{0.42}, retaining its HCP structure, but showing an increase in the crystal lattice parameters. Increasing the oxygen content above TiO_{0.42} forms titanium oxides of increasing oxygen content. Figure 3.1 is the titanium – oxygen phase diagram.

Alpha titanium monoxide, α -TiO, has a NaCl (rock salt) crystal structure and can exist with both titanium and oxygen vacancies. Stoichiometric TiO has ~15% of the titanium and oxygen sites vacant. Titanium sesquioxide, Ti₂O₃, has a corundum (Al₂O₃) structure, whilst titanium pentoxide, Ti₃O₅, has a

monoclinic structure at low temperatures and a pseudobrookite structure above 177°C. Glassman and Papas (1994) have calculated the decomposition temperature of Ti_3O_5 to be 4000K at atmospheric pressure.

The most common titanium oxide is TiO_2 . TiO_2 can have three different crystal structures, anatase, rutile and brookite. Rutile is the most thermodynamically stable and therefore most common of the structures. Rutile has a tetragonal crystal structure. Table 3.2 details some physical properties of the titanium oxides. Fischer (1997) has detailed the thermodynamics of the Ti – O system, whilst detailed investigations into the atomic structure of the oxides have been presented by Leung *et al.* (1996) and Sousa and Illas (1994).

Property	TiO	Ti ₂ O ₃	Ti ₃ O ₅	TiO ₂
Colour	Golden-Yellow	Violet	Blue-Black	Grey-White
Density / g cm ⁻³	4.89	4.49	4.21	4.25
Melting Temperature / °C	1737	2127	1780	1860

3.1.2 Titanium and Iron Alloys

Titanium and iron form a variety of phases when alloyed together. Figure 3.2 is a detailed phase diagram of the alloy (Okamoto 1996). The two intermetallic phases that form are FeTi and Fe₂Ti. The FeTi and Fe₂Ti reactions are weakly exothermic, $\Delta H_{FeTi} = -30.6 \text{ kJ mol}^{-1}$ and $\Delta H_{Fe_2Ti} = -26.8 \text{ kJ mol}^{-1}$. Pribytkov *et al.* (1983) found that a self-propagating reaction would occur between iron and

titanium if the adiabatic reaction temperature was above the alloys eutectic melting temperature of $\sim 1080^{\circ}\text{C}$. If FeTi was being formed it was calculated that the reactants had to be preheated to 700°C to initiate the reaction. In the case of Fe₂Ti formation, the preheat temperature had to be 800°C . Kivalo *et al.* (1988) sintered finely divided iron and titanium powders and found that the interface between iron and titanium powders consisted of FeTi and Fe₂Ti with the profile being Fe > Fe₂Ti > FeTi > Ti. It was found that during sintering at 1100°C the 70at% Ti / 30at% Fe eutectic liquid phase forms. Upon contact with the iron particles the eutectic liquid solidifies as the solid FeTi and Fe₂Ti phases form. Around the titanium particles, the eutectic alloy remains liquid with the eutectic composition. The heat capacities of these phases have been calculated by Wang *et al.* (1993), whilst the effect of titanium on the lattice parameters of iron has been studied by Rickerby (1982).

3.2 Iron and Iron Oxides

By virtue of their wide range of mechanical, physical and chemical properties, iron based alloys are among the most useful of metals. Iron can either have a BCC or FCC crystal structure. Between 912°C and 1394°C iron has a FCC structure and is termed *austenite*. Below 912°C is the *ferrite* phase and above 1394°C is the *delta* phase. Under atmospheric conditions iron will easily oxidise. The oxide layer is multiphase, with FeO adjacent to the metal, followed by Fe₃O₄, followed by Fe₂O₃ on the outside. The oxide layer is not passive, as in TiO₂, and thus does not inhibit further oxidation when formed.

Table 3.3 details some of the physical properties of metallic iron. Figure 3.3 is the Fe – O phase diagram.

Property	Value
Atomic Number	26
Crystal Structure	BCC
Lattice Parameter / nm	a = 0.2866 c = 0.46831
Atomic Mass / g mol ⁻¹	55.85
Atomic Radius / nm	0.1241
Valence	+2
Density / g cm ⁻³	7.87
Melting Temperature / °C	1538
Boiling Temperature / °C	2860

Iron (II) oxide, FeO, is black in colour. It has a NaCl crystal structure and is unstable, decomposing to Fe and Fe₃O₄ below 575°C. Glassman and Papas (1994) have reported that FeO decomposes above 3400K. Iron (III) oxide, Fe₂O₃, is red – orange in colour. It exists in two different crystal structures, named *hematite* and *maghemite*. Hematite has a corundum structure whilst maghemite is a spinel. Iron (II, III) oxide, Fe₃O₄, is a mixture of Fe (II) and (III) oxides. It is black in colour and occurs naturally in the mineral ‘Lodestone’. Table 3.4 details some physical properties of iron oxides. Figure 3.3 is the Fe - O phase diagram.

Property	FeO	Fe ₂ O ₃	Fe ₃ O ₄
Colour	Black	Red - Orange	Blue-Black
Density / g cm ⁻³	5.98	5.25	5.24
Melting Temperature / °C	1378	1597	1594

3.3 Reactions Between Bulk Titanium and Air

3.3.1 Isothermal Oxidation

It has been known for some time that the oxidation of titanium can be described with reference to the Wagner model (Kubaschewski and Hopkins 1953 and Kofstad 1966). The model assumes that in titanium oxidation, oxygen diffuses inward through the oxide coating, to be consumed by the growth of the oxide and the dissolution of the oxygen into the metal. This process is shown schematically in figure 3.4. It is composed of two individual oxygen concentration profiles, one corresponding to the oxide TiO_2 and the other relating to the substrate which is a solid solution of oxygen in titanium. The diffusion of oxygen through the oxide layer is the rate controlling factor in this case. Kofstad (1966), in his review book, states that the oxidation of titanium in the 600-900°C range was seen to be parabolic, changing to linear above this temperature. However, he stated that the reason for the change was not clear.

Dechamps *et al.* (1976) investigated the oxidation of titanium in air within the temperature range of 700-875°C. They found that the oxidation kinetics change as the oxide layer grows, initially starting with a parabolic kinetic and moving into a linear one when the film thickness reached around 10 μm -20 μm over the testing temperature range. The change in reaction kinetics was attributed to the break down of the oxide layer due to the build up of internal compressive stresses within it, as it reached these thickness'. Titanium / TiO_2 has a Pilling-

Bedworth ratio of 1.5 – 1.75 (Askeland 1992 and Dechamps *et al.* 1976). Below the 10-20 μ m threshold the oxide was seen to be very adherent and of grey colour. The grey oxide was seen to be non-stoichiometric rutile, TiO₂.

Cismaru and Momirlan (1977) worked on the oxidation of titanium discs in air within the range 300°C - 1250°C. The films formed were analysed by XRD. No measurable oxidation was seen in the sample held at 300°C for 17 hours, or the sample held in the 300-500°C temperature range for 17 hours. However, in the sample held at 550°C for 12 hours non-stoichiometric TiO₂ was detected along with the titanium. In the sample held at 700°C for 4 hours stoichiometric TiO₂ was the only phase detected. Whilst the work is by no means detailed it is possible to infer that only a thin oxide layer was formed in the 550°C sample, as titanium was still detected in the XRD analysis. No titanium was detected in the 700°C sample, suggesting that the oxide layer was thicker. Additionally the stoichiometry of the TiO₂ (rutile) was seen to change from a non stoichiometric TiO₂ at 550°C to a near stoichiometric TiO₂ at 700°C, suggesting a fuller transformation at the higher temperature.

Maksimovich *et al.* (1986) investigated the mechanism of titanium oxidation at 600, 850 and 1000°C. The experiments consisted of heating commercially pure titanium specimen, of unspecified dimensions, in air. The heating and cooling of the sample occurred at 0.25°C / second. The specimens were held for 1-10 hours at the testing temperature. This research was specifically investigating the mechanism of oxidation, in particular, cation and anion movement.

There were two areas that they investigated, namely the formation of the oxide scale and the formation of the gas (oxygen) impregnated layer in the titanium metal. By measuring the thickness of the scale and its relative position to the initial surface of titanium it was seen that the oxide scale grows outward from the surface of the metal. The analysis of the hardness of the matrix behind the oxide layer was employed to determine the extent of penetration of oxygen into it. This is possible as oxygen in solution in titanium greatly increases its hardness. A hardness of 0.5GPa above that of the base titanium hardness was used as a minimum value to infer the presence of oxygen in the matrix (Maksimovich *et al.* 1986).

A sample held for 1hr at 850°C showed impregnation of oxygen into the matrix to a depth of ~100µm and the formation of a 10µm thick dense oxide scale occurring above the surface of the titanium. The scale formation above the initial surface of the titanium is cited as evidence for titanium cation diffusion through the oxide layer as the oxide formation mechanism. Oxygen that diffuses through the oxide layer to the metal is held in solid solution in the metal at these low concentration levels. Whilst titanium cation movement may have a role to play in titanium oxidation, the literature suggests that the primary oxidation method is one oxygen diffusion into the titanium metal through the oxide shell.

Samples held for up to 3 hours showed an increase in oxide thickness to 25µm and an increased oxidation rate, but no increase in the thickness of the oxygen

impregnated layer. The oxide was seen to grow primarily into the metal, rather than away from it as in the previous sample. The oxide was also seen to contain cracks perpendicular to the surface of the titanium. The cracking of the oxide was attributed to be the cause for the increase in oxidation rate, by allowing oxygen to easily reach the metal-oxide interface without having to initially diffuse through the oxide layer. The oxide formed is thus determined by the oxygen diffusion rate through the oxide layer. The cracked porous structure also inhibits titanium cation diffusion to the oxide-gas interface, thus reducing outward development of the oxide.

Similar additional experiments confirmed that the physical structure of the oxide determines the mechanism of titanium oxidation. In summary, the literature suggests that when the scale is porous, oxide diffusion through the scale to the metal-oxide interface dominates, and when the scale is dense and coherent, titanium cation diffusion to the oxide-gas interface is the controlling factor.

The detailed investigation of Unman *et al.* (1986) into the oxidation kinetics of titanium in air between 593°C and 760°C confirms and expands on the previously reviewed research. Thermogravimetric, microhardness and metallographic data were employed to elucidate the oxidation process. Thermogravimetric data confirms that in the range from 593°C to 704°C the oxidation of titanium is essentially parabolic for at least 100 hours. At 732°C and 760°C the parabolic kinetics are only observed for 30 hours and 10 hours

respectively. The kinetics then move into linear kinetics. Data also reveals a slight transition occurring in the weight gain of the sample after a certain time, in one instance after 6.25 hours at 649°C. The weight gain per unit was seen to increase after the time threshold. The time threshold is seen to decrease with increasing temperature. A simultaneous heating and XRD analysis investigation of the sample revealed that the increase in oxygen absorption (as measured by an increase in sample weight) coincides with an increase in the oxygen solubility at the metal – oxygen interface. No reason for the increase in the oxygen solubility was given. Additional XRD data revealed all of the oxide formed to be TiO₂, rutile.

Microhardness data, showing good correlation to the thermogravimetric and metallographic data, revealed that there was no porosity in the oxide layers formed in the samples investigated. Approximate values for the ratio of oxygen diffused into the matrix to the total oxygen pick up is given as 0.31 ± 0.05 . This figure is consistent with data produced by other authors that were reviewed in the paper.

An interesting phenomenon revealed in the metallographic samples was the presence of a visible boundary that occurs within the titanium matrix. The boundary is highlighted when the sample is etched and corresponds to a composition of $5.0 \pm 0.5\text{at}\% \text{ O}$ in solid solution in the titanium (Unman *et al.* 1986). It appears that at this composition the titanium – oxygen solid solution preferentially etches to reveal a boundary. The boundary is seen to have a

definite correlation to time and exposure temperature. The distance of the boundary from the oxide – metal interface is seen to increase with both parameters.

Customarily, it is assumed that the saturation limit of 34at% oxygen in alpha titanium is reached immediately at the metal – oxide interface. This was seen not to be true, the maximum solubility only being achieved in the sample held at 760°C for 100 hours. Due to the time and temperature dependant nature of this oxygen concentration the lower temperature samples had lower oxygen concentrations. For samples oxidised between 593°C and 677°C the oxygen concentration at the metal – oxide interface was calculated to be ~20 at%. Additional data reviewed in the paper agree with these findings.

The work was completed with the finding that the diffusion coefficient for oxygen through TiO₂ is about 50 times greater than for its diffusion through the titanium matrix.

3.3.2 Anisothermal Oxidation

The previous literature deals with oxidation of titanium when the surrounding temperature has been constant. Anisothermal oxidation is a more complex process, as the temperature, and thus the rate law, is constantly changing. To aid the understanding of anisothermal oxidation, researchers have attempted to mathematically model the process. This has occurred alongside the advent of computers, which significantly simplified the process.

Initially Wolf and Grochowski (1975) presented a model for anisothermal oxidation which assumed that the system had an oxidation rate that was parabolic under isothermal conditions and that the temperature of the system increased linearly with time. The model is based on differentiating the isothermal parabolic oxidation rate law with temperature to give the weight gain according to the temperature and time. The isothermal parabolic rate law is described as:

$$W^2 = K_p t \quad (3.1)$$

where W is the specific weight change, t the time over which oxidation has taken place and K_p a rate constant, taken to have the form of:

$$K_p = A \exp(-Q / RT) \quad (3.2)$$

where A is the pre-exponential factor, Q the activation energy, R the gas constant and T the absolute temperature. The temperature was assumed to increase linearly with time, which was described as:

$$T = T_i + r t \quad (3.3)$$

where T_i is the temperature at $t = 0$, and r ($K s^{-1}$) is the fixed rate at which T changes with time. The heating rate is linear. The final solution to the

integration being:

$$W_m^2 = -\frac{AQ}{rR} \int_{Z_i}^{Z_m} e^{-Z} (Z^{-2} + Z^{-1} - Z_i^{-1}) dZ \quad (3.4)$$

where

$$Z_i = Q / RT_i \text{ and } Z_m = Q / RT_m \quad (3.5)$$

Subscript i and m relate to the initial and final conditions of that term. Markworth (1977) criticised the mathematical process, changing the method of integration and stating that the initial equation should be the mass gain rate differential equation:

$$dW/dt = K_p / 2W \quad (3.6)$$

as K_p is itself time dependant. Markworth's (1977) final equation, the mass gain due to anisothermal oxidation, is:

$$W_m^2 = AQ / rR [(Z_m^{-1} \cdot e^{-Z_m}) - (Z_i^{-1} \cdot e^{-Z_i}) + E_1(Z_m)] \quad (3.7)$$

Where the E_1 function can be expressed in terms of certain polynomial and rational expansions of polynomials.

It was found that the *Markworth* model was very mathematically complex when the heating rate was non linear. Both the *Markworth* and *W-G* (Wolf-

Grochowski) models are based on linear heating rates. With this in mind Liu and Gao (1998a) developed the model to make non linear heating easier to incorporate. They expressed the continuously varying temperature of anisothermal oxidation as many small isothermal holding steps. The sum of the holding steps leads to the total mass gain over the time period. This can be mathematically modelled as:

$$\Delta W_i^2 = \Delta W_{i-1}^2 + K_p^i \cdot \delta t_i \quad (3.8)$$

where:

$$\delta t_i = \delta T / \alpha(T_i) \quad (3.9)$$

and

$$K_p^i = A \cdot \exp(-Q / RT_i) \quad (3.10)$$

where α is the heating or cooling rate, T is the temperature, i is the time step number, = 1, 2, 3,n, δt is the differential time step, δT is the differential temperature step and $\Delta W_0 = 0$.

By re-writing the model with a linear heating rate it was seen to be consistent with the *Markworth* model, thus the *Markworth* model is a special expression of *L-G* (Liu and Gao) model with a linear heating rate. Predicted mass gain

curves for the *Markworth* and *L-G* models with linear heating rates gave the same results, whilst the *W-G* model gave much higher predictions.

The *L-G* model gave very accurate predictions when tested against the authors own anisothermal oxidation experimental work on stainless steel, and against work previously done by other authors on mild steel and Fe-Cr-Al alloys. In all cases the model closely matched the experimental data.

The work of Wolf *et al.* (1976) specifically investigated the anisothermal oxidation of titanium. Experiments consisted of heating 99.8% pure titanium strips, 0.01-0.158cm thick by 5cm by 1cm, in a sealed reaction chamber containing oxygen gas at 200 torr. The volumetric, gravimetric and temperature data from the equipment enabled the analysis of the titanium oxidation reaction rate. Heating cycles of the chamber specifically investigated linear and non linear heating rates.

By analysing a number of different conditions it was found that the anisothermal oxidation of titanium is accurately described by parabolic reaction kinetics at low heating rates of $\sim 0.5^{\circ}\text{C} / \text{sec}$ and by sequential asymptotic – parabolic kinetics at intermediate heating rates $\sim 10^{\circ}\text{C} / \text{sec}$. The asymptotic kinetics describe the initial oxidation of titanium, which was seen to proceed at a faster rate than that described by the parabolic kinetics. The reaction rate is seen to reach its asymptote and then proceed with parabolic kinetics after a short while.

The asymptotic and parabolic kinetics therefore apply sequentially to the system. The parabolic rate law was found to be:

$$K_p = 1.94 \times 10^7 \exp(-54300 / RT) \quad (3.11)$$

where K_p is in $\text{mg}^2 / \text{cm}^4 \text{ s}^{-1}$. The asymptotic rate law is described in terms of oxygen fixation, as detailed in Evans (1960):

$$N = N_0 + K_a (1 - \exp[-ct]) \quad (12)$$

where N is the number of pores in the oxygen scale, N_0 the initial number of pores in the oxide scale, $c = 0.03\text{s}^{-1}$ and t is the time. K_a is the asymptotic rate constant which can be expressed as:

$$K_a = 2.82 \times 10^{-2} \exp(-17100 / RT) \quad (3.13)$$

where K_a is expressed in terms of moles O_2 / cm^2 .

Faster heating rates, in the case of the experiments conducted, $\sim 22^\circ\text{C} / \text{sec}$, could not be described by asymptotic or parabolic reaction rates. Under rapid heating conditions the titanium was seen to have an increased reactivity which occurred at lower temperatures than in the slower heating experiments. It was postulated that this increased reactivity was due to an increase in the effective reactive surface area. Stresses, imposed upon the titanium during the rapid

heating, were thought to cause the increase in specimen surface area; however oxygen solubility in the metal, oxide grain boundary oxidation, differential thermal expansion (metal / oxide) and thermal gradients were all noted as other possible causes.

The increased reactivity of the rapidly heated samples was seen to lead to sample ignition. This was thought to be due to the liberation of the exothermic oxidation energy at the sample surface, leading to the 'thermal runaway' of the sample. Calculations, based on one set of experiments, concluded that ignition would occur if the heat input was greater or equal to $\sim 4.2 \text{ J / cm}^3 \text{ s}^{-1}$. However, with this rate of heat input it was calculated that the temperature rise over the whole sample would only be $2^\circ\text{C} \setminus \text{second}$. It was therefore assumed that localised, rather than general, heating of the sample substrate lead to ignition.

3.3.3 Burning

Until recently there had been little detailed research into the burning of metals due to the complex reactions involved and the physical difficulties in investigating them. However, there is sufficient research to draw some broad conclusions.

A thorough work by Sirca *et al.* (1991), using a real time gravimetric technique, investigated the burning of $3.2\text{mm}\varnothing$ titanium rod in oxygen. The rod was held by a load beam, in the vertical orientation, in a sealed reaction chamber and ignited at the bottom surface by a magnesium promoter. The

burning of the rod and the formation of droplets was recorded by high speed video camera. The mass gain due to oxidation and mass loss due to droplet formation was measured by the load beam and recorded by a data logger.

Burning of metals can be classified via the *Glassman* criterion, which states that if the boiling points of the metals oxides are below the boiling point of the metal, combustion proceeds in the liquid phase. If the reverse is true then combustion proceeds in the vapour phase. Given the quoted data for the boiling point of titanium as 3550 K and the boiling points of TiO, TiO₂ and Ti₂O₃ as 3270 K, 3000 K and 3300 K respectively, it was expected and experimentally verified that titanium should burn in the liquid state (Glassman and Papas 1994).

The incorporation of oxygen into the metal as oxide during burning signifies burning of the metal in the liquid state. This can be measured as a sample weight gain during burning. It was additionally seen that incorporation of oxygen into the material was the rate limiting step in the reaction. An increase in oxygen pressure increased the burning rate, but not the amount of oxygen in the product, which stayed constant at ~10wt%. This figure is seen to agree with a quoted first-order heat-balance equation that indicated that 10wt% oxygen in a sphere of titanium will support sustained combustion.

Recent investigations by Abbud-Madrid *et al.* (1996) into the ignition and combustion of bulk titanium samples agree and expand on the findings of Sirca

et al. Cylindrical titanium specimens, 4mm \varnothing by 4mm long, were placed in a sealed reaction chamber, filled with oxygen at atmospheric pressure. The samples were heated to ignition by a 1000 W xenon lamp. Burning of the sample was recorded by video, thermocouple, imaging spectrograph and a diode array detector.

During the heating cycle an intermediate plateau is seen in the time-temperature plot at the α - β titanium transition temperature, due to heat energy supplied to the sample being used to change the crystal structure of the metal and not heat the sample. Above this transition temperature the gradient of the graph is seen to increase. This is attributed to the change from a parabolic oxidation rate to a linear one. A critical temperature (T_{crit}) is defined as the point at which the heat generated by the exothermic surface oxidation of the titanium equals the heat losses from the sample. Typically T_{crit} was around 1700K. If the sample temperature passes T_{crit} , ignition will eventually occur, even if the heat source is removed.

Ignition, defined as a runaway increase in temperature of the sample, is seen to occur when the sample is a few degrees below the melting point of titanium (1933K). This finding agrees with the conclusion of Sirca *et al.* (1991), that titanium burns in the liquid phase. Ignition of the sample was observed to coincide with the appearance of a luminous combustion reaction front. Combustion temperatures were recorded to be over the 3000K limit of the thermocouples used in the experiments. The combustion wave was seen to

travel at an average speed of 16.2mm s^{-1} . Several studies have shown that diffusion and convection of oxygen to the sample surface was the rate controlling step in burning (Sirca *et al.* 1991).

Linking in to the above findings, a mathematical description of the ignition of titanium plate in an air flow by laser beam has been developed by Poyurovskaya and Ryabcwuk (1989). The work highlighted a few interesting points.

The heat source for the ignition of the plate was assumed to be the exothermic oxidation reaction of titanium. The oxidation reaction was initiated by the laser, but was sustained by the exothermic oxidation reaction. A calculated minimum energy intensity of 130000 W cm^{-2} was required to ignite the plate. It was seen that the reaction was only self sustaining if the oxidation reaction kept the titanium surface molten. They calculated the radiative and convective heat loss from the surface of the titanium to be $\sim 200\text{ W cm}^{-2}$. This was calculated to be significantly less than the rate of heat conduction through the metal.

It was seen that the melting of TiO_2 (2185K) hinders the evaporation of titanium by forming a liquid film on the surface of the molten titanium. If the temperature increases to above the decomposition temperature of TiO_2 (3200K), no burning can take place, as TiO_2 becomes thermodynamically unstable. At this temperature titanium is still liquid, but cannot oxidise.

An interesting paper by Gunaji and Sinclair (1995) found that the burning characteristics of titanium rod, ignited in a similar way to those in the work of Sirca *et al.*, changed with oxygen pressure. At low pressures (13.8kPa) titanium burned violently, sparking considerably. Increasing the pressure changed the burning mode to quiescent. This observation could indicate that the burning of titanium at low pressures is in the vapour stage, as classified by the *Glassman* criterion and investigated in the burning of aluminium Sirca *et al.* (1991) and magnesium Abbud-Madrid *et al.* (1996).

Additionally, Gunaji and Sinclair (1995) found that alloyed titanium requires a greater threshold oxygen pressure to burn than that of pure titanium.

3.4 Reactions Between Powdered Titanium and Air

Tavgen *et al.* (1992) investigated by differential thermal analyser (DTA), the behaviour of <40 μ m titanium powder, heated at 5°C / min, under atmospheric conditions. From 280°C to 495°C the specimen increases in weight as oxygen combines with the titanium. The rate of specimen weight gain was recorded to increase linearly with the temperature. Upon reaching ~ 495°C rapid oxidation was seen to occur, indicated by a significant exothermic effect on the Differential Scanning Calorimetry (DSC) graphs and an increase in the actual sample temperature. This effect subsided in the 620-680°C region but was seen to reappear afterwards, up to a maximum testing temperature of 960°C. The

rate of oxidation was seen to increase with temperature. The subsidence in the exothermic effect between 620-680°C was attributed to the build up of oxide scale on the powder surface, limiting oxygen diffusion to the titanium. The subsequent increase in oxidation after the lull is attributed to the break up and cracking of the thickening oxide shell, leading to direct metal – air contact and therefore to the observed increase in oxidation rate.

The observed effects of oxide scale thickening on the reaction rate agrees with the theories and experimental results reviewed in the texts of Kubaschewski and Hopkins (1953) and Kofstad (1966) and seen in the papers of Dechamps *et al.* (1976), Maksimovich *et al.* (1986) and Unman *et al.* (1986).

Tavgen *et al.* (1992) also held powdered samples at isothermal temperatures from 300-800°C for a time of 1 hour. X-ray phase analysis reveals that TiO₂ was the only detectable oxide and it was only found in samples held at 600°C or greater. The amount of TiO₂ detectable was seen to increase with the holding temperature.

Rode and Hlavcek (1994) worked on the reactivity of titanium powder in oxygen and their work is in agreement with Tavgen *et al.* (1992). They conducted a wide ranging simultaneous thermogravimetric / differential thermal analyser (TGA/DTA) investigation into the oxidation of three different types of titanium powder; 40µm-130µm, 30µm-150µm and 16µm-41µm. Experiments were conducted in pure oxygen at atmospheric pressures. Oxidation was seen to start from 455°C, with ignition of the sample, defined as

a runaway temperature increase resulting in melting of the sample, occurring in the $500^{\circ}\text{C} \pm 10^{\circ}\text{C}$ region for all powder sizes.

No direct relationship between powder size and the oxidation start temperature was found; this was attributed to the fact that the onset of oxidation is not just controlled by powder size, but by prior oxygen content in the powder, powder morphology, chemical composition and the powder's previous thermal history. Other results show that an increase in the sample size decreased the ignition temperature, due to the reduced relative heat loss effect of the sample, figure 3.5, and that increasing the heating rate decreased the ignition temperature, as shown in figure 3.6.

An interesting feature of the low heating rate (5 or $10^{\circ}\text{C} / \text{min}$) experiments were the presence of flat spots in the DTA graphs that occurred just after exothermic oxidation started. Subsequent analysis by SEM revealed that this effect was due to the build up of a passive oxide layer, that inhibits direct metal / oxygen contact. Continuing to heat the sample led to cracking and spalling of the oxide layer. This promoted to the reappearance of the exotherm which lead to complete ignition. This ties in with the findings of various other authors reviewed in this text.

Additionally, pre-oxidised powders were compared with as-received powders. The pre-oxidised powders have limited low temperature oxidation, but spontaneously ignite at around 600°C , figure 3.7. This is contrasted with the

gradual oxidation and ignition of the as-received powders. The behaviour of the pre-oxidised powders is attributed to the presence of the pacifying oxide layer already on the powders. This subsequently breaks down at the higher temperatures, allowing direct metal-gas oxidation that spontaneously ignites the powder.

Merzhanov *et al.* (1995) in their paper using time resolved x-ray diffraction (TRXRD) found that ignition of a bulk sample of powdered titanium heated in air occurred at around 500-540°C. The process of reaction was the formation of TiO₂ and a solid solution of oxygen in α -titanium. Interestingly it was noted that if the reaction front temperature exceeded the α - β titanium transition temperature (1155 K) then titanium reacted with nitrogen as well as oxygen in the air, the final oxide product being a TiO₂-xN_y modified rutile. The TiO₂ oxide product found here agrees with the work of the previously mentioned authors.

Bakhman *et al.* (1998) in their paper on the critical conditions for ignition of pressed titanium powder compacts found that there is an upper and lower limit of pellet density in which a powder pellet would burn at a certain oxygen concentration. Compressed rectangular samples were held in a flowing argon / O₂ atmosphere. They were ignited via a Nichrome wire placed close to the top surface of the sample (SHS mode). The oxygen concentration and sample densities were altered so that a comprehensive map of sample burning at different densities and oxygen concentrations could be obtained.

When the density was above the upper limit no steady combustion occurred. Two reasons were cited for this phenomenon. Firstly, it was attributed to the increased heat conduction away from the surface of the specimen. Quoted data shows that the heat conduction of a sample more than doubles as the density changes from 60% of theoretical to 80% of theoretical. The data is shown in table 3.5.

Table 3.5 Heat Conduction Through a Titanium Powder Compact with Respect to the Compact Density. Bakhman *et al.* (1994).

% of theoretical density	60	65	70	75	80
$\lambda / \text{Wm}^{-1}\text{k}^{-1}$	2.6	3.0	3.8	4.4	5.4
$\lambda / \lambda_{\text{density} = 100\%}$	0.16	0.19	0.24	0.28	0.34

Secondly, the thickness of the reacting surface layer was seen to reduced with increasing compact density. This also contributed to non-steady combustion, as there is less material combusting for a given compact size. If the pellet was under the lower limit for steady combustion the pellet melted and lost its shape as is burnt. The final product was then an oxide ‘puddle’.

The density range in between these two limits produces steady state burning of the pellet. This is characterised by the formation of a dense oxide film on the surface of the sample, with unburned titanium remaining within the bulk of the sample. The completeness of combustion was calculated by measuring and weighing the burnt sample. By assuming that the titanium oxidises only to TiO_2 , the increase in weight can be attributed to the absorption of oxygen. It is

then simple to calculate the amount of TiO₂ formed. They found that the completeness of combustion, expressed as a percentage, decreases with increasing density, as shown in figure 3.8. This was also found with titanium compacts were burnt in nitrogen, figure 3.9 (Dunmead *et al.* 1989).

Results show that at an oxygen concentration of 10%, no burning took place at any density. At 15% oxygen concentration, combustion just starts to occur in 25% dense samples. At 20% oxygen concentration, steady combustion is seen to occur in samples up to 50% dense. At 50% oxygen concentration, samples up to 60% dense burn steadily. Combustion with splashing and melting is seen in all samples up to 74% dense in 100% oxygen atmospheres. The complete results are shown in table 3.6. Figure 3.10 is a graphical representation of the results, comparing the density of the sample and the lowest oxygen concentration in which combustion of the sample is possible.

Table 3.6 Combustion Stability of Titanium Powder Compacts in Various Oxygen – Argon Atmospheres. Bakhman *et al.* (1994).

O_2/Ar ratio	Compact density in g cm ⁻³ and % of theoretical density								
	1.11, 24.6	1.34, 29.7	1.51, 33.4	1.56, 34.6	1.96, 43.5	2.22, 49.2	2.67, 59.2	2.69, 59.6	3.33, 73.8
10 / 90	-	-	-	-	-	-			
15 / 85	+ / -		-			-	-		-
20 / 80	+		+			+	-		
50 / 50	+	+	+		+	+	+	+	-
75 / 25	++	++	++	++			+	+	-
100 / 0	++		++			++	++		++

Key: No combustion (-), combustion with very low completeness (+ / -), stable combustion (+) and combustion with melting and splashing (++). In the combustion of Ti in 75% O₂ + 25% Ar, stable combustion (+) was also observed when the density = 2.37, 2.45, 2.56 and 2.63 g / cm³.

In agreement with Bakhman *et al.* (1998), Dunmead *et al.* (1989) and Filonenko and Barzykin (1996) both found that the density of a sample of powdered titanium affects the burning reaction. In their experiments of igniting, in the SHS mode, compacted cylindrical powdered titanium samples in a nitrogen atmosphere, it was seen that the critical nitrogen pressure for burning of the sample decreased with density, as shown in figure 3.8. Kudo and Odawara (1989) and Filonenko and Barzykin (1996) both found that the combustion velocity decreased with increasing compact density (figures 3.11 and 3.12). Additionally it was noted that burnt samples had a thin surface layer of TiN, with the internal titanium containing a quantity of nitrogen in solid solution. This finding is in agreement with Kume *et al.* (1992) who found that the compositional profile of combustion nitrified titanium was $\text{TiN} > \text{Ti}_2\text{N} > \alpha\text{-Ti} > \beta\text{-Ti}$.

Li and Ge (1996) investigated the combustion nitriding of compacted powdered silicon and reported similar phenomena to those mentioned by other authors. The adiabatic reaction temperature of the reaction $3\text{Si} + 4\text{N} \Rightarrow \text{Si}_3\text{N}_4$ is above the melting point of silicon. As the reaction occurred on the surface of the compact, silicon beneath the reaction layer melted. This nitrified and formed an impervious layer that stopped further rapid nitrogen penetration into the compact. The exothermic heat generated by the reaction was sufficient to melt the whole of the remaining unreacted internal silicon.

3.5 Reactions Between Titanium and Al_2O_3

Zhuravlev and Turchanin (1997) reviewed and investigated the interaction of pure titanium and titanium in solution with Al_2O_3 . It is known that up to 6 wt% Al_2O_3 can dissolve in α -titanium at 1200°C and that titanium can reduce Al_2O_3 above 700°C. However, results were only analysed after 60 hours of reaction. In the 750-1600°C range titanium interacts with Al_2O_3 , solid solutions of aluminium and oxygen in titanium are produced. Titanium in solution with other metals was seen to react with Al_2O_3 to form various titanium oxides at the interface. This is in agreement with Kritsalis *et al.* (1991) and Chidambaram *et al.* (1996) who both found that solute titanium in liquid copper reacts with solid Al_2O_3 to form solid TiO on the Al_2O_3 . This reduces the solid – liquid interfacial tension and subsequently increases the wettability.

3.6 Reactions Between Titanium and Fe_2O_3

An exhaustive and thorough examination of the available literature found no specific work published concerning the reactions between titanium and Fe_2O_3 . However, a paper by Bickley *et al.* (1991) investigated the reaction between TiO_2 and Fe_2O_3 at elevated temperatures. As all titanium has a nano film of TiO_2 on its surface, the reactions described in the paper could relate to those which occur in the initial stages of titanium - Fe_2O_3 reactions.

To investigate the reaction between Fe_2O_3 and TiO_2 Bickley *et al.* (1991) produced a reaction mixture of equimolar quantities of powdered Fe_2O_3 and

TiO₂. It was mixed, sealed in silica tubes and then heated in air for 24 hours. The mixture was then analysed by XRD to investigate the changes occurring in the chemical composition. The TiO₂ had an initial structure of 80% anatase + 20% rutile. It was seen in the sample held at 500°C that the anatase to rutile ratio had changed to 60% - 40%. This temperature is some 200°C below the temperature at which the transformation occurs in pure titanium dioxide. It was thought that the incorporation of iron (III) ions into the TiO₂ lattice facilitated the transition. Higher holding temperatures increased the degree of transformation from anatase to rutile. At 700 °C the ratio was 15% - 85% anatase to rutile; at 800°C no anatase was detected. At the testing temperatures of 800°C and 1000°C a third phase of pseudo-brookite (Fe₂TiO₅) was seen. At 800°C it is a minor phase, at 1000°C it is the major product phase, formed by the reaction of Fe₂O₃ with TiO₂.

Vacuum reduction of pure TiO₂, Fe₂O₃ and samples consisting of mixed equimolar quantities of Fe₂O₃ and TiO₂ revealed some interesting phenomena, as shown in figure 3.13. The reaction powders were held in a vacuum of 10⁻⁶ torr, and heated at 5 K min⁻¹ from 450°C to 1000°C. The partial pressure of O₂ in the chamber was recorded as a function of temperature. It was seen that TiO₂ did not significantly decompose over the experimental run, which was in agreement with other authors. The reduction of Fe₂O₃ followed three distinct stages of reduction, which correspond to the formation of Fe₃O₄ from Fe₂O₃ (680°C), then the formation of FeO from Fe₃O₄ (780°C), and finally the reduction of FeO to metallic iron (1030°C).

Interestingly, when the mixed equimolar powders were vacuum heated, significant differences were seen. The initial release of oxygen from the formation of Fe_3O_4 is virtually absent and the release due to the formation of FeO is reduced by roughly 50%. However a release of oxygen, approximately equal to that suppressed at the lower temperatures is seen to occur in the 860°C-920°C region. The reason for the change in decomposition profile is not fully understood. However, the change was hypothesised to have been due to the formation of a new phase. This new phase must have formed before the onset of the Fe_2O_3 to Fe_3O_4 transformation. Additional magnetic susceptibility studies found that the maximum solubility of iron (III) ions in rutile to be ~ 3 at%.

3.7 Summary

The literature seems to be conclusive in the analysis of isothermal oxidation kinetics. The kinetics are described as parabolic in the initial stages, changing to linear after an extended period of time or an increase in temperature. The changeover point is thought to be related to the thickness of the oxide scale formed on the titanium, rather than purely as a function of time or temperature.

Linear oxidation kinetics were seen to occur in titanium with a scale thicker than $\sim 10\mu\text{m}$. This is due to a change in the structure of the scale above this thickness. Initial scales are coherent, the kinetics are parabolic and oxygen diffusion through the TiO_2 scale is the controlling factor. Above $\sim 10\mu\text{m}$ the internal stresses in the scale cause it to crack, thus allowing oxygen gas to

easily diffuse along the cracks to the metal surface. Under these conditions the oxidation kinetics are linear.

Various researchers have concluded that the anisothermal oxidation of titanium varies with the heating rate. Below a heating rate of $\sim 20^{\circ}\text{C s}^{-1}$ the kinetics can be described as parabolic, with perhaps an initial asymptotic kinetic in the early stages of the higher heating rates. Above a heating rate of $\sim 20^{\circ}\text{C s}^{-1}$ the oxidation rate is above that described by parabolic and asymptotic kinetics. This is thought to be due to an increase in the reacting surface area, caused by stress within the sample. In general, it has been seen that increasing the heating rate increases the oxidation rate of the titanium. This subsequently reduces the ambient temperature at which the sample ignites and starts to burn.

Additionally, the sample size, or more importantly the surface area to volume ratio of the sample, has been highlighted as a controlling factor in whether a sample will ignite under fixed conditions. Samples with high surface area to volume ratios have an increased tendency to ignite. Ignition of a sample when the ambient temperature is below the melting point of titanium is caused by the exothermic oxidation reaction, which increases the temperature of the sample producing a 'thermal runaway' effect. If the conditions are correct, this effect leads to ignition and burning of the sample.

The burning of titanium is known to occur only in the liquid phase at atmospheric pressures, with the incorporation of oxygen into the material being

the burning rate limiting factor. A minimum of 10 wt% oxygen in titanium was experimentally and theoretically seen to support sustained combustion. Combustion of titanium produces temperatures over 3000K. For a given sample and experimental procedure, defined sample temperatures and ambient temperatures at which ignition will occur, exist.

When titanium is in powdered form, DSC experiments reveal exothermic peaks caused by oxidation, occurring from 495°C onwards. The thickness and morphology of the scale on the oxide is seen to influence the oxidation rate and hence the exothermicity. Initially the exothermic oxidation rate is high as oxygen and titanium quickly diffuse through the thin oxide shell to react. The oxidation rate then slows as a coherent oxide scale forms, leaving the oxidation process governed by the diffusion of titanium cations through the oxide scale. It then starts to increase as the scale cracks under its own internal stress and direct metal – oxygen contact occurs.

Further heating can cause the sample to ignite. When the powder is pressed into a cylindrical form, the sample density and gas pressure effect the burning of the sample. Higher oxygen pressures and lower densities aid burning, as the flow of gas to the reacting surface is the controlling factor.

Researchers conclude that the oxidation of titanium powder is heavily influenced by the powder's previous thermal history, oxide thickness, diameter, morphology, pellet density and ambient atmosphere.

With respect to the modelling of anisothermal oxidation, a consensus has appeared in the literature. Analysis reveals that the recent work of Liu and Gao (1998a) on the development of the *Markworth* model is the most accurate way to describe anisothermal oxidation.

Chapter 3

Figures

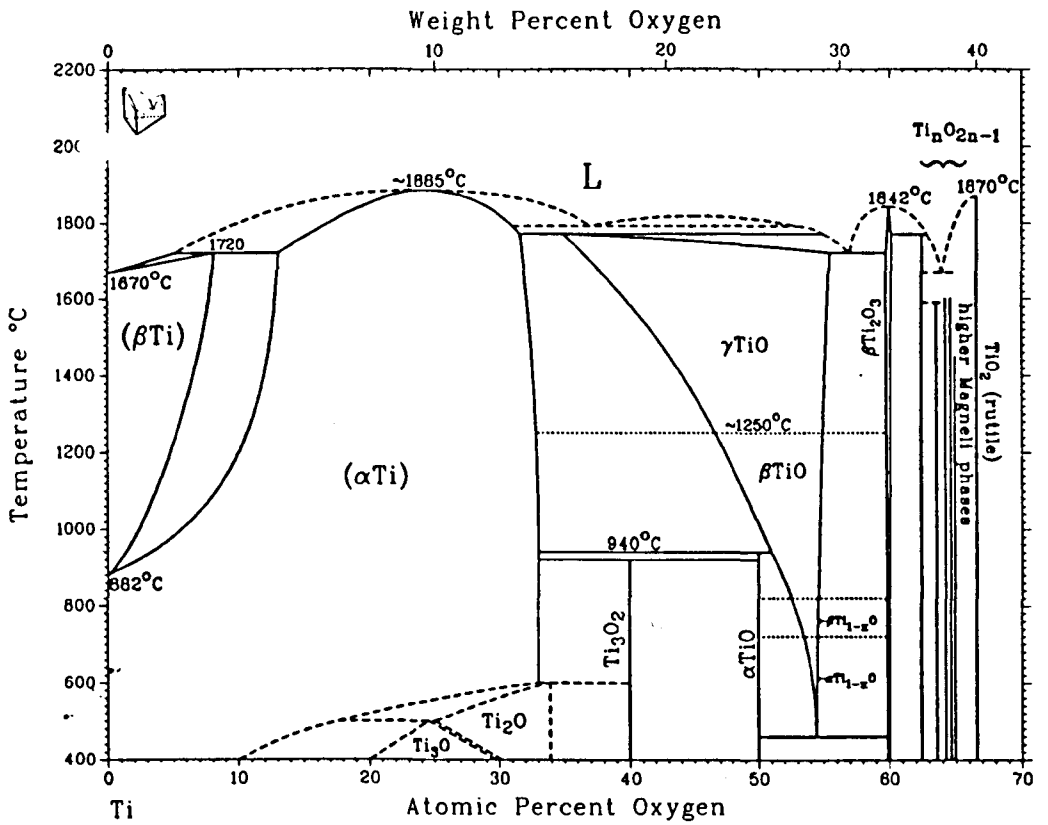


Figure 3.1 The Ti – O Phase Diagram. ASM Handbook (1992b).

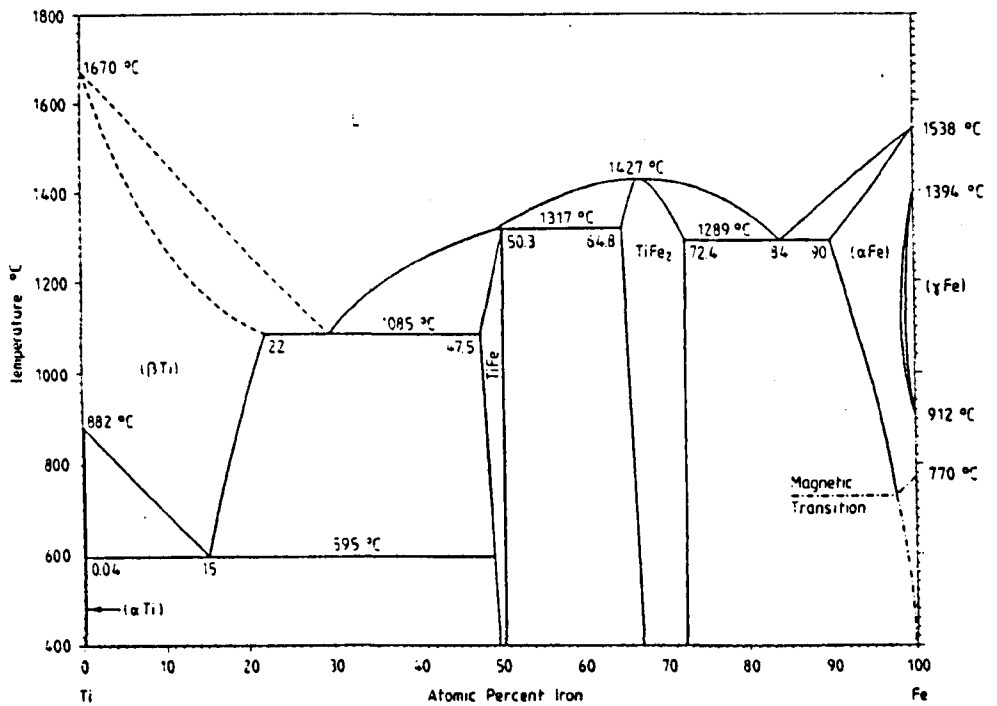
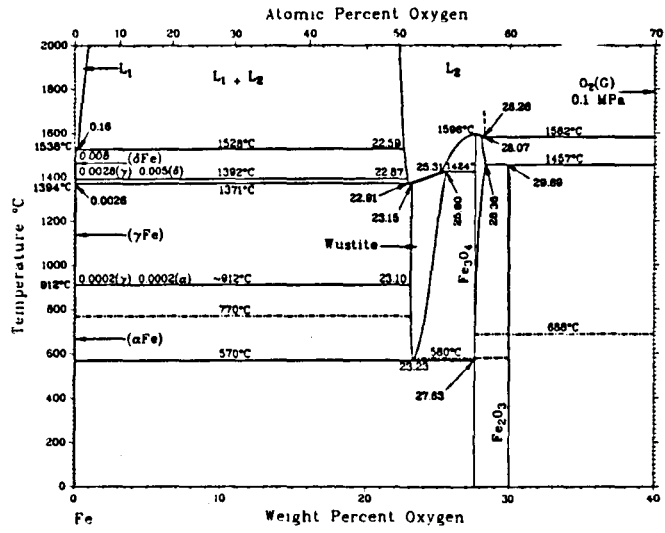


Figure 3.2 The Fe – Ti Phase Diagram. Okamoto (1996).

Fe-O



Fe-O phase diagram from 22 to 31 wt% O

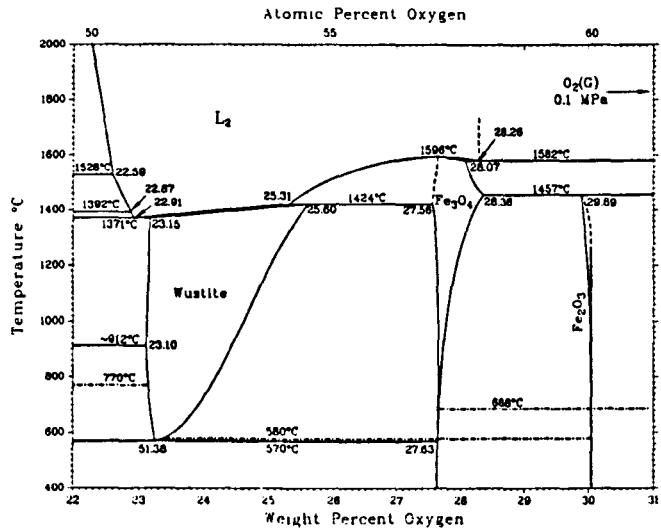


Figure 3.3 The Fe – O Phase Diagram. ASM Handbook (1992a).

Figure 3.4 The Oxygen Concentration Profile Across TiO_2 and the Titanium Metal Substrate. Kubaschewski and Hopkins (1953).

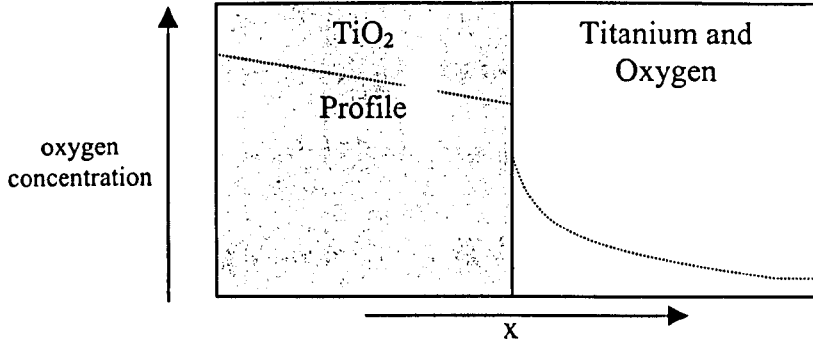
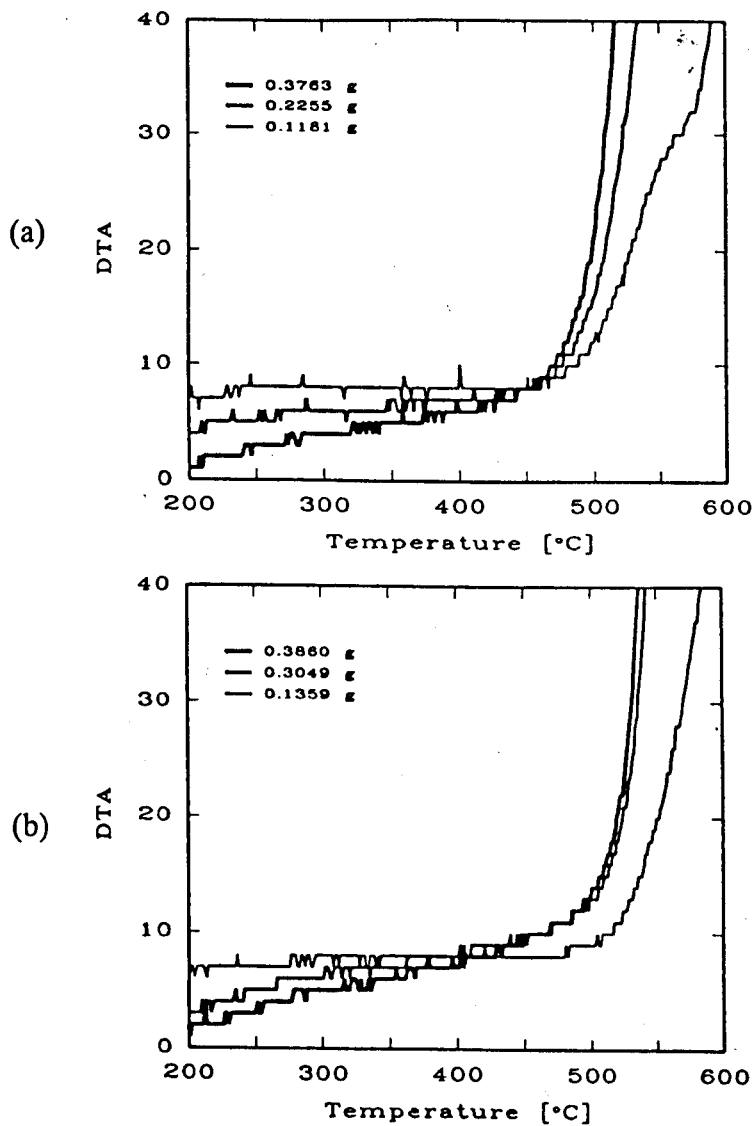


Figure 3.5 The Reduction in the Compact Ignition Temperature with Increasing Size, for -100 Mesh (a) and -325 Mesh (b) Titanium Powder Compacts Heated in Air. Rode and Hlavcek (1994).



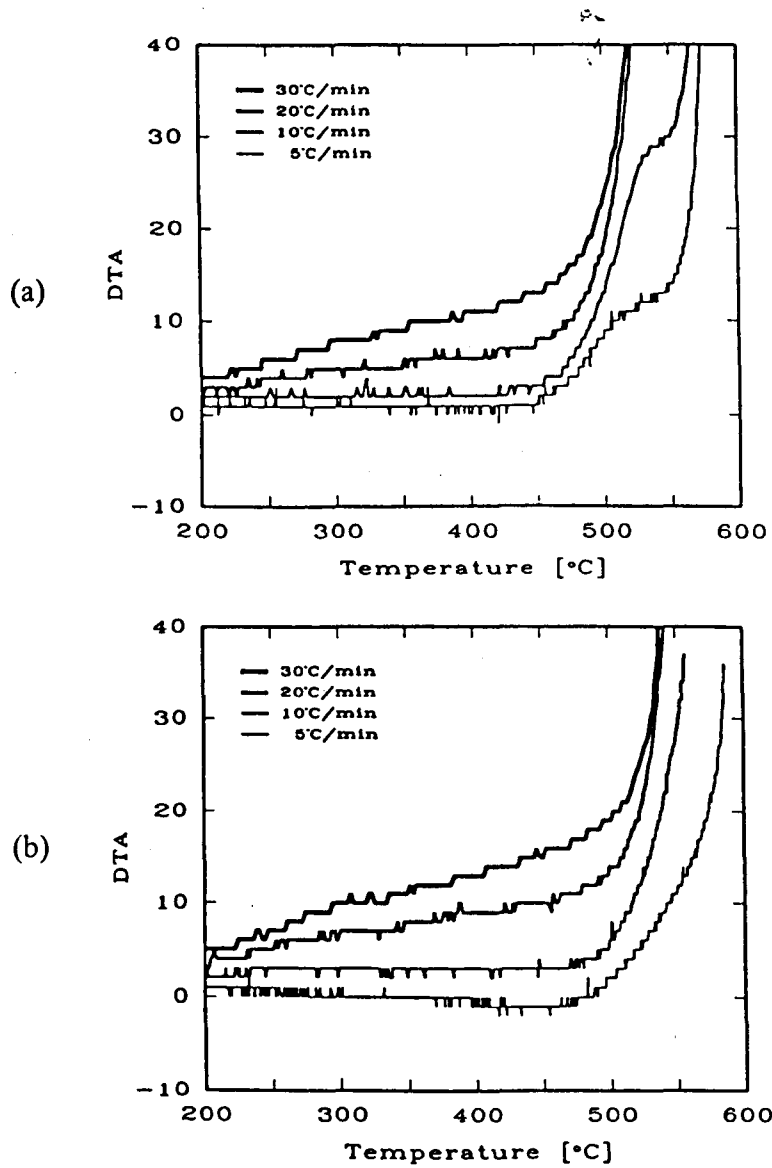


Figure 3.6 The Effect of the Heating Rate on the Ignition Temperature of -100 mesh (a) and -325 mesh (b) Titanium Powder Compacts, Heated in Air. Rode and Hlavcek (1994).

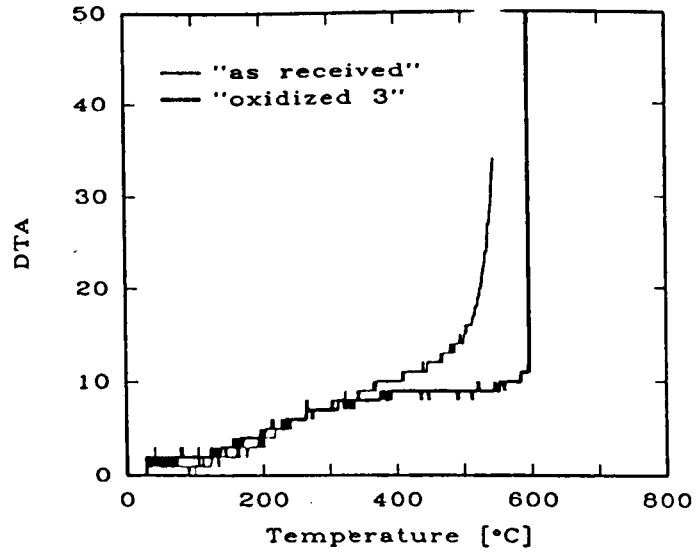


Figure 3.7 Spontaneous Ignition of Compacts Pressed from Pre-Oxidised Titanium Powders Heated in Air. Rode and Hlavcek (1994)

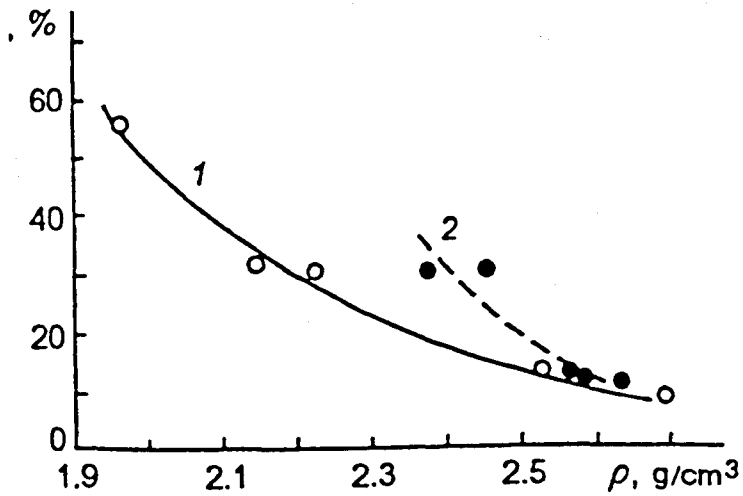


Figure 3.8 The Effect of Sample Density on the Completeness of Combustion of Titanium Powders Burning in a 50 / 50 Argon-O₂ Atmosphere (Curve 1) and a 25 / 75 Argon-O₂ Atmosphere (Curve 2) at a Pressure of 0.1MPa. Bakhman *et al.* (1998)

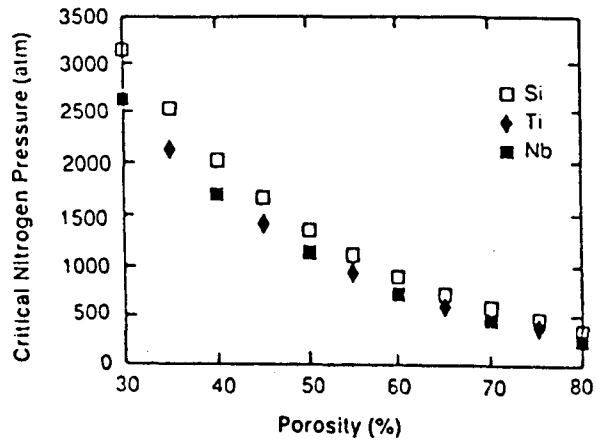
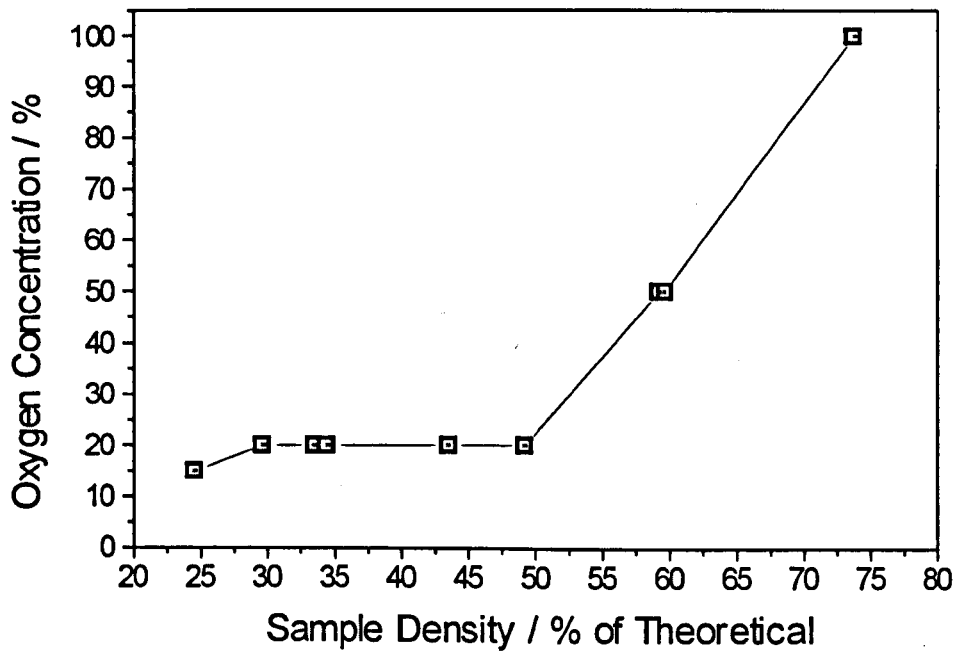
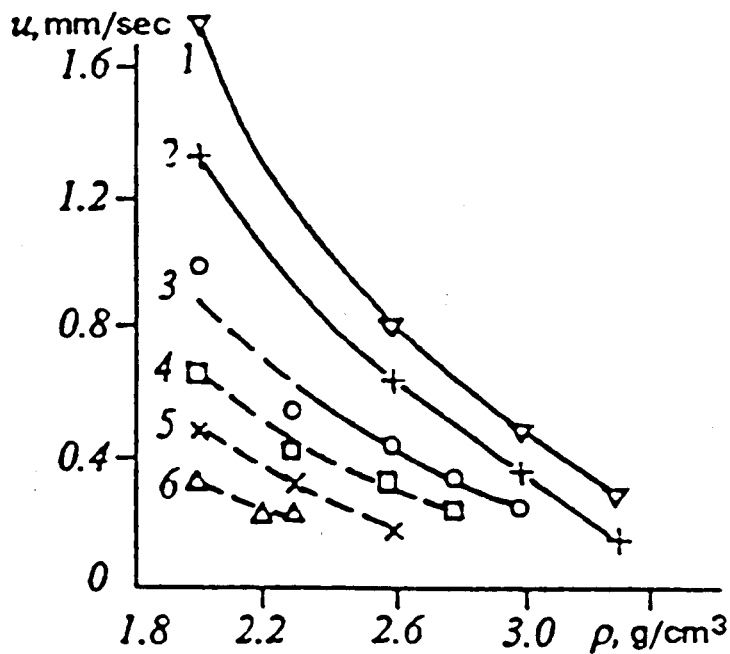


Figure 3.9 The Critical Nitrogen Pressure Required for Complete Combustion of a Titanium Powder Compact to Stoichiometric TiN. The Critical Nitrogen Pressures for Silicon and Niobium Powder Compacts are Also Shown. Dunmead *et al.* (1989).

Figure 3.10 Graphical Representation of Table 3.6 Data, The Effect of Sample Density on the Lowest Oxygen Concentration at which Stable Combustion of Titanium Powder Compacts is Possible.





Nitrogen Pressure: 1: 1800 Torr, 2: 1100 Torr, 3: 700 Torr, 4: 400 Tor, 5: 300 Torr, 6: 200 Torr

Figure 3.11 The Effect of Density on the Combustion Wave Velocity of Titanium Powders Burning in Nitrogen. Kudo and Odawara (1989).

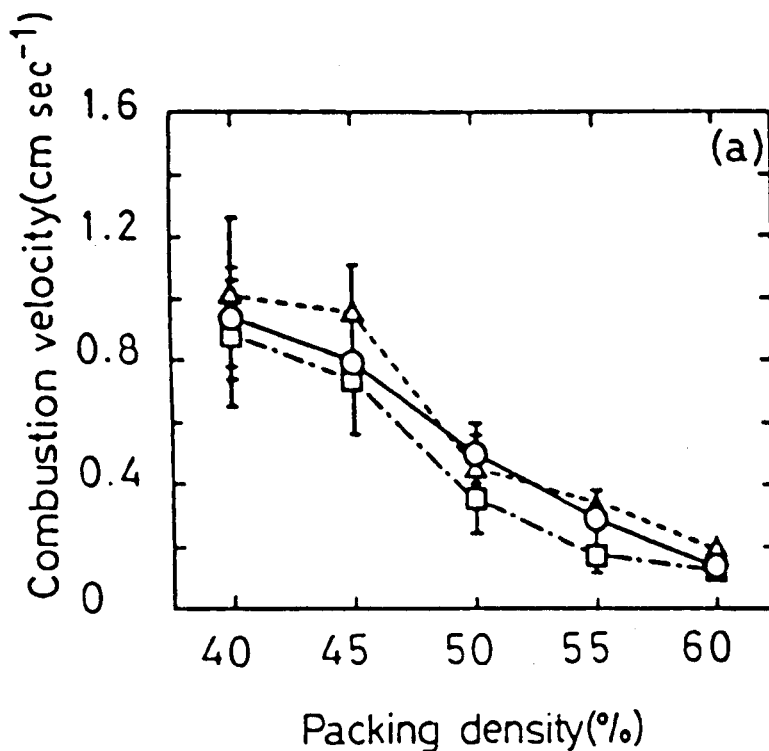


Figure 3.12 The Effect of the Sample Density on the Combustion Wave Velocity of Titanium Powder Burning in Nitrogen under Three Different Gas Flow Regiems. Filonenko and Barzykin (1996).

Partial Pressure of Oxygen in the Vacuum Chamber

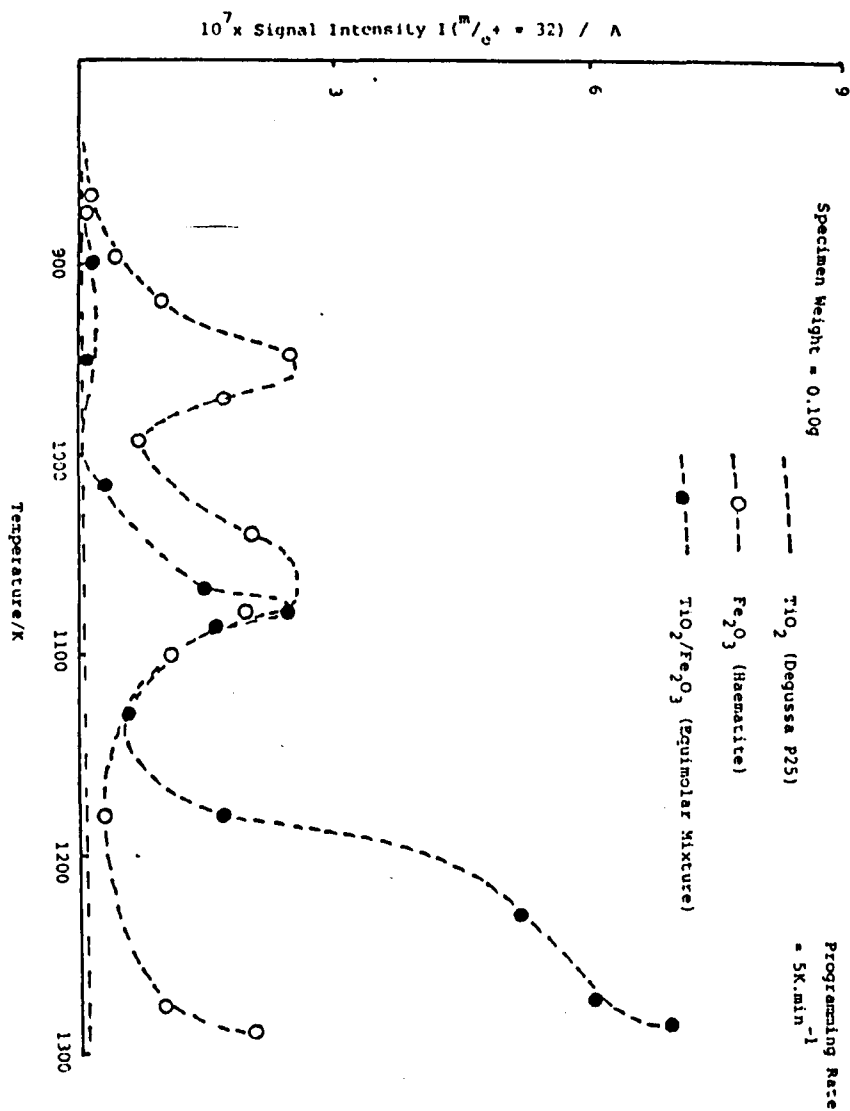


Figure 3.13 The Effect Of Vacuum Reduction on TiO_2 , Fe_2O_3 and an Equimolar $\text{TiO}_2 / \text{Fe}_2\text{O}_3$ Compacted Mixture as they are Heated at $5 \text{ K} \cdot \text{min}^{-1}$. Peaks in the Graphs Denote Regions of Phase Decomposition. Bickley *et al.* (1991).

Chapter 4

Experimental Procedure

4.1 Introduction

The experimental procedures used in the research are recorded here, with additional discussion to clarify certain points and methodologies. Any additional detail specific to certain experiments is recorded in the relevant chapters. The experimental programme involved the formation of compressed cylindrical pellets from mixed starting powders. The pellets could then be heated to react the powders in a SHS type reaction, forming a product phase.

4.2 Materials used

To enable the experiments to be compared to one another, all powders used came from the same batch. Powders used in this research were:

- **Titanium:** Goodfellows UK Ti006020, <150 μ m, 99.5 wt% titanium according to manufacturer. Prepared by the hydride-calcium reduction method and crushed to size. The hydride-calcium reduction method of producing titanium results in a porous titanium foam. Crushing breaks up the foam; however, the particles are still irregular, and thus have a larger surface area than they would have if they had been spherical. Figure 4.1 shows the morphology of the powder. Table 4.1 details the major impurities and table 4.2 details the powder size fractions:

Table 4.1 Chemical Analysis of <150µm Titanium Powder Values are in wt%.					
C	N	O	S	Cl	Fe
0.04	0.15	0.36	0.003	0.17	0.09

Table 4.2 < 150µm Titanium Powder Mesh Analysis (Cumulative)			
Mesh/µm	Test 1	Test 2	Average % of Powder in Fraction
>150	1.1	1.1	1.1%
>125	13.0	13.3	12.05%
>90	37.1	37.5	24.15%
>75	47.7	47.1	10.1%
>63	70.7	68.5	22.2%
>45	83.3	80.7	12.4%
<45	100	100	18%

- **Titanium:** PyroGenesis Inc; Montreal, Quebec, Canada. Spherical titanium powder, one-off order, 75-125µm. Commercially Pure. The titanium powder was made by the novel plasma gun method. Solid titanium rod is fed into the meeting point of the hypersonic hot gases from three plasma guns, under inert conditions. The resultant gas vortex and high heating rates melts the titanium and blows it away from the solid feed stock. The titanium produced is fine, of high purity and spherical. Figure 4.2 shows the product.
- **Titanium:** <355µm. Supplied by the London and Scandinavian Metallurgical Company U.K. (L.S.M.) Prepared by the hydride-calcium

reduction method and crushed to size. Figure 4.3 shows the morphology of the powder. It has a porous structure that is characteristic of the production method. Chemical analysis of the powder is detailed in table 4.3 and the powder size analysis is detailed in table 4.4:

Table 4.3 Chemical Analysis of <355μm Titanium Powder Values are in wt%.					
C	N	O	S	Cl	Fe
0.12	0.23	0.73	0.004	0.21	0.12

Table 4.4 <355μm Titanium Powder Mesh Analysis (Cumulative)			
<u>Mesh μm</u>	<u>Test 1</u>	<u>Test 2</u>	<u>Average % of Powder in Fraction</u>
>250	15.9	17.6	16.75%
>180	47.0	48.6	31.05%
>125	66.7	68.2	19.65%
>90	78.7	83.2	13.5%
>63	90.8	96.3	12.6%
>45	97.1	99.0	4.5%
<45	100	100	1.95%

- Iron oxide: Aldrich UK 31,005-0, Fe₂O₃, <5 μ m, 99+% according to manufacturer. Figure 4.4 shows the powder. Chemical analysis : Fe = 69.89%. Powder size analysis is shown in table 4.5

Table 4.5 Powder Size Analysis of Fe₂O₃ via 'Microtrac' Analysis									
Size / μm	0.9	1.4	1.9	2.8	3.9	5.5	7.8	11	16
Cumulative vol % Below size	1.3	5.3	12.1	31.7	58.2	79.0	91.9	97.8	100
Powder Size Distribution - Powder Diameter at:									
10 th Percentile - DV ₁₀	50 th Percentile - DV ₅₀			90 th Percentile - DV ₉₀					
1.75μm	3.56μm			7.46μm					

Other powdered materials used in the experiments were:

- Graphite: Aldrich UK 28,286-3, Synthetic, <1μm. Produced from a bonded granular carbon body that has been heated to above 2400°C.
- Alumina: Al₂O₃, <5μm. Stoichiometric composition.

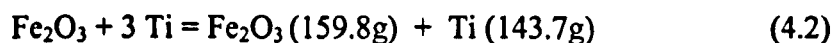
4.3 Sample Preparation

4.3.1 Weighing, Mixing and Pressing

The mass of the powders used in the compositions was determined by molar masses. A typical reaction composition of Fe₂O₃ + 3 Ti, employs 1 mole of Fe₂O₃ and 3 moles of titanium. The molar mass of Fe₂O₃ is:

$$(2 \times 55.9) + (3 \times 16) = 159.8 \text{ g mol}^{-1} \quad (4.1)$$

The molar mass of titanium = 47.9 g mol⁻¹. This is multiplied by 3 to equal 143.7g. Therefore, the balanced masses of Fe₂O₃ and titanium for the reaction of:



These values were translated into manageable quantities, e.g. 15.98g Fe₂O₃ and 14.37g Ti per mixed batch of powder. For each sample the reactant powders were weighed to an accuracy of ± 0.01g on a electronic digital scale. The weighed powders were then sealed in a plastic container and mixed for at least 20 minutes by a *Turbular* mixer (Glen Creston, UK). Due to the low density and fine particle size of the powders, 10mm Ø steel ball bearings were added to the mix, to break up powder agglomerations and aid particle interaction. Without the ball bearings the powder tended to settle within the container and not mix. Once mixed the powder was sieved to retrieve the ball bearings and to break up any small powder agglomerations that had formed.

Pellets were produced by cold pressing the powder under an uniaxial load of ~350MPa in a steel die of 12mmØ. A pellet length of between 15mm and 20mm was sufficient to allow easy manipulation, viewing and analysis. Such a pellet contains around 8g of material. Pressing was performed in a Moore (UK) 40 ton uniaxial press. Before each pressing cycle the die was cleaned to remove any previous powder and coated in a suspension of lithium stearate in acetone, which acted as a lubricant. The acetone quickly evaporated leaving a fine lithium stearate film on the die.

All weighing, mixing and pressing of the powders was carried out under normal atmospheric conditions. Once pressed, the pellets were either reacted immediately or placed in an sealed inert atmosphere to prevent any degradation

due to atmospheric contamination such as oxidation or water vapour absorption.

4.4 Combustion Methods

4.4.1 Radiant Heat, Box Furnace (Ambient Atmosphere)

A Carbolite UK series LMF 12 / 3 radiant heat, electric box furnace was used to facilitate the heating of pellets in air. The furnace was held at the desired temperature for at least 30 minutes prior to experimentation, so that an even temperature was achieved throughout it. Pellets were placed on alumina furnace boats and placed in the furnace for the desired length of time.

4.4.1.1 Deducing the Reaction Time



The time to the start of the reaction of these pellets was deduced to the nearest 10 seconds by optical observations of the pellet in situ, via the chimney, over typically 5 runs. Once the reaction time was deduced from the previous trials a final experiment was run for the full standard length of time. This was required for experimental completeness as the reaction occurred after a few minutes in some samples, but longer in others. At the end of this time the pellet was removed from the furnace and allowed to cool to ambient temperatures.

Ti + Fe₂O₃

The time to reaction for these compositions was deduced via an audible explosion and puff of smoke which accompanies the reaction. Visual inspection confirmed the pellet had reacted. Again, once the reaction time had been deduced over a number of runs an pellet was placed in the furnace for the standard length of time. The pellet was then removed from the furnace and allowed to cool to ambient temperatures.

4.4.2 Radiant Heat, Tube Furnace (Argon Atmosphere)

A sealed Carbolite UK series STF 15 / 50 tube furnace was used to facilitate the heating of the samples in a flowing argon atmosphere. The samples were placed on alumina / silica ceramic wool on a steel furnace boat in the centre of the furnace tube, so the samples were in the middle of the heating zone. The tube furnace was sealed and flushed with argon for 10 minutes before heating commenced. The flow rate was decreased to limit any thermal shock occurring from the cold gas touching the tube and the furnace turned on. The heating rate from 20°C - 300°C was 10°C / min, from 300°C to the desired temperature was 20°C / min. After the heating cycle had finished the samples were left to cool in the furnace, still in a flowing argon atmosphere.

4.4.3 Tungsten Filament (Argon Atmosphere)

An in house constructed vacuum glove box was used to facilitate the heating of pellets by a tungsten filament. The glove box is required to provide an inert atmosphere that enables the filament to operate at high temperatures. Without

the inert atmosphere the filament oxidises rapidly and fails within 5-10 seconds. A schematic of the apparatus is shown in figure 4.5, whilst figures 4.6 and 4.7 show the actual apparatus and the internal set up.

The pellet was placed atop the graphite block. A tungsten filament, constructed from 0.38mm pure tungsten wire, in the shape of a W, was positioned roughly 1mm from the top surface of the pellet. The glove box is then sealed and evacuated for at least 1 hour. Once evacuated the chamber is back filled with argon gas. The process is conducted three times, keeping the third fill of gas in the chamber. It is under these conditions that the pellets are ignited. A current is passed through the filament to resistively heat it. The radiative heat from the glowing filament is absorbed by the pellet thus raising the temperature of its top surface. Once the top surface reaches the ignition temperature, T_{ig} , the reaction starts and a reaction wave is seen to propagate down the pellet.

4.5 Data Recording

4.5.1 Temperature Measurements

The combustion reaction temperature is an important factor in the understanding and analysis of SHS reactions. An *Ircon 2* colour pyrometer was employed to measure this parameter. A 2 colour pyrometer was required as considerable smoke and fume are produced during the reaction. In such a situation, the reading from a single colour pyrometer records a reduction in temperature in relation to the decrease in signal strength occurring. A 2 colour pyrometer takes its reading from the difference between two different recorded

wave lengths and is therefore less sensitive to smoke and obstruction of the sample.

The pyrometer employed has a temperature range of 1000°C - 3000°C. It is accurate to within 1% of the full scale. A analysed spot size of 4mm diameter can be achieved when the pyrometer is placed at around 350mm from the sample. Pre-heating by the tungsten coil increases the reaction rate and temperature in the top section of the pellet. Therefore to obtain an accurate reading of the actual reaction temperature, and reducing the effect of any pre-heat interference, the pyrometer was focused at the mid point on the pellet.

The analogue voltage output data from the pyrometer was sampled, at a frequency of 100Hz, by an IBM compatible personal computer running a 'Waveview' software package.

4.6 *Microstructural Examination*

4.6.1 *Sample Preparation*

4.6.1.1 *Mounted and Polished Samples*

SHS reaction products were mounted in 'Edge Retaining' Bakelite for analysis by optical microscope. The samples were crushed to a rough powder. High ceramic content products easily crushed to <2mm pieces, products with a high metallic content were harder to crush, resulting in >5mm particles. Once mounted the samples were polished on progressively finer silicon carbide and

diamond abrasive laps, to a final finish of 1µm. No etching was required on these samples.

4.6.1.2 SEM Samples

Samples for analysis in the SEM were mounted in 'Conductive' Bakelite. The same polishing regime as above was used. For use in the SEM conducting aluminium tape was used to eliminate any build up of charge on the samples.

4.6.1.3 XRD samples

All samples for XRD analysis were roughly crushed before being hand-ground to a very fine powder. The powder was then pressed into a depression in the XRD powder holder and smoothed over so that the surface of the powder was at the same height as that of the holder. In this way the possibility of peak shifting in the spectra, due to the height differential, was minimised.

4.6.2 Optical Microscopy

A Nippon Optiphot facilitated the examination of microstructural features in the samples. Magnifications up to 1000x were employed. The use of polarised and coloured light help bring out certain metallographic features.

4.6.3 Scanning Electron Microscopy (SEM)

A JOEL Winsem 6400 Scanning Electron Microscope and Philips FEG-ESEM Microscope were used to investigate the samples.

4.6.3.1 JOEL 6400

The JOEL was the primary piece of investigative equipment. Operating conditions varied depending on the application, however a typical accelerating voltage of 15-20kV was utilised at a working distance of between 15-39mm. In secondary electron imaging (SEI) mode high resolution and depth of field images, photographic negatives and digital printouts, were obtained. Back scattered electron imaging (BSI) enabled distinctions between chemical composition to be seen. Elements with high atomic numbers backscatter more electrons and therefore appear brighter.

The attached 'Noran' energy dispersive X-ray (EDX) analysis system was used to determine the chemical composition of the samples. Spot analysis facilitated the examination of discrete areas within the sample. Quantitative chemical analysis of the samples down to the atomic number of 6 (carbon) is possible, however, for accuracy the system was only used to quantitatively analyse the elements of aluminium and higher. The minimum spot size is dependant on the spot size / dead time set up. The spot size directly affects the dead time which has to be in the range of 20 to 30%. Thus the spot size is usually in the 2-5 μ m range.

4.6.3.2 Philips FEG-ESEM

The ESEM is a high resolution environmental scanning electron microscope. The magnification and resolution are significantly greater than those of the JOEL 6400. The inclusion of an accurate EDX system on the microscope makes it an impressive investigatory tool. The system was used to chemically

spot analyse specific areas in the samples and optically examine the sintered samples in fine detail. The spot size for such EDX analysis was $<1\mu\text{m}$ although the volume of analysis was governed by beam spreading. The field emission gun (FEG) produces a greater electron density in the beam than a conventional SEM gun. It was therefore necessary to use a reduced voltage to stop degradation of the material. Typical voltages are in the region of 5-15kV, operating under a high vacuum.

4.6.4 X-Ray Diffraction Analysis (XRD)

XRD analysis was used to determine the phases present in a bulk sample of material. A 'Siemens Kristalloflex' using $\text{Cu K}\alpha$ radiation, operating at 40kV and 20mA was used to facilitate this. The standard analysis method utilised a 2θ step rotation of 0.03° with a dwell time of 2 seconds. Samples for examination were prepared as detailed previously. Problems were encountered as the metallic phases present in the samples did not easily crush into a fine powder. Thus they are left as large particles in the bulk sample and sieved out before analysis. The ceramic phases easily comminute and consequently the XRD analysis is primarily of the ceramic phase and contains only a small amount of the metallic phase. The results were subsequently only used to determine the nature of phases in the sample, not their relative amounts. Analysis of the spectra was via a 'Siemens Diffrac-AT v3.0' PC based computer system, using PDF-2 standards, sets 1-41.

Chapter 4

Figures

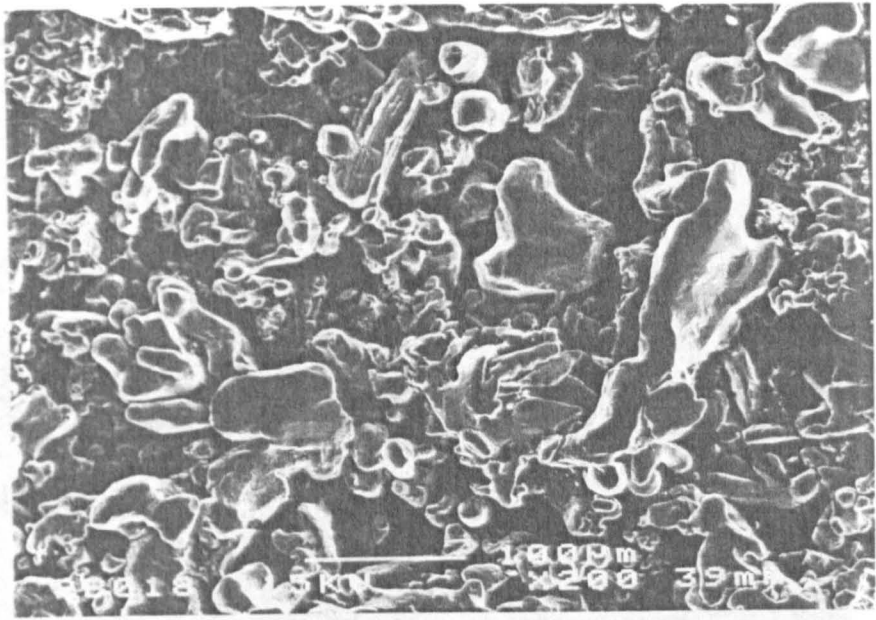


Figure 4.1 SEM Micrograph of *Goodfellows* <150μm Titanium Powder

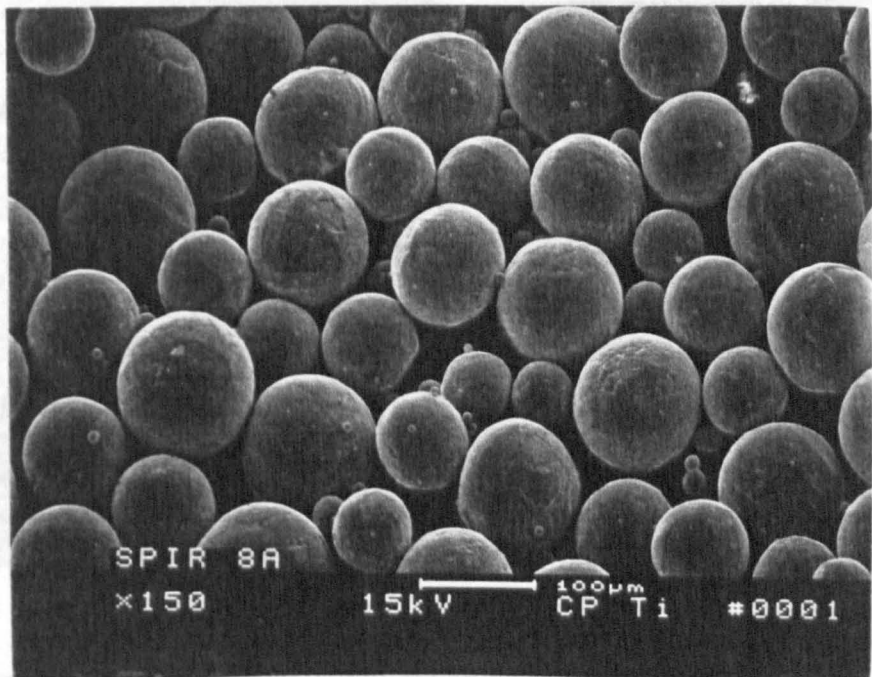


Figure 4.2 SEM Micrograph of *Pyrogenesis* Spherical Titanium Powders

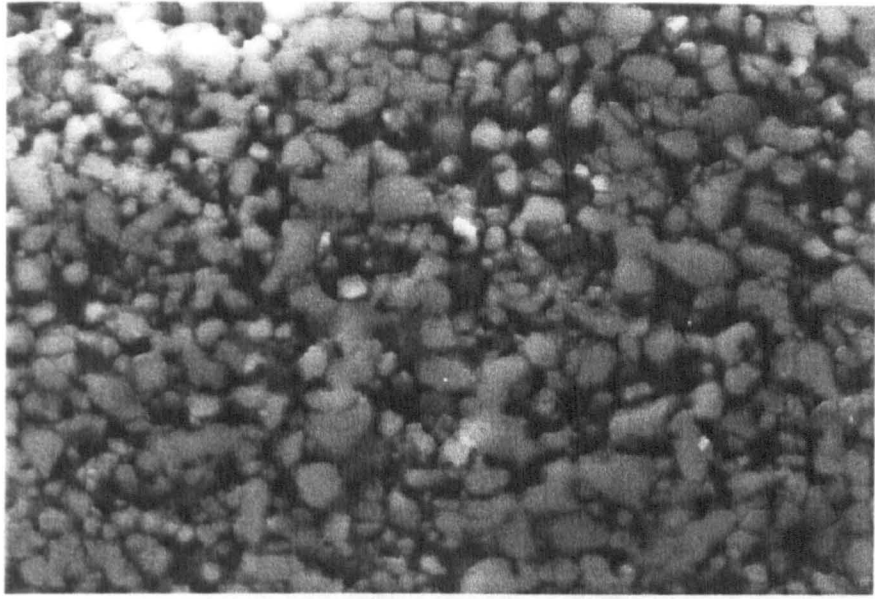


Figure 4.3 SEM Micrograph of the Surface of *Aldrich* $<5\mu\text{m}</math> $\text{Fe}_2\text{O}_3</math> Powders$$

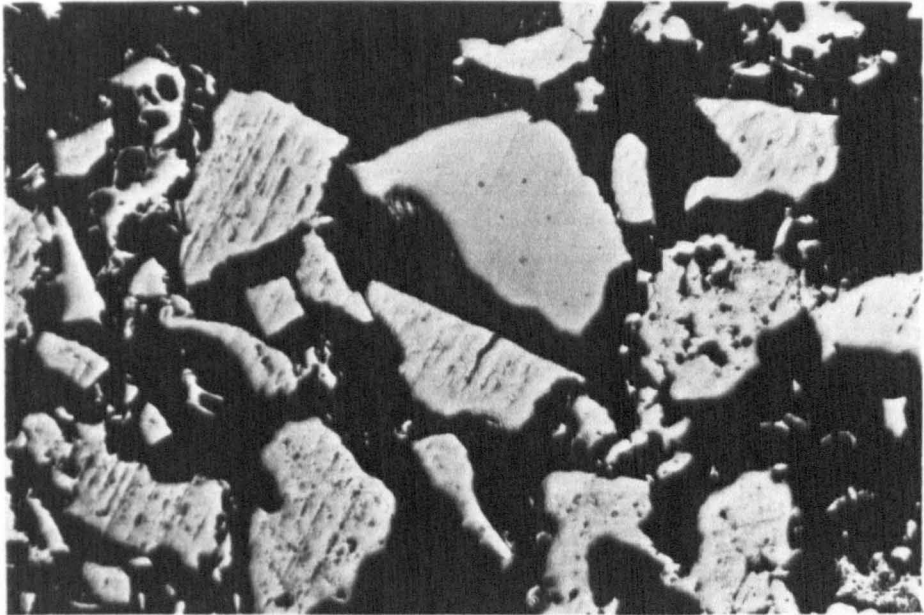


Figure 4.4 Optical Micrograph of Sectioned *LSM* $<355\mu\text{m}</math> Titanium Powders$

Figure 4.5 Schematic of the in-house built Vacuum Box and Experimental set up.

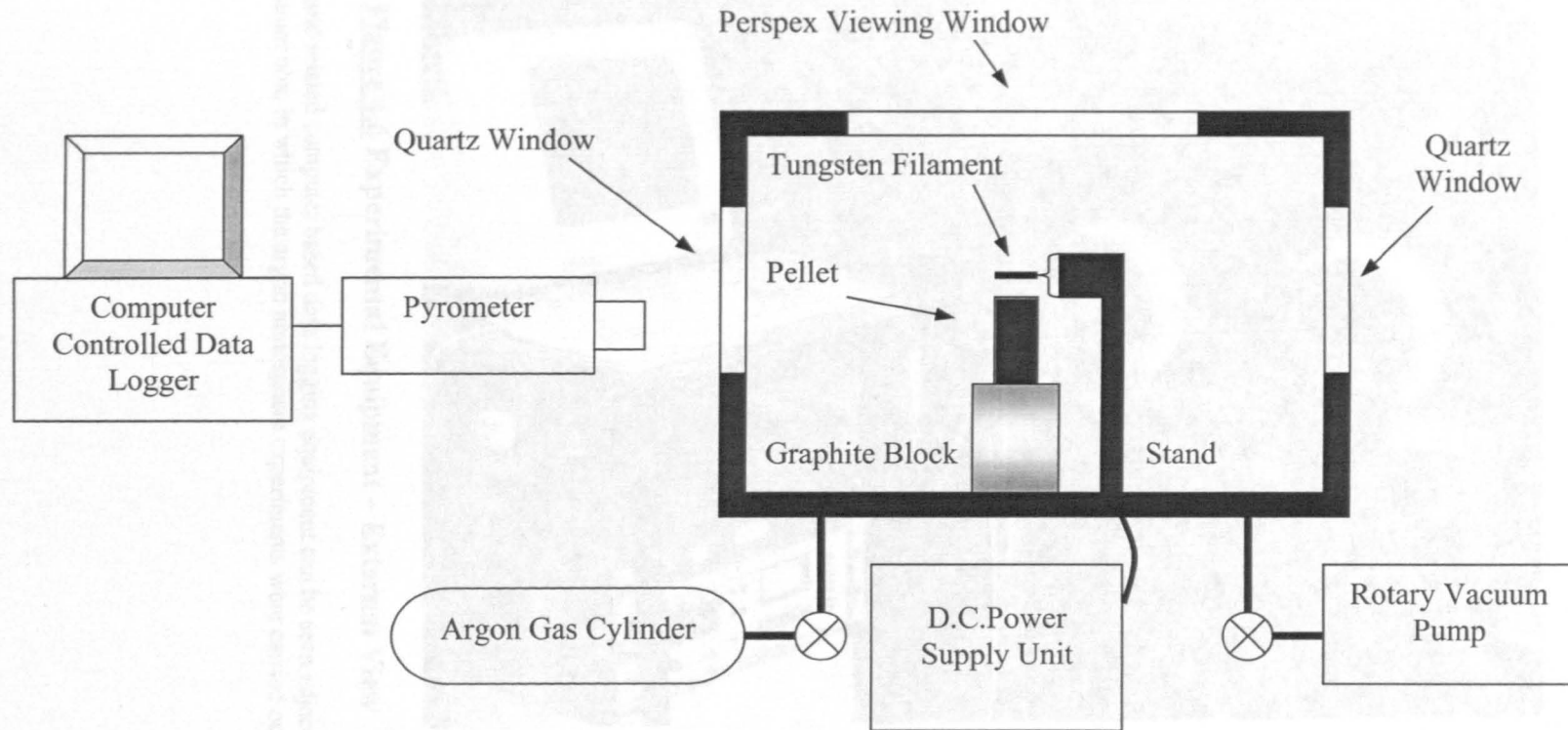




Figure 4.6 Experimental Equipment – External View

The pyrometer and related computer based data logging equipment can be seen adjacent to the blue vacuum box, in which the argon atmosphere experiments were carried out.

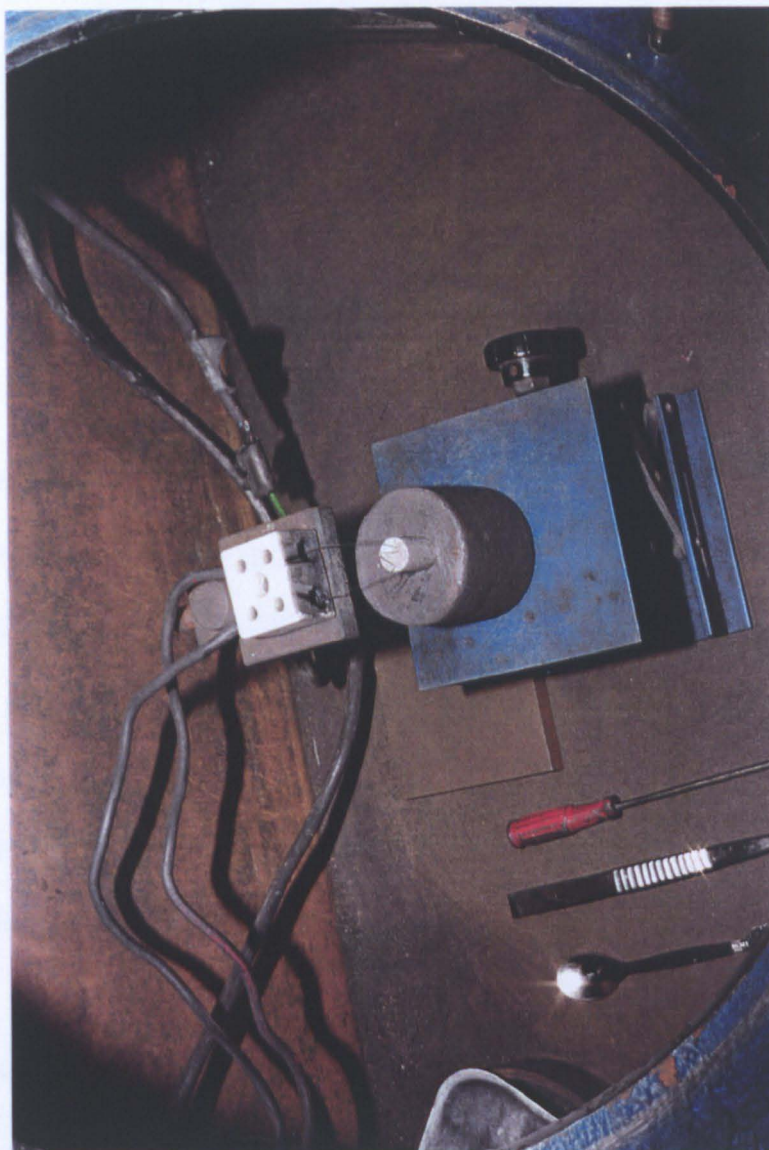


Figure 4.7 Experimental Equipment – Detail inside the Vacuum Box

A pressed titanium powder pellet is seen sitting on top of the graphite mount. The height of this can be adjusted by the carrier. A tungsten filament can be seen in position, ready for heating.

Chapter 5

The Reaction Between Titanium and Air, and Titanium and Iron (III) Oxide, Heated in the Thermal Explosion Mode.

5.1 Introduction

The aim of this work is to understand the oxidation behaviour of titanium and titanium + Fe_2O_3 powder compacts, as they are heated in air and argon atmospheres. The results of these investigations will form the theoretical basis for the understanding of the self-propagating reaction that occurs between powdered titanium and Fe_2O_3 . By subjecting whole pellets to different heating regimes, covering temperatures that are above and below the ignition point of the pellet, the processes that occur in the powders prior to and during ignition and reaction can be inferred. This data can then be related to the processes that occur when pellets are ignited in the SHS mode.

Due to the complex, interrelated nature of the parameters involved in the process of oxidation, this chapter specifically investigates the physical observations of compressed powder oxidation. Explanations and models of oxidation are produced in the following two chapters.

5.2 Experiments

A series of experiments has been conducted that investigate the oxidation reaction that occurs between titanium and air and between titanium and Fe_2O_3 .

There are 4 series of experiments.

- Series 1: Examination of the effect that heating has on compressed titanium powder compacts in an air atmosphere.
- Series 2: Examination of the effect that heating has on compressed mixed titanium and Al_2O_3 powder compacts, in an air or argon atmosphere.
- Series 3: Examination of the effect that heating has on compressed, mixed titanium and Fe_2O_3 powder compacts, in an air or argon atmosphere.
- Series 4: Examination of the reaction that occurs between bulk titanium and Fe_2O_3 powder under an inert atmosphere.

5.2.1 Series 1: Titanium Powder Compacts Heated in Air

It is known from the literature that titanium exothermically oxidises. Powdered titanium compressed into a compact has been seen to ignite when heated to relatively low temperatures i.e. $<50\mu\text{m}$ titanium powder heated to 550°C (Tavgen *et al.* 1992). This is due to the compact heating up due to exothermic oxidation, leading to an increased oxidation rate and thus thermal runaway of the compact. This leads to compact ignition and combustion (Rode and

Hlavcek 1994). The research here looks at the oxidation process of titanium powder compacts as a starting point in the understanding of the $\text{Fe}_2\text{O}_3 + 3\text{Ti}$ combustion reaction.

Pellets were produced in the standard way as described in Chapter 4 except that hand pressing was employed to compact the pellet. It was found that pressing the pellets in the uniaxial hydraulic press to $\sim 350\text{MPa}$ caused sufficient plastic deformation to close the surface porosity of the pellets. The pellets then behaved as bulk samples and as such did not meet the requirements of the experiment.

Pellet morphologies were kept as similar as possible across all the experimental series, so that information gained during the experiments could be related to one another. It was calculated that the density of titanium within a hydraulically pressed $\text{Fe}_2\text{O}_3 + 3\text{Ti}$ pellet is $\sim 36.5\%$. Pellet densities were found by weighing and measuring the pellets. A digital electronic balance with an accuracy of $\pm 0.01\text{g}$ was employed to weigh the pressed pellets. The dimensional measurements were found with the use of Vernier Callipers. As can be seen from Table 5.6, hand pressing produces whole pellet densities that are of comparable value to the density of Ti in a hydraulically compressed $\text{Fe}_2\text{O}_3 + 3\text{Ti}$ pellet, the effect being that both pellets have similar titanium powder distributions, and results can be compared. The series was broken down into 2 heating regimes:

- A: Experiments conducted in a pre-heated furnace of constant temperature.

- B: Experiments conducted in a furnace that was heated from ambient temperatures at 10°C / min to the desired holding temperature.

In all experiments the pellet was held at the desired temperature for 20 minutes. It was found from initial experiments that a time of 20 minutes was sufficient for the sample to reach the furnace temperature. Initial experiments showed that if the pellet had not ignited after 20 minutes, then it would not ignite at all. The maximum hold time for this test was 24 hours.

Both sets of experiments were conducted with a variety of powder size fractions as shown in Table 5.2 and 5.3. The powder fractions were obtained by sieving the LSM grade titanium (<355µm) with an Endecotts (UK) Octagon Digital vibratory sieve.

In these experiments, the ignition temperature is defined as the temperature of the furnace which promotes ignition – and consequently burning of the pellet. Burning of the pellet is characterised as self-sustaining oxidation of liquid titanium (Glassman and Papas 1994). It can be determined in a number of ways.

- Bright white optical radiation, accompanied with flames, smoke and possible melting of the pellet.
- Optical pyrometry records an increase in temperature of the surface of the compact above the melting point of titanium metal, 1670°C.

- Post reaction analysis of the pellet reveals significant morphological and chemical changes in the titanium – evidence of liquid phase titanium metal.

Pellets that had not ignited exhibited none of the characteristics described above.

Experiments were conducted at furnace temperature intervals of 25°C. Internal temperature fluctuations within the furnace precluded greater accuracy. Tables 5.1 and 5.2 detail the experimental parameters that were employed in the series A and series B experiments respectively.

Table 5.1 Titanium Powder Diameters and Furnace Holding Temperatures Employed in Series 1A Experiments	
<u>Powder Size / μm</u>	<u>Holding Temperatures / $^{\circ}\text{C}$</u>
(l) <355	475, 500, 525, 550, 575, 600, 625
(l) 355-250	
(l) 250-150	
(g) <150	
(g) 150-90	
(g) 90-53	
(g) <53	
(l) denotes powder from LSM (g) denotes powder from Goodfellows	

Table 5.2 Titanium Powder Diameters and Furnace Holding Temperatures Employed in Series 1B Experiments	
<u>Powder Size / μm</u>	<u>Holding Temperatures / $^{\circ}\text{C}$</u>
355-250	475, 500, 525, 550, 575, 600, 625, 650, 700, 750, 800, 850. (Heating rate 10°C / min)
150-90	
>53	

5.2.2 Series 2: Titanium Powder + Al₂O₃ Compacts Heated in Air and Argon

In this series of experiments, <5 μ m Al₂O₃ powder is utilised to produce a pellet morphology similar to that of a titanium and Fe₂O₃ pellet i.e. provide packing between the Ti particles. The Al₂O₃ was mixed into the titanium powder at a powder volume identical to that of Fe₂O₃ for a pellet of composition 3 moles Ti + 1 mole Fe₂O₃. It was calculated that, by volume, 1mole of Fe₂O₃ \equiv 1.2 moles of Al₂O₃.

In this way the reaction of the titanium with air could be examined under similar conditions to its reaction with air in a Ti + Fe₂O₃ pellet. Titanium has only been seen to react with Al₂O₃ when the titanium is in solution in a molten carrier metal (Zhuravlev and Turchanin 1997). This situation will not occur in these experiments and the Al₂O₃ can therefore be classed as an inert packing material. The pellets were produced as described in the Chapter 4. Ignition was again determined by insitu examination and post heating-cycle examination. Hydraulic pressing was chosen as the compaction method to produce a pellet with similar density characteristics as a hydraulically pressed 3Ti + Fe₂O₃ pellet.

The behaviour of the pellets heated under an argon atmosphere was examined. Whilst these pellets were predicted not to react, the experiments were done for experimental completeness. Due to the heating regime of the furnace the minimum holding time was 60 minutes. Table 5.3 details the experimental parameters employed in both air and argon atmosphere experiments.

Table 5.3 Pellet Compositions, Titanium Particle Size and Furnace Temperatures and Holding Times Employed in Series 2 - Air Atmosphere Furnace Experiments			
<u>Composition</u>	<u>Titanium Particle Size</u>	<u>Holding Temperature /°C</u>	<u>Hold Time /min</u>
Al ₂ O ₃ + 3Ti	<150µm	550, 600	20
Al ₂ O ₃ + 3Ti	<355µm	550, 600	20
Pellet Compositions, Titanium Particle Size and Furnace Temperatures and Holding Times Employed in Series 2 - Argon Tube Furnace Experiments			
Al ₂ O ₃ + 3Ti	<150µm	550, 600	60
Al ₂ O ₃ + 3Ti	<355µm	550, 600	60

5.2.3 Series 3: Titanium Powder + Fe₂O₃ Compacts Heated in Air and Argon

The first two series of experiments investigated the reaction of pure titanium with air and argon. This series incorporates Fe₂O₃ into the compact. The Fe₂O₃ is expected to react with the titanium and act as an oxygen source during combustion.

Pellets of composition 3Ti + Fe₂O₃ were produced and pressed into pellets as described in Chapter 4. These pellets are similar to those in Series 2 except for the change from the inert Al₂O₃ to the reactive Fe₂O₃. The reaction between the two powders was examined under air and argon atmospheres. Heating the pellets in an inert argon atmosphere allows the examination of the reaction between titanium and Fe₂O₃ without any influence from elements or compounds found in air, notably O₂ and N₂. The tube furnace, used for heating in an inert, argon atmosphere precluded optical observation of the pellet. It was still possible to determine if ignition had occurred by analysis of the pellet after

the heating cycle. Due to the heating regime of the furnace the minimum hold time at the desired temperature was 60 minutes. Table 5.4 details the experimental parameters employed.

Table 5.4 Pellet Compositions, Titanium Particle Size and Furnace Temperatures and Holding Times Employed in Series 3 - Air Atmosphere Furnace Experiments			
<u>Composition</u>	<u>Titanium Particle Size</u>	<u>Holding Temperature /°C</u>	<u>Hold Time /min</u>
Fe ₂ O ₃ + 3Ti	<150µm	550, 600, 650, 700	20
Fe ₂ O ₃ +3Ti	<355 µm	550, 600, 700	20
Pellet Compositions, Titanium Particle Size and Furnace Temperatures and Holding Times Employed in Series 3 - Argon Tube Furnace Experiments			
Fe ₂ O ₃ + 3Ti	<150µm	550, 600, 700	60
Fe ₂ O ₃ + 3Ti	<355µm	550, 600, 700	60

5.2.4 Series 4 : Bulk Titanium and Fe₂O₃ Reactions

The experiments in Series 3 investigated the effect of heating a compact of composition Fe₂O₃ + 3Ti. Ignition of the compact completely changed the morphology and chemical composition. Examination of the interactions between Fe₂O₃ and titanium was only possible in compacts that did not ignite. The experiments in series 4 were designed to allow observation of the interaction between titanium and Fe₂O₃ at higher temperatures and in greater detail.

Experiments comprised of heating a polished commercially pure titanium disc, 6mm Ø by 1mm thick, surrounded by >10mm of Fe₂O₃ powder, in an argon atmosphere tube furnace for a desired period of time. The interface reaction

between the two materials was then examined by carefully removing the disc from the Fe₂O₃, sectioning and mounting it, and analysing it by SEM. XRD analysis of the flat side of a non-sectioned disc allowed the surface, down to a depth of about 5µm to be analysed. Any iron oxide that was still bonded to the disc was also included in the analysis. Experiments that were conducted are shown in table 5.5.

Table 5.5 Furnace Temperatures and Hold Times Employed in Series 4 - Bulk Titanium Samples Experiments	
Furnace Temperature / °C	Hold Time / minutes
800	45
900	30
1200	15

5.3 Results

5.3.1 Series 1 : Titanium Powder Pellets Heated in Air

5.3.1.1 Series 1A : Titanium Powder Pellets Held in a Pre Heated Furnace in Air.

Table 5.6 details the densities of the pellets. The values are rounded to the nearest whole percent. Table 5.7 records the temperature of the furnace that was required to promote ignition of the pellet and the effect of the furnace temperature on the time it took for a <150µm titanium pellet to ignite.

Table 5.6 The Calculated Pellet Densities for Various Pellet Compositions Under Hand and Hydraulic Compaction		
<u>Titanium Powder Size</u>	<u>Density of Hand Pressed Pellet</u>	<u>Density of Hydraulic Pressed Pellet</u>
(l) <355 μ m	41%	68%
(l) 355-250 μ m	38%	68%
(l) 250-150 μ m	37%	66%
(g) <150 μ m	42%	67%
(g) 150-90 μ m	36%	75%
(g) 90-53 μ m	39%	76%
(g) <53 μ m	42%	79%
(l) denotes powder from LSM (g) denotes powder from Goodfellows		

Table 5.7 The Furnace Temperature Required to Promote the Ignition of Compacts from Experimental Series 1A in Air.	
<u>Powder Size / μm</u>	<u>Ignition Temperatures / $^{\circ}$C</u>
<355	650
<150	600
355-250	575
250-150	575
150-90	525
90-53	525
<53	500
The Effect of the Furnace Holding Temperature on the Time Taken for Experimental Series 1A Compacts to Ignite in Air.	
<u>Furnace Temperature / $^{\circ}$C</u>	<u>Time to Ignition / minutes</u>
950	0.5
850	0.5
750	1.5
650	3.5
600	4.5

Figure 5.1 shows a <355 μ m titanium powder pellet after hydraulic pressing.

Figure 5.2 is the same pellet after being placed in an air atmosphere furnace at

650°C for 20 minutes. The pellet has a white / yellow outer surface and there is evidence in the sectioned pellet, of a change in colour of the titanium powder that is close to the pellet surface. The bulk of the titanium powder remains visibly the same as the as-pressed pellet, retaining its original colour and still in powder form.

In comparison, figure 5.3 shows a hand pressed <355µm titanium powder pellet after heating under the same conditions as the hydraulically pressed pellet seen in figure 5.2. The left hand pellet shows the top outer surface, the right hand pellet is sectioned. The top surface is again predominately a yellow / white colour. The grey area on the surface of the pellet is caused by incomplete combustion, due to that area touching the furnace boat.

The sectioned pellet reveals the internal morphology. The outer most layer is again white / yellow, the next layer is grey. A thin gold layer separates the grey layer from the internal purple / blue colour titanium.

The dimensions of a typical hydraulically pressed <150µm titanium powder pellet are shown in figures 5.4 and 5.5. Figure 5.6 shows the pellet after it had been placed in the furnace at 600°C. The left hand pellet is sectioned and the right hand pellet details the outer surface. As in the <355µm titanium pellets, the outer surface is a yellow / white colour. The sectioned pellet reveals three distinct layers; the white / yellow outer coating, an intermediate golden with purple / blue layer and the internal grey area.

Figures 5.7 and 5.8 show the results from hand pressed pellets that have undergone the same heating process. Figure 5.8 is taken under different lighting conditions. In figure 5.7, the upper sample shows a side view of the pellet. The typical white / yellow outer coating is apparent. It is seen to have a 'shiny' appearance. The bottom two samples are sections. It can be seen that significant changes have occurred. Four distinct regions exist within both the pellets. They can be more clearly seen in figure 5.8. The layers can be categorised as follows.

1. A white / yellow colour, shiny outer surface.
2. A grey, porous layer beneath.
3. A blue / purple / gold coloured layer.
4. A foam like central core.

Closer microscopic observations reveal additional features. Layer 2 is a grey foam of ceramic appearance and consistent morphology across its width. Layer 3 is still powdery and can be scraped away with tweezers. Layer 4 (the internal core) is of metallic appearance and has a coarse foam structure.

The optical pyrometer was employed to record the temperature profiles of the $<355\mu\text{m}$ and $<150\mu\text{m}$ hand and hydraulically pressed titanium powder pellets as they burnt in the air furnace set at 650°C . Figure 5.9 plots the recorded temperature against time for the pellets. The effect of the powder size and the pressing conditions can be seen. From optical observations it was possible to see the pellet heat up before a visible combustion wave passed through the

pellet. The combustion wave always originated from the corner of the pellet nearest the rear furnace wall, the hottest place in the furnace. The maximum recorded combustion temperatures for the pellets under investigation are shown in Table 5.8.

Table 5.8 The Maximum Recorded Combustion Temperatures of Pellets of Different Titanium Particle Size and Pressing Conditions, as they Burn in an Air Atmosphered Furnace Held at 650°C	
<u>Powder Size / μm and Pressing Condition</u>	<u>Maximum Burning Temperature / °C</u>
<150 Hand	1825
<150 Hydraulic	1660
<355 Hand	1650
<355 Hydraulic	1350

5.3.1.2 Series 1B : Titanium Powder Pellets Heated at 10 °C / Min in Air

Table 5.9 records the temperature of the furnace required to promote ignition of the pellets.

Table 5.9 The Recorded Furnace Temperature Required to Promote Ignition in Compacts from Series 1B Experiments in a Air Furnace with a 10°C min⁻¹ Heating Rate	
<u>Powder Size / μm</u>	<u>Minimum Furnace Temperature Required to Promote Pellet Ignition / °C</u>
355-250	800
150-90	550
>53	500

Pellets that had undergone ignition had similar morphologies to those seen in pellets that had ignited in pre-heated furnaces e.g. figure 5.8. Figure 5.10

shows the relationship between the furnace temperature required to promote ignition of the pellets in both series A and B.

5.3.2 Series 2 : Titanium Powder + Al₂O₃ Pellets Heated in Air and Argon

Table 5.10 details the temperature of the furnace required to promote ignition of the pellet. Table 5.11 details the calculated densities of the pellets used in the experiments.

Table 5.10 The Temperature of the Air Atmosphere Furnace Required to Promote Ignition of the Hydraulically Pressed Al₂O₃ + 3Ti Pellets from Experimental Series 2.		
<u>Composition</u>	<u>Titanium Particle Size</u>	<u>Minimum Furnace Temperature Required to Promote Ignition of the Compact / °C</u>
Al ₂ O ₃ + 3Ti	<150µm	600
Al ₂ O ₃ + 3Ti	<355µm	650
The Temperature of the Argon Tube Furnace Required to Promote Ignition of Hydraulically Pressed Al₂O₃ + 3Ti Pellets from Experimental Series 2.		
Al ₂ O ₃ + 3Ti	<150µm	No ignition
Al ₂ O ₃ + 3Ti	<355µm	No ignition

Table 5.11 The Calculated Densities of Hydraulically Pressed Pellets of Al₂O₃ + 3Ti with Different Titanium Powder Sizes as used in Experimental Series 2.	
<u>Titanium Powder Size</u>	<u>Density of Pellet</u>
<355µm	72%
<150µm	73%

Figure 5.11 is an optical photograph of a hydraulically pressed <150µm titanium powder pellet prior to heating in the furnace. Figures 5.12 and 5.13 are

optical micrographs of powder taken from the pellet surface after heating at 650°C for 20 minutes. At this furnace temperature the pellet has ignited. Optically, the pellets that have ignited have a similar morphology to those seen in figure 5.2. The pellets have a yellow / white surface coating, followed by a grey porous intermediate layer. The core material still remains powdery and is of a yellow / purple / blue colour.

Two additional interesting features of the powders from these experiments are noted. In the figures the black background matrix is mounting compound, Bakelite. Lower centre (mark X) in figure 5.12 is a silver particle with a thick grey outer layer. EDX analysis reveals the silver material to be titanium and the grey outer layer to be TiO_2 . Other powders in these figures exhibit similar characteristics. Central (mark X) in figure 5.13 is a grey particle with a dispersion of a dark grey secondary phase. EDX analysis reveals the dark grey dispersion to be Al_2O_3 and the surrounding grey material to be TiO_2 . The diameter of the Al_2O_3 particles is similar to the size of the starting Al_2O_3 powder.

A coherent piece of the surface from the reacted pellet is shown in figure 5.14. Central to the figure (mark X) is a silver particle, EDX analysed to be Ti, surrounded by a dark grey layer (mark Y) of TiO_2 . The light grey background matrix (mark Z) was EDX analysed to contain Ti, Al and O.

The grey, porous intermediate layer is shown in figure 5.15. A larger silver particle (mark X), EDX analysed to be titanium, is in the top left corner of the

figure. The remainder of the figure depicts the grey layer (mark Y). EDX analysis reveals the layer to be TiO_2 , with the dispersion of dark grey particles as Al_2O_3 . Titanium metal is found around the outside of the grey TiO_2 foam (mark Z). Figure 5.16 is an XRD analysis of the crushed pellet. Titanium, TiO_2 (rutile) and Al_2O_3 are the only phases detected. No detectable Al / Ti compounds are formed.

Figure 5.17 is an optical micrograph of powders taken from a pellet heated to 650°C in the argon atmosphered furnace. No sign of reaction is detected, the powders have the same morphology as the as received material. XRD analysis of the powder detected no TiO_2 .

5.3.3 Series 3 : Titanium Powder + Fe_2O_3 Pellets Heated In Air and Argon

Table 5.12 records the experimental results for this series.

Table 5.12 The Minimum Temperature of the Air Atmosphere Furnace Required to Promote Ignition of the Hydraulically Pressed Fe₂O₃ + 3Ti Pellets of Various Titanium Powder Sizes from Experimental Series 3.				
<u>Composition</u>	<u>Titanium Particle Size</u>	<u>Hold Time /minutes</u>	<u>Minimum Furnace Temperature Required to Promote Ignition of the Compact / °C</u>	<u>Time to Ignition / minutes</u>
Fe ₂ O ₃ + 3Ti	<150µm	20	600	3.0
Fe ₂ O ₃ + 3Ti	<150µm	60	600	3.0
Fe ₂ O ₃ + 3Ti	<355 µm	60	650	3.5
The Minimum Temperature of the Argon Atmosphered Tube Furnace Required to Promote Ignition of the Hydraulically Pressed Fe₂O₃ + 3Ti Pellets of Various Titanium Powder Sizes from Experimental Series 3.				
Fe ₂ O ₃ + 3Ti	<150µm	60	600	Not Recorded
Fe ₂ O ₃ + 3Ti	<355µm	60	650	Not Recorded

Table 5.13 records the densities of the pellets used in the experiments.

Table 5.13 The Calculated Densities of Hydraulically Pressed Fe₂O₃ + 3Ti Pellets Containing <355µm or <150µm Titanium Powders.	
<u>Titanium Powder Size</u>	<u>Pellet Density</u>
<355µm	74%
<150µm	74%

Figures 5.18 and 5.19 show a <150µm titanium and Fe₂O₃ pellet prior to heating. The even dispersion of titanium powder in the Fe₂O₃ can be seen by examination of the top surface of the pellet in figure 5.18. The pellet after heating in an air atmosphere furnace at 600°C is shown in figure 5.20. The product consists of solidified 'puddles' of material. The outer coating of the material is white / yellow in colour. A schematic of the product morphology is shown in figure 5.21

When crushed, the 'puddle' was seen to consist of a ceramic shell surrounding a metallic lump. XRD analysis of the crushed ceramic shell is shown in figure 5.22. The shell consists of TiO and Ti₂O₃ oxides. Whilst the morphology of the product was consistent under both atmospheres the XRD data detected the presence of Fe₂Ti in the reactions that occurred in air. No Fe₂Ti was detected in the argon atmosphere reactions. The XRD analysis was based on a powder sample and therefore the metallic lump was not included.

Figure 5.23 is an SEM micrograph of the metallic part of the sample. Some dark grey ceramic phase is seen in the lighter grey metallic phase. EDX analysis of the metallic phase reveals it to be ~90% iron / 10% titanium. The ceramic phase was EDX analysed to be the composition of TiO.

Pellets that had not ignited after the period of time in the furnace were analysed. These 'sintered' samples may provide information concerning the reaction mechanisms that occur between the powders prior to ignition.

5.3.3.1 *'Sintered' Compacts Heated in Air*

Figure 5.24 is a E-SEM photo of powder taken from a pellet containing <150µm titanium powder that had been heated to 650°C for 3 minutes. A titanium particle (mark 1) surrounded by Fe₂O₃ powder (mark 2) is seen. The Fe₂O₃ powder has sintered and there is intimate contact between the sintered Fe₂O₃ and the titanium particle in the form of a bridge between the two (mark 3).

Figure 5.25 is an E-SEM photo of two titanium powders, in contact with one another and some Fe₂O₃ powder. The Fe₂O₃ powder at the upper left hand side of the figure (mark 1) appears to be sintered to the titanium. Figure 5.26 is the backscattered electron image of figure 5.25. Table 5.14 details the EDX analysis obtained at the points marked on figure 5.26.

Mark	Ti at%	O at%	Fe at%
1	15	48	38
2	10	44	47
3	86	8	7
4	60	33	7

Figure 5.27 and the related close up image in figure 5.28 are backscattered electron images of two titanium powder particles, surrounded by Fe₂O₃, taken from the same pellet. Table 5.15 details the EDX analysis obtained at the relevant marks on figure 5.28.

Mark	Ti at%	O at%	Fe at%
1	4	45	51
2	37	43	20
3	50	46	4

Figure 5.29 and the related backscattered image in figure 5.30 detail a ~80µm titanium powder particle surrounded by Fe₂O₃. Close up images of the titanium powder particle are shown in figure 5.31 and the related backscattered image in

figure 5.32. The obtained EDX analysis of areas marked on figure 5.32 are shown in table 5.16

Mark	Ti at%	O at%	Fe at%
1	100	0	0
2	100	0	0
3	83	17	0
4	48	52	0
5	42	58	0
6	44	56	0
7	4	51	45
8	2	49	49

5.3.3.2 'Sintered' Compacts Heated in Argon

A difference was observed in the oxide shell around the titanium particles when it was heated in an air or argon atmosphere.

Figure 5.33 is an optical micrograph of a pellet containing $355\mu\text{m}$ titanium that had been held at 650°C for 60 minutes. An oxide shell (mark 1) around a titanium powder particle (mark 2) is seen, the oxide shell contains bright metallic looking particles. The larger particles appear on the outer edge of the oxide layer, and smaller particles are scattered within it.

Figure 5.34 is a SEM SEI micrograph of powder taken from the same sample. Bright particles are seen within the oxide shell (mark 1) that has broken away from the central titanium particle (mark 2).

Figures 5.35 and 5.36 are SEM micrographs of powder taken from a pellet containing $<150\mu\text{m}$ titanium that had been held at 550°C for 60 minutes. The two micrographs show the same area of sample, figure 5.35 is taken with secondary electrons, figure 5.36 from backscattered electrons. In figure 5.36 titanium particles (marks 1) with a substantial oxide layer (mark 2) surround some iron oxide powder (mark 3). The presence of the secondary phase within the oxide layer is clear to see. The atomic number of the secondary phase is far higher than the titanium metal, the oxide layer or iron oxide powder. The fineness of the secondary phase precluded it from accurate EDX analysis.

5.3.4 Series 4 : Bulk Titanium and Fe_2O_3 Reactions

Figure 5.37 is a XRD analysis of Fe_2O_3 powder, heated in an air or argon furnace at 800°C for 1 hour. The results are used as control for the experiments. XRD analysis of the surface of the discs after heating in argon are shown in table 5.17.

<u>Furnace Temperature / °C</u>	<u>Hold Time / minutes</u>	<u>Phase Identified by XRD Analysis</u>
800	45	TiO ₂ , FeO
900	30	TiO ₂ , FeO
1200	15	TiO ₂ , Ti

Some titanium metal was detected within the 1200°C sample as the surface of the disc had substantially flaked, and thus was revealing the internal material. The peaks detected for titanium metal were very small and had shifted slightly along the 2 θ scale, which is probably due to the absorption of oxygen into solution within the matrix.

The interface between the titanium and the Fe₂O₃ was investigated by E-SEM. Figure 5.38 shows an intact area of the reaction interface. Figure 5.39 is a close up region 1 in figure 5.38. The EDX analysis of the material at the points highlighted on the figure are shown in table 5.18

<u>Mark</u>	<u>Ti at%</u>	<u>O at%</u>	<u>Fe at%</u>
1	100	0	0
2	41	59	0
3	46	54	0
4	2	50	48

The small scale of the interface precludes accurate analysis of finer areas.

A cracked section of the interface from the same sample is shown in figure 5.40. EDX analysis of the material at the points detailed is shown in table 5.19

Mark	Ti at%	O at%	Fe at%
1	32	67	1
2	45	55	0
3	33	67	0

The morphology of the interface of the 1200°C sample is shown in figure 5.41. EDX spot analysis at a number of places around the area conclusively place the composition as TiO₂. The outside layer (mark 1) has a denser morphology to the inner areas (mark 2).

5.4 Discussion

5.4.1 Series 1: Titanium Powder Pellets Heated In Air

Series 1 experiments investigated the oxidation and ignition characteristics of pressed titanium powder compacts, heated in air. Experiments have been conducted that examine the influence of the ambient temperature, the titanium powder diameter and the pellet density, on the oxidation and ignition mechanisms of the pellet in air.

It is well known that the oxidation of titanium is exothermic (Kubaschewski and Hopkins 1953). When the oxidation rate is small enough and the sample

large enough, the energy released by the oxidation results in a negligible temperature rise within the sample. However Sirca *et al.* (1991) have shown that by reducing the size of the sample, maximising its surface area and increasing the oxidation rate, the energy released by oxidation can cause significant rises in the temperature of the sample. These temperature rises can be large enough to cause localised melting of the sample that consequently leads to ignition and combustion.

Previous researchers (Tavgen *et al.* 1992, Rodes and Hlavacek 1994, Merzhanov *et al.* 1995 and Bakhman *et al.* 1998) have examined the oxidation of titanium powder, pressed and loose, under various conditions. It is clear that oxidation of titanium is detectable from around 455°C, with powder ignition or detectable rises in sample temperature occurring from around 500°C.

5.4.1.1 *The Effect of the Pellet Size and Density*

The pellet density is known to have a considerable effect on the ignition of pellets of titanium heated in gaseous environments (Bakhman *et al.* 1998, Filonenko and Barzykin 1996 and Dunmead *et al.* 1989). In this research the pellets had densities between 36-42% of theoretical and were of consistent size, at 12mmØ and 15mm length. It was found that the pellet density is not dependent on the titanium powder size used in the pellet (table 5.6), however, this variation of pellet density across the powder size range can be discounted as it is small and not consistent with the effect that pellets made from smaller powders ignite at lower furnace temperatures (table 5.7). As such the effect of pellet density and size were not investigated in this research.

5.4.1.2 *The Effect of the Titanium Powder Diameter*

It is seen that there is a clear relationship between the temperature required to promote ignition in a pellet and the titanium powder diameter (table 5.7). The results show that the furnace temperature required to promote ignition decreases as the diameter of the titanium powder decreases.

This effect has not been critically examined in the literature. No conclusions could be drawn from Rode and Hlavacek's (1994) work as the previous thermal history of the powder and the powders chemical purity overrode any powder diameter effect on the ignition temperature of the sample. However, it was shown that an oxygen content of ~1.5 at% of the powder particle was enough to influence its ignition temperature. In the experiments conducted in the current research, two sources of titanium powder were used. They were both manufactured by the same method and stored under the same conditions. The chemical analysis of the powders revealed that the <355 μm titanium powders have twice as much oxygen than the <150 μm powders (tables 4.1 and 4.3), however, the quantities are still less than 1 at% and therefore are not seen as an overriding factor in the reactivity of the powder.

The tendency of small diameter powder pellets to ignite at lower temperatures than those made from larger diameter powders is due to the surface area to volume ratio. Smaller diameter powders have a larger surface area to volume ratio than larger powders. For an ideal particle oxidising exothermically at a constant rate, $X \text{ J} / \text{mm}^2$ of surface area would be liberated. The smaller powder has a higher energy liberated per volume of material than the larger.

Therefore, under fixed conditions, the temperature rise of the smaller powder would be greater. This, in turn, leads to an increased oxidation rate and heat energy output (Rode and Hlavcek 1994).

5.4.1.3 *The Effect of the Heating Rate*

The pellets used in the research were of consistent size and density. For a certain powder fraction it is therefore assumed that the thermal conductivity would be the same for all pellets (Kalpakjian 1992). In series 1A experiments (where cold pellets were placed into heated furnaces) the heating rate of the pellets increases with the furnace temperature, the net effect being that the time spent at the lower temperatures decreases as the furnace temperature increases. This effect is fully investigated in the next two chapters. The recorded time to ignition fell as the furnace temperature increased, although this was not critically examined, table 5.7.

Series 1B (10 °C / min heating rate) revealed that a higher furnace temperature is required to ignite the pellets when they are heated at a slow rate when compared to the rapid heating that occurs when they are placed in the furnace at a constant temperature, figure 5.10. This effect was seen by Rode and Hlavacck (1994) who proposed that the thickness of the oxide shell influences the ignition temperature of the titanium powders (figures 3.5 and 3.6). Powders heated at slow rates have more time to grow an oxide layer than powders placed into a hot furnace. The thicker oxide layer slows additional oxidation, and thus heat energy release. It is only when the oxide reaches a thickness sufficient for it to crack, leading to metal air contact, that ignition occurs. The

experimental evidence detailed in figure 5.10 verifies this theory. The <355 titanium powder, which ignites when placed in a hot furnace at 650°C, required the furnace to be at ~800°C when heated at 10°C / min., to promote ignition.

It has been proposed that oxidation of titanium is only significant above ~500°C (Tavgen *et al.* 1992 and Merzhanov *et al.* 1995); thus small diameter powders (<53µm) which ignite at around that temperature have no time to gain a significant oxide layer before ignition. The <355µm powders require rapid exothermic oxidation before they ignite, evidenced by the 650°C furnace temperature that promoted ignition. The slow growth of the oxide layer when the heating rate is 10 °C / min is not sufficiently exothermic to promote ignition as the exothermic heat is lost to the surroundings. The oxide's growth additionally stifles the oxidation rate. This raises the ambient temperature required to ignite them. It is therefore possible to either reduce the heating rate, or increase the particle size, to such an extent that ignition would never occur. The sample would just oxidise completely without ever combusting.

5.4.1.4 Oxidation Characteristics of the Pellet

The oxidation of the pellet is of great interest in the understanding of the mechanisms which promote pellet ignition. In the experiments conducted in this research the size of the titanium powder and the pellet density are the two factors which influence these mechanisms.

The combustion temperatures of the pellets as they oxidise is related to the pellet density and the powder diameter. Figure 5.9 and table 5.8 shows that the low density, hand pressed, $<150\mu\text{m}$ titanium pellets have the highest combustion temperature, whilst the hydraulically pressed $<355\mu\text{m}$ titanium pellets have the lowest. It is known that the melting point of one of the reaction phases is often the maximum temperature a reaction will reach (Glassman and Papas 1994). This relationship is observed in the burning of titanium powder pellets in air. The hand pressed $150\mu\text{m}$ pellet has a maximum reaction temperature of $\sim 1830^\circ\text{C}$. Taking into account any errors in the measurement, this is very close to the melting point of TiO_2 (1855°C). The maximum reaction temperatures of the hydraulically pressed $150\mu\text{m}$ titanium and hand pressed $<355\mu\text{m}$ titanium pellets are 1660°C , which is exactly the same as the melting point of titanium metal. The hydraulically pressed $<355\mu\text{m}$ pellet has a lower recorded reaction temperature of 1350°C . If this is accurate, it is evidence that the compact has only undergone a solid state exothermic oxidation reaction.

Figure 5.9 reveals additional information about the combustion waves of the pellets. As the pyrometer is focused on one discrete area of the pellet it records the time the combustion wave is in that area. A shorter time indicates a faster combustion wave. The combustion speed is seen to increase with maximum combustion temperature, indicating that pellets with lower densities and smaller powder diameters have higher reaction rates. This observation is in agreement with Filonenko and Barzykin (1996), figure 3.11 and Kudo and Odawara (1989), figure 3.12. The lower density of the compact (higher

porosity) facilitates oxygen penetration into the pellet. This increases the amount and rate of powder reacting, raising the combustion wave temperature. Small diameter powders ignite at lower temperatures and are consumed at a faster rate than larger powders, hence the combustion wave is smaller in width (rapid ignition and consumption) but is hotter (more powder reacting and heat output) and travels faster (powder ignites at lower temperatures) than that of a larger powder pellet.

An interesting phenomena recorded for the hand pressed $<355\mu\text{m}$ titanium pellet is the occurrence of an 'after burn' as described by Dunmead *et al.* (1989) and shown in figure 5.42 . The 'after burn' occurs when the combustion wave progresses back up the compact, converting more of the metal to the product. Dunmead *et al.* (1989) observed the effect when burning titanium in nitrogen. The product of the primary combustion wave is a layer of TiN around the titanium powders. There is also substantial nitrogen in solid solution in the titanium. The second (afterburn) combustion wave increased the thickness of the TiN layer and the amount of nitrogen in solid solution in the titanium.

It is seen from figures 5.2, 5.3, 5.7 and 5.8 that the totality of conversion of the titanium metal to oxide is greatly affected by the pellet density, and to a lesser extent, the powder diameter. The degree of morphological change is directly linked to the pellets maximum combustion temperature as referenced above (table 5.8). The hand pressed pellets show significant changes to their morphology when compared to their initial state. The hydraulically pressed pellets show less evidence of oxidation. The changes have been classified in

section 5.3 and can be attributed to the high temperature oxidation of the titanium. The white / yellow layer outer skin colour and morphology is characteristic of a thick, defect rich, layer of TiO_2 (Rode and Hlavacek 1994 and Abbud-Madrid *et al.* 1996). Beneath that, the grey porous layer is characteristic of a thin layer of TiO_2 . In next layer the colour change of titanium from blue \Rightarrow purple \Rightarrow violet \Rightarrow gold reflects the changing oxides present on the remaining powders. TiO_2 is white, but oxygen deficiencies darken its colour to grey or blue, Ti_3O_5 is blue / purple, Ti_2O_3 is violet and TiO is golden yellow (table 3.2). It is therefore obvious that the amount of titanium oxidation decreases towards the centre of the pellet. Within the centre of the hand pressed $<150\mu\text{m}$ titanium pellet is a porous mass of titanium metal.

The change in morphology within the pellet can be attributed to the presence of oxygen within the pellet and the exothermic heat generated by that oxidation. Obviously, titanium can only oxidise if there is oxygen present. Thus, in all cases, the surface has undergone the most significant oxidation and is consistent across all the samples. The pellet density and powder diameter have a greater effect on the internal oxidation. A highly dense pellet has a much lower porosity than a low density pellet, thus, oxygen has difficulty travelling inward to the centre of a highly dense pellet. Work by Dunmead and Munir (1989) and Bakhman *et al.* (1998) confirm the effect of pellet density on the conversion of titanium by gaseous media, figure 3.8. In the case of a pure nitrogen atmosphere, conversion of the titanium to TiN , is increased as the nitrogen pressure is increased and / or the pellet density decreased, figure 3.9. In agreement with this, it has been shown that the limiting factor in the

combustion of titanium is the availability of oxygen, and its ability to get to the combustion front (Abbud-Madrid *et al.* 1996). The work presented here agrees with these findings. The oxidation is seen to greatest on the outside and least in the centre.

The two interesting features found in the pellets are the porous TiO₂ layer just under the surface of the hand pressed pellets and the porous titanium mass found, in particular, at the centre of the <150µm titanium pellet. The TiO₂ layer could only have formed in the presence of a liquid phase, as it is not a sintered powder (individual powders sintered together exhibiting necks and solid state diffusional bonds), but a porous solid (a foam). In pellets where the exothermic oxidation of the pellet is sufficient to raise the temperature of the pellet above the melting temperature of titanium, the titanium will be liquid. The effect of the combustion wave, only melting a certain part of the pellet at one time, could form the porous solid. This phenomena is expanded upon in series 2, figure 5.15.

The lack of complete combustion of the pellet can be explained by the formation of the outer oxide layer. This inhibits the free passage of oxygen toward the centre of the pellet and limits the reaction. The effect has been seen previously by Bakhman *et al.* (1998). The metallic foam in the centre of the hand pressed <150µm titanium pellet can be explained by the high temperature of the reaction and the lack of oxidising conditions caused by the oxide shell. This enables the central core to liquefy but not to oxidise. The metal is not in a solid lump as the combustion wave passes down the pellet and therefore the

internal powders do not liquefy at the same time, but rather particle by particle. This causes the porous structure. The same effect may cause the porosity in the TiO_2 layer.

At high pellet densities the oxidation of the internal powders is considerably reduced, figure 5.2. The outer skin is still present but there is very limited oxidation of the internal powders. The lack of porosity and probable rapid sealing over of the external pores by the surface oxidation reaction, limit the oxidation of the powder. The lack of conversion of the powders is a common trait in the gas-phase SHS reaction of high density pressed powder pellets. (Kudo and Odawara 1989, Filonenko and Barzykin 1996 and Dunmead and Munir 1989)

5.4.2 Series 2 : Titanium Powder + Al_2O_3 Pellets Heated in Air and Argon

Series 2 experiments analysed the effect that small particles within the titanium powder would have on the oxidation and ignition characteristics of the pellet. These pellets were designed to have a similar morphology to that of a $\text{Fe}_2\text{O}_3 + 3\text{Ti}$ pellet. Due to this similarity in morphology, the oxidation of these pellets would reveal the effect of separating the titanium particles and the effect that gaseous oxidation has on the titanium present in the $\text{Fe}_2\text{O}_3 + 3\text{Ti}$ pellets. The effect of just the Fe_2O_3 on the oxidation can then be deduced.

Titanium powder pellets containing Al_2O_3 were pressed hydraulically, and show an increased density over pure titanium pellets due to the pore filling

effect of the fine Al_2O_3 , table 5.11. The Al_2O_3 containing pellets had densities of ~72%; similar pure titanium pellets had densities of ~67%. For the size of titanium powder in question, both the Al_2O_3 containing and pure titanium pellets are seen to require the same furnace temperature to promote ignition. As the pellet densities are not significantly different, in this context, Al_2O_3 has no effect on the temperature that was required to promote ignition of the pellet.

The reacted pellets had similar morphologies to the titanium pellets. As they were hydraulically pressed, oxidation was limited but still evident. As in the pure titanium pellets from Series 1, a TiO_2 skin is seen to have formed over the surface of the pellets. The structure of the oxide skin is detailed in figure 5.14. Beneath the skin, the porous TiO_2 layer (mark Y) is found, figure 5.15. A comparison of this layer and the titanium powder (mark X) typifies the degree of change in the morphology. The TiO_2 is clear to distinguish from the silver titanium metal (mark Z).

The presence of a liquid phase was found conclusively in the Series 1 experiments. Proof of the presence of liquid titanium or TiO_2 is found in figure 5.13 and figure 5.15 where Al_2O_3 particles are found within the formed TiO_2 oxide. Thus, even at these high densities with the presence of inert particles, the exothermic oxidation of titanium is sufficient to cause localised melting of the titanium. The titanium is thought to have melted rather than the TiO_2 as the maximum combustion temperature of a pure hydraulically pressed $<150\mu\text{m}$ titanium pellet is seen to be 1660°C , close to the melting point of titanium.

XRD analysis of the reacted pellet, figure 5.16 shows that the oxidation product is TiO_2 and that there is no detectable Al_2O_3 / Ti reaction. As expected, pellets that were heated under an argon atmosphere show no signs of oxidation or reaction.

5.4.3 Series 3 : Titanium Powder and Fe_2O_3 Pellets Heated in Air and Argon

Series 3 experiments investigated the reaction that occurs when pressed pellets of $\text{Fe}_2\text{O}_3 + 3\text{Ti}$ powders are heated in air or inert atmospheres. An understanding of this reaction is the initial step in understanding the complex interactions that occur between Fe_2O_3 and titanium when they heated.

Many self-propagating SHS reactions between two solid reactant compounds are initiated by the formation of a liquid phase. The liquid phase allows the reaction rate to increase by orders of magnitude, facilitating the self-propagating exothermic reaction. Experiments in Series 1 and 2 reveal that a titanium based liquid phase (titanium metal or TiO_2) occurs during the combustion of titanium in air, although this may not be the initiating step.

In these experiments, pellets of composition $\text{Fe}_2\text{O}_3 + 3 \text{Ti}$ were pressed hydraulically. Titanium powders of $<355\mu\text{m}$ and $<150\mu\text{m}$ were used in the pellets. The densities of the pellets were $\sim 74\%$ of theoretical, table 5.13. This slight increase in density in the Fe_2O_3 containing pellets over those in Series 2 was due to the Fe_2O_3 's inherent moisture content, that aids compressibility over the dry Al_2O_3 powders. However, the pellet morphology - porosity, density and particle arrangement in the pellet - was similar between the two.

Under both air and argon atmospheres, the $<355\mu\text{m}$ Ti + Fe₂O₃ pellets required a furnace of 650°C to promote ignition, whilst the $<150\mu\text{m}$ Ti + Fe₂O₃ pellets required a 600°C furnace. These temperatures are the same as those that were required to promote ignition in the Al₂O₃ + 3Ti pellets of Series 2. The time to ignition of the pellets is also similar to the pure titanium powder pellets, table 5.12.

5.4.3.1 *Reactions In Air*

In the case of the air furnace, the furnace temperature and time that was required to promote ignition in the Al₂O₃ and Fe₂O₃ containing pellets was the same. There is no difference between these temperatures as the liquid phase that forms during the oxidation of titanium by air, as seen in Series 1 and 2, would have initiated the reaction between the Fe₂O₃ and titanium. Whatever the composition of the first liquid phase, the reaction is initiated in the same time frame as pure titanium pellets. This is indicative of similar reaction kinetics and thus a similar ignition mechanism – the exothermic oxidation of solid titanium by gaseous oxygen reaching a sufficient temperature that a liquid phase forms.

The product of the reaction is seen to be completely different to that of those in Series 1 or 2, figure 5.20. The exothermicity of the reaction has completely melted both the products to form a 'puddle' in the furnace boat. Upon examination the 'puddle' was seen to consist of a ceramic shell containing a discrete metallic lump within, figure 5.21. To form this morphology the products must have been liquid at some point. The additional energy required

to melt the products is produced by the exothermic oxidation – reduction reaction that occurs between the titanium and the Fe_2O_3 . As the Fe_2O_3 is dispersed throughout the pellet and in stoichiometric quantities, there is no oxygen deficiency and conversion of all the titanium to oxide occurs.

The ceramic shell and predominately iron metallic core both contain small quantities of each other. The SEM micrograph in figure 5.23 shows a portion of the metallic phase. Within the light metallic part of the sample, clearly defined darker TiO areas are seen. Some of the areas appear to have dendritic features which is evidence of the TiO precipitating from the melt.

As these reactions have been carried out in air, it is not clear what reactions are occurring as the pellet is heated. It is probable that the initial reaction is between titanium and gaseous oxygen. This oxidation becomes increasingly exothermic and at a point, the Fe_2O_3 and titanium reaction will initialise. Whether this reaction occurs before or after the formation of a liquid phase is impossible to determine from these experiments.

From figure 5.9 it is seen that the reaction temperature reached by a hydraulically pressed $<150\mu\text{m}$ pure titanium pellet is 1650°C . Fe_2O_3 and iron have melting temperatures of 1565°C and 1535°C respectively, titanium melts at 1670°C . It is therefore conceivable that the first liquid phase to form contains iron. This could be confirmed as the XRD analysis in figure 5.22 shows that Fe_2Ti is present in the ceramic shell product. This is evidence that titanium / iron intermetallics are forming.

5.4.3.2 'Sintered' Samples Heated in Air

The actual course of the reaction between the Fe_2O_3 and the titanium can be investigated by the analysis of pellets which have been heated to below the ignition promoting temperature. These pellets reveal the process of oxidation and reduction that occurs between titanium and Fe_2O_3 powders that are in intimate contact. There is free oxygen available from the atmosphere that will influence the process of oxidation.

The E-Sem photomicrographs in figures 5.24 through to 5.32 reveal in detail the reaction between Fe_2O_3 and titanium powder when heated in air. All the figures come from identical samples.

Figures 5.24, 5.25 and 5.26 show the initial stages of the reaction between titanium and Fe_2O_3 . Sintering of Fe_2O_3 particles occurs, figure 5.24, and Fe_2O_3 sinters to the titanium as well, figure 5.25. The morphology of the pellet clearly enables Fe_2O_3 powders to be in intimate contact with the titanium, figures 5.25 and 5.26 and table 5.14. In marks 1-3 the oxygen concentration decreases in accordance with the visible reduction in the amount of Fe_2O_3 present between the titanium pellets. This is evidence of a pure titanium and Fe_2O_3 reaction as opposed to a titanium and air reaction. Interestingly, the oxygen concentration found under mark 4 of figure 5.26 is roughly the maximum solubility of oxygen in α titanium.

The next stage of the reaction is seen in figures 5.27 and 5.28. From the EDX analysis of figure 5.28, table 5.15, it is clear that TiO is forming around the

titanium particle (mark 3). The Fe_2O_3 is being reduced to FeO during this process (mark 1). Between these phases is a mixed titanium / iron oxide. The Fe_2O_3 powder is additionally sintering together. This is evidence of localised heating of the powder, as the surrounding Fe_2O_3 remains unsintered. Morphologically, these reaction sites are where Fe_2O_3 is pressed between titanium powders. The titanium oxide is forming on the titanium metal surface – as can be seen in figure 5.28. This is evidence that the titanium cations are moving into the Fe_2O_3 . This is characteristic of the initial stages of titanium oxidation. The portion of oxide under mark 3 could have easily been a Fe_2O_3 powder that has been changed to TiO . This theory is supported by the presence of Fe in this area.

The next stage in the reaction can be seen in figures 5.29, 5.30, 5.31 and 5.32. Figures 5.29 and 5.30 show a whole titanium powder particle that has areas of oxidation throughout it. The morphology of the titanium means that there are plenty of areas in which Fe_2O_3 is in close contact with the titanium. The close up SEM micrographs in figures 5.31 and 5.32 clearly show the reaction mechanism. In figure 5.32 Fe_2O_3 is sintered to the outer edge of the titanium oxide that forms over the particle. As the oxidation method is titanium cation movement outwards, the Fe_2O_3 is being consumed by the titanium. The titanium oxide has a composition around that of $\text{TiO} / \text{Ti}_2\text{O}_3$ (marks 4, 5 and 6 in table 5.16). The EDX analysis under mark 3 would include too much of the titanium substrate for an accurate analysis. The iron oxide has a composition near that of FeO (mark 7 and 8 in table 5.32), evidence of Fe_2O_3 reduction by the titanium. Observations of other Fe_2O_3 powders not touching any titanium

show that they have not sintered. It could be that the localised heating caused by the oxidation process is aiding the sintering process. The lack of oxygen found within the titanium powder at marks 1 and 2 is due to the early stage of the reaction.

5.4.3.3 *Reactions in Argon*

The argon furnace experiments differ from the air furnace experiments in two ways, the heating rate of the sample and the inert atmosphere. It was not possible to deduce the ignition time of the argon heated pellets, but it is known from the heating rate of the tube furnace (20 °C / min from 300°C) and their ignition temperature (600°C) that it must take at least 15 minutes to get to the ignition temperature. This is 5 times longer than the air furnace experiments.

In the argon atmosphere, the Al₂O₃ containing titanium powder pellets of Series 2 did not react. As Fe₂O₃ only decomposes slightly in an argon environment up to 800°C, figure 5.37, there must be a reaction occurring between the titanium and Fe₂O₃ that promotes ignition of the pellet. The reaction product of the Fe₂O₃ + 3Ti pellet looks similar to that of a pellet that has reacted in air. Figure 5.22 shows that no Fe₂Ti is detected in the ceramic shell. The reason for this is not known as data such as the combustion temperature and ignition time could not be obtained.

5.4.3.4 *'Sintered' Samples Heated in Argon.*

It is conclusively shown that metallic particles are found within the oxide shells of samples heated under argon, figures 5.33, 5.34, 5.35 and 5.36. These

metallic particles are almost certainly iron, figure 5.36. The particles have come from the reduction of the Fe_2O_3 by the titanium, as it is seen that Fe_2O_3 will not significantly reduce by itself in argon up to 800°C , figure 5.37. The presence of iron particles within the oxide shell, in the argon atmosphere experiments, is due to a different oxidation mechanism than that in the air atmosphere experiments. In an air atmosphere there is an abundance of free oxygen. This can easily combine with the titanium at the surface of the pellet. It is here that combustion is initiated.

In argon, there is no gaseous oxygen to combine with the titanium. All of the oxygen has to come from the reduction of Fe_2O_3 . The reaction is initially solid state as at the furnace temperature that promotes ignition all of the constituents are solid. To promote ignition, the reaction must be exothermic and must form a liquid phase at some point.

It is clear that the $\text{Fe}_2\text{O}_3 + \text{Ti}$ reaction is complex. At present it is impossible to determine the actual reaction mechanism. However, theoretically the reaction between titanium and Fe_2O_3 could occur by titanium cation movement into the Fe_2O_3 . This would form a reaction product layer consisting of a titanium oxide shell containing reduced metallic iron particles. Titanium cations would reach the trapped iron and the possibility of forming iron / titanium intermetallics exists. The formation of FeTi and Fe_2Ti is exothermic and requires a temperature of 700°C or 800°C respectively to initiate (Pribytkov *et al.* 1983). This temperature is only slightly more than the furnace temperature, and as the titanium cations move outward from the titanium particle the first iron -

titanium phase to form would be Fe_2Ti (mtp of 1427°C). The low melting point (1080°C) eutectic (68%Ti – 32%Fe) would possibly occur at a later stage. The iron - titanium intermetallics will be in the centre of the 'hot zone' – the area where most of the exothermic oxidation heat is generated, and as their melting temperatures are some 250°C and 100°C below those of pure titanium and iron respectively, they are the most likely first liquid phases. It is known that the metallic core in the reacted $\text{Fe}_2\text{O}_3 + 3\text{Ti}$ samples contains ~10wt% Ti, so not all the titanium is taken up as oxide.

5.4.4 Series 4 : Bulk Titanium and Fe_2O_3 Reactions

It is known that Fe_2O_3 will not significantly reduce by itself in argon up to 800°C . Thus, any reduction must come from its reaction with titanium. XRD analysis of the surface of the disc heated at 800°C reveals FeO. This has been observed in the reaction zone around titanium particles (figure 5.32, mark 7 and 8). The interface between the titanium and the Fe_2O_3 reveals four distinct layers, figure 5.39. The outer edge is of composition ~FeO (mark 4). Attached to that is a coherent ~TiO layer (mark 3). Beneath that is a powder like ~TiO layer (mark 2). This layer could be sub divided into two distinct areas. The outside edge is the 'powdery' layer, the inner the coherent edge. In from that layer is the titanium metal (mark 1). The outer FeO layer is produced from the reduction of Fe_2O_3 . The sintering effect coming from the exothermic heat generated by the oxidation of the titanium. The TiO layer attached to this is caused by the migration of titanium cations into the material. The diffusion of oxygen into the titanium appears to have formed the layer under mark 2. This is characterised by the appearance of the 'limit of diffusion' band at the

interface between this phase and the actual titanium metal. The layer separating this layer and the outer FeO / TiO layer is of uncertain origin.

A closer examination of the interface in figure 5.40 shows that a ~TiO layer (mark 2) separates two TiO₂ layers. The layers under marks 1, 2 and 3 are equivalent to the layers under mark 3, 2(powdery) and 2(coherent) respectively, in figure 5.39. The layers being TiO₂ rather than TiO could be due to the level of completeness in the reaction. TiO₂ is more stable than TiO and thus is the final product of the reaction if oxygen is abundant. This could be the case in this instance.

5.5 Summary

The reaction mechanism between Fe₂O₃ and titanium has been investigated and the processes that occur when they are heated in intimate contact with one another have been demonstrated. The oxidation of pure titanium in air has been related to the oxidation of a compact of Fe₂O₃ and titanium heated in an inert environment and comparisons have been drawn as to their respective oxidation / reaction mechanisms. To test the theories put forward in this chapter a numerical model has to be constructed to investigate the feasibility of the above described reaction mechanisms. The model is developed and presented in the following chapters.

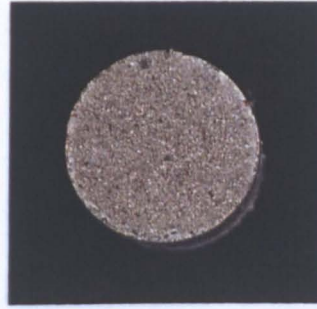
5.6 Conclusions

- The oxidation rate of pressed pellets of titanium powder, and hence its exothermic heat release rate increase as the pellet density and the powder diameter decreases.
- The diameter of the titanium powder effects the surrounding temperature that is required to cause a compact to ignite. Smaller particles require lower ambient temperatures.
- The heating rate of the compact will affect the temperature that is required to promote ignition of the pellet. Slower heating rates increase the required ignition promoting temperature.
- The oxidation of the titanium is seen to be largely confined to the surface of the pellet as the density of the pellet and the formation of a TiO_2 reaction shell reduces air penetration.
- Molten titanium is the first liquid phase to form in pure titanium compact combustion.
- Titanium and Fe_2O_3 powder compacts exhibit the same ignition behaviour as pure titanium powder compacts when heated in air.

- The first liquid phase to form in titanium and Fe_2O_3 combustion in air was not possible to deduce. However, it is likely that the first reaction is between Ti and oxygen from the air.
- Titanium and Fe_2O_3 powder compacts heated under argon have different oxidation characteristics to those heated under air. The first reaction is that of titanium reducing Fe_2O_3 to form titanium oxides and metallic iron.

Chapter 5

Figures



12mm

Figure 5.1 $<355\mu\text{m}$ Titanium Powder Compact, as Hydraulically Pressed.



(a)

(b)

12mm

Figure 5.2 $<355\mu\text{m}$ Titanium Powder Compact, Hydraulically Pressed, After Heating at 650°C for 20 Minutes. (a) Top Surface, (b) Cross-section.



(a)

(b)

12mm

Figure 5.3 $<355\mu\text{m}$ Titanium Powder Compact, Hand Pressed, After Heating at 650°C for 20 Minutes. (a) Top Surface, (b) Cross-section.

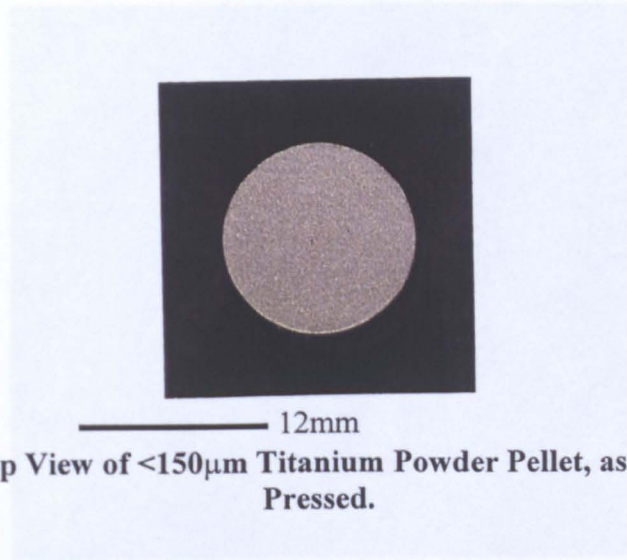


Figure 5.4 Top View of $<150\mu\text{m}$ Titanium Powder Pellet, as Hydraulically Pressed.

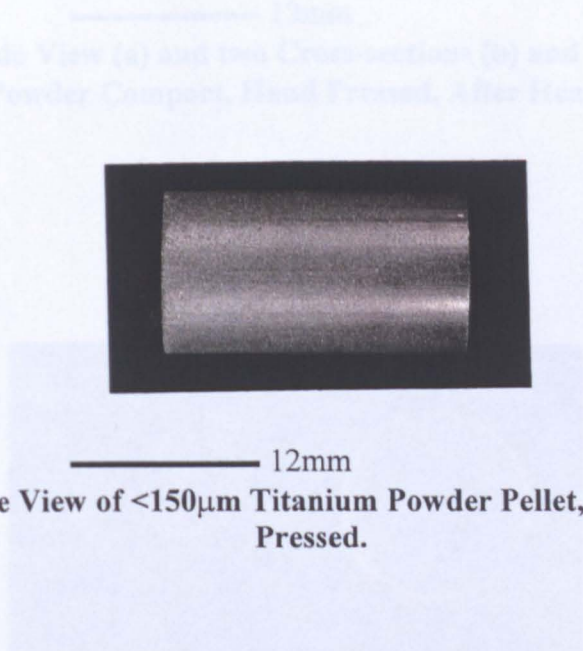


Figure 5.5 Side View of $<150\mu\text{m}$ Titanium Powder Pellet, as Hydraulically Pressed.

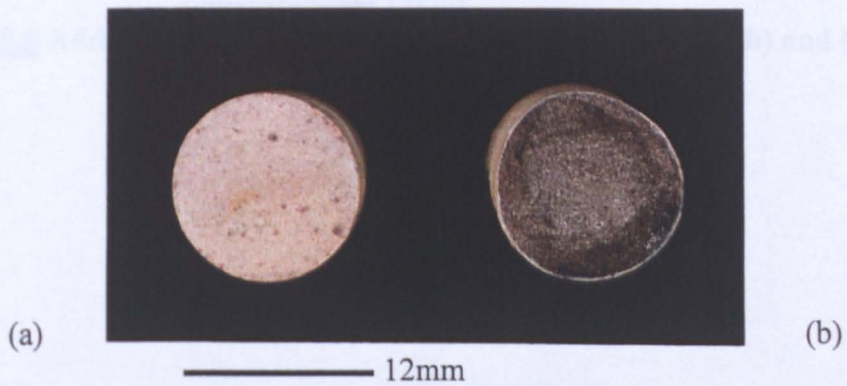


Figure 5.6 $<150\mu\text{m}$ Titanium Powder, Hydraulically Pressed, After Heating at 600°C . (a) Top Surface, (b) Cross-section.



Figure 5.7 Side View (a) and two Cross-sections (b) and (c) of a $<150\mu\text{m}$ Titanium Powder Compact, Hand Pressed, After Heating at 600°C .



Figure 5.8 Additional Photograph of the Two Cross-sections (b) and (c) Seen Above in Figure 5.7

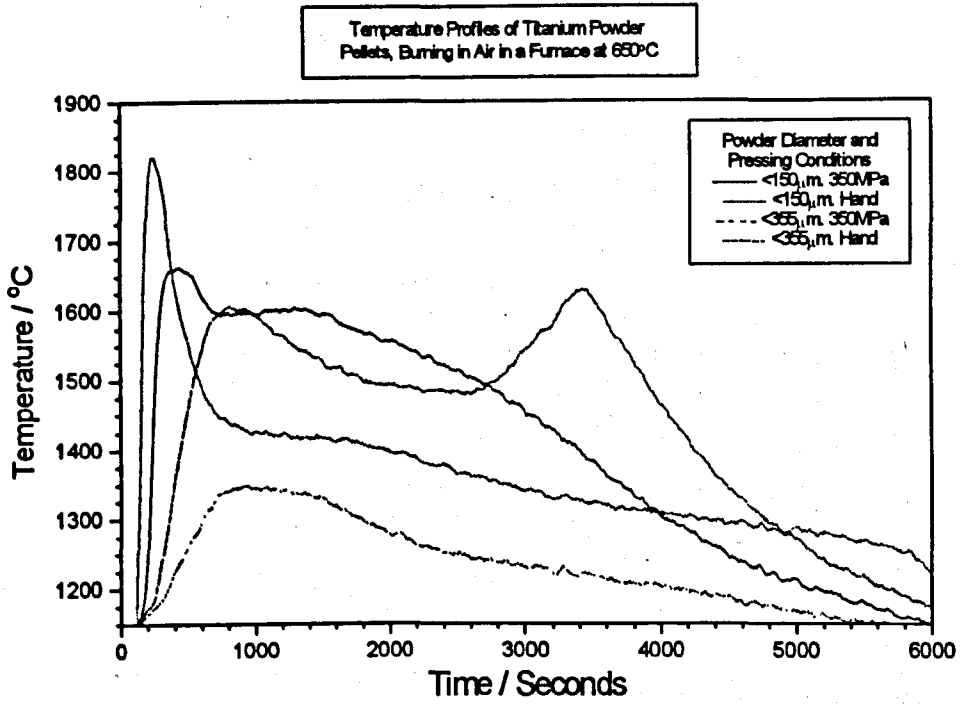


Figure 5.9

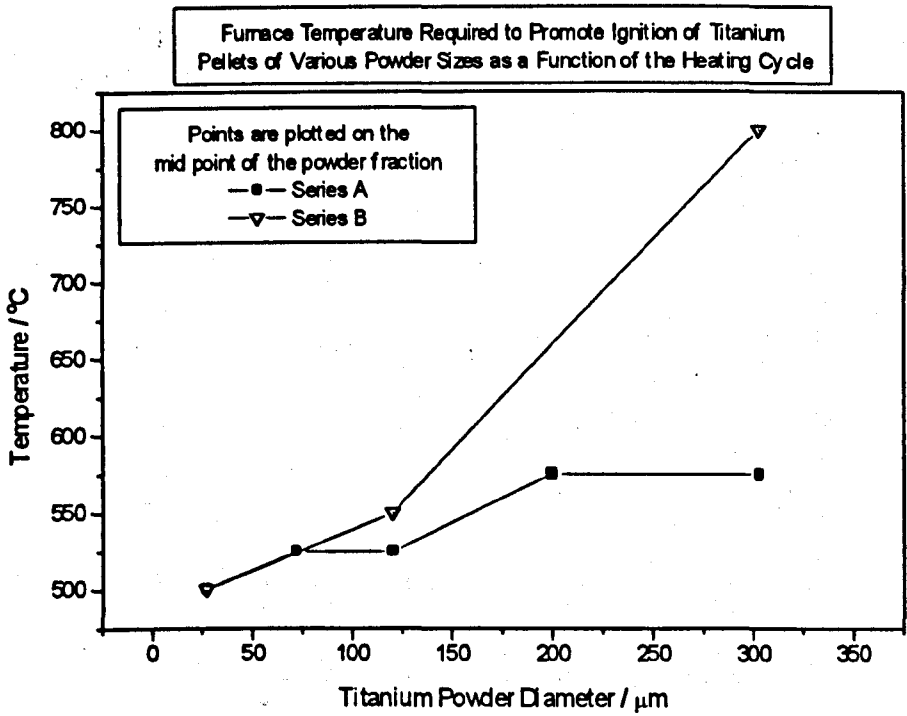
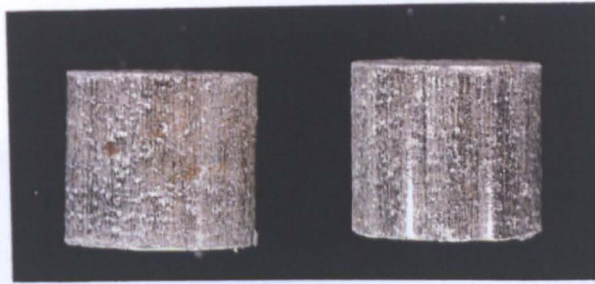
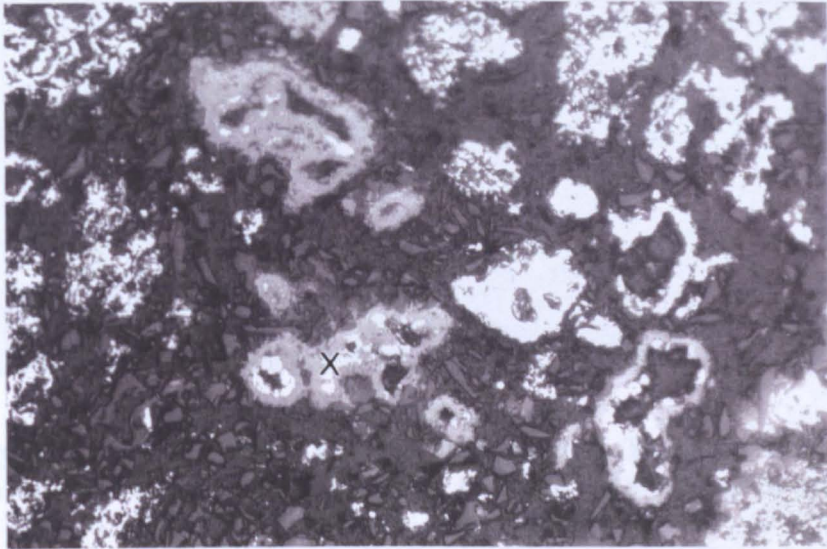


Figure 5.10



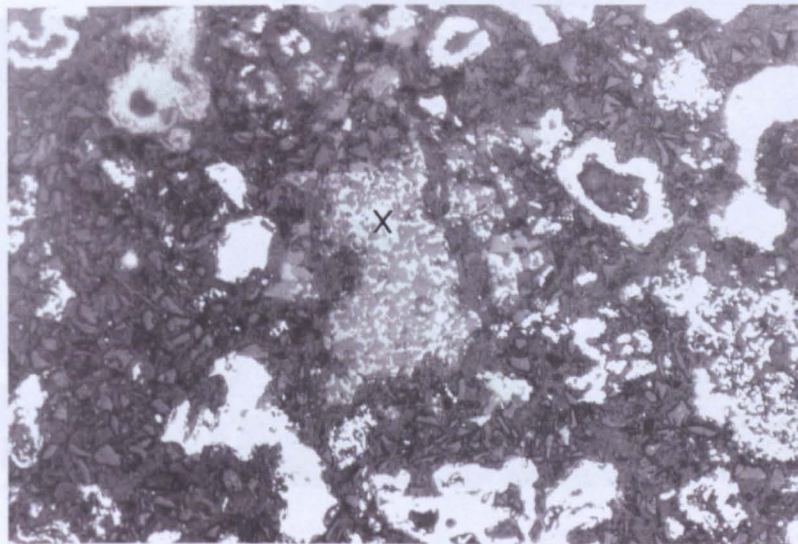
12mm

Figure 5.11 <150 μ m Titanium and Al₂O₃ Compacts, as Hydraulically Pressed.



50 μ m

Figure 5.12 Powders Taken from a <150 μ m Titanium and Al₂O₃ Compact, Hydraulically Pressed, After Heating at 650 $^{\circ}$ C for 20 Minutes.



50 μ m

Figure 5.13 Powders Taken from a <150 μ m Titanium and Al₂O₃ Compact, Hydraulically Pressed, After Heating at 650 $^{\circ}$ C for 20 Minutes.

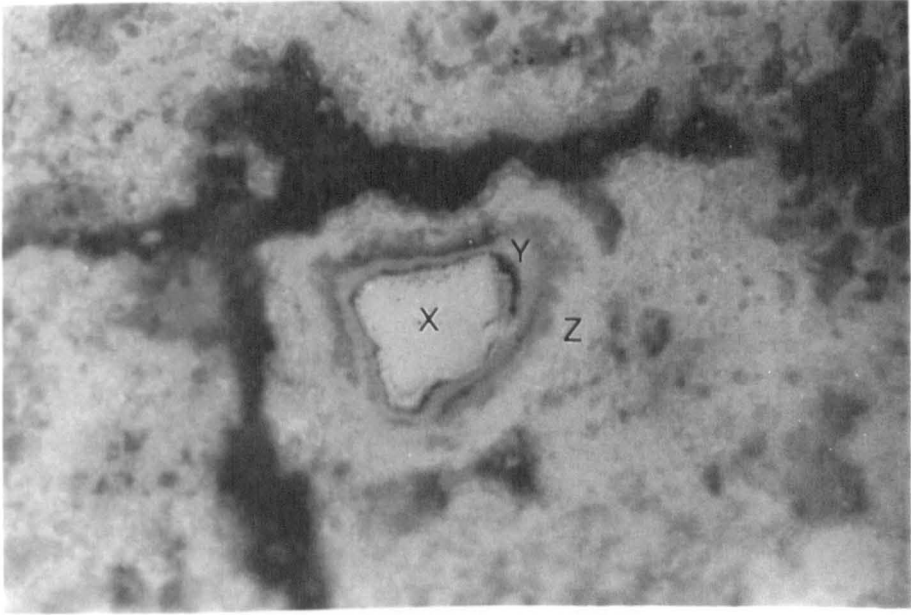


Figure 5.14 Surface Section Taken from a $<150\mu\text{m}$ Titanium and Al_2O_3 Compact, Hydraulically Pressed, After Heating at 650°C for 20 Minutes

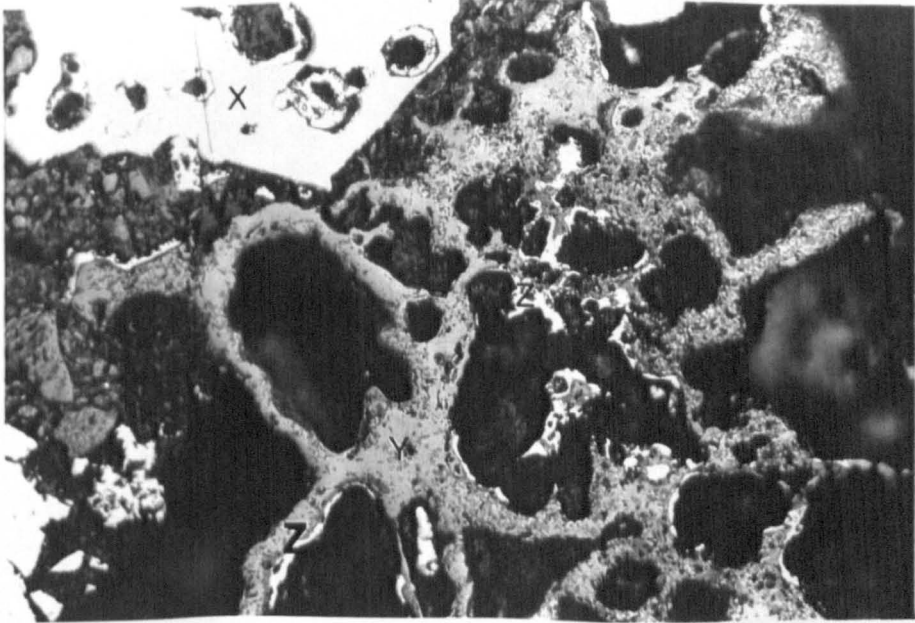


Figure 5.15 Intermediate Layer Taken from a $<150\mu\text{m}$ Titanium and Al_2O_3 Compact, Hydraulically Pressed, After Heating at 650°C for 20 Minutes

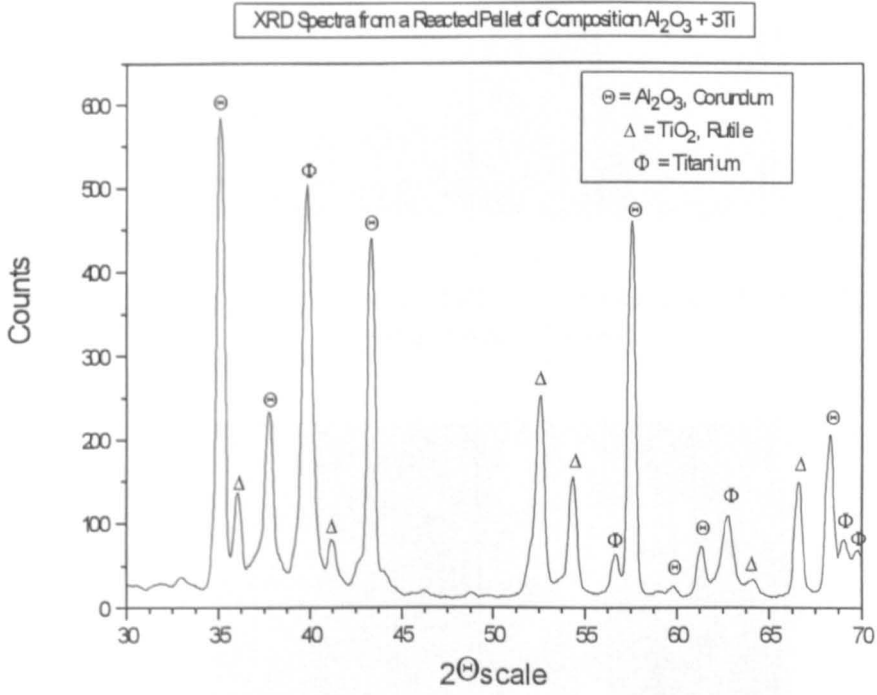


Figure 5.16

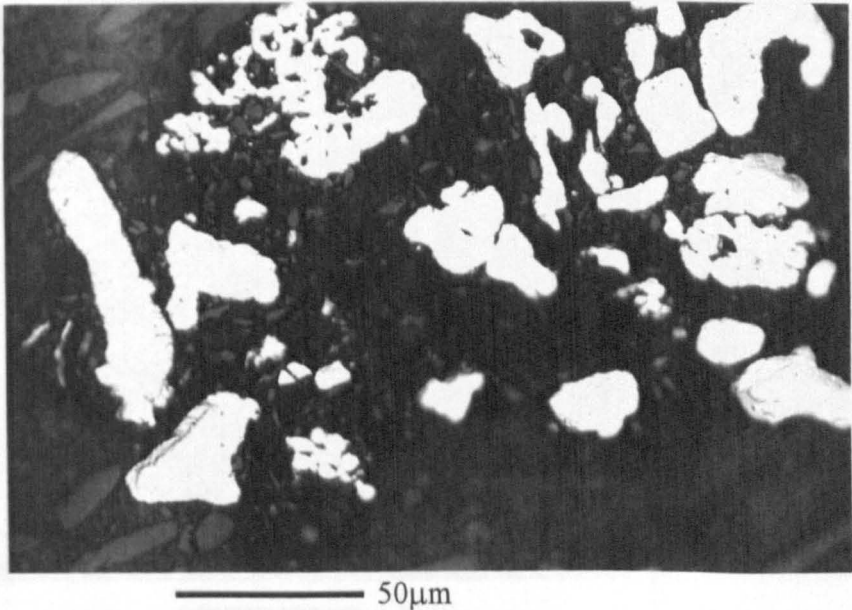
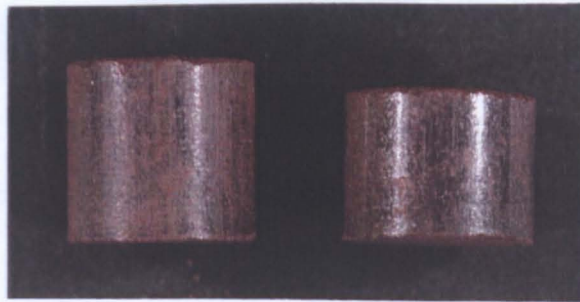


Figure 5.17 Powders Taken from a $<150\mu\text{m}$ Titanium and Al_2O_3 Compact, Hydraulically Pressed, After Heating at 650°C for 20 Minutes in Argon



12mm

Figure 5.18 Top Surface of a $<150\mu\text{m}$ Titanium and Fe_2O_3 Compact, Hydraulically Pressed.



12mm

Figure 5.19 Side View of a $<150\mu\text{m}$ Titanium and Fe_2O_3 Compact, Hydraulically Pressed.



15mm

Figure 5.20 Reacted $<150\mu\text{m}$ Titanium and Fe_2O_3 Compact, Hydraulically Pressed, After Heating in Air at 600°C .

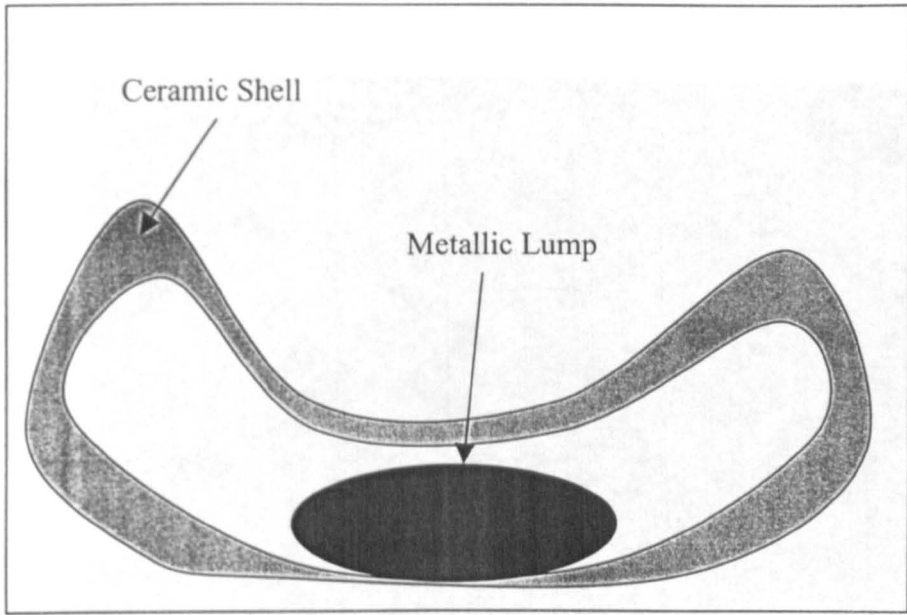


Figure 5.21 Schematic of the Product Morphology of a $\text{Fe}_2\text{O}_3 + 3 \text{Ti}$ Pellet Reaction

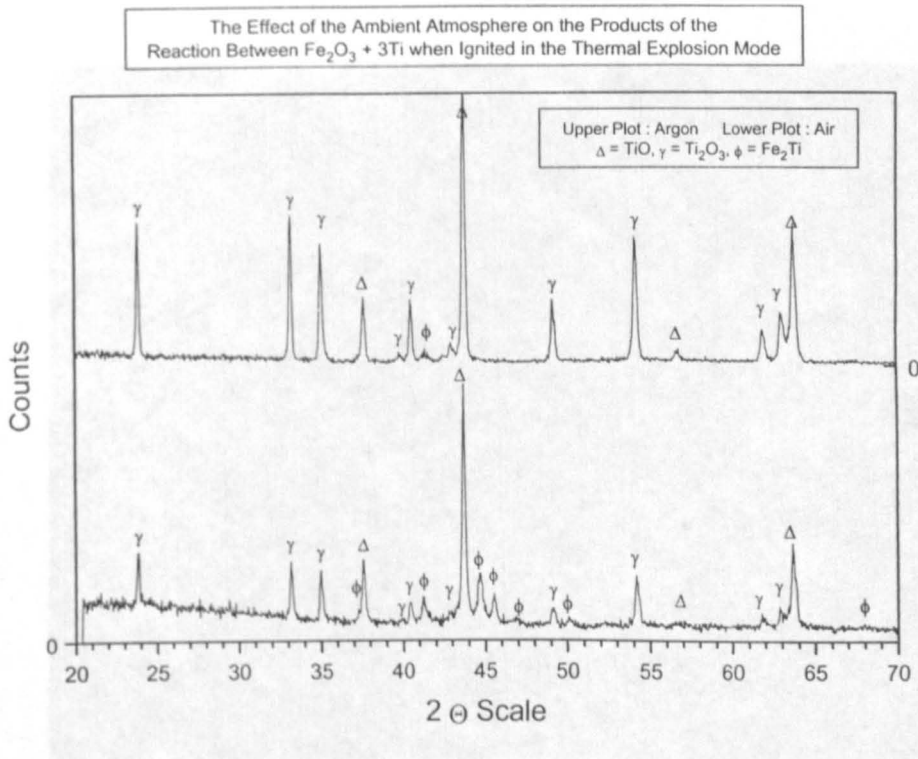


Figure 5.22 XRD Patterns of the Products of the Reaction Between $\text{Fe}_2\text{O}_3 + 3\text{Ti}$ when Ignited in the Thermal Explosion Mode in Argon and Air Atmospheres. The Reaction was Ignited at 500°C for 3 Minutes.

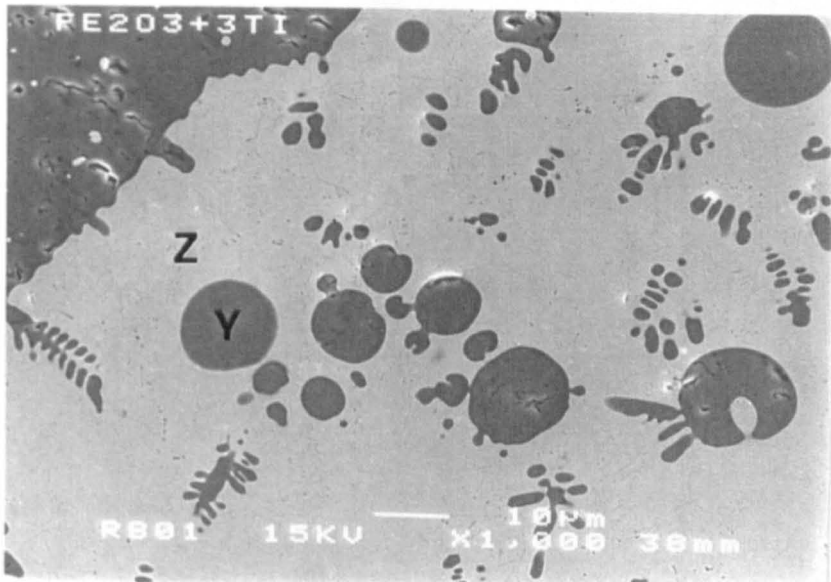


Figure 5.23 SEM Micrograph of the Metallic Part of the Product from a Reacted $\text{Fe}_2\text{O}_3 + 3 \text{ Ti}$ Compact. Y = dark grey ceramic phase, Z = light grey metallic phase.

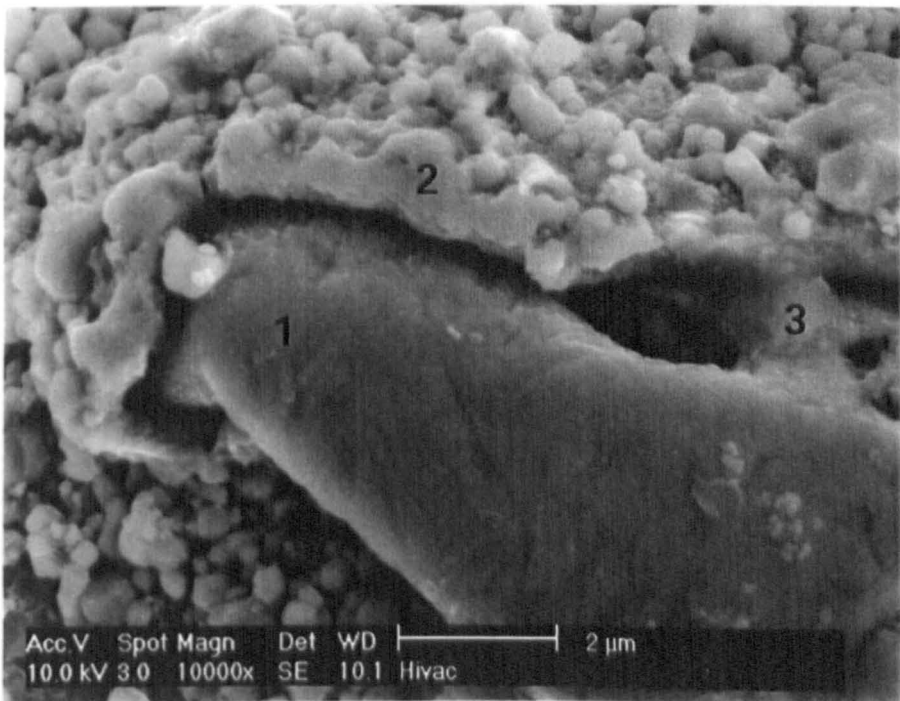


Figure 5.24 E-SEM Photo of Powder Taken From an Unreacted $<150\mu\text{m}$ Titanium and Fe_2O_3 Compact, Heated at 650°C for 3 Minutes.

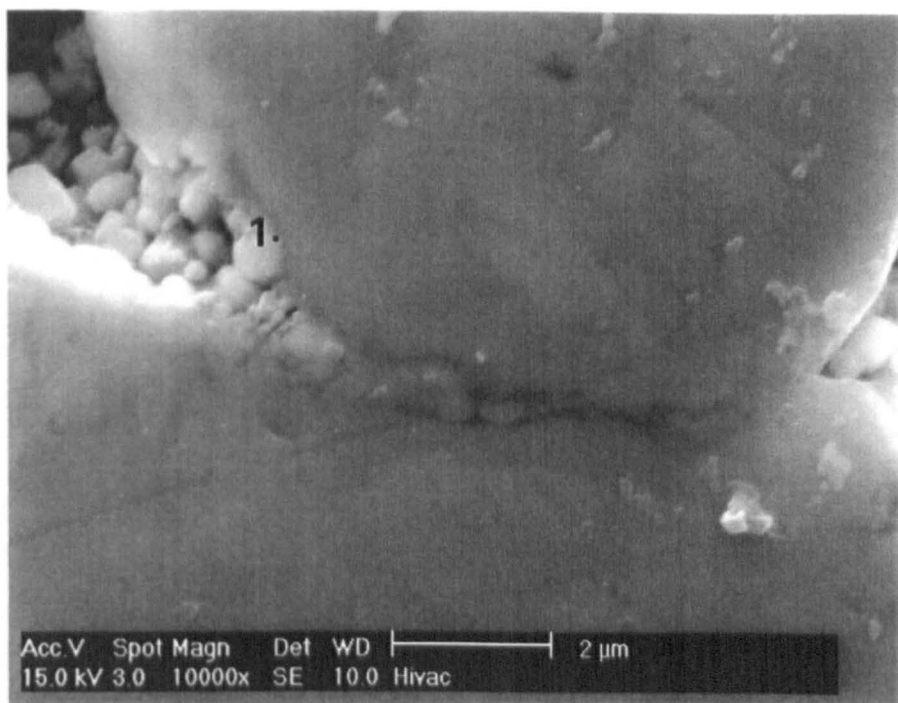


Figure 5.25 E-SEM Photo of Powder Taken from a <math><150\mu\text{m}</math> Titanium and Fe_2O_3 Compact, Heated at 650°C for 3 Minutes in Air, Showing Two Titanium Powders in Contact with Each Other and some Fe_2O_3 Powder.

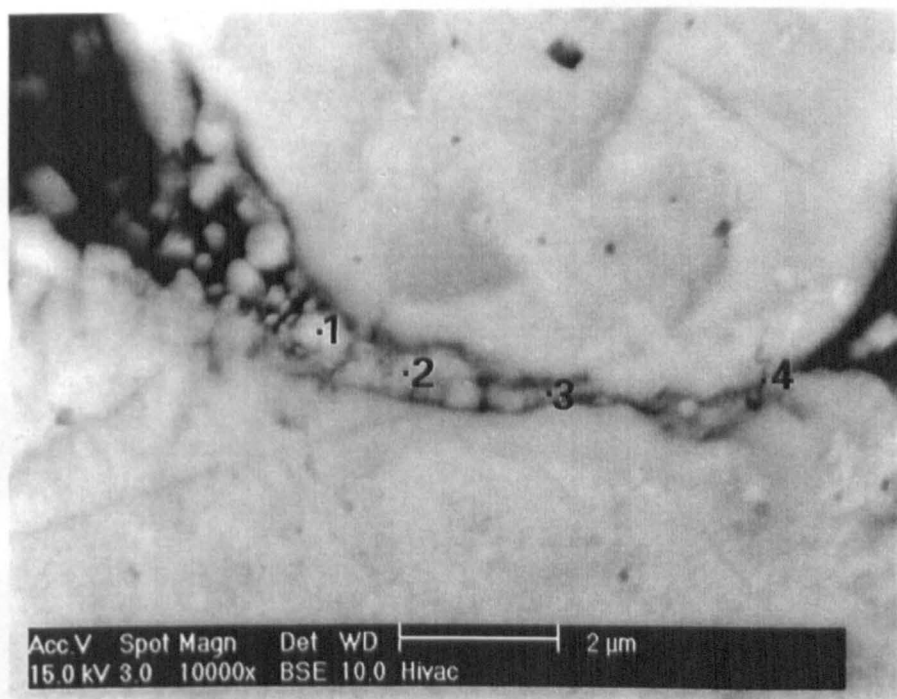


Figure 5.26 Back Scattered Electron Image of the Above Photo.

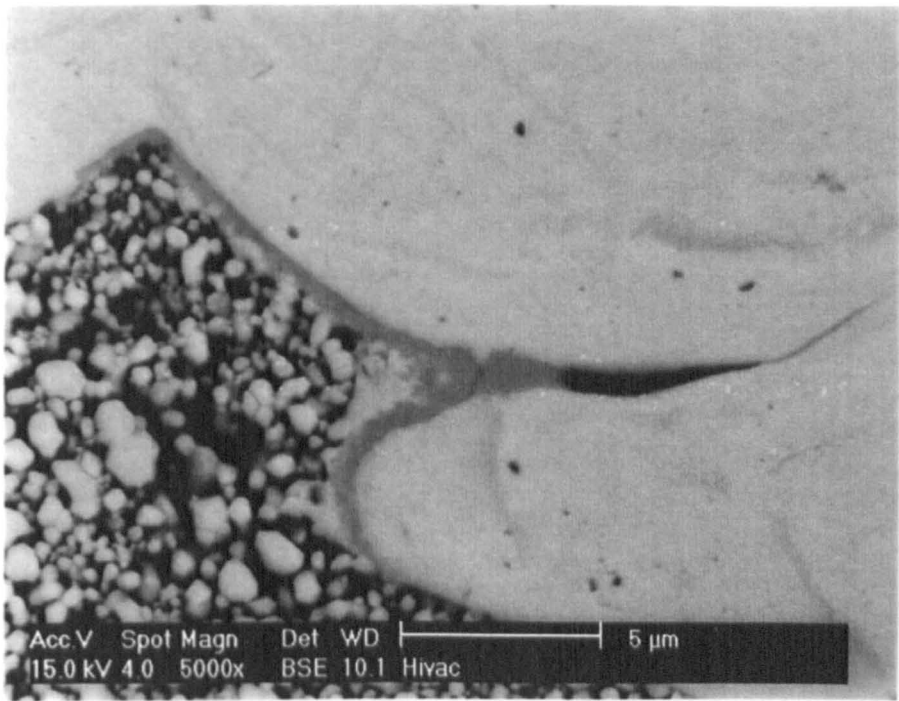


Figure 5.27 Back Scattered Electron E-SEM Photo of Titanium Powder in Contact with Fe₂O₃ Powder, Taken from a <150μm Titanium and Fe₂O₃ Compact, Heated at 650°C for 3 Minutes in Air.

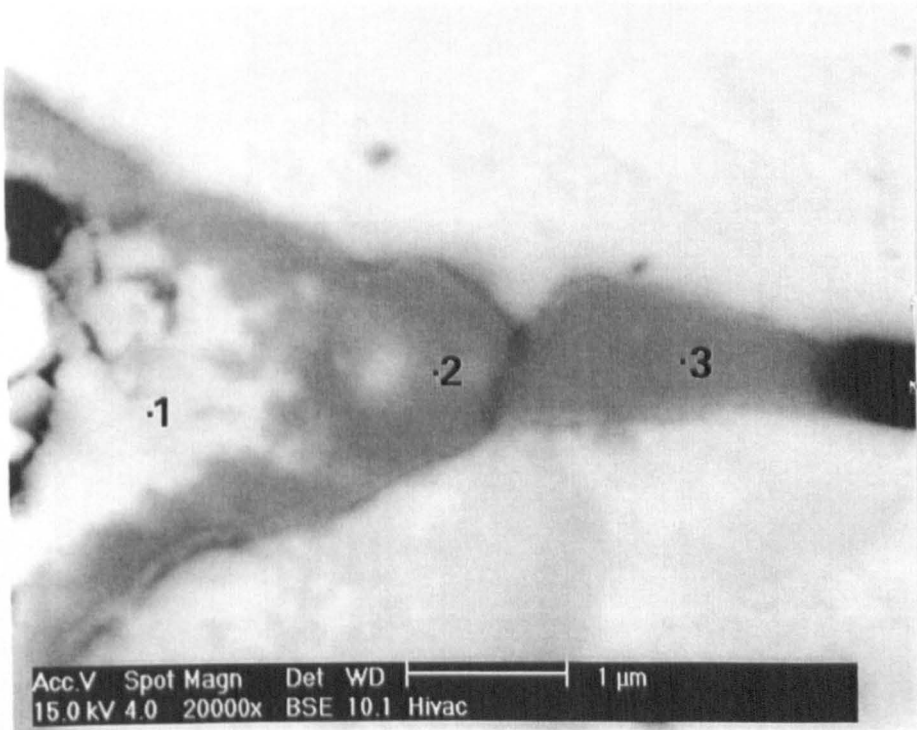


Figure 5.28 Close Up Image of the Above Photo

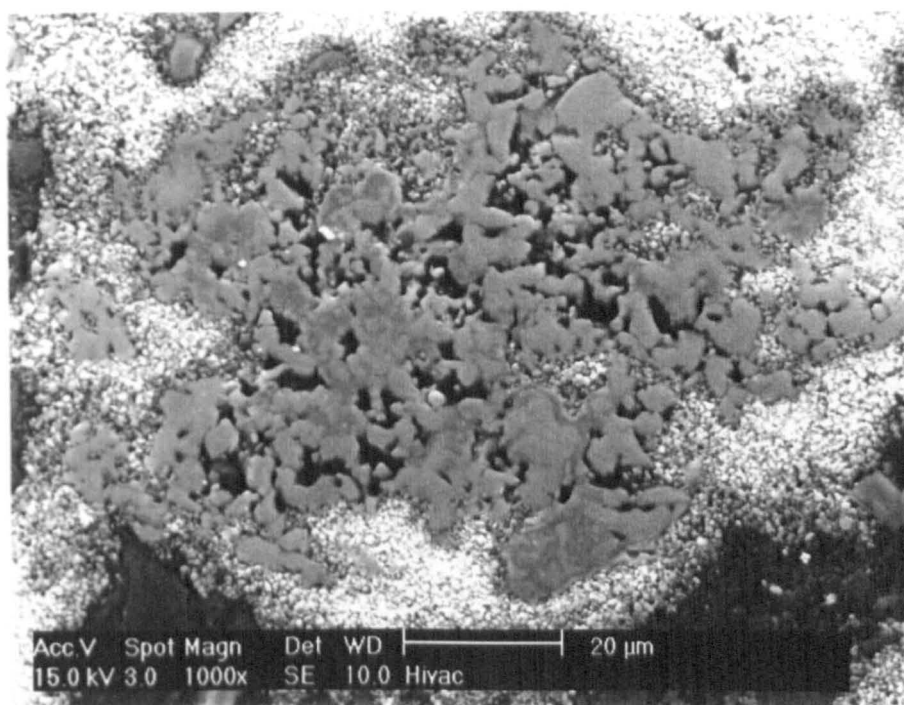


Figure 5.29 E-SEM Photo of a Titanium Powder in Contact with Fe₂O₃ Powder, taken from a <150μm Titanium and Fe₂O₃ Compact, Heated at 650°C for 3 Minutes in Air.

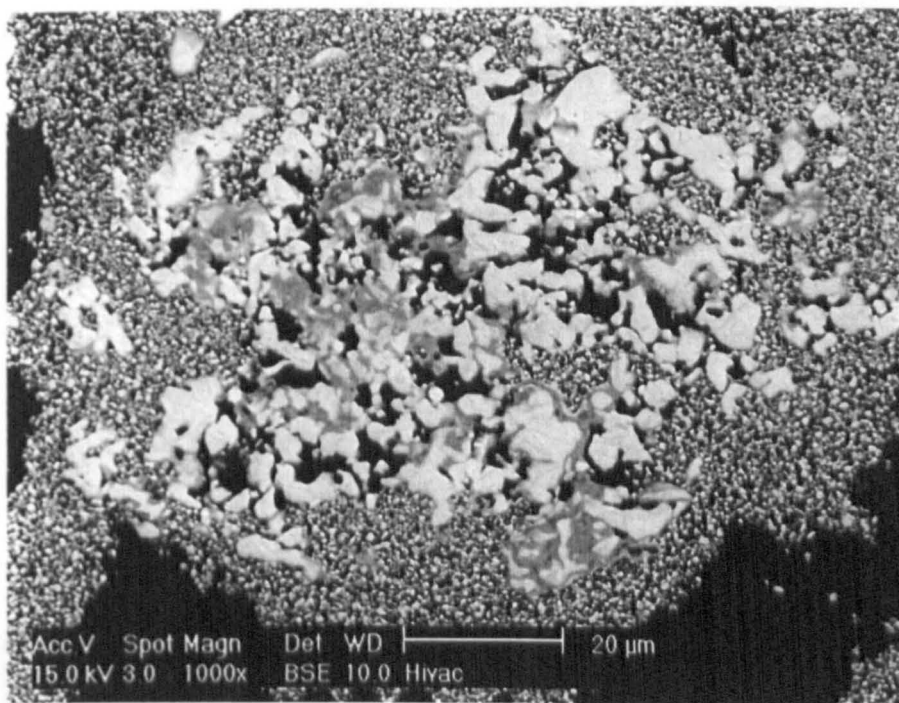


Figure 5.30 Back Scattered Electron E-SEM Image of the Above Photo.

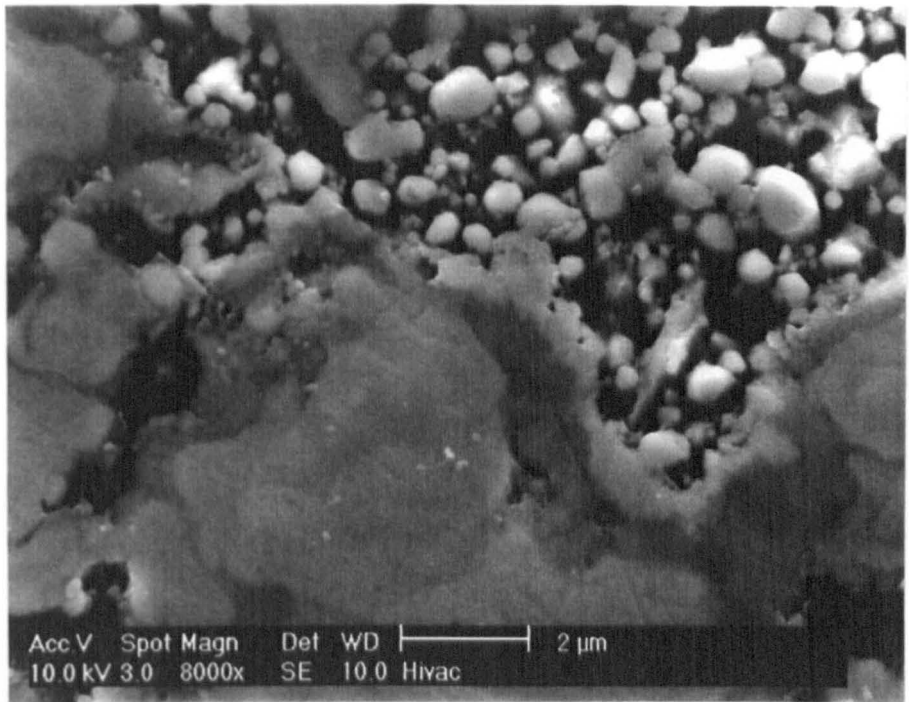


Figure 5.31 Close Up E-SEM Photo of Part of the Powder Seen in Figures 29 and 30

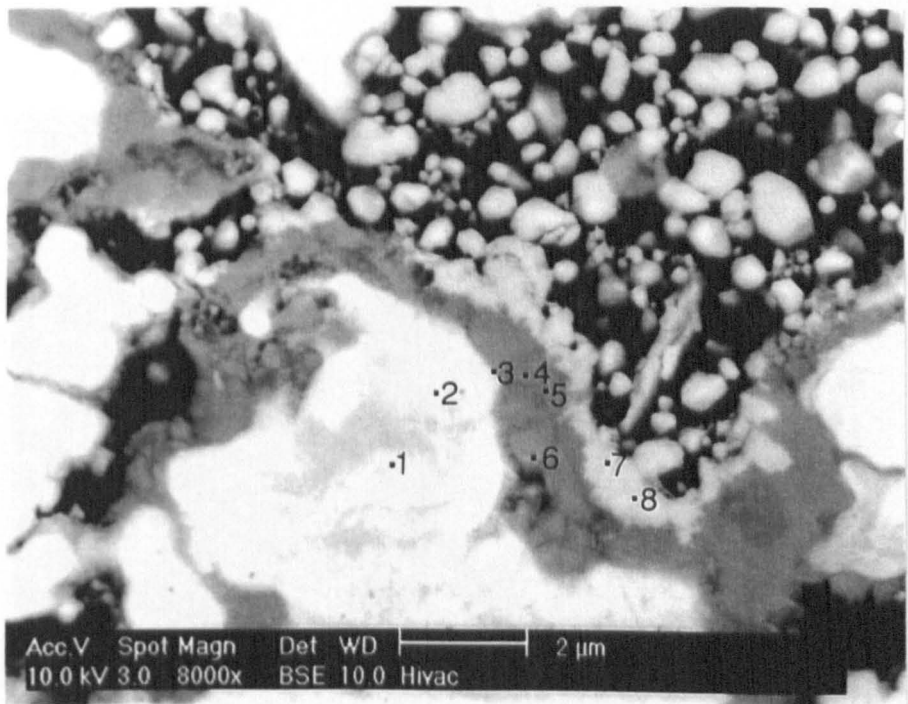
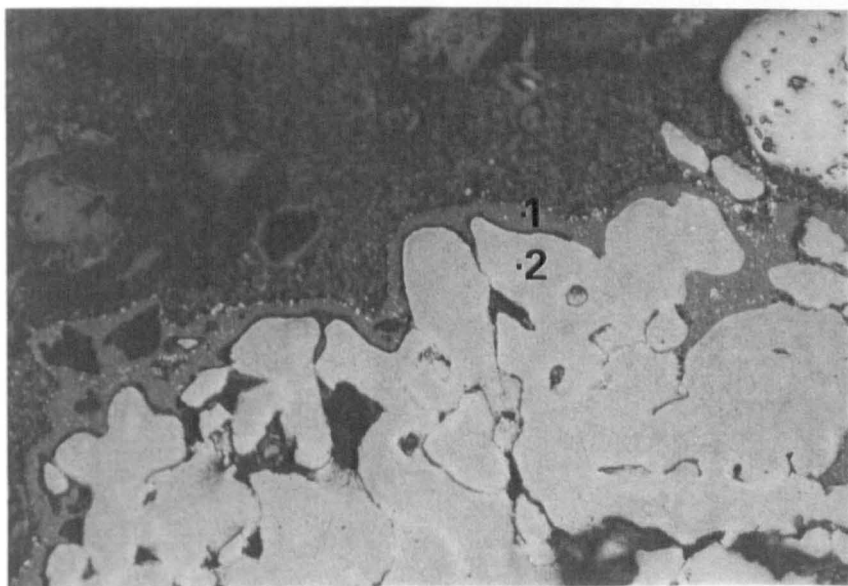


Figure 5.32 Back Scattered Electron E-SEM Image of the Above Photo



————— 50 μm

Figure 5.33 Optical Micrograph of a Compact Containing $<355\mu\text{m}$ Titanium and Fe_2O_3 Powder, Held at 650°C for 60 Minutes.

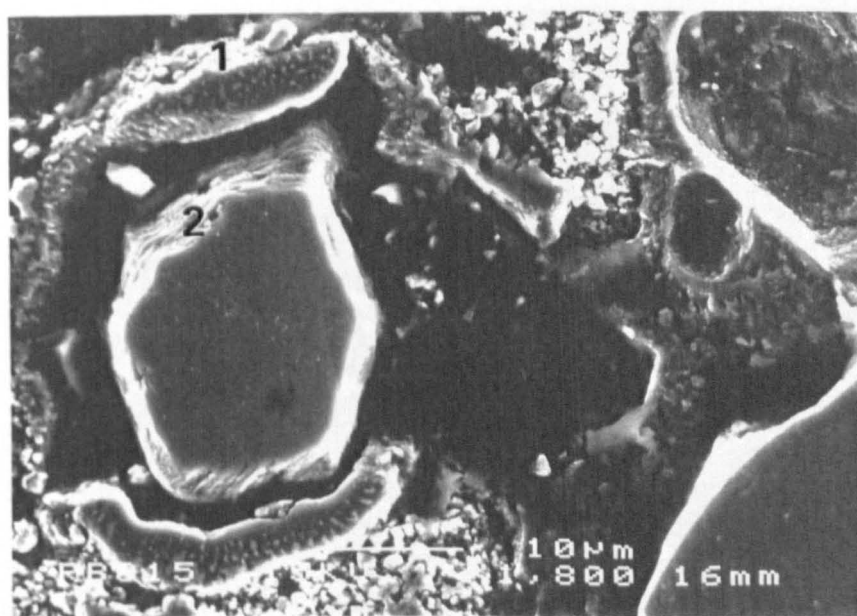


Figure 5.34 SEM Image of Powders Taken From the Same Sample as Above.

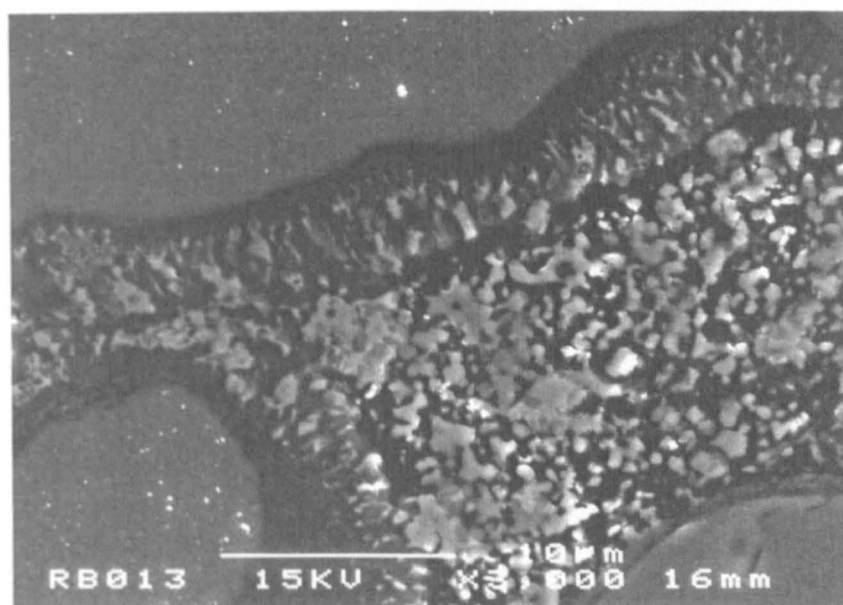


Figure 5.35 SEM Image of a Compact Containing $<150\mu\text{m}$ Titanium and Fe_2O_3 Powder, Held at 550°C for 60 Minutes.

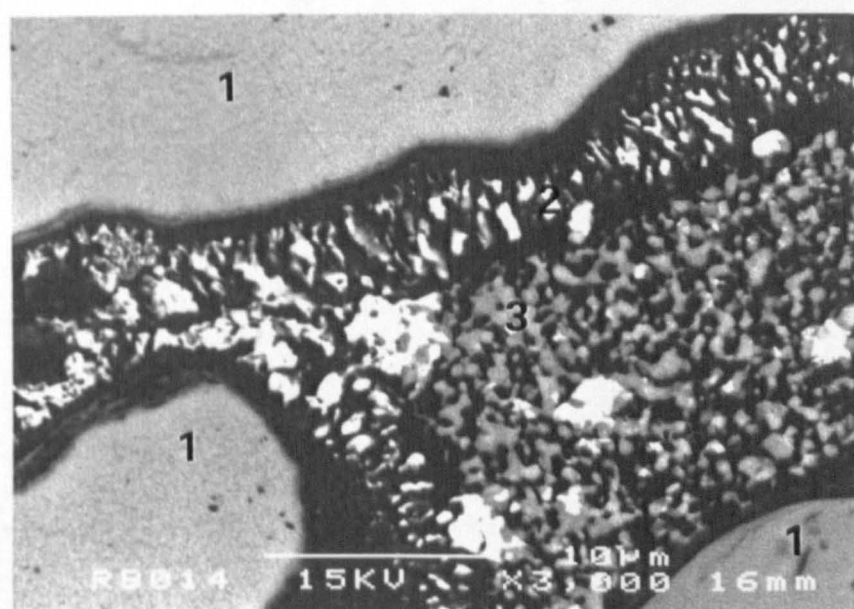


Figure 5.36 Back Scattered Electron Image of the Above Image.

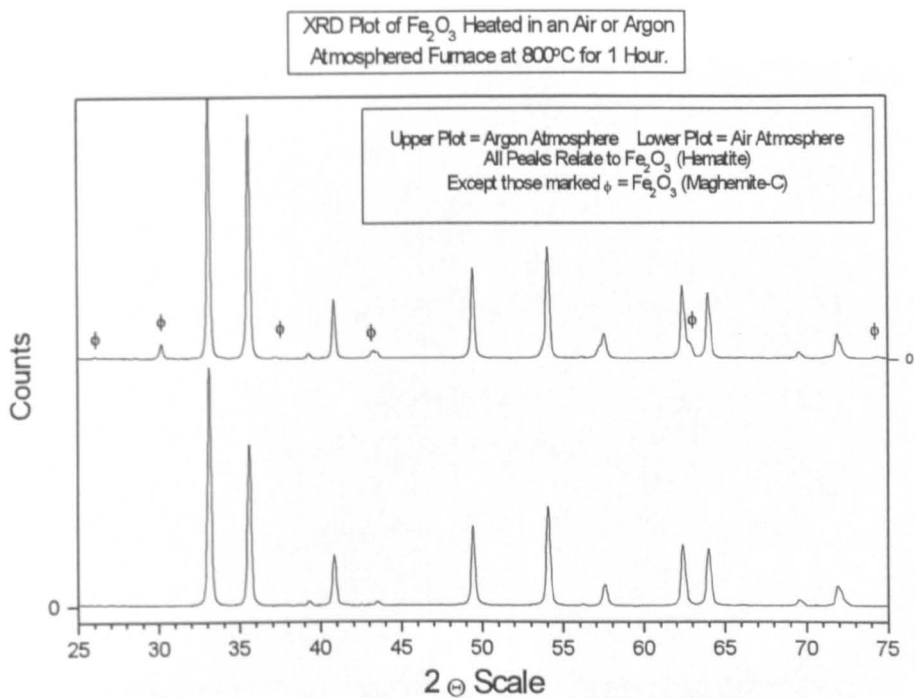


Figure 5.37

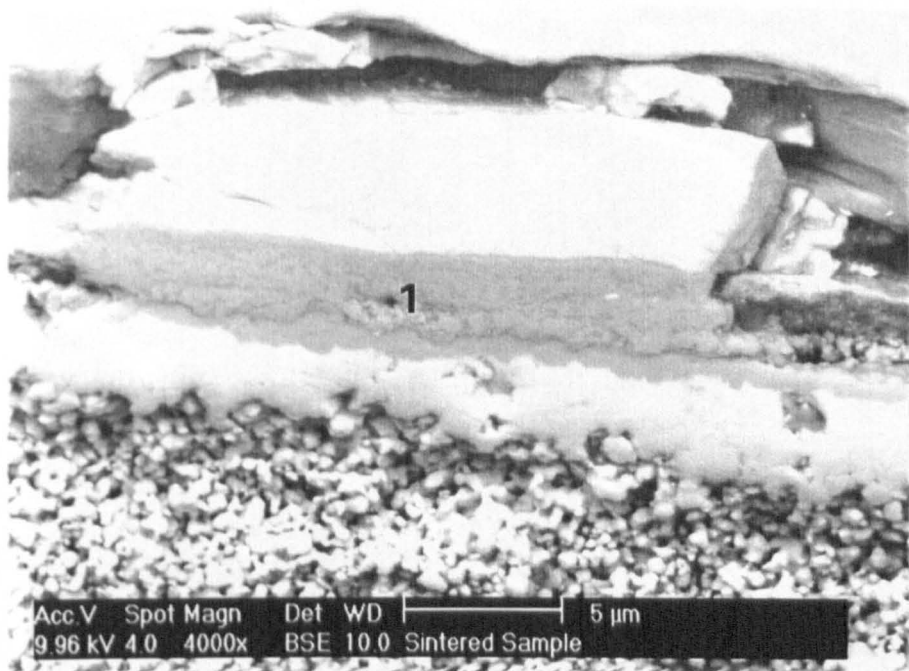


Figure 5.38 E-SEM Image of the Interface Between Titanium and Fe_2O_3 After Heating at 900°C for 30 Minutes in Argon.

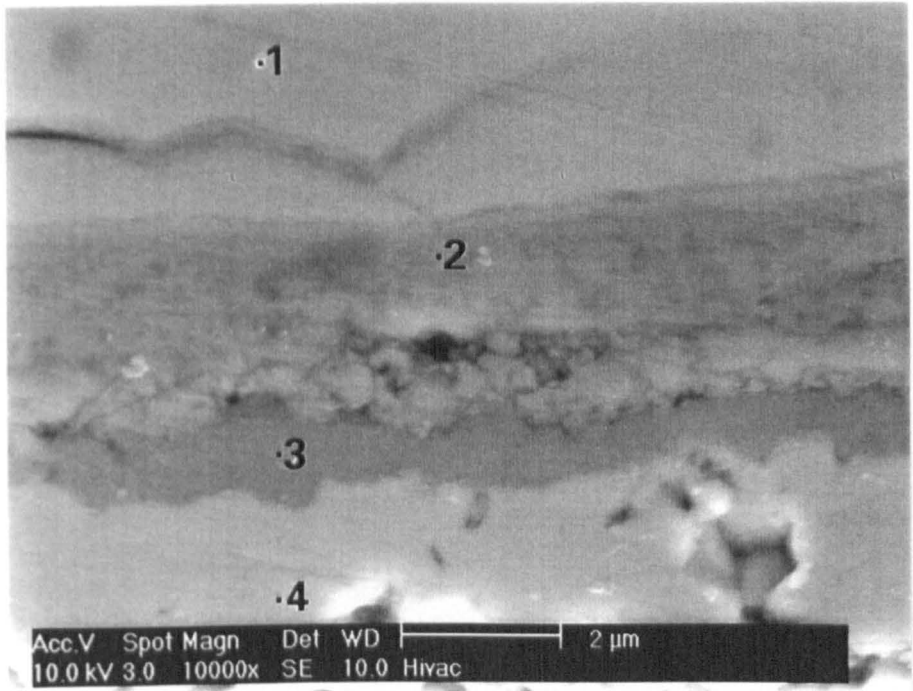


Figure 5.39 Close Up of the Interface Seen in Figure 38

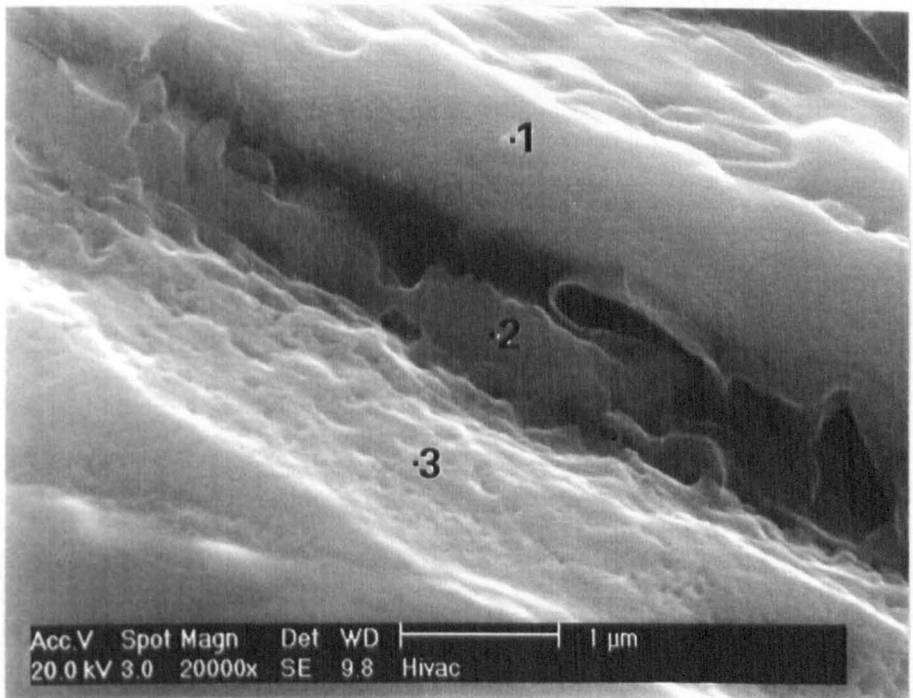


Figure 5.40 E-SEM Image of a Cracked Section of the Interface from the Sample seen in Figure 38

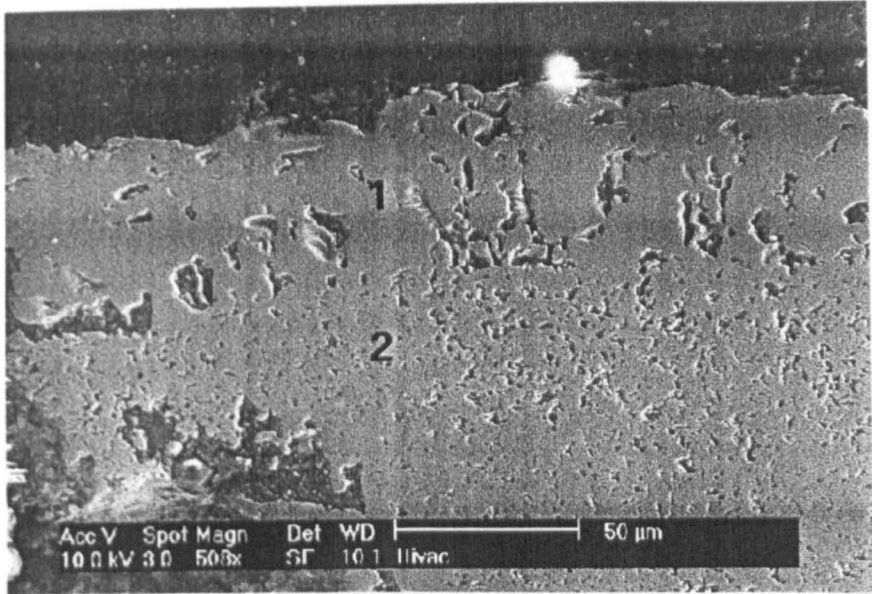


Figure 5.41 E-SEM Image of the Interface Between Titanium and Fe_2O_3 Powder after Heating at 1200°C for 15 Minutes in Argon.

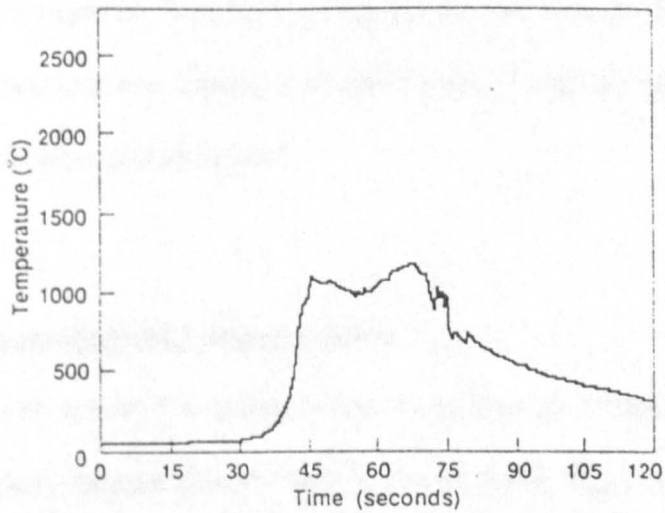


Figure 5.42 'Afterburn' Occurring in the Combustion of Titanium Powder Compacts in Nitrogen. Dunmead *et al.* (1989).

Chapter 6

Numerical Calculations for the Oxidation Reaction of Titanium in Air or Titanium in Fe_2O_3 .

6.1 Introduction

It is thought that the ignition of pure titanium or titanium + Fe_2O_3 powder compacts is initiated by the formation of a liquid phase at the titanium / Fe_2O_3 boundary, produced by localised heating from the exothermic oxidation reaction. It is the production of the liquid phase that marks the ignition of the pellet.

This chapter investigates the feasibility of the theory that a layer of titanium oxide formed instantaneously around a titanium powder particle can liberate sufficient heat to produce a liquid phase.

6.2 Basic Calculation and Assumptions

The theory is based around the instantaneous formation of a titanium oxide layer around an ideal titanium powder particle. From the previous chapter it is known that the oxides in question are TiO_2 for pure titanium air reactions and TiO for the reaction between $\text{Fe}_2\text{O}_3 + 3\text{Ti}$. The oxide is said to form instantaneously and be $1\mu\text{m}$ thick. From an examination of the 'sintered' samples in the previous chapter it is seen that this is roughly the thickness of

the oxide layers that are observed in the samples that have nearly combusted. The oxide is said to form instantaneously to simplify the calculation.

The powder particle was taken to be spherical and of 75 μ m diameter. The idealised shape aids the calculation and the 75 μ m diameter was taken as an arbitrary figure, representative of the sizes employed in this work. The heat energy of the oxidation reaction is said to go only into the body of the powder. There are no conductive / convective / radiative heat losses.

The heat liberated by the formation of the oxide layer is calculated. The heat energy required to raise the temperature of a titanium powder particle above its melting point is also calculated. A comparison of the two values reveals in broad terms whether the said theory is the possible method for liquid phase formation.

The powder particle is said to ignite when placed in surroundings at 500°C as this is the lowest furnace temperature at which titanium powders have been seen to ignite. As such, the powder particle has to increase in temperature by:

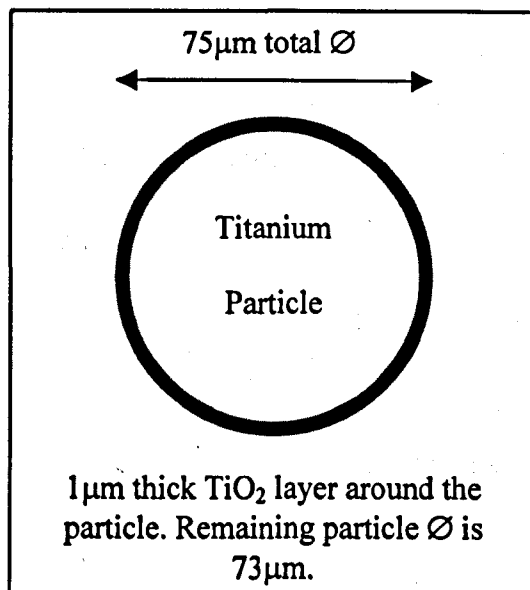
$$1170^{\circ}\text{C} = \text{mpt of titanium } 1670^{\circ}\text{C} - \text{initial temperature } 500^{\circ}\text{C} \quad (6.1)$$

The oxidation of titanium to TiO by Fe₂O₃ and the oxidation of titanium to TiO₂ by gaseous oxygen (air) are both included for comparison of their exothermicities.

6.3 Assumptions and Constants

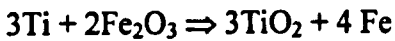
- Titanium particle size: 75 μm , spherical. See Figure 6.1.
- Reaction layer: 1 μm thick titanium oxide. Forms instantaneously.
- Specific heat capacity of titanium: 523 J kg⁻¹ K⁻¹
- Density of titanium: 4510 kg m⁻³
- Molar Mass: 47.9g mol⁻¹
- Density of TiO₂: 4.260 kg m⁻³
- Melting Point of Titanium: 1670°C
- Starting Temperature of Powder : 500°C

Figure 6.1 Schematic Diagram of the Model



6.4 Calculations

6.4.1 Reaction Energy Calculation for the Formation of TiO₂ by Fe₂O₃



$$\Delta H_f(\text{Fe}_2\text{O}_3) = -196.3\text{kcal mol}^{-1} \Rightarrow -821.61\text{ kJ mol}^{-1} \quad (6.2)$$

$$\Delta H_f(\text{TiO}_2) = -225.8\text{kcal mol}^{-1} \Rightarrow -945.06\text{kJ mol}^{-1} \quad (6.3)$$

$$\begin{aligned} \text{Products} - \text{Reactants} &= 3\text{TiO}_2 - 2\text{Fe}_2\text{O}_3 = (3 \times -945.06) - (2 \times -821.61) = \\ &= -2835.26 - -1643.23 \Rightarrow -1192.03\text{ kJ} \end{aligned} \quad (6.4)$$

- ΔH for 1 mole of TiO₂ = -1192.03 kJ / 3 = -397.34 kJ

6.4.2 Reaction Energy Calculation for the Formation of TiO by Fe₂O₃



$$\Delta H_f(\text{TiO}) = -129.7\text{ kcal} \Rightarrow -542.86\text{ kJ mol}^{-1} \quad (6.5)$$

$$\begin{aligned} \text{Products} - \text{Reactants} &= 3\text{TiO} - \text{Fe}_2\text{O}_3 = -1628.58 - -821.61 = \\ &= -806.96\text{ kJ} \end{aligned} \quad (6.6)$$

- ΔH for 1 mole of TiO = -806.96 kJ / 3 = -268.99 kJ

6.4.3 Reaction Energy Calculation for the Formation of TiO₂ or TiO by Gaseous Oxygen (air)

$$\Delta H_f(\text{TiO}_2) = -945.09 \text{ kJ mol}^{-1} \quad (6.7)$$

$$\Delta H_f(\text{TiO}) = -542.86 \text{ kJ mol}^{-1} \quad (6.8)$$

6.4.4 Powder Calculations

Volume of 1 particle of titanium = $4\pi r^3 / 3$:

$$= 4\pi(37.5 \times 10^{-6})^3 / 3 = 2.208932335 \times 10^{-13} \text{ m}^3 \quad (6.9)$$

With a 1 μm thick reaction layer the titanium volume becomes:

$$= 4\pi(36.5 \times 10^{-6})^3 / 3 = 2.036888249 \times 10^{-13} \text{ m}^3 \quad (6.10)$$

Mass of the particle = density x volume = mass:

$$= 4510 \times (2.03689 \times 10^{-13}) = 9.186366003 \times 10^{-10} \text{ kg} \quad (6.11)$$

Moles of titanium in particle = $(9.186366003 \times 10^{-7} / 47.9) =$

$$1.91782171 \times 10^{-8} \text{ mols} \quad (6.12)$$

The volume of the reaction layer is therefore:

$$2.208932335 \times 10^{-13} - 2.036888249 \times 10^{-13} = 1.720440856 \times 10^{-14} \text{ m}^3 \quad (6.13)$$

6.4.5 Calculation of Energy Released when the Reaction Layer is TiO₂

$$\text{Mass of TiO}_2 \text{ formed} = 4260 \text{ kg m}^{-3} \times 1.720440856 \times 10^{-14} =$$

$$7.329078045 \times 10^{-11} \text{ kg} \quad (6.14)$$

$$\text{Moles of TiO}_2 \text{ formed} = 7.329078045 \times 10^{-8} \text{ (grams)} / 79.9 =$$

$$9.172813573 \times 10^{-10} \text{ mols} \quad (6.15)$$

- TiO₂ formed from Fe₂O₃ ⇒ 397.34 kJ mol⁻¹ x moles TiO₂ = 3.646 x 10⁻⁴ J
- TiO₂ formed from air ⇒ 945.09 kJ mol⁻¹ x moles TiO₂ = 8.669 x 10⁻⁴ J

6.4.6 Calculation of Energy Released when the Reaction Layer is TiO

$$\text{Mass of TiO formed} = 5100 \times 1.720440856 \times 10^{-14} =$$

$$8.774248366 \times 10^{-11} \text{ kg} \quad (6.16)$$

$$\text{Moles of TiO formed} = 8.774248366 \times 10^{-8} / 63.9 =$$

$$1.37312181 \times 10^{-9} \text{ mols} \quad (6.17)$$

- TiO formed from Fe₂O₃ ⇒ 268.99 kJ mol⁻¹ x moles of TiO = 3.694 x 10⁻⁴ J
- TiO formed from air ⇒ 542.86 kJ mol⁻¹ x moles of TiO = 7.454 x 10⁻⁴ J

6.4.7 Calculation of the Energy Required to Melt the Titanium Powder Particle

To melt the titanium, the particle needs to be heated to at least 1670°C. From the lowest ignition point of 550°C this equates to a 1120°C rise in temperature.

Energy required to heat the titanium particle \Rightarrow

(Cp of Titanium) x (Mass of particle) x (Temperature Rise) =

$$523 \times 9.186366003 \times 10^{-10} \text{ kg} \times 1120 \text{ K} = 5.381 \times 10^{-4} \text{ J} \quad (6.18)$$

6.5 Results

The calculations have produced the results:

- Energy Required to Melt Particle = $5.381 \times 10^{-4} \text{ J}$

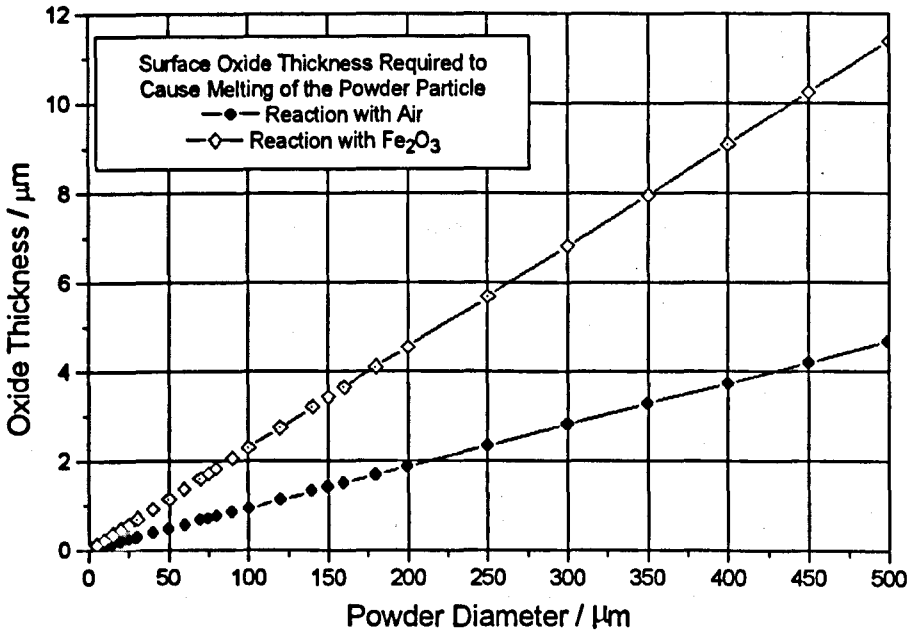
Energy released by the formation of a 1 μm thick layer of oxide on the particle

- TiO_2 from Fe_2O_3 = $3.645 \times 10^{-4} \text{ J}$
- TiO_2 from AIR = $8.669 \times 10^{-4} \text{ J}$
- TiO from Fe_2O_3 = $3.694 \times 10^{-4} \text{ J}$
- TiO from AIR = $7.454 \times 10^{-4} \text{ J}$

A graph created from data calculated by a computer programme of this calculation (Powder.bas in the appendix) showing the required thickness of oxide layer that has to form to melt a powder particle of a certain diameter, is shown in figure 6.2. The data marks the point at which the heat liberated by the

formation of the oxide layer equals the energy required to melt the remaining titanium metal in the particle subject to the assumptions previously made.

Figure 6.2 The Thickness of the TiO_2 Oxide Layer Required to Cause Melting of the Titanium Powder.



6.6 Discussion

It can be seen that the energy produced by the formation of a $1\mu\text{m}$ thick oxidation layer around the particle can produce enough energy to melt the titanium powder particle. The result; even with its coarse assumptions as to the heat losses, the instantaneous formation of the oxide layer and its total absorption into the powder, indicates that the theory that the ignition of titanium powder compacts depends upon the melting of the titanium is not unreasonable. Figure 6.2 makes it clear that the oxidation of titanium in air is more exothermic than its oxidation by Fe_2O_3 . This feature is not seen in the experimental data on the furnace temperature required to promote ignition of

pellets, presented in the previous chapter. This is probably due to the combined inaccuracy of the furnace temperature, the effect of the morphology of the powder used in the experiments and the composition of the first liquid phase to form. The first liquid phase to form will ignite the pellet, therefore, the effect of the reduced exothermicity of the Fe_2O_3 oxidised titanium powders may be counteracted by the fact that both Fe_2O_3 , metallic iron and iron – titanium alloys melt at lower temperatures than metallic titanium. As it is likely that some of the heat of oxidation is absorbed by the surrounding environment these could be the first melting phases, rather than metallic titanium.

Morphologically, the titanium powder used experimentally is highly porous, being a crushed foam, and thus has areas which are of significantly smaller diameter than the said size of the powder. These areas are the likely place for the formation of the first liquid. As such, the effect of the oxidation medium is insignificant when the effective particle size is below $\sim 30\mu\text{m}$, as shown in figure 6.2.

On a more general note, the thickness' of oxide layer required to cause melting are sufficiently small when the powder diameter is small, that they could form instantaneously. Dunmead *et al.* (1989), Tavgen *et al.* (1992) and Bakhman *et al.* (1998) have seen the ignition of titanium powders at the onset of oxidation ($\sim 500^\circ\text{C}$) which could be attributed to the rapid formation of the critical thickness of oxide required to cause melting, and thus ignition.

6.7 Conclusions

The instantaneous formation of a $\sim 1\mu\text{m}$ thick, oxide layer on $75\mu\text{m}$ spherical titanium powder is seen to liberate sufficient heat to cause melting of the powder particle. The formation of the liquid phase causes the pellet to ignite. In the context of Fe_2O_3 and titanium pellets, the reduced exothermicity of the oxidation reaction by Fe_2O_3 may be counteracted by the lower melting temperature of Fe_2O_3 or metallic iron – titanium alloys over pure metallic titanium. The influence of the oxidation medium is seen to reduce with the reduction in the powder diameter.

Chapter 7

Numerical Model to Predict the Behaviour of a Titanium Powder Pellet Heated in Air

7.1 Introduction

A numerical model has been presented in Chapter 6, that explores the theory that exothermic oxidation of titanium by air or Fe_2O_3 is sufficient to cause melting of the oxidising titanium powder. This chapter builds on that theory, adding complexity and real physical constraints to the model.

A computer programme was written to utilise and explore the model. The model was constructed to test the theory of ignition of the $\text{Ti} + \text{Air}$ and $\text{Ti} + \text{Fe}_2\text{O}_3$ reactions put forward in the previous chapter. At the heart of the programme is the concept that the oxidation of titanium powder will raise the temperature of the pellet body above that of its surroundings. The experimental evidence shows that pellets of titanium powders will ignite at ambient temperatures as low as 550°C . Ignition is thought to occur when liquid phases are present (Sirca *et al.* 1991). Obviously there are no liquid phases present at this temperature, indicating that the pellet body must be at a higher temperature than the surroundings, one at which liquid phases will form. The numerical model investigates this phenomena.

The model breaks the system into two parts, namely the oxidation of titanium powder and the subsequent release of energy into the compact (raising its temperature) and the rate of heat loss (or gain) to the surroundings. From these, the thermal behaviour of the pellet can be modelled.

7.2 Model Outline

The basic model is described in the flowchart diagram, figure 7.1. A more complex flowchart is shown in figure 7.2 (in the Appendix), which goes into greater detail as to the actual written computer programme of the numerical model. The model works on a time basis, cycling through the calculations for a given time-step size.

Initially the mass of oxide formed in the time interval is calculated assuming parabolic oxidation kinetics dependant on the oxide thickness. The oxidation of titanium is exothermic and thus heat energy is released. It is assumed that the pellet absorbs all of this energy and that the pellet is at a uniform temperature throughout.

Next, the heat flow to or from the surroundings is calculated taking into account heat transfer due to radiation and conduction. If the pellet temperature is less than the furnace temperature, energy is absorbed by the pellet. If the pellet temperature is higher than the furnace temperature, energy is lost by the pellet. The sum of the energy input to the pellet from the oxidation of titanium and the energy absorbed or lost by the pellet due to the surroundings is calculated, allowing the temperature change of the pellet (taking into account

possible phase transformations in the pellet such as the alpha \Rightarrow beta titanium transformation) to be determined.

If the pellet temperature is above the defined ignition temperature (the melting point of titanium) the pellet is said to ignite. The adiabatic temperature of the reaction following ignition (assuming all remaining reaction occurs instantaneously), taking into account phase transformations, is calculated as well as the cooling profile of the pellet. If molten phases solidify the latent heat of fusion of those phases must be lost before the pellet temperature will drop any further. If the pellet temperature is not above the ignition temperature at the end of the particular timestep, the cycle repeats itself.

The model is expanded and detailed below. A print out of the computer programmes along with a full programme commentary can be found in the appendix.

7.3 Defining the Pellet

Initially, the make up of the cylindrical pellet in terms of its physical size and the size and condition of the powders from which it is made has to be defined.

Factors that need to be known to define the pellet are:

- Pellet radius.
- Pellet length.
- Titanium powder radius.
- Initial TiO₂ thickness on the titanium powder.

The *standard pellet* is defined as:

- 12mmØ.
- 20mm length.
- 75µm Titanium powder diameter.
- 0.01µm TiO₂ Initial oxide thickness.
- 100% ActiveFactor (see section 7.4.1).
- 35% Conversion Factor upon ignition.

The *standard furnace routine* is defined as:

- 1000°C Furnace start temperature.
- 20°C Pellet start temperature.
- 0°C / min. Furnace heating rate.
- 1000°C Furnace holding temperature.
- 10 min Furnace holding time.
- 250°C / min. Cooling rate.

Additional values that are set as constants in the calculations are detailed below.

7.3.1 Pellet Dimensions

The radius and length of the pellet affect the surface area and volume of the pellet. These factors play an important part in defining the amount of heat loss

or gain from the pellet to the surroundings. The pellet surface area is defined as:

$$P_{\text{surf}} = (2 \pi P_{\text{rad}} P_l) + (2 \pi P_{\text{rad}}^2) \quad (7.1)$$

where P_{rad} is the pellet radius and P_l is the pellet length. It is seen that the pellet surface area has a linear relationship with the pellet length, but an 'squared' relationship with the pellet diameter. The pellet volume is defined as:

$$P_{\text{vol}} = \pi P_{\text{rad}}^2 P_l \quad (7.2)$$

Due to the squared term in the calculation of the pellet volume it too will have an 'squared' relationship with the pellet diameter. Graph 7.1 records the effect of changing the pellet length, diameter or both these variables, on the pellet surface area.

7.3.2 Titanium Powder Data

The diameter of the powder and the initial thickness of TiO_2 on the powder alter the powder volume and the actual volume of titanium in the powder. The volume of one titanium powder particle is defined as:

$$Ti_{\text{totvol}} = (4 \pi Ti_{\text{rad}}^3) / 3 \quad (7.3)$$

where Ti_{rad} is the powder radius. The actual volume of the titanium in the powder particle, taking into account the thickness of the initial oxide layer on the particle is defined as:

$$Ti_{vol} = (4 \pi (Ti_{rad} - Ox_{th})^3) / 3 \quad (7.4)$$

where Ox_{th} is the initial TiO_2 thickness on the powder. The initial oxide thickness on the powder will strongly affect the subsequent oxidation of the titanium. Graph 7.2 records the effect of increasing initial oxide thickness on the powder in relation to the number of moles of titanium in the pellet and the number of moles of TiO_2 in the pellet.

7.3.3 Pellet Data

The schematic in figure 7.3. details the form of the pellet and powders that are used within the numerical model. The powder particles are assumed to be spherical and it is assumed that the spheres pack with maximum efficiency (74%) within the pellet. Thus, the number of titanium powder particles in the pellet is defined as:

$$Ti_{num} = 0.74 P_{vol} / Ti_{totvol} \quad (7.5)$$

where the 0.74 factor is the packing density of the titanium powder. The number of powder particles in the pellet is therefore controlled directly by the diameter and length of the pellet and the diameter of the powder particles. The total surface area of titanium powder within the pellet can be defined as:

$$Ti_{surf} = 4 \pi Ti_{rad}^2 Ti_{num} \quad (7.6)$$

Again this is related directly to the pellet dimensions and powder diameter. Graph 7.3 details the effect of the titanium powder diameter on the surface area of the powder. A decrease from 150 μ m \varnothing powder to 70 μ m \varnothing powder increases the powder surface area to (150 / 70) x 100% (~200%) of its original value. Graph 7.4 shows the effect of the titanium powder diameter on the number of particles in a standard pellet. Decreasing the powder size from 150 μ m to 70 μ m increases the number of powder particles in the standard pellet to (150 / 70)³ x 100% (~1000%) of its original value. Additional factors can also be calculated. The number of moles of titanium in the pellet is defined as:

$$Ti_{mol} = (Ti_{num} Ti_{vol} \rho_{ti}) / M_{ti} \quad (7.7)$$

where M_{ti} is the molar mass of titanium and ρ_{ti} the density of titanium. The initial mass per m² of TiO₂ on the surface of the titanium particles (Ox_{mas}) can be defined as:

$$Ox_{mas} = Ox_{th} \rho_{ox} \quad (7.8)$$

where ρ_{ox} is the density of TiO₂. The number of moles of TiO₂ in the pellet as a whole can then be defined as:

$$Ox_{mol} = (Ox_{mas} / M_{ox}) Ti_{surf} \quad (7.9)$$

where M_{ox} is the molar mass of TiO_2 .

It can be clearly seen that the values calculated above are related to the pellet dimensions, the powder diameter and the initial oxide thickness of the titanium particles.

7.4 Oxidation

Titanium oxidises when heated in an oxygen containing environment. In this model the oxide that forms as titanium is oxidised in air is assumed to be TiO_2 (Unman *et al.*, 1986). The oxidation of titanium is independent of oxygen pressure as the diffusion of oxygen through the oxide coating is the rate controlling process (Dechamps and Lehr, 1976). Oxidation is assumed to be parabolic; the total mass of TiO_2 produced per unit area as a function of time, t , is defined as:

$$\Delta m^2 = kt \quad (7.10)$$

where Δm is the mass of TiO_2 formed per unit area after a time t and k the rate constant. The oxidation rate constant, k , exhibits an Arrhenius type behaviour and is defined as:

$$k_p = C e^{(-Q/RT)} \quad (7.11)$$

where C is a constant having the same dimensions as k_p ($kg^2cm^{-4}s^{-1}$) and is derived from experimental values, Q is the activation energy, R is the Gas

Constant and T the absolute temperature. The equation used in the model defines the parabolic oxidation of titanium and is said to be accurate from 550°C to 850°C (Kubaschewski and Hopkins, 1952). Below 500°C the oxidation kinetics are seen to be logarithmic; however Tavgen *et al.* (1992) showed that there is no significant oxidation below 500°C, and therefore the logarithmic kinetics are not modelled. Instead the same parabolic kinetics are employed below 550°C.

Dechamps and Lehr (1976) argued that the transition from parabolic to linear oxidation was a function of the thickness of the oxide layer, and not due to the change in temperature, as others had claimed. The change in kinetics was seen to occur when the oxide was around 10µm thick. Due to the fact that the pellets modelled here ignite when the oxide is around 1µm thick, the kinetic change from parabolic to linear behaviour is not modelled. The reaction of titanium with nitrogen from air is seen to be negligible at these temperatures (Merzhanov *et al.* 1995) and is therefore not included in the equation or calculations.

By differentiating equation 7.10 with respect to time, the incremental mass gain in any given time can be calculated:

$$\Delta m^2 = kt \quad \Rightarrow \quad \frac{d \Delta m}{dt} = \frac{\sqrt{k} \sqrt{k}}{2 \Delta m} = \frac{k}{2 \Delta m} \quad (7.12)$$

However:

$$\sqrt{t} = \frac{\Delta m}{\sqrt{k}} \quad (7.13)$$

and thus:

$$\frac{d\Delta m}{dt} = \frac{\sqrt{k}}{2\sqrt{t}} \quad (7.14)$$

Thus the increment in mass gain in a time period, dt , can be calculated as:

$$d\Delta m = \frac{k}{2\Delta m} \cdot dt \quad (7.15a)$$

or

$$d\Delta m = \frac{\sqrt{k}}{2\sqrt{t}} \cdot dt \quad (7.15b)$$

Thus the increment of mass increase can be calculated at any temperature (k is a function of temperature) as long as the mass of oxide already in existence is known, or the total time of oxidation (with that value of k) up to that point is known. Within the model, the incremental oxidation has been calculated using the concept of a 'dummy time' which takes into account that k varies with temperature and thus with time. Graph 7.5 describes the notion of a dummy time. Starting from a time, t_0 , the equation calculates the mass of oxide, Δm_1 , formed in the time period t_{step} at the temperature T_1 . The model then calculates the new temperature, T_2 , attributed to the combined effect of furnace heating or cooling and the energy released by the oxidation of the titanium. The model then determines how much time it would have taken to form the existing total mass of oxide, Δm_1 of TiO_2 at the new temperature, T_2 . This is now referred to as the dummy time, t_{dum} . The model then calculates the mass of oxide formed, Δm_2 , in the time period t_{step} from t_{dum} to $(t_{\text{dum}} + t_{\text{step}})$. In this way it is possible to

calculate the mass of oxide formed for any thermal history of the sample. The model assumes that the oxidation is isothermal over the timestep. In this way anisothermal oxidation can be expressed as a series of small isothermal oxidation's of time period t_{step} , as shown in graph 7.6.

After k_p has been calculated for a given temperature the model defines dummy time in seconds as:

$$t_{\text{dum}} = \text{Ox}_{\text{mas}}^2 / k_p \quad (7.16)$$

The mass of TiO_2 per m^2 formed in the time period t_{step} , Ox_{minc} is then calculated:

$$\text{Ox}_{\text{minc}} = k_p^{1/2} \cdot ((t_{\text{dum}} + t_{\text{step}})^{1/2} - t_{\text{dum}}^{1/2}) \quad (7.17)$$

This value is not linked to the surface area of titanium since it is a generic value that describes the mass of TiO_2 formed per m^2 of available surface area at temperature T , after time period t_{step} . The Ox_{mas} is recalculated to take into account the new mass of oxide / m^2 . Again the value is generic and not linked to the pellet dimensions:

$$\text{Ox}_{\text{mas}} = k_p^{1/2} \cdot (t_{\text{dum}} + t_{\text{step}})^{1/2} \quad (7.18)$$

7.4.1 Temperature Increase Due to Oxidation

The mass of $\text{TiO}_2 / \text{m}^2$ formed in a time period is known as Ox_{minc} . An 'Active Percentage' factor, α , is also incorporated into the model. It is a user-defined constant that determines the amount of titanium surface area that is said to be active in oxidation. This factor is included as it is seen experimentally and in the literature (Bakhman *et al.*, 1998) that full oxidation only occurs on the outer surface of the pellet. Oxygen does not significantly get to the core of the pellet to oxidise the titanium. Typically, titanium powder to a depth of $\sim 1\text{mm}$ has oxidised to TiO_2 , where as the remaining powder does not oxidise or oxidises to TiO or Ti_2O_3 . The 'Active Factor' takes into account the uneven distribution of oxidation throughout the pellet.

For a typical pellet size of $12\text{mm}\varnothing$ and 20mm length a 1mm thick crust of TiO_2 will account for $\sim 37.5\%$ of the total volume of the pellet. It should be noted that the amount of surface area reacting exothermically is in reality not limited to the TiO_2 crust material. The titanium oxidising within the pellet, prior to ignition, will contribute to the heat output of the pellet in experiments. Considering this fact, α is usually greater than the figure calculated from the thickness of the formed TiO_2 reaction layer.

Thus, the actual mass of TiO_2 formed in the time period is calculated by the usable surface area of titanium, which is determined by an 'Active Percentage' factor α :

$$\text{Ox}_{\text{mas}} = \text{Ox}_{\text{minc}} (\text{Ti}_{\text{surf}} \cdot \alpha) \quad (7.19)$$

The amount of energy released by the oxidation of titanium is defined as:

$$E_{\text{ox}} = O_{\text{X,mas}} (O_{\text{X,enth}} / M_{\text{ox}}) \quad (7.20)$$

where $O_{\text{X,enth}}$ is the molar enthalpy of formation of TiO_2 at temperature T . The enthalpy of the oxidation reaction, $O_{\text{X,enth}}$, is calculated at the temperature of reaction by Kirchoffs Law, as shown in figure 7.4.

7.5 Heating and Cooling of the Pellet

The heating and cooling of the pellet is defined by the summation of the conductive and radiative heat gains or losses. The energy absorbed or lost by the pellet by conduction is modelled on one dimensional steady heat flow from the pellet to the surrounding. For the purposes of the model, the pellet is said to have no temperature gradients, thus Fourier's first law is defined as:

$$Q_c = H \cdot A \cdot (T_2 - T_1) \quad (7.21)$$

where Q_c is the energy absorbed by the body per unit time in W, H is the heat transfer coefficient of the body in $\text{W} / \text{m}^2 \text{K}$, A is the surface area of the body in m^2 , $(T_2 - T_1)$ is the relative difference between the body temperature, T_2 , and the ambient atmosphere temperature, T_1 . This equation is written in the model as:

$$Q_c = H (P_{\text{temp}} - F_{\text{temp}}) P_{\text{surf}} \quad (7.22)$$

The energy emitted or absorbed by the pellet by radiation per unit time is calculated by a derivation of the Stefan-Boltzmanns Law. For black body radiation, the total energy emitted or absorbed per unit time by unit area of a black body surface (Q_b) is proportional to the fourth power of the absolute temperature T . This ratio is expressed by the Stefan-Boltzmann Law:

$$Q_b = S \cdot T^4 \cdot A \quad (7.23)$$

Where S is the Stefan-Boltzmanns constant, equal to $56.7 \times 10^{-12} \text{ kW} / \text{m}^2 \text{ K}^4$, T is the absolute temperature in K and A is the surface area of the body in m^2 . In reality there are no materials that act as true black bodies, all materials are classed as grey bodies. For a grey body the amount of energy absorbed or emitted by it in radiation is altered by the emissivity of the material. The emissivity of a material is defined as:

$$Em = [Q / Q_b]_T \quad (7.24)$$

where Q is the energy emitted per unit time by the body at T and Q_b is the energy emitted by a black body at T . Therefore the energy emitted or absorbed by the material at temperature T is now:

$$Q = Em \cdot S \cdot T^4 \cdot A \quad (7.25)$$

This equation is written in the programme as:

$$Q_b = (S \cdot Em) (P_{temp}^4 - F_{temp}^4) \cdot P_{surf} \quad (7.26)$$

where P_{temp} is the temperature of the pellet and F_{temp} is the temperature of the furnace. The addition of the two equations (7.22 and 7.26) in the model allows calculation of the total energy absorbed or emitted from the pellet in a time period, t_{step} , and takes the form:

$$E_{fur} = ((H (P_{temp} - F_{temp})) + ((S \cdot Em) (P_{temp}^4 - F_{temp}^4))) P_{surf} \cdot t_{step} \quad (7.27)$$

If E_{fur} is negative, the energy is said to be absorbed by the pellet, and if it is positive the energy is released by the pellet. Both H and Em are unknown variables, however, the effect of each on the heating of the pellet has been investigated. It is seen from graph 7.7 that H has a relatively small part to play within the equation. Typical values are between 5 and 15 $W / m^2 K$ (Zemansky and Dittman 1997) so there is little variance in the calculated time to ignition, only 30 seconds over a change in the heat transfer coefficient of 100 $W / m^2 K$. The behaviour is more sensitively dependant on the emissivity term as it can change from 0.3-0.4 for titanium metal to 0.8-0.9 for titanium oxide (Zemansky and Dittman 1997). As can be seen from graph 7.8, such a range of values greatly effects the time it takes for the pellet to ignite, in this case by over 500 seconds over the full emissivity range. With greater values of either, emissivity or H , the pellet not only absorbs, but also loses, heat energy more quickly. All this implies that heat losses throughout the process are dominated

by radiation. As such, H was set at the middle value of $10 \text{ W / m}^2 \text{ K}$. A value of 0.6 for the pellet emissivity was chosen as a compromise value between titanium metal ($E_m = 0.3$) and titanium oxide ($E_m = 0.9$).

7.6 Pellet Temperature Changes

The total amount of energy either absorbed or lost from the pellet in a timestep depends on the enthalpy of oxidation and the heat transferred to or from the surroundings and is defined as:

$$E_{\text{tot}} = E_{\text{ox}} + E_{\text{fur}} \quad (7.28)$$

The actual temperature change of the pellet in K attributed to this energy change is defined by:

$$T_{\text{chg}} = \frac{-E_{\text{tot}}}{(Ti_{\text{mol}} \times \int C_p(Ti) dT) + (Ox_{\text{mol}} \times \int C_p(TiO_2) dT)} \quad (7.29)$$

The new pellet temperature is then simply:

$$P_{\text{temp}}(\text{new}) = P_{\text{temp}}(\text{old}) + T_{\text{chg}} \quad (7.30)$$

If the pellet temperature rises above the titanium $\alpha \Rightarrow \beta$ transition temperature (1155K) then the latent heat of transformation for that reaction is included in the calculation. This is modelled by ensuring that there is no pellet temperature increase until the total amount of energy required for transformation has been absorbed by the pellet. Additionally, whilst the pellet is cooling after the

reaction any transformations or solidifications that are exothermic are modelled such that there is no pellet temperature fall until the energy of that transformation has been liberated from the pellet.

7.7 Pellet Ignition

It has been seen that titanium only burns in the liquid state (Sirca *et al.* 1991 and Abbud-Madrid *et al.* 1996). Pellet ignition, the point at which the pellet starts to burn, is therefore set at the melting point of titanium, 1943K. The burning of the titanium pellet liberates a massive amount of energy which drives the temperature of the pellet considerably higher than the surrounding temperature (Abbud-Madrid *et al.* 1996). The pellet continues to burn only if the exothermic heat liberated by the pellet produces a liquid phase (Poyurovskaya and Ryabwuk 1989). This is in contrast to oxidation, which is controlled by diffusion of oxygen through the oxide layer (Rode and Hlavacek 1994), and is only mildly exothermic (Tavgen *et al.* 1992).

Experiments detailed previously have shown that the burning of the pellet is not instantaneous, but takes place over a number of seconds. The length of time it takes the pellet to burn can be attributed to a number of factors. The main influences are the size of the titanium powder, the pellet density and the ambient temperature. In the model, the burning of the pellet is not modelled, instead an instantaneous adiabatic reaction temperature is assumed. (This is due to the fact that the model was designed to describe the ignition of an Fe₂O₃ and Ti pellet. The reaction between these powders happens rapidly, as bulk oxygen diffusion is not a limiting factor, and is therefore faithfully modelled)

A 'Conversion Factor' is introduced at the point of calculating the adiabatic reaction temperature. The factor is required as it has been seen experimentally and in the literature (Tavgen *et al.* 1992 and Bakhman *et al.* 1998) that pellets do not fully react to the product phase. Thus, only a percentage of the titanium in the pellet is contributing to the exothermic heat and subsequently, the adiabatic temperature of the reaction. The 'Conversion Factor' is different from the 'Active Factor' because the titanium within the pellet does not continue to oxidise and contribute to the exothermic heat output of the pellet. This is due to the TiO₂ layer being formed primarily from liquid titanium. As such, the formed TiO₂ is a solid layer and acts as a very strong diffusional barrier to subsequent oxygen penetration into the pellet. In the model the 'Conversion Factor' acts to describe what percentage of the pellet will react, and is modelled as:

$$E_{ad} = E_{tot} \cdot C_f \quad (7.31)$$

where E_{ad} is the energy used in the calculation of the adiabatic temperature, E_{tot} is the total energy of the system (the energy released by the reaction $Ti + O_2 \Rightarrow TiO_2$) and C_f is the Conversion Factor. The 'Conversion Factor' is also used to describe what percentage of the pellet does not react to form TiO₂. This remaining titanium metal acts as a heat sink for some of the energy of reaction. Its liquefaction and possible vaporisation limits the adiabatic temperature of the pellet. Graph 7.9 describes the effect of the 'Conversion Factor' on the calculated adiabatic temperature.

The numerical model only determines the adiabatic reaction temperature of the pellet. This is calculated under the conditions that the reaction happens instantaneously, i.e. there is no heat loss from the pellet and the reaction is $\text{Ti} + \text{O}_2 \Rightarrow \text{TiO}_2$. As mentioned earlier, experiments have shown that the reaction does not occur instantaneously, with the length of the burn time being measured in seconds. Additionally, heat loss from the pellet whilst it is reacting is considerable. These factors result in the calculated adiabatic temperature for the model being considerably higher than experimentally derived values.

The adiabatic reaction temperature for the reaction between titanium (liquid) and oxygen (gas) to form the product TiO_2 , is specifically calculated by using an iterative process to solve the integration:

$$\Delta H_{T_{ig}} = -\left[\int_{T_{ig}}^{T_p} \sum C_{p(1)} dT + Li_{(1 \rightarrow 2)} + \int_{T_p}^{T_{ad}} \sum C_{p(2)} dT \right] \quad (7.32)$$

where T_{ad} is the adiabatic temperature of reaction in K, T_p is the temperature of a phase change, $C_{p(1)}$ and $C_{p(2)}$ are the heat capacities for the phases before and after the phase change, Li is the latent heat of transformation and where $\Delta H_{T_{ig}}$ is the enthalpy of reaction at the ignition temperature and is shown schematically in figure 7.4 as:

$$\Delta H_{T_{ig}} = \sum \Delta H_{f, T_{ig}}(P) - \sum \Delta H_{f, T_{ig}}(R) \quad (7.33)$$

where $\Delta H_{f, T_{ig}}(P)$ and $\Delta H_{f, T_{ig}}(R)$ are the enthalpies of formation at the ignition temperature of the products and reactants respectively.

7.8 Results from Running the Programme

7.8.1 Introduction

To gain a full understanding of the model it is necessary to analyse the effect of each parameter. However, the programme is constructed from equations that are related to one another and produce dynamically changing results as the programme runs. To analyse the effect of the individual parameter it is therefore necessary to run the programme using a set input scheme and only alter the parameter that is of interest. In this way, the effect of that particular piece of parameter on the model can be determined.

7.8.2. Standard Input Variables

The standard pellet is defined as:

- 12mmØ.
- 20mm length.
- 75µm Titanium powder diameter.
- 0.01µm TiO₂ Initial oxide thickness.
- 100% ActiveFactor.
- 35% Conversion Factor upon ignition.

The standard furnace routine is defined as:

- 1000°C Furnace start temperature.
- 20°C Pellet start temperature.
- 0°C / min. Furnace heating rate.
- 1000°C Furnace holding temperature.
- 10 min Furnace holding time.
- 250°C / min. Cooling rate.

Due to the number of dynamic variables in the programme a simple furnace routine with no heating rate has been used. In this way interpretation of the graphical data and visualisation of the particular effect of the tested parameter is simpler. However, the model allows the temperature of the furnace to be varied as required e.g. a heating > hold > cooling cycle.

7.8.3. Graphical Outputs

Graph 7.10 is a plot of the standard pellets temperature profile and the standard furnace temperature profile, but of reduced hold time, against time.

7.8.3.1. *The Effect of the Pellet Parameters*

- The variation of the pellet diameter; graphs 7.11, 7.12 and 7.13.
- The variation of the titanium powder diameter; graphs 7.14, 7.15, 7.16.
- The effect of the furnace temperature; graphs 7.17 and 7.18.
- The combined effect of pellet size and powder diameter. Graphs 7.19, 7.20, 7.21.

- The variation of the initial oxide thickness and the formed oxide thickness on the titanium powder; graphs 7.22, 7.23, 7.24.
- The effect of the 'Active Factor'; graph 7.25.

7.8.3.2. *The Effect of the Furnace Parameters.*

- The effect of the furnace heating rate; graphs 7.26, 7.27, 7.28, 7.29, 7.30, 7.31.
- The effect of furnace holding time; graph 7.32.

7.9 Experimental Verification of Programme Results

7.9.1 Introduction

A model cannot be critically analysed unless its predictions are tested against experimental evidence. In the light of this, an experiment has been conducted that finds the minimum furnace temperature that is required to ignite a pellet of spherical titanium powder. The titanium, being spherical and of limited size fraction ($<125\text{-}75\mu\text{m}$) will be comparable to the parameters the model is using to calculate the ignition temperature of the powder.

7.9.2 Experimental

To test the model an experiment has been conducted (repeated 8 times for accuracy) that represents the model by using spherical titanium powder. The limited availability and cost of spherical commercially pure titanium powder precluded its use throughout the research. The experiment tested the minimum furnace temperature that facilitated ignition of the powder. The powder could not be pressed and was thus held in a tubular furnace boat. As no deformation of the powders occurred through pressing, true point contacts were obtained. Additionally, the flow of oxygen through the powders was increased, thus representing a true 'active factor' of 100%. The powders were placed and held in a pre heated furnace for 20 minutes. Ignition of the powders was observed through the viewing port.

7.9.3 Results

The powders were seen to ignite and burn exothermically at $800^{\circ}\text{C} \pm 10^{\circ}\text{C}$. The model, when run with the same parameters used in the experiment (the 'standard' pellet parameters) but with different powder diameters, to take into account the variability in the experimental powder size fraction, produced comparable results, seen below, in table 7.1.

Powder Diameter / μm	Temperature Required to Promote Ignition / $^{\circ}\text{C}$
75	778
100	823
125	854

7.9.4 Discussion

In actual experiments it will be the smallest powders that ignite first; thus the model accurately predicts the onset of ignition at around the correct, experimentally verified, temperature.

7.10 Discussion

7.10.1 The Effect of the Pellet Parameters

7.10.1.1 *The Variation in Pellet Diameter and Size*

Graph 7.11 details the effect of just increasing the pellet diameter, whilst the length is kept constant at 12mm, on the time it takes for the pellet to ignite in a furnace at a constant temperature. The pellet becomes more disc shaped as the diameter increases, and in doing so the main gain in surface area is through the increase in the top and bottom surfaces of the pellet. The surface area of the pellet and its volume effect the heating rate of the pellet in a furnace of fixed temperature. The surface area governs the amount of heat energy absorbed or lost by the pellet (equation 7.27) and the pellet volume determines how much material is in the pellet and thus the increase in pellet temperature caused by the absorption of that amount of energy (equation 7.29).

Thus, the ratio of pellet surface area to pellet volume (S-V ratio), when related to changing pellet dimensions, is an expression of the effect of those dimensions on the pellets heating rates in a furnace of fixed temperature. The S-V ratio when the diameter is only changed is asymptotic, reaching its asymptote around 100-150mm \varnothing for the standard pellet. This is shown in the graph as a levelling off of the time to ignition at around this pellet size. Above this point there is no significant change in the S-V ratio and thus the heat input into the pellet and temperature rise with respect to the heat input, determined by the pellet volume, remain constant. The only way to decrease the time to ignition is to increase the furnace temperature which increases the rate of heat

input into the pellet. An interesting effect seen in the 800°C furnace is that the smallest pellets do not ignite. This effect is discussed later with reference to Graph 7.13.

Graph 7.12 details the effect of pellet size with respect to the standard size, on the time it takes for the pellet to ignite in a furnace at constant temperature. The size of the pellet is expressed as a ratio of the standard size, thus a 10x standard size pellet has dimensions of 120mm \varnothing and 200mm length. The time taken for the pellet to ignite increases linearly with the pellet size. In this case the S-V ratio increases linearly with the pellet dimensions. This produces the linear time to ignition output as the gain in pellet surface area is matched by the gain in pellet volume. Again, increasing the furnace temperature reduces the time taken for the pellet to ignite. The smallest 800°C pellets are again seen not to ignite. The pellet temperature data from those pellets is presented in graph 7.13.

Graph 7.13 shows the actual temperature plots of a number of pellets from graph 7.12, when placed in the furnace at 800°C. Some of the pellets illustrate ignition whilst others do not. As the S-V ratio is linear then so the heat loss from the pellet to pellet volume ratio must also be linear. In effect the % of heat energy lost is constant for any given pellet size ratio and temperature.

A simple way to understand the relative 'reactivity' of a powder / pellet composition is to describe the quantity of exothermic energy released in

relation to the volume of metal in the pellet in J / cm^3 . The J / cm^3 term is constant for a certain powder size.

In the case of the 0.25x pellet the S-V ratio is high and there is a large amount of relative heat loss, there is only enough exothermic energy from the oxidation to raise the pellet temperature slightly above the ambient atmosphere. As soon as the pellet temperature exceeds the furnace temperature only the energy from the oxidation of the titanium is available to increase the temperature of the pellet. As the oxide layer thickens, the rate of reaction at any given temperature reduces. To ensure that the reaction proceeds, the reaction rate must be promoted by an increase in temperature due to oxidation.

Increasing the size of the pellet to 0.75x standard size increases the amount of available exothermic energy, which drives the pellet temperature above the furnace temperature, into the $\alpha - \beta$ transformation temperature. The exothermic energy of oxidation then has to supply enough energy to complete the transformation before the energy is used to raise the temperature of the pellet again. It can be seen that there is only enough energy after the $\alpha - \beta$ transformation to increase the pellet temperature slightly. The pellet then cools, going through the $\beta - \alpha$ transformation and onto the ambient furnace temperature.

Increasing the pellet size ratio to 1.25x increases the amount of available energy to such an extent that a 'thermal runaway' of the pellet take place, which leads to ignition of the pellet. It can be seen that the time taken to pass

through the $\alpha - \beta$ transformation is considerably less than taken by the 0.75x pellet. The x2 pellet also ignites. It can be seen that the time taken for the pellet to reach the furnace temperature increases with the size of the pellet, the effect of which can be seen in graph 7.12.

7.10.1.1.1 Experimental Verification

Rode and Hlavacek (1994) analysed the time and temperature taken to ignite various sized samples of titanium powder. The samples were heated at a constant 10°C / minute, not placed into pre-heated furnaces. They found that larger samples ignited quicker and at lower temperatures due to the reduced relative heat loss from them. This is not to be taken as a comparison with larger samples placed into a pre-heated furnace, graph 7.12, as larger samples take longer to heat up and thus ignite. The effect of reduced relative heat loss with increasing sample size is modelled in the programme and shown later, in graph 7.21.

7.10.1.2 The Variation of Powder Diameter

Graph 7.14 displays the time taken for the standard pellet to ignite with respect to titanium powder diameter, over a number of furnace temperatures. It can easily be seen that a smaller powder size or an increases furnace temperature reduces the time taken for the pellet to ignite. Additionally, the maximum powder diameter that will allow ignition at a certain furnace temperature is shown. Higher furnace temperatures allow the use of larger powder diameters. The surface area of the powder is related to the diameter of the powder, as

shown in graph 7.3. A larger powder surface area gives a larger area for oxidation, and thus a larger release of exothermic energy.

The number of moles of titanium (the volume of titanium) stays constant for a given pellet size and therefore a smaller powder size has a greater amount of active surface area available for a given volume of titanium. Thus, smaller powders enable the pellet to heat up more quickly due to oxidation and ignition can take place at lower furnace temperatures. The larger amount of exothermic oxidation energy compensates for the lack of furnace supplied energy at the lower temperatures.

Graph 7.15 contains similar data to graph 7.14 with the time to ignition plotted against the furnace temperature for a range of powder particle sizes. It can be seen that for a certain powder size, an increase in the furnace temperature reduces the time it takes for the pellet to ignite. Additionally, the data points to a convergence in the time taken for the pellet to ignite across the range of titanium powder particles sizes. On the graph the convergence is seen to occur around 2000°C, which is above the melting point of titanium, and thus the time to ignition is primarily determined by the time it takes for the pellet to heat up to this temperature. This value is related to the pellet dimensions, as it has already been shown in graph 7.12, that an increase in pellet size effects the time it takes for the pellet to ignite. The powder diameter is seen to be irrelevant as oxidation is not a determining factor in whether the pellet temperature goes above the ignition temperature.

Graph 7.16 shows the actual pellet temperature profiles for pellets with different powder diameters. It is clearly seen that the whilst the pellets heat up at the same rate initially (for pellets of the same size) the exothermic oxidation effect is much more pronounced in the smaller diameter powder pellets. The 85 μm powder pellet takes over 200 seconds longer to ignite than the 10 μm powder pellet. The lack of any observable α - β transformation holding period in the 10 μm powder gives some idea of the amount of energy released. The comparison of the temperature plot of the 10 μm and 85 μm powder pellet shows that the exothermic reaction in the 10 μm powder pellet starts to overtake the effect of the furnace heating at around 850 K. The pellet is seen to ignite, characterised by a temperature above the melting point of titanium (1943K), a few seconds later. The 85 μm powder pellet has a long period of exothermic activity above the furnace temperature before eventually igniting. Characteristically, small diameter powders ignite easily and rapidly, whilst larger powders take longer and require higher furnace temperatures.

Graph 7.17 shows the effect of the furnace temperature on the heating rate of the pellet. As expected, higher furnace temperatures increase the heating rate, and promote ignition of the pellet. In the case of the standard pellet, a furnace set at 775°C (1048K) will not ignite the pellet. Graph 7.18 highlights the same effect in a 10 μm powder pellet in a furnace at 600 and 800°C.

7.10.1.2.1 Experimental Verification

In chapter 5 it was clearly show in table 5.7 that the furnace temperature required to ignite the pellet increases as the powder diameter increases. This effect is clearly modelled in figure 7.20. The actual figures seen in the experiments are not comparable due to the large difference in the powders used in the experimental and that used in the model. The experimental powders are not spherical, but a crushed highly porous foam, and thus have a larger surface area to that of a spherical powder. The powders, if meaningful comparisons wish to be made, therefore have to be modelled as a smaller diameter than they are, which introduces complications in the calculations of a number of pellet properties. The model predicts that the powder particle size has to be less than $19\mu\text{m}$ to ignite at 600°C .

In the $<150\mu\text{m}$ titanium powder, $\sim 18\%$ of the powder is below a particle size of $45\mu\text{m}$. In the $<355\mu\text{m}$ titanium, only $\sim 2\%$ is below a particle size of $45\mu\text{m}$. This fact does explain why the $<355\mu\text{m}$ powder requires a higher furnace temperature to promote ignition.

The model fundamentally works with the surface area of titanium and so it would be simple to input the surface area of the experimental powder rather than use the in-built calculation of surface area, based on spherical powders.

7.10.1.3 The Combined Effect of Pellet Size and Powder Diameter

Graph 7.19 details the combined effect of pellet size and powder diameter on the time taken for the pellet to ignite. Larger powder diameters increase the time taken for the pellet to ignite in an almost linear fashion. The 10 and 20 μm powder pellets seem to ignite in times that are slightly less than would be predicted by a linear line. This effect is most significant in the larger pellet sizes. Larger pellet sizes increase the time to ignition of the pellet equally across all the powder diameters. This is shown in the transposition of the lines up the graph with increasing pellet size.

Graphs 7.20 and 7.21 show the minimum furnace temperature, to the nearest degree, at which the pellet will ignite. The minimum temperature at which a pellet will ignite is governed by the amount of exothermic energy released with respect to the volume of titanium powder, J / cm^3 . As shown in graph 7.14, the smaller diameter powder pellets ignite at lower temperatures. Additionally, the pellets ignite at lower temperatures as they get larger. This is due to the S-V ratio, larger pellets have less surface area to volume than smaller pellets and will thus lose less heat than a smaller pellet for a given volume of powder.

7.10.1.4 The Effect of the Oxide Layer on the Pellet Ignition

All titanium that has been exposed to air has an adherent oxide coating on it. In this work the pre-existing oxide layer acts as a thickness of oxide that exists, but has not contributed to the heating of the titanium. In effect, the oxidation process is not starting from initial oxygen – metal contact, but from oxygen – oxide contact and this has to be taken into account in the model. Graph 7.22

shows the effect of the initial oxide thickness on the titanium powder on the time it takes for the pellet to ignite. As can be seen, the initial oxide thickness is most potent at the lower furnace temperatures, where pellet ignition is very sensitive to the pellet and furnace parameters. When the furnace temperatures are high (+1000°C) the pellet needs only supply a little exothermic oxidation energy to promote ignition. The oxidation of the pellet has to supply most of the energy to promote ignition when the furnace is at a low temperature.

The initial oxide layer has the effect of increasing the time to ignition for a certain furnace temperature and also limiting the maximum furnace temperature at which the pellet will ignite.

Graph 7.23 shows the total thickness of the oxide layer formed on the powder at the point of pellet ignition. This value includes the starting initial oxide thickness of 0.01 μ m. The total thickness of oxide on the powder at the point of ignition gives an idea as to the energy liberated by the powder. It is seen that the total oxide thickness on the powders at the point of ignition decreases slightly with increasing furnace temperature. This is due to the increased heating effect of the furnace graph 7.17, reducing the amount of energy that needs to be supplied by the exothermic oxidation of the titanium to promote ignition of the pellet. Larger powder diameters also require a thicker oxide layer, as the volume of the powder particle requires an increased amount of energy to cause melting of it.

Graph 7.24 shows that pellet size has a very limited effect on the total oxide thickness on the powder at the point of ignition. There is a slight increase in the thickness as the size increases, due to the longer times the pellet takes to heat up. Again the main influence on the oxide thickness is the powder particle diameter.

7.10.1.4.1 Experimental Verification

The work of Rode and Hlavacek (1994) on the oxidation of titanium powder at different heating rates highlights the fact that the onset of oxidation occurs at higher temperatures with increasing initial oxygen content due to a thicker oxide layer on the surface of the powder acting as a transport barrier. Powders oxidised prior to heating from room temperature, ignited at higher temperatures than that had not been oxidised. The effect is modelled in the programme and shown in graph 7.22.

7.10.1.5 The Variation in Active Factor

Graph 7.25 details the effect of the AF (Active Factor) on the time it takes for the standard pellet to ignite in a furnace of set temperature. Low furnace temperatures require a high AF for the pellet to ignite, the AF governing the amount of powder surface area that is said to be active and therefore contributing to the exothermic oxidation energy. At any given temperature the time for the pellet to ignite will decrease with increasing AF.

The percentage of pellet energy that is required to cause pellet ignition at any given furnace temperature can be found by the minimum AF value that causes pellet ignition to occur. Obviously, the pellet requires this amount of energy to be supplied above the furnace temperature to promote ignition.

7.10.1.5.1 Experimental Verification

The 'active factor' can be thought of as an effect of the density of the pellet, higher density pellets do not allow the internal titanium to oxidise and thus liberate heat energy. More porous pellets allow the free flow of oxygen and thus oxidation is increased. Experimentally, this has been seen in chapter 5 in table 5.7 and 5.8. Additionally, Bakhman *et al.* (1998), Dunmead and Munir (1989), Filonenko and Barzkin (1996) and Hiroshi and Odawara (1989) have all reported the increased combustion / conversion of powder pellets with increased porosity.

7.10.2 The Effect of the Furnace Parameters

As we have seen the furnace parameter of temperature has a considerable effect on the ignition of the pellet. Graph 7.26 details the averaged heating rate the pellet exhibits up to its ignition point, when placed into a furnace at a set temperature. As can be seen, the graph is not linear, but exhibits an exponential effect due to the increasing role of oxidation and radiation effects at the higher temperatures.

Graph 7.27 shows the effect on the ignition temperature and the oxide thickness on the powder at the ignition temperature, when the pellet is heated from room temperature at a fixed rate. It is seen that the oxide thickness on the powders and the furnace temperature at which they ignite is more or less constant when the heating rate is above $10^{\circ}\text{C} / \text{min}$ ($0.167^{\circ}\text{C} / \text{Sec}$). Slower heating rates cause an increase in the oxide thickness and the furnace temperature at which they ignite.

It is interesting to note that the furnace temperature at which the pellets ignite is around 1150K, the α - β transformation temperature. The pellets do not liberate enough exothermic energy to get them past the transformation temperature, and require the furnace energy to accomplish it.

For a certain heating rate it is shown in graph 7.28 that the thickness of the oxide on the pellet at the time of ignition increases linearly with the powder size. The oxide thickness expressed as a percentage of the powder radius gives a asymptotic graph, nearing 4.65% at a powder diameter of $200\mu\text{m}$. This is considerably larger than those of the pellets put into hot furnaces, as the heating rates are so much lower, as shown in graph 7.26.

The effect of various heating rates on the temperature pellet profile are shown in graph 7.29. The effect of the powder diameter on the temperature profile of the pellet is shown in graph 7.30. Pellets with smaller diameter powders ignite quicker and have a smaller oxide thickness on the powders. It is seen in graph

7.31 that pellets made from even the largest powder diameters will eventually ignite at the melting point of titanium.

The effect of the furnace holding time is also important in determining if ignition of the pellet will occur. Graph 7.32 demonstrates that if the pellet is only mildly exothermic then a drop in the furnace temperature, by the onset of furnace cooling, can increase the heat loss of the pellet such that the pellet cannot compensate for it and starts to cool. In such a case the pellets cease to undergo thermal runaway. Holding the furnace at temperature for a longer period of time reduces the heat loss from the pellet and allows the exothermic energy to be devoted to pellet temperature increase, thus thermal runaway occurs with subsequent ignition of the pellet.

7.10.2.1.1 Experimental Verification

The work of Rode and Hlavacek (1994) show that increased heating rates reduce the temperature at which the ignition of a powder sample will occur.

7.11 Conclusions

It has been shown that there are complex interactions that occur in the computation and modelling of the oxidation of the pellet and powder. The fact that a change in one variable effects many others sometimes makes it hard to determine why the output results are as they are. However, each aspect of the model is based on sound principles, which when taken as a whole and acting in

a dynamically changing way, faithfully represents the effect of the powder, pellet or furnace parameters.

The model has been shown to be accurate in the prediction of the furnace temperature required to promote the ignition of spherical titanium powder. The model is therefore accurate in its theory and operational procedure.

The interaction between the furnace parameters (maximum temperature, holding time, etc.) and the pellet and powder parameters (pellet size, powder diameter, initial oxide thickness, etc.) ultimately produces a relationship between heat loss and heat gain for the pellet. It is this relationship which will govern whether a pellet will ignite.

Chapter 7

Figures

Figure 7.1 Simple Flowchart of the Numerical Model

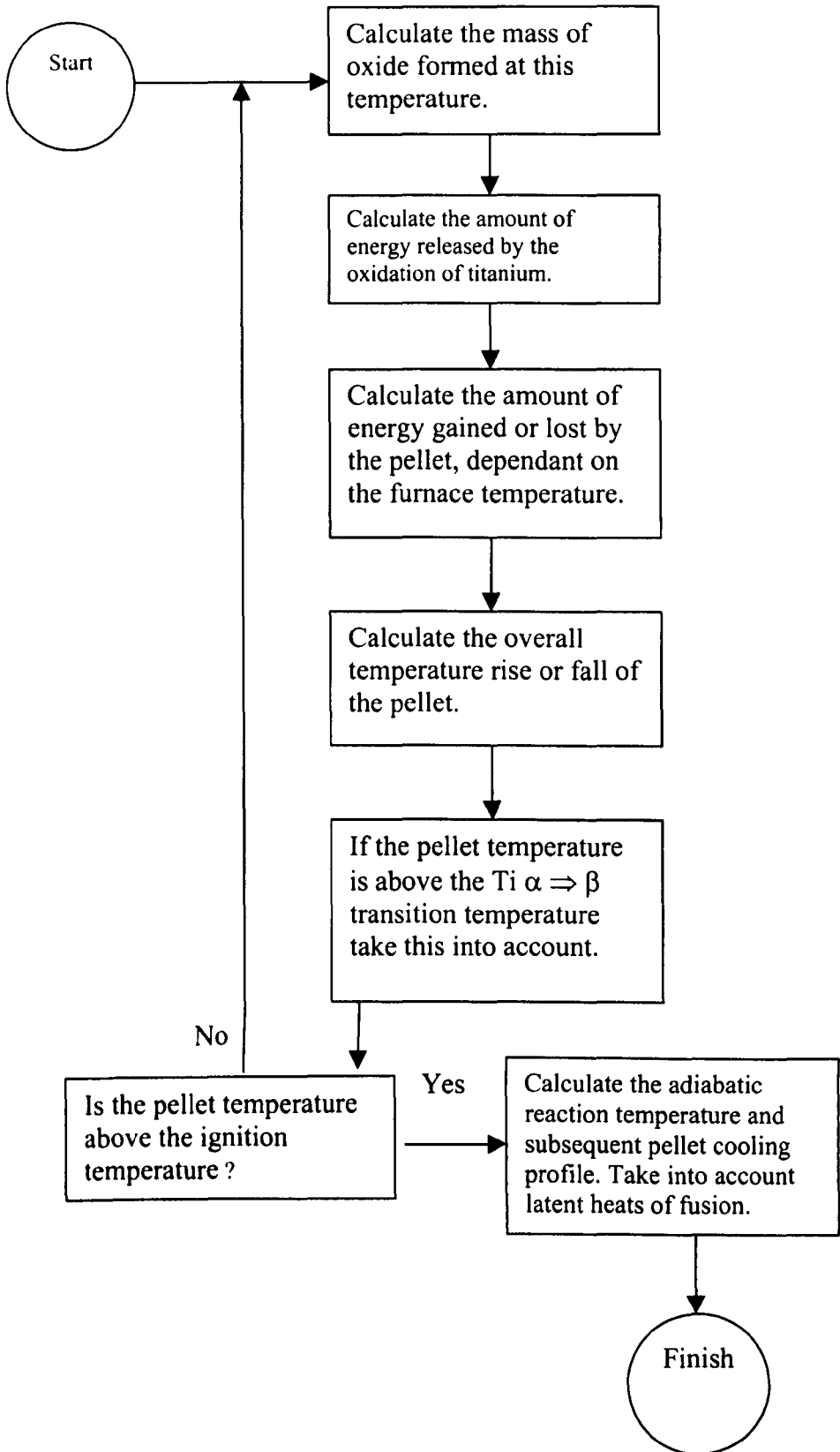


Figure 7.3 Schematic of Pellet and Titanium Powder, as used in the Model

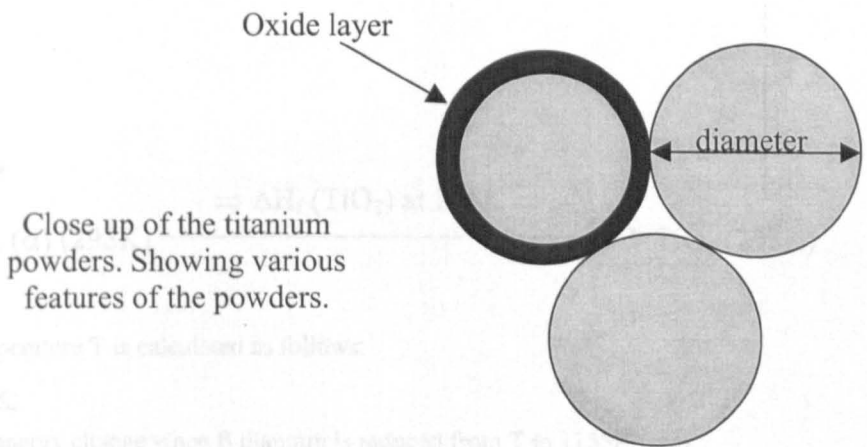
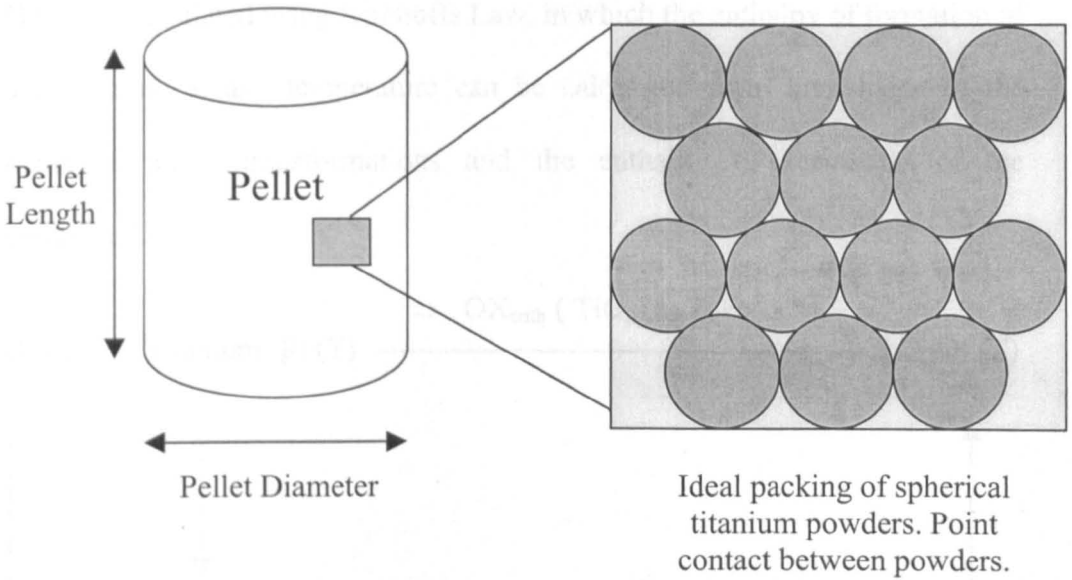
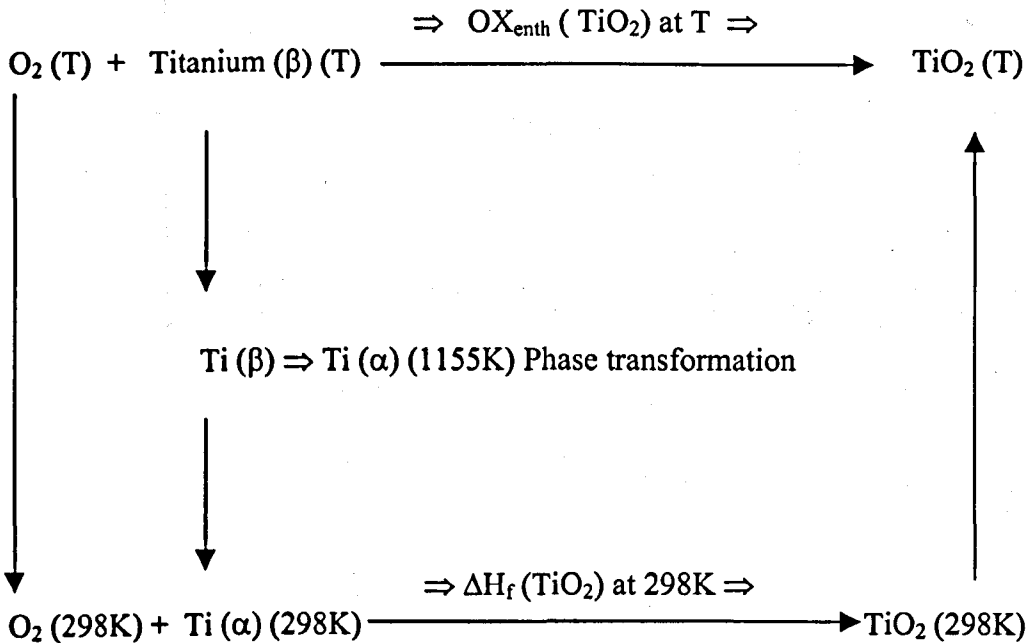


Figure 7.4 Schematic Representation of Kirchoffs Law

OX_{enth} is calculated using Kirchoffs Law, in which the enthalpy of formation of a compound at any temperature can be calculated from knowledge of the materials phase transformations and the enthalpy of formation of the compound.



OX_{enth} for any temperature T is calculated as follows:

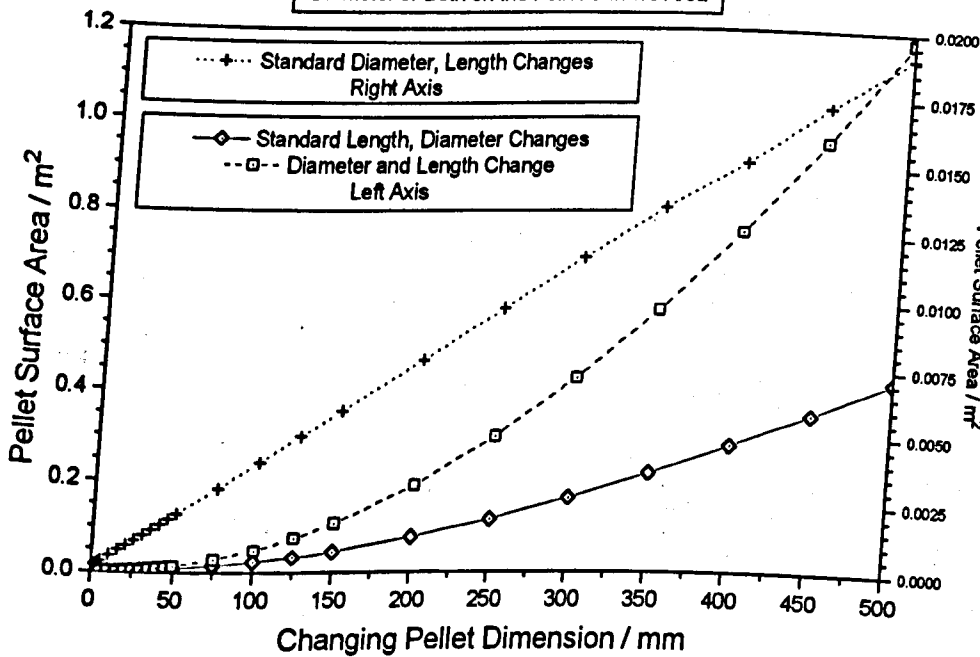
If T is above 1155K:

1. Calculate the energy change when β titanium is reduced from T to 1155K (-ve).
2. Calculate the latent heat of transformation from $\beta \Rightarrow \alpha$ titanium (-ve).
3. Calculate the energy change when α titanium is reduced from 1155K to 298K (-ve).
4. Calculate the enthalpy of formation of TiO_2 at 298K from $Ti + O_2$ (-ve).
5. Calculate the energy required to raise TiO_2 from 298K to TiO_2 at T (+ve).
6. Sum 1 \Rightarrow 5, this value is equal to the enthalpy of formation of TiO_2 at T from $Ti + O_2$ at T .

If T is below 1155K:

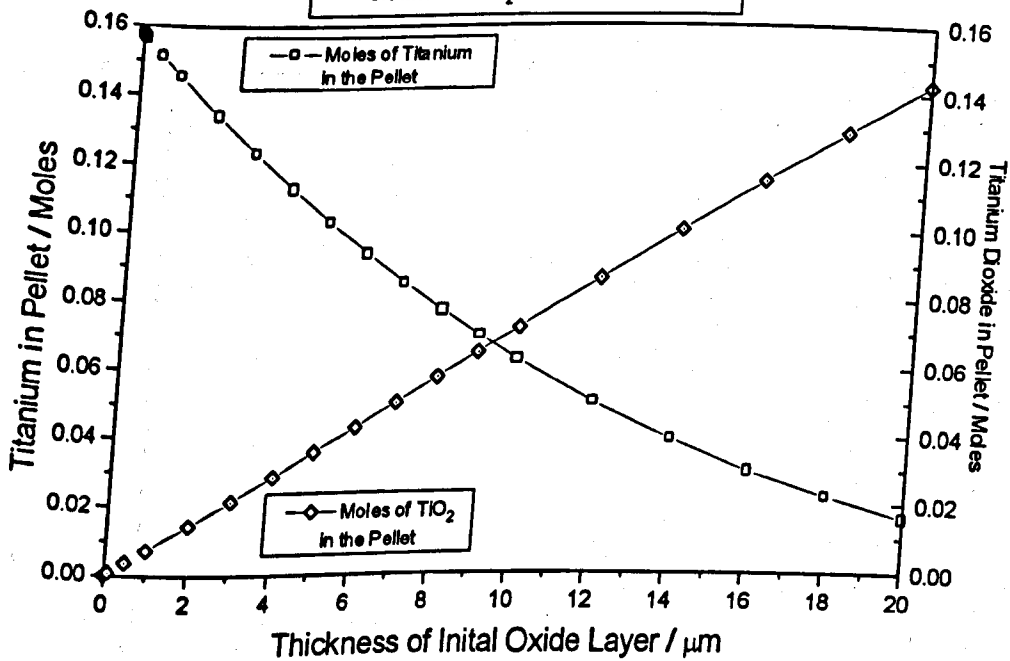
1. Calculate the energy change when α titanium is reduced from T to 298K (-ve).
2. Calculate the enthalpy of formation of TiO_2 at 298K from $Ti + O_2$ (-ve).
3. Calculate the energy required to raise TiO_2 from 298K to TiO_2 at T (+ve).
4. Sum 1 \Rightarrow 3, this value is equal to the enthalpy of formation of TiO_2 at T from $Ti + O_2$ at T .

The Effect of Altering the Pellet Length, Diameter or Both on the Pellet Surface Area

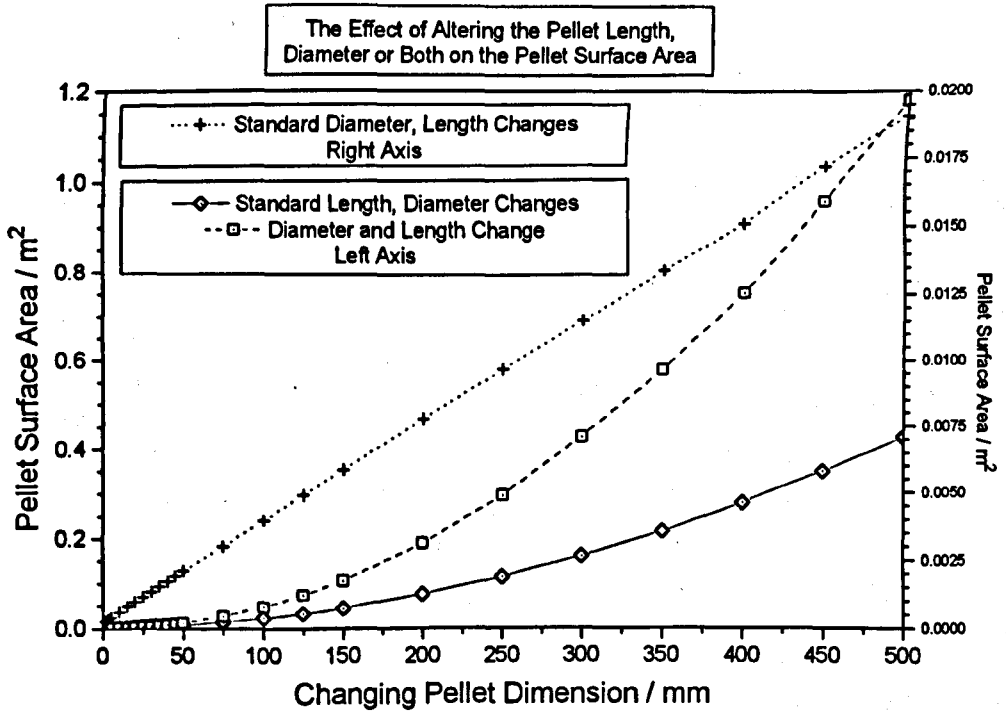


Graph 7.1

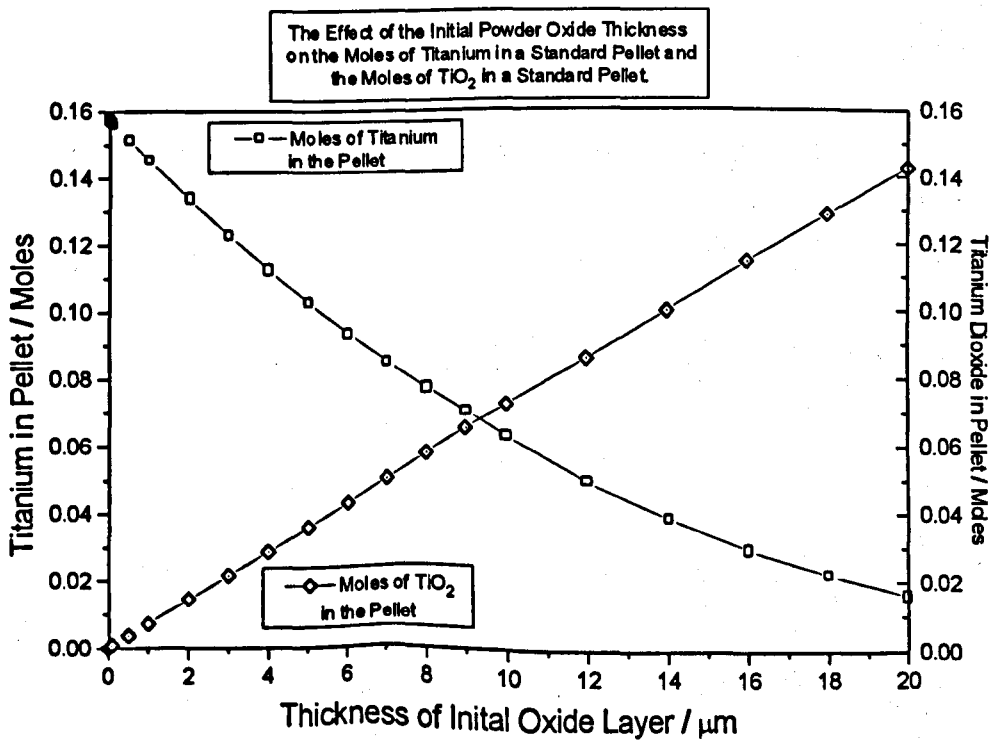
The Effect of the Initial Powder Oxide Thickness on the Moles of Titanium in a Standard Pellet and the Moles of TiO₂ in a Standard Pellet



Graph 7.2

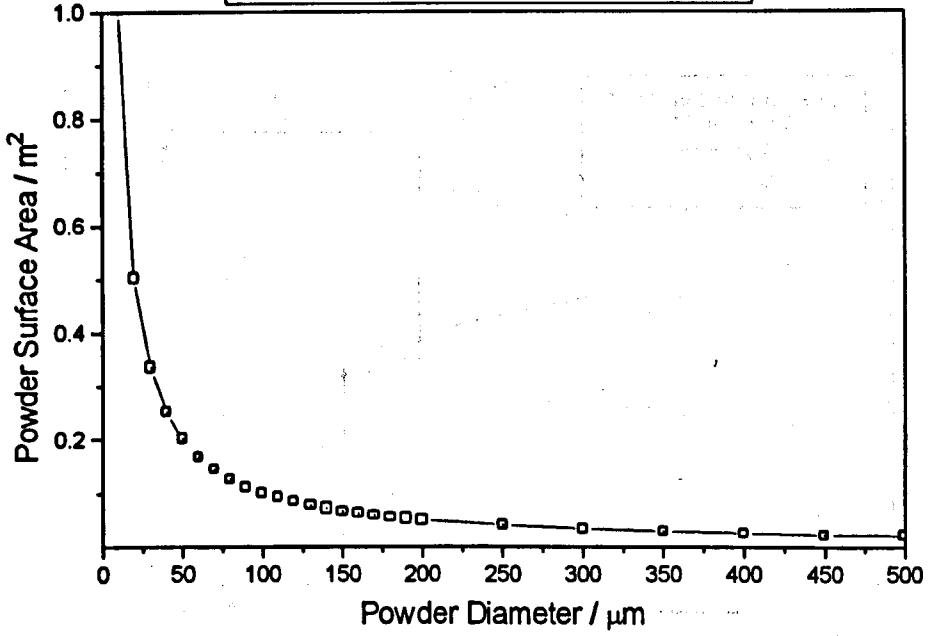


Graph 7.1



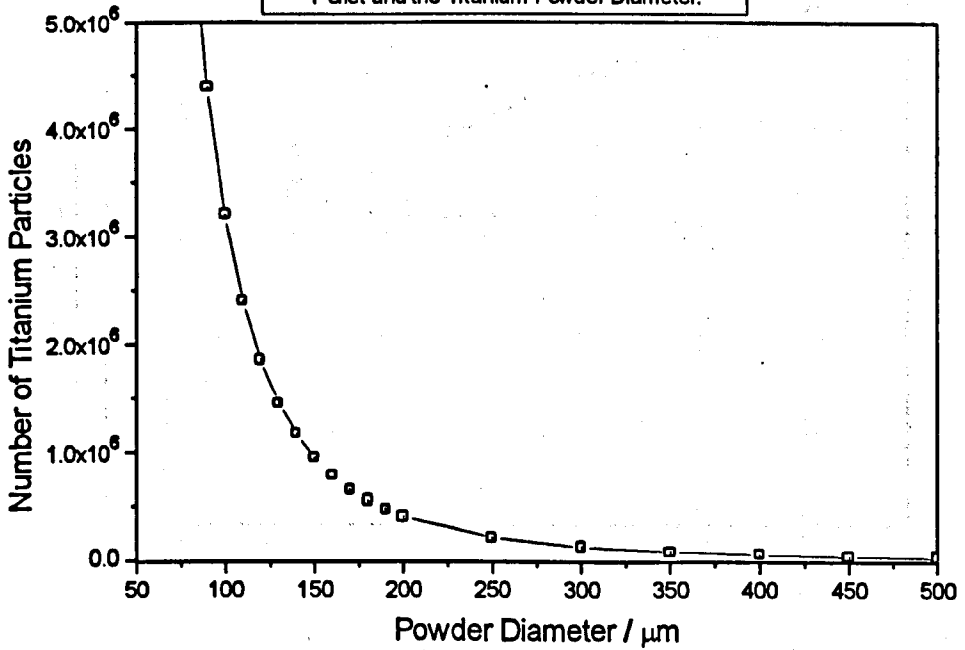
Graph 7.2

The Relationship Between the Total Titanium Powder Surface Area in a Standard Pellet and the Titanium Powder Diameter.



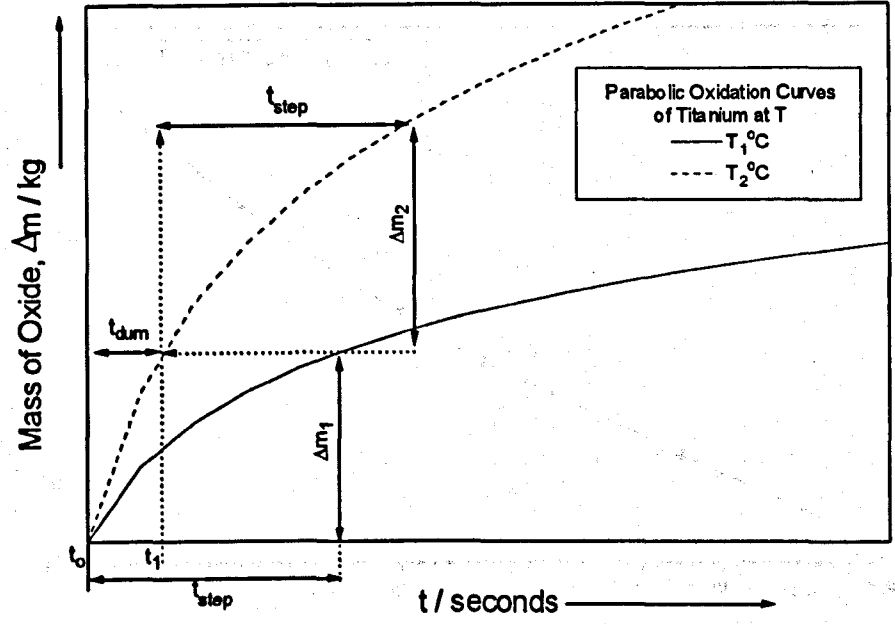
Graph 7.3

The Relationship Between the Number of Titanium Powder Particles in a Standard Pellet and the Titanium Powder Diameter.



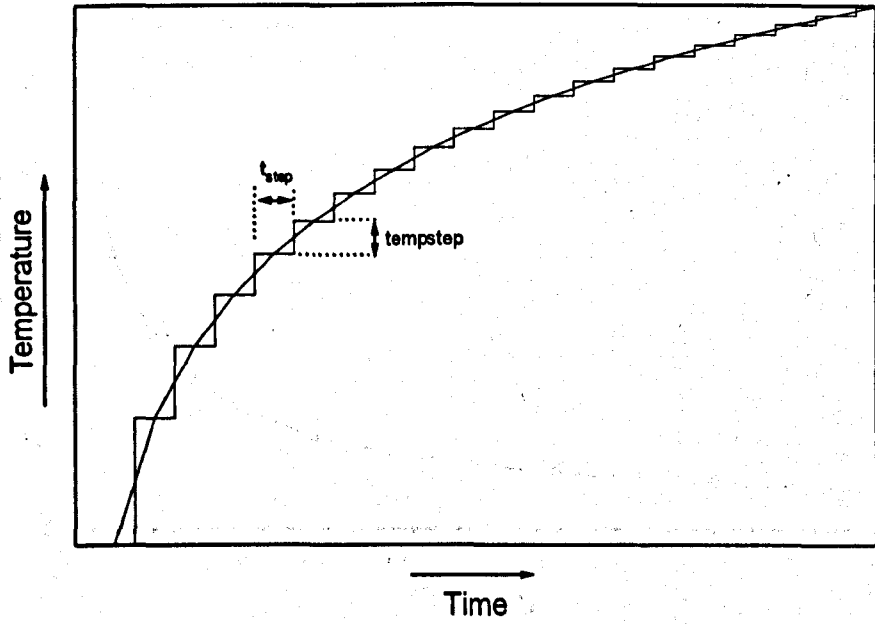
Graph 7.4

Schematic Representation of the Concept of 'Dummy Time'.



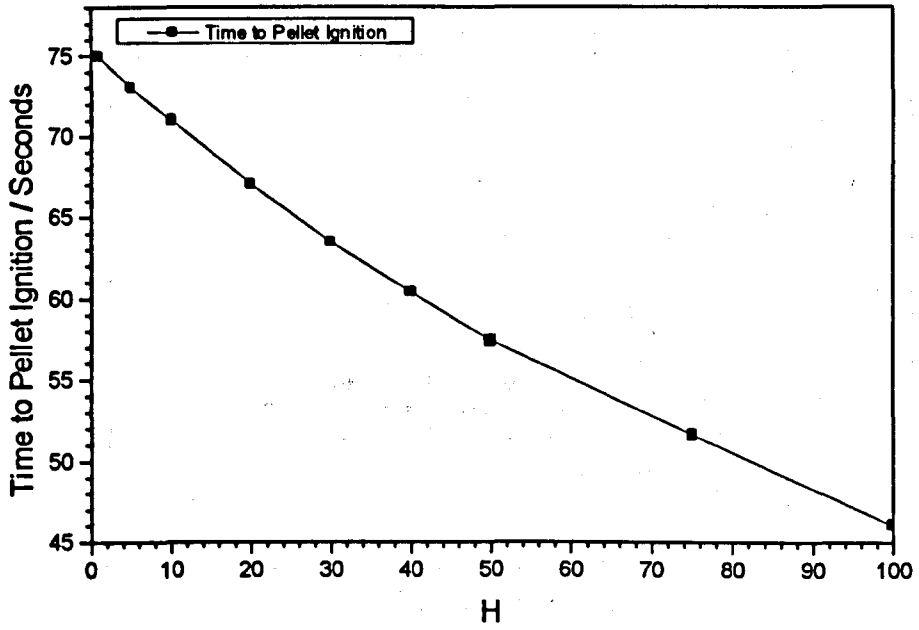
Graph 7.5

Schematic Representation Showing how Anisothermal Oxidation can be Modeled as Many Small Isothermal Time Steps.



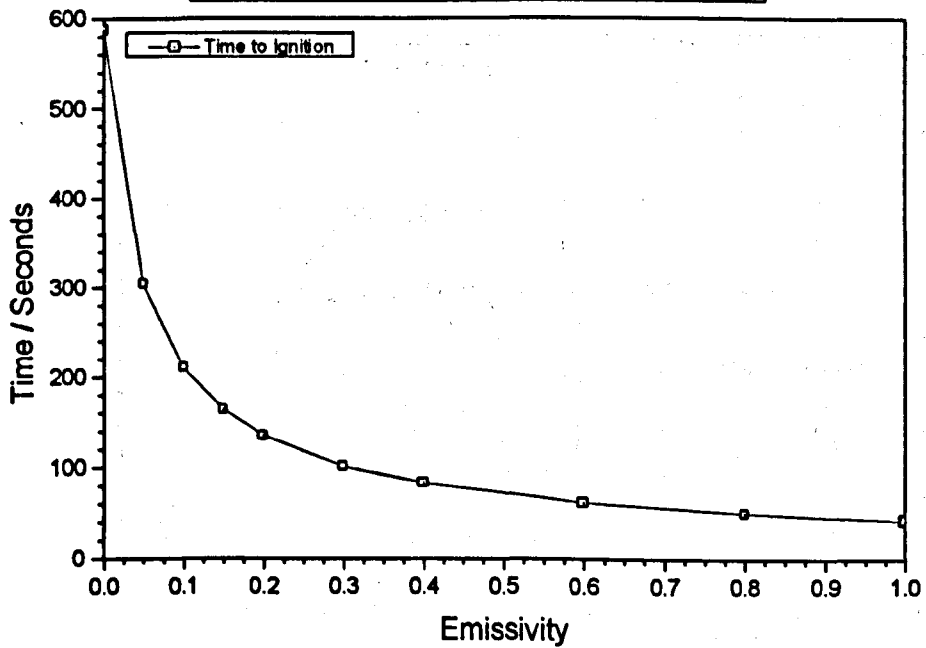
Graph 7.6

The Effect of H, the Heat Flow Constant on the Time Taken for a Pellet to Ignite in a Furnace set at 1000°C. $\epsilon_m = 0.5$



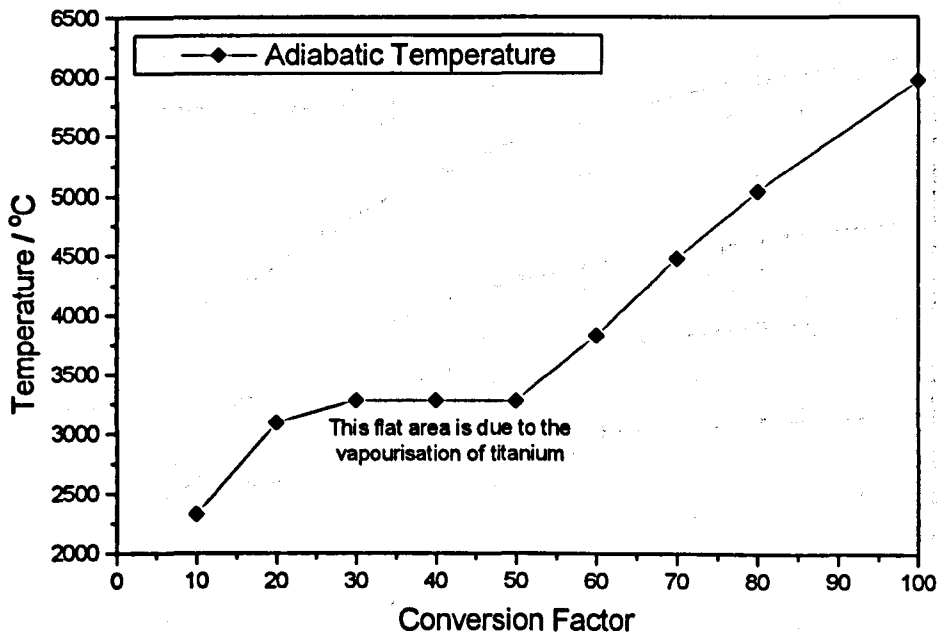
Graph 7.7

The Effect of the Titaniums Emissivity on the time it takes for a Pellet to Ignite in a Furnace set at 1000°C. $H = 10$.



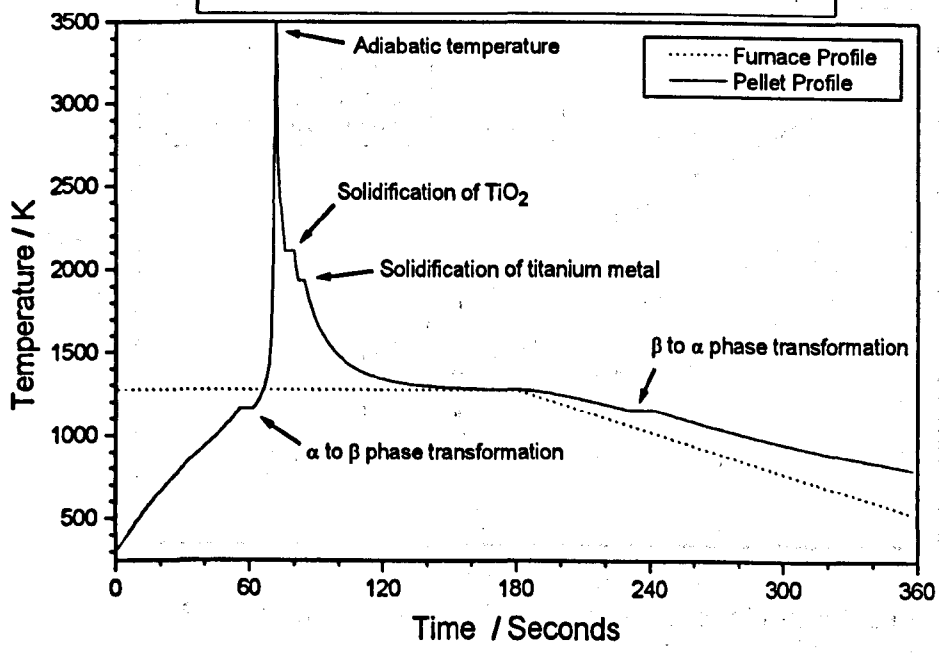
Graph 7.8

Relationship Between the Calculated Adiabatic Reaction Temperature and the Conversion Factor for a Standard Pellet.



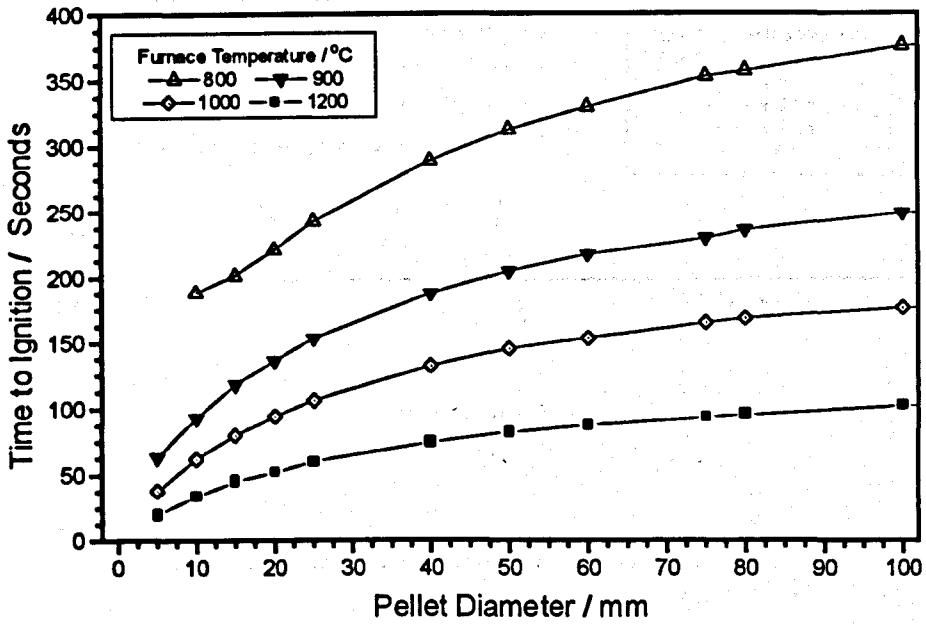
Graph 7.9

The Time / Temperature Profile for the Standard Pellet in the Standard Furnace. (3min hold time)



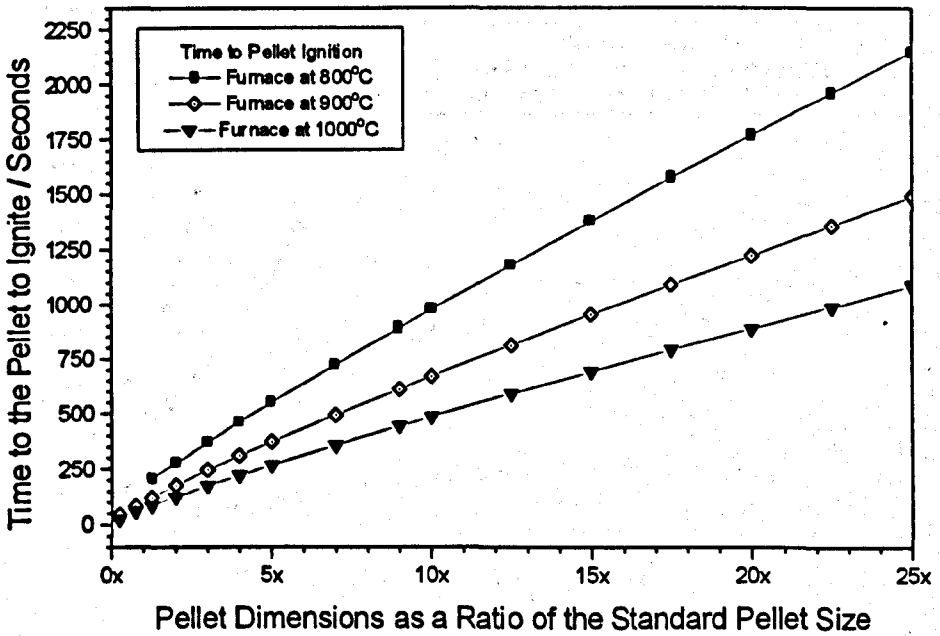
Graph 7.10

The Effect of the Pellet Diameter on the Time to Ignition of a Standard Pellet in a Furnace Held at Various Temperatures.

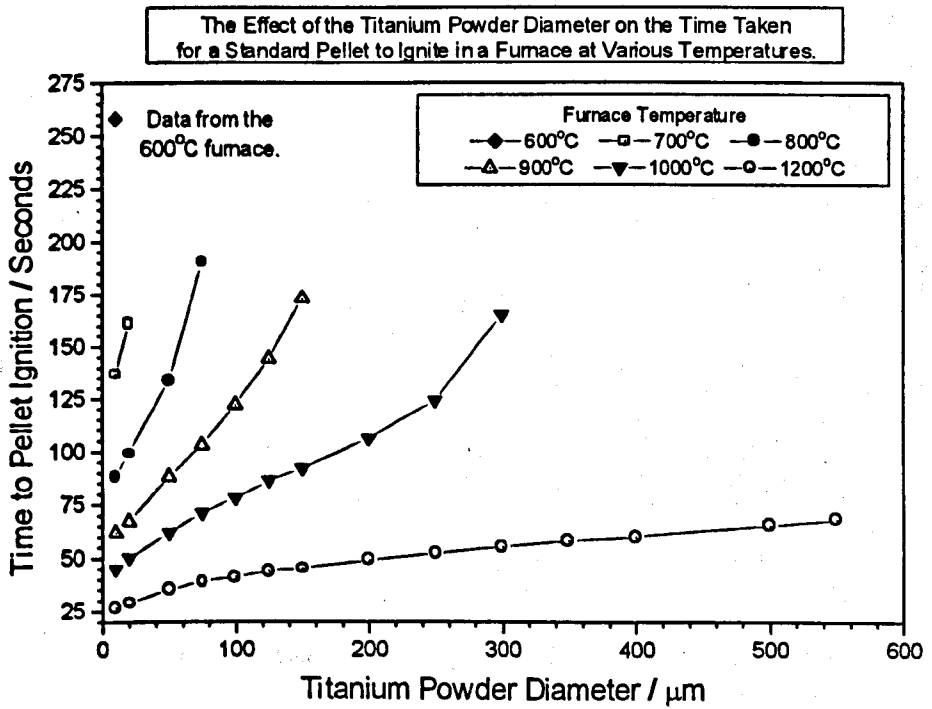
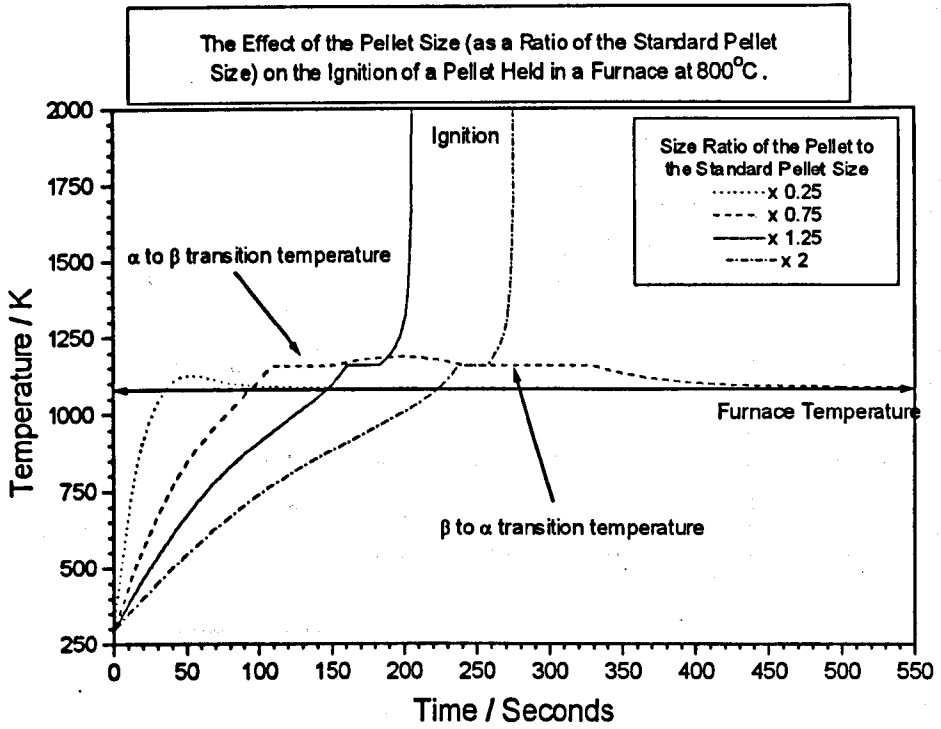


Graph 7.11

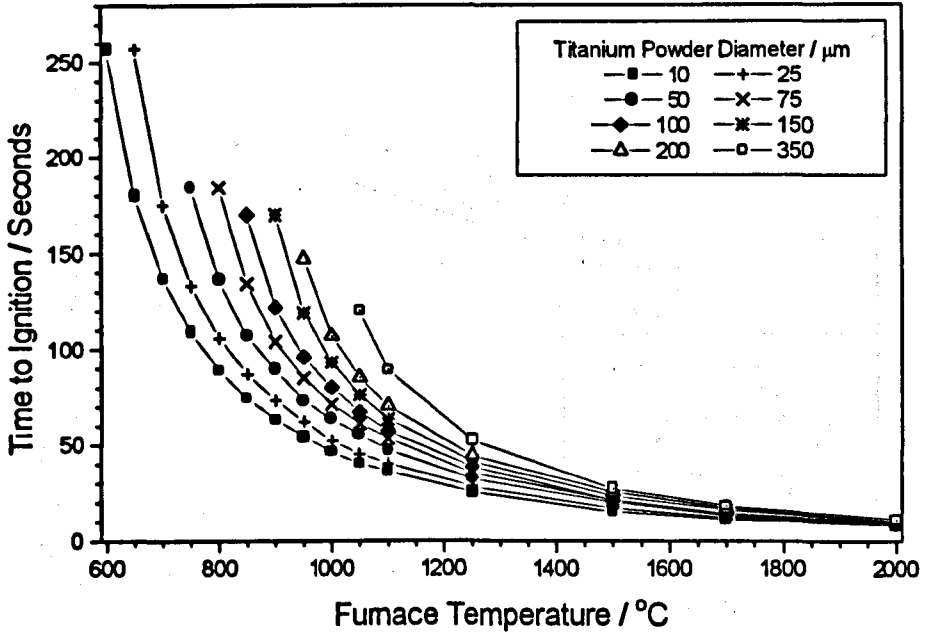
The Effect of the Pellet Dimensions (as a Ratio of the Standard Pellet Dimensions) on the Time Taken for the Pellet to Ignite in a Furnace Held at Various Temperatures.



Graph 7.12

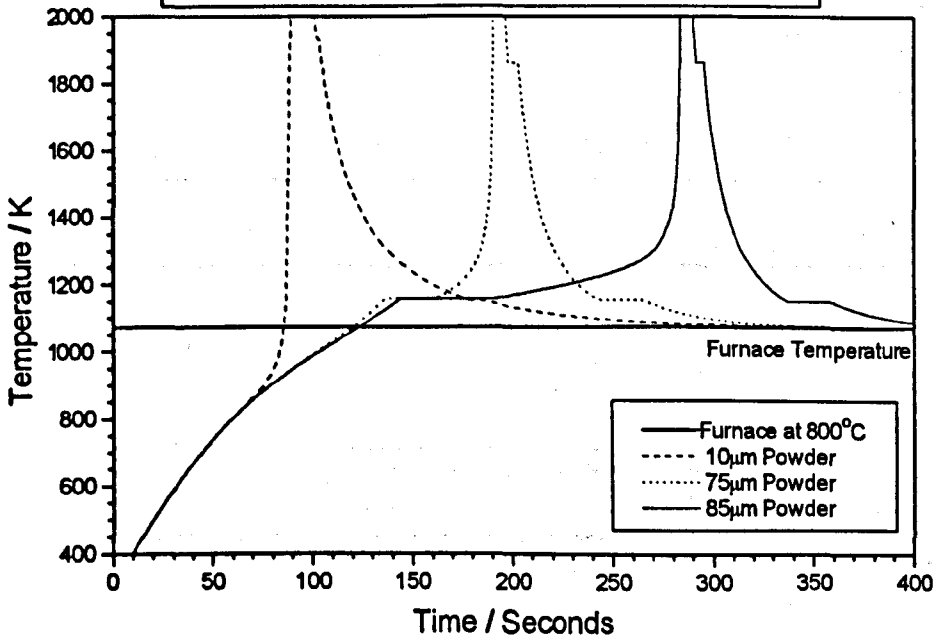


The Effect of the Titanium Powder Diameter on the Time Taken for a Standard Pellet to Ignite in a Furnace at Various Temperatures.

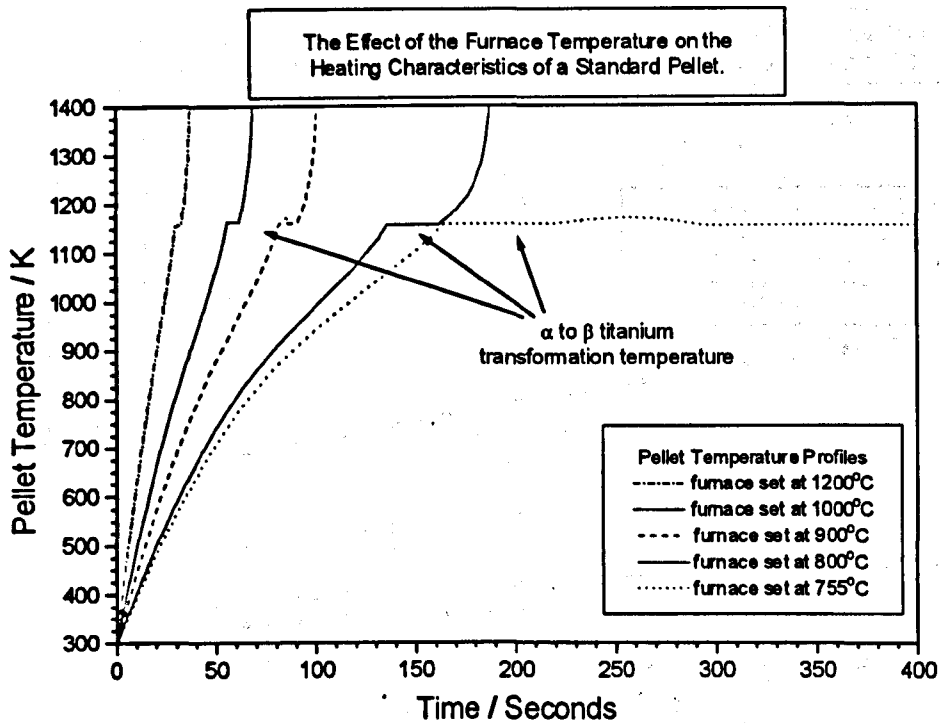


Graph 7.15

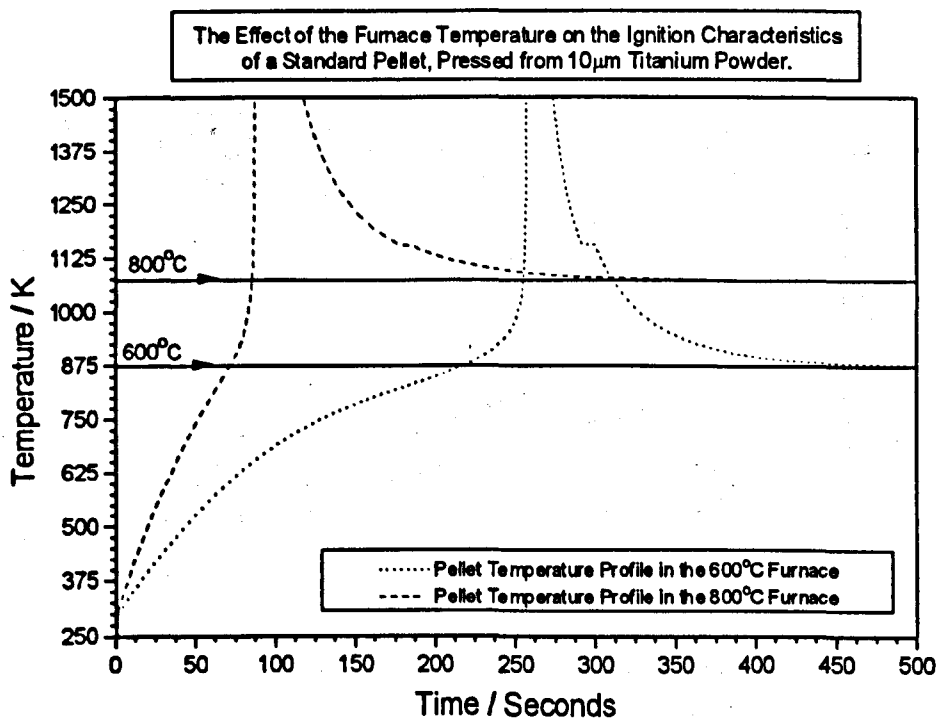
The Effect of the Titanium Powder Diameter on the Ignition Characteristics of a Standard Pellet Held in a Furnace at 800°C.



Graph 7.16

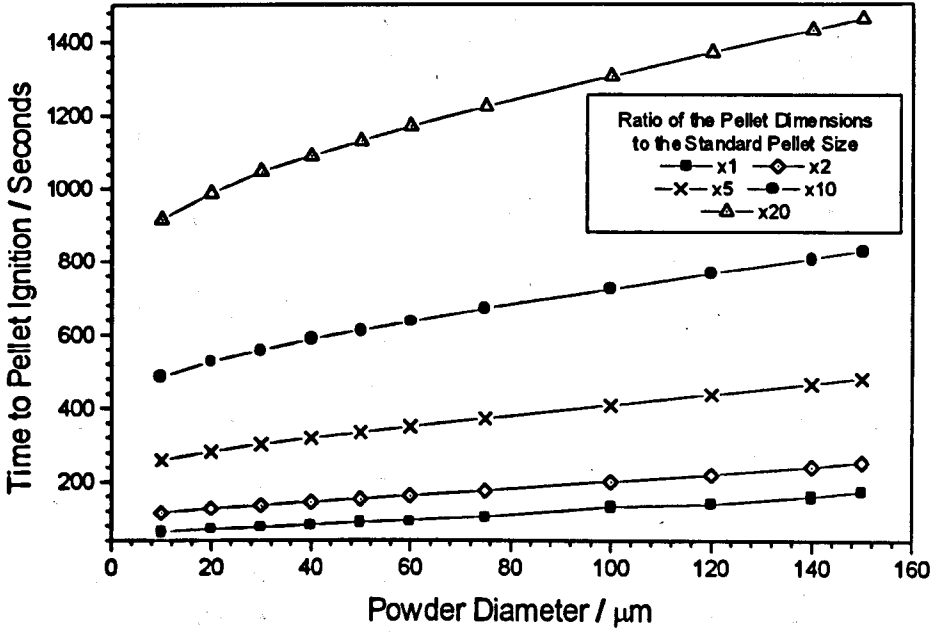


Graph 7.17



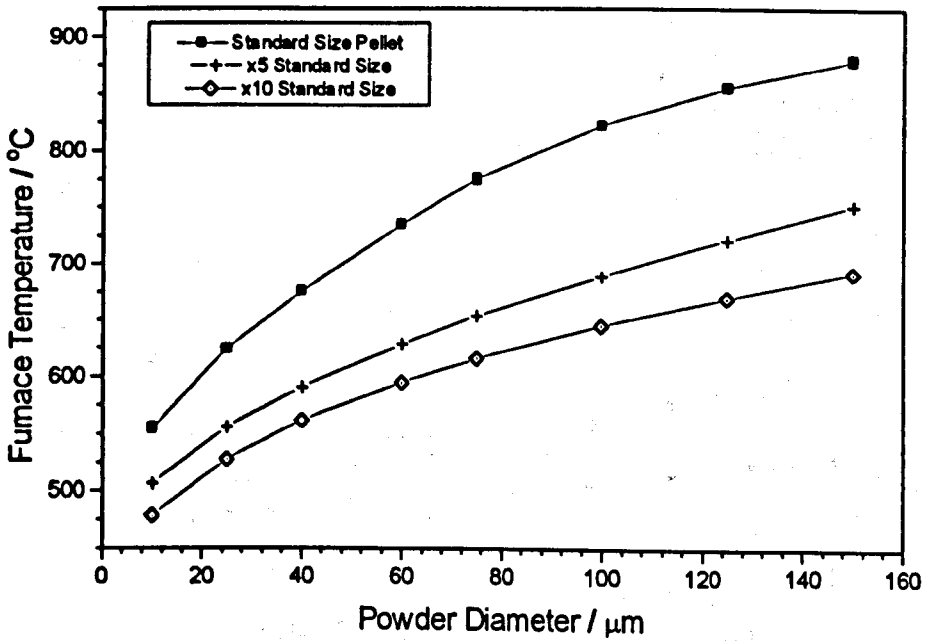
Graph 7.18

The Effect of the Powder Diameter and the Pellet Dimensions (as a Ratio of the Standard Pellet Size) on the Time Taken for the Pellet to Ignite in a Furnace set at 900°C.



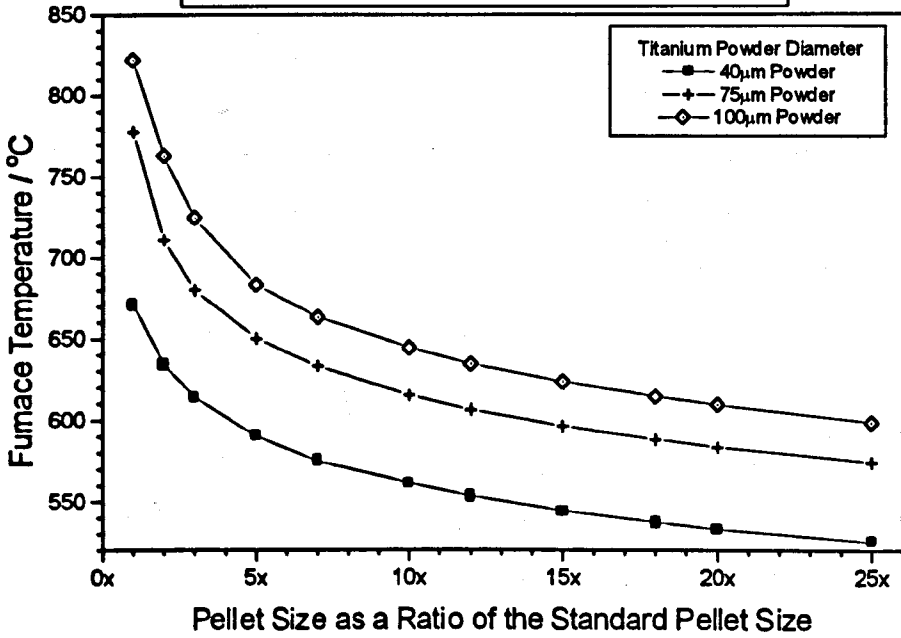
Graph 7.19

The Effect of the Powder Diameter on the Minimum Furnace Temperature that Promotes Ignition of Various Sized Pellets.



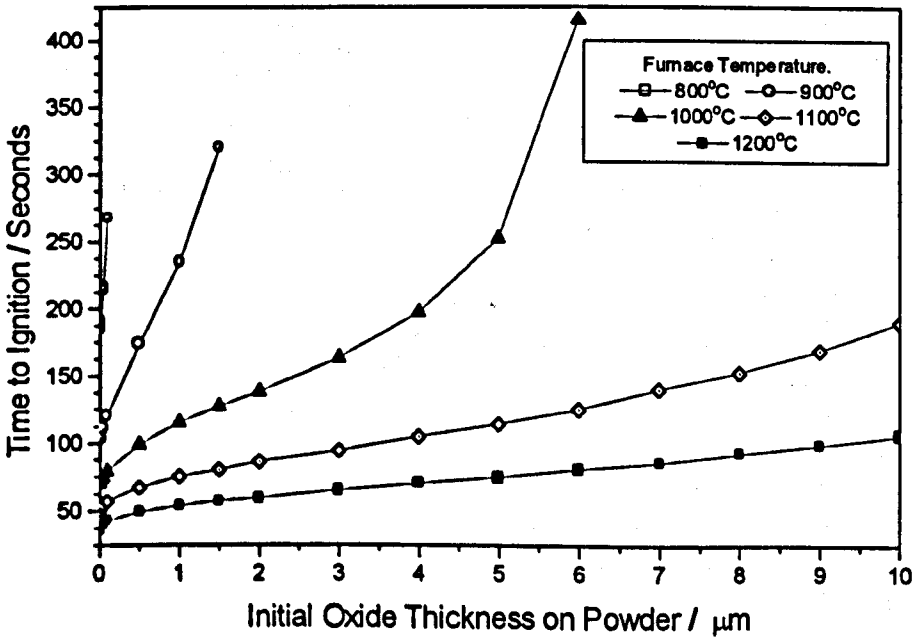
Graph 7.20

The Effect of the Pellet Size (as a Ratio of the Standard Pellet Size) on the Minimum Furnace Temperature that Promotes Ignition of a Pellet Constructed from Various Diameters of Titanium Powder.



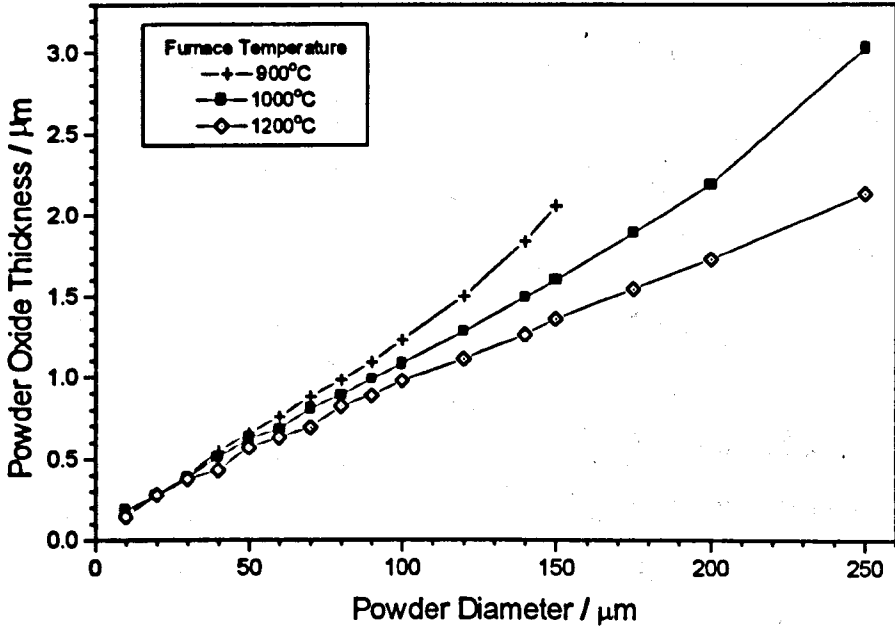
Graph 7.21

The Effect of the Initial Oxide Thickness on the Powder, on the Time Taken for a Standard Pellet to Ignite at Various Furnace Temperatures.



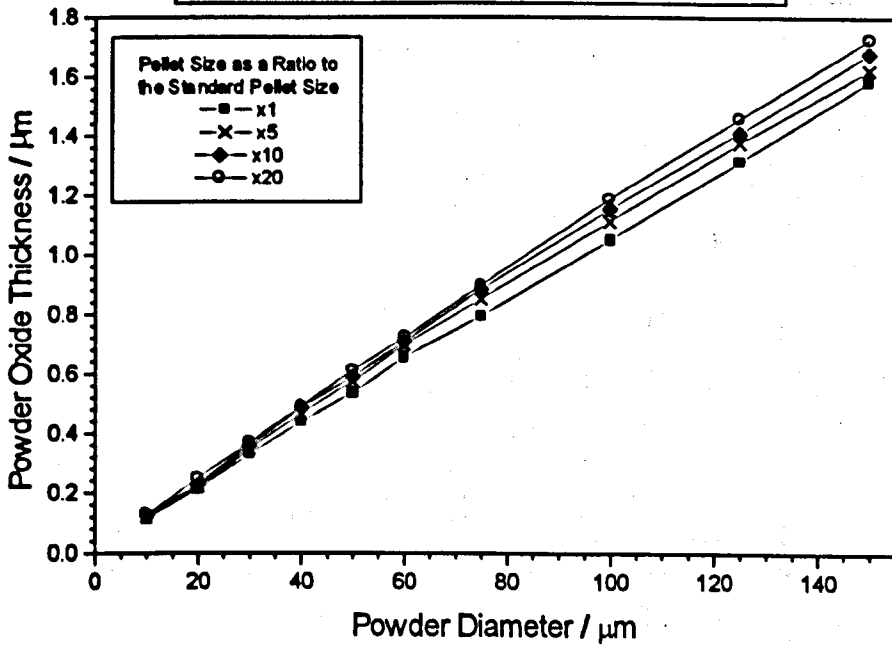
Graph 7.22

The Effect of the Titanium Powder Diameter on the Powder Oxide Thickness at the Time of Pellet Ignition for Various Furnace Temperatures.



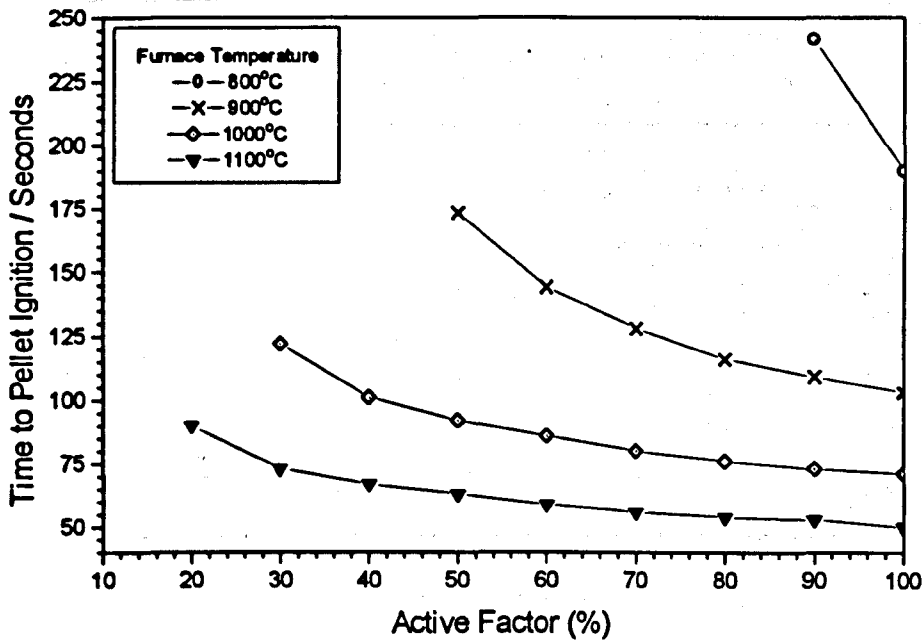
Graph 7.23

The Effect of the Titanium Powder Diameter on the Powder Oxide Thickness at the Time of Pellet Ignition in a Furnace Set at 1000°C for Various Pellet Sizes (as a Ratio of the Standard Pellet Size).



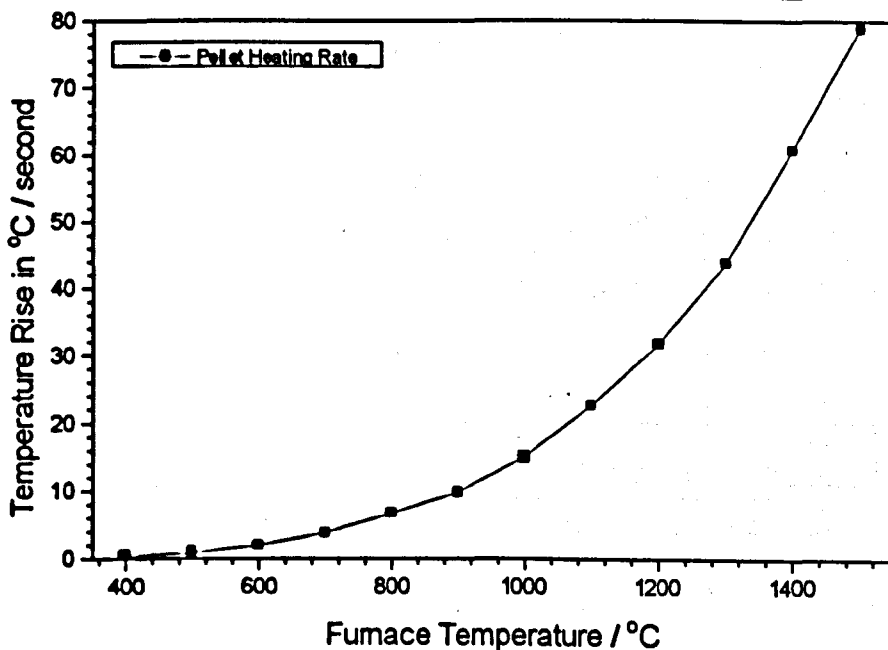
Graph 7.24

The Effect of the Pellets 'Active Factor' on the Time Taken for a Standard Pellet to Ignite in a Furnace at Various Temperatures.

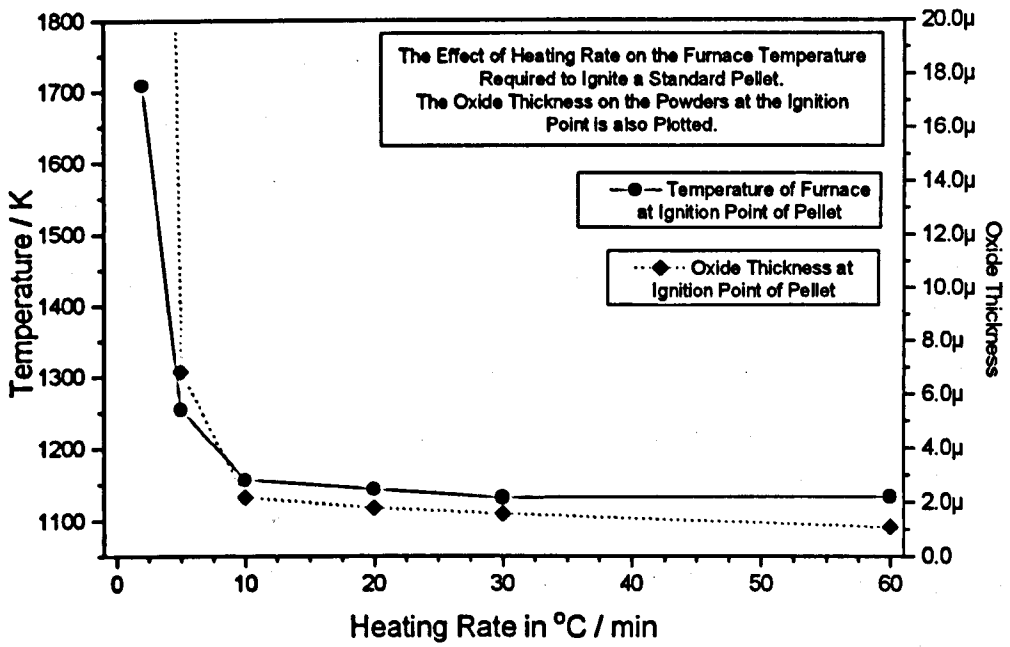


Graph 7.25

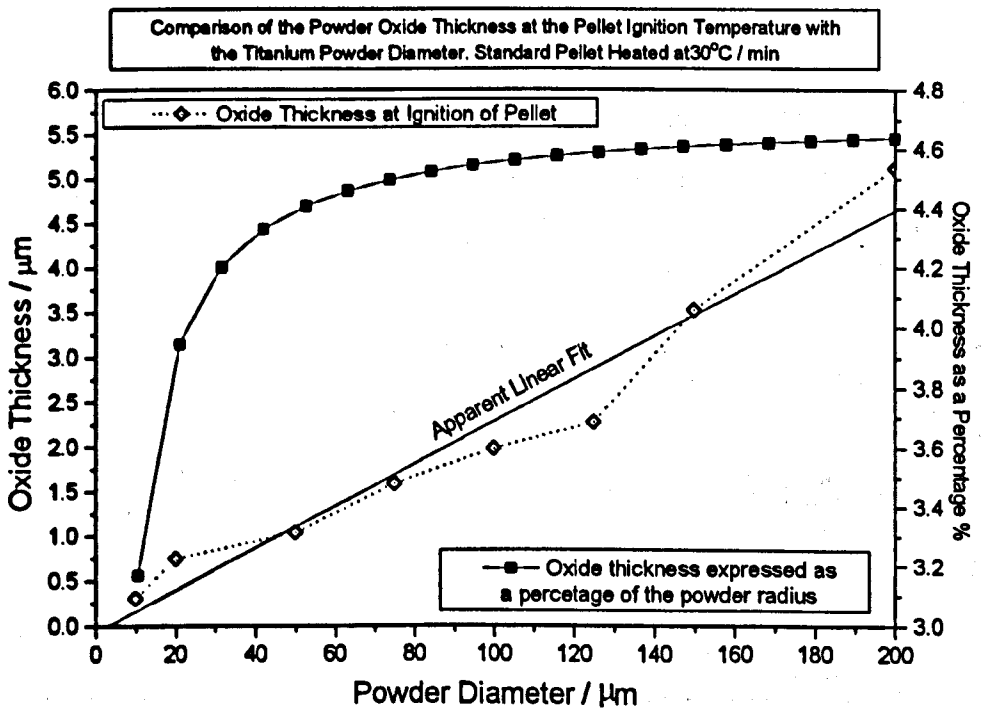
The Averaged Temperature Rise of a Standard Pellet (up to the Furnace Temperature) when in a Furnace at Various Temperatures.



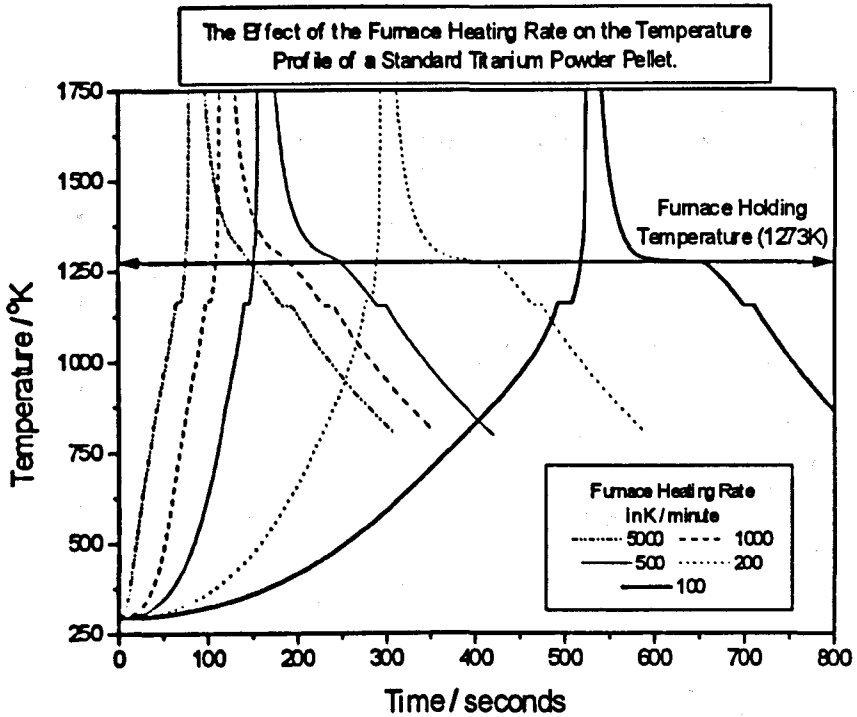
Graph 7.26



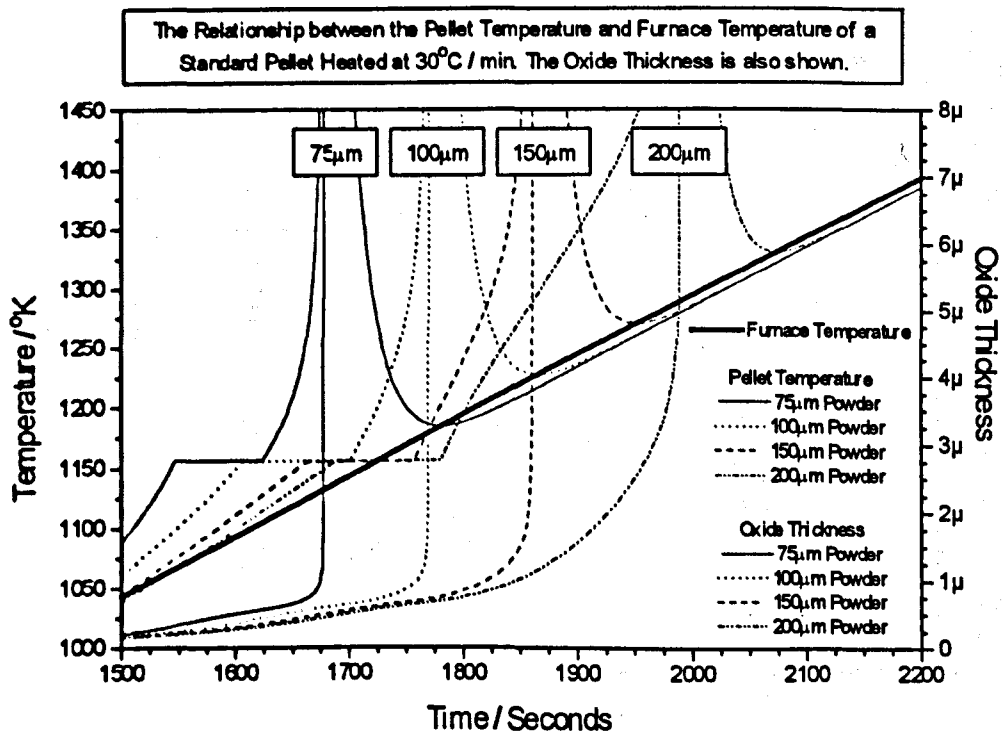
Graph 7.27



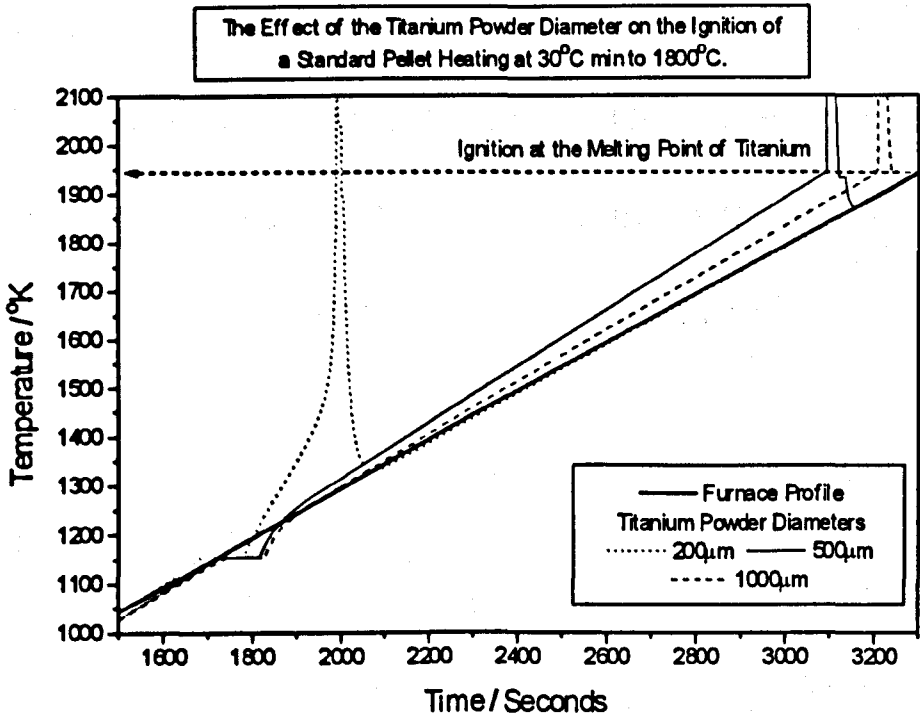
Graph 7.28



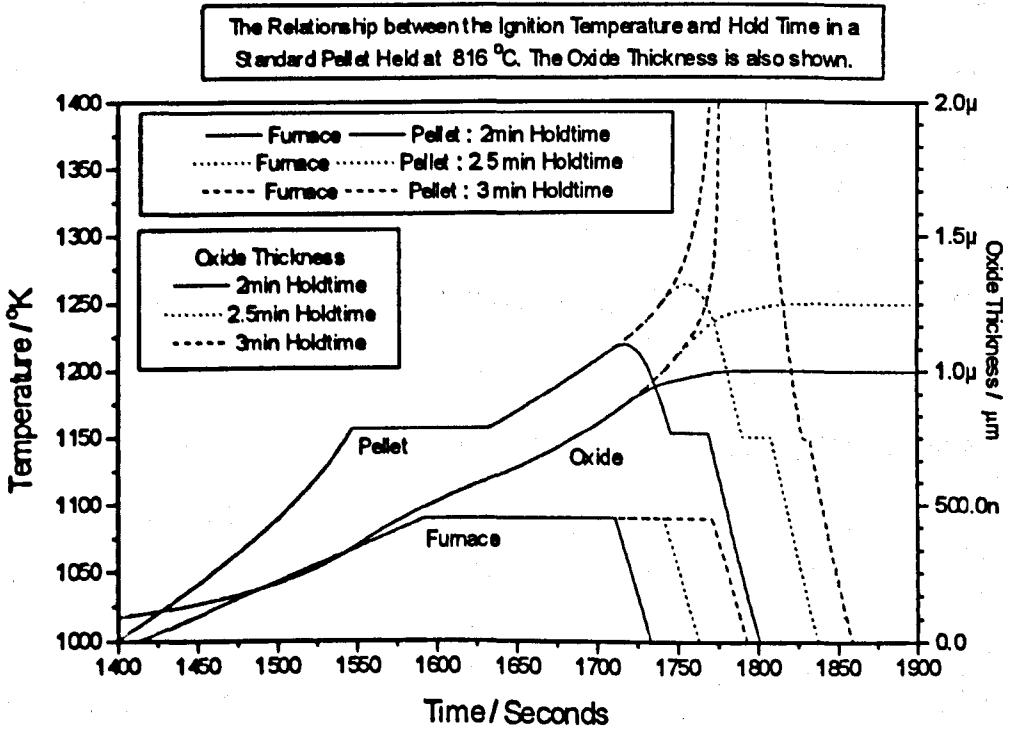
Graph 7.29



Graph 7.30



Graph 7.31



Graph 7.32

Chapter 8

The Effect of the Initial Powder Composition and the Addition of an Iron Powder Diluent on the Products of the SHS Reaction Between Fe_2O_3 and Titanium.

8.1 Introduction

One of the aims of this research was to produce, via the SHS method, a titanium oxide dispersed iron matrix master alloy. It has been seen in the previous chapters that the reaction $\text{Fe}_2\text{O}_3 + 3\text{Ti}$ is highly exothermic, forming a product that is highly segregated. The metallic phase is completely separate from the surrounding ceramic phase. Other researchers, for example Saidi (1995), have shown that by changing the initial composition of the reactant powders, or by adding a diluent, the final product is modified. It has been seen that the addition of a diluent reduces the SHS reaction temperature, thus producing a finer ceramic particle morphology. In this chapter the SHS reaction between Fe_2O_3 , titanium and iron powders is investigated, from a view of changing the initial starting composition to form a final product morphology that is a fine dispersion of ceramic phase in the metallic matrix.

8.2 Experiments

Pellets of compositions summarised in table 8.1 were constructed from $<5\mu\text{m}$ Fe_2O_3 , $<150\mu\text{m}$ titanium and $<60\mu\text{m}$ Fe powders. The pellets were ignited in the argon backfilled glove box, via an electrically heated tungsten filament.

The temperature profile of the pellets was recorded by optical pyrometry.

Comprehensive details of the experimental routine are found in chapter 4.

Table 8.1 Compositions of Pellets Used in the Experiments, Constructed from $<5\mu\text{m Fe}_2\text{O}_3$, $<150\mu\text{m Ti}$ and $<60\mu\text{m Fe}$: $\text{Fe}_2\text{O}_3 + X$ (moles Ti) + Y (wt% Fe)

<u>X (moles of titanium)</u>	<u>Y (wt % of added iron)</u>
1.5	0, 10, 20, 30, 40, 50
2	0, 10, 20, 30, 40, 50
3	0, 10, 20, 30, 40, 60, 65
4	0, 10, 20, 30, 50, 60
5	0, 10, 20, 30, 50, 60
6	0, 10, 20, 30, 40, 50

Stoichiometric reaction products and their exothermicities are detailed in table 8.2

Table 8.2 The Stoichiometric Reaction Products of Pellets with Various Initial Starting Compositions and the Reactions Total Exothermic Energy

<u>Initial Pellet Composition</u>	<u>The Stoichiometric Reaction Product</u>	<u>The Total Exothermic Energy of the Reaction</u>
$\text{Fe}_2\text{O}_3 + 1.5\text{Ti}$	TiO_2	~125 kJ
$\text{Fe}_2\text{O}_3 + 2\text{Ti}$	Ti_2O_3	~700 kJ
$\text{Fe}_2\text{O}_3 + 3\text{Ti}$	TiO	~810 kJ
$\text{Fe}_2\text{O}_3 + 4\text{Ti}$	TiO_{1-x}	~810 kJ
$\text{Fe}_2\text{O}_3 + 5\text{Ti}$	~ Ti_3O_2	unknown
$\text{Fe}_2\text{O}_3 + 6\text{Ti}$	$\text{Ti}_2\text{O} + \alpha\text{-Ti solid solution}$	unknown

8.3 Results

The XRD analysis of the crushed products of the reacted pellets is shown in table 8.3. In some reactions the metallic product phase segregated from the ceramic phase, forming a pea sized lump. This could not be included in the XRD analysis due to the crushed powder method used to analyse the product. Pellets that did not react are included so that the compositional limit of the reaction is known.

<u>Initial Powder Compositions : Fe₂O₃ + X</u>	<u>XRD Analysis</u>
1.5 Ti	Ti ₃ O ₅ FeTi Fe
1.5 Ti + 10wt% Fe	Fe ₂ TiO ₅ Fe
1.5 Ti + 20wt% Fe	Fe ₂ TiO ₅ Fe
1.5 Ti + 30wt% Fe	Fe ₂ TiO ₅ Fe
1.5 Ti + 40wt% Fe	Fe ₂ TiO ₅ Fe
1.5 Ti + 50wt% Fe	Did Not React
2 Ti	Ti ₂ O ₃ TiO Fe ₂ Ti
2 Ti + 10 wt% Fe	Ti ₂ O ₃ TiO Fe ₂ Ti
2 Ti + 20 wt% Fe	Ti ₂ O ₃ TiO Fe ₂ Ti
2 Ti + 30 wt% Fe	Ti ₂ O ₃ Ti ₃ O ₅ Fe
2 Ti + 40 wt% Fe	Ti ₂ O ₃ Ti ₃ O ₅ Fe
2 Ti + 50 wt% Fe	Ti ₂ O ₃ Ti ₃ O ₅ Fe
2 Ti + 60 wt% Fe	Did Not React
3 Ti	TiO Fe ₂ Ti
3 Ti + 10 wt% Fe	TiO Fe ₂ Ti
3 Ti + 20 wt% Fe	TiO Fe ₂ Ti Fe
3 Ti + 30 wt% Fe	TiO Ti ₂ O ₃ Fe ₂ Ti Fe
3 Ti + 40 wt% Fe	TiO Ti ₂ O ₃ Fe ₂ Ti Fe
3 Ti + 60 wt% Fe	Ti ₂ O ₃ + Fe
3 Ti + 65 wt% Fe	Did Not React
4 Ti	TiO Fe ₂ TiO ₄
4 Ti + 10 wt% Fe	TiO Fe ₂ TiO ₄
4 Ti + 20 wt% Fe	TiO Fe ₂ TiO ₄ Fe ₂ Ti

4 Ti + 30 wt% Fe	TiO Fe ₂ TiO ₄ Fe ₂ Ti
4 Ti + 40 wt% Fe	TiO Ti ₂ O ₃ Fe ₂ Ti
4 Ti + 50 wt% Fe	TiO Ti ₂ O ₃ Fe ₂ Ti
4 Ti + 60 wt% Fe	Did Not React
5 Ti	TiO Fe ₂ Ti ₄ O
5 Ti + 10 wt% Fe	TiO Fe ₂ Ti ₄ O
5 Ti + 20 wt% Fe	TiO Fe ₂ Ti ₄ O Fe ₂ Ti FeTi
5 Ti + 30 wt% Fe	TiO Fe ₂ Ti ₄ O Fe ₂ Ti FeTi
5 Ti + 40 wt% Fe	TiO Fe ₂ Ti ₄ O Fe ₂ Ti FeTi
5 Ti + 50 wt% Fe	Ti ₂ O ₃ Fe ₂ Ti
5 Ti + 60 wt% Fe	Did Not React
6 Ti	Fe ₂ Ti ₄ O Ti ₂ O FeTi
6 Ti + 10 wt% Fe	Fe ₂ Ti ₄ O Ti ₂ O FeTi
6 Ti + 20 wt% Fe	Fe ₂ Ti ₄ O Ti ₂ O FeTi
6 Ti + 30 wt% Fe	Fe ₂ Ti ₄ O Ti ₂ O FeTi
6 Ti + 40 wt% Fe	Fe ₂ Ti ₄ O Ti ₂ O Fe ₂ Ti FeTi
6 Ti + 50 wt% Fe	Did Not React

The pyrometer recorded the temperature of the reaction wave as it passed through the pellet. The pyrometer makes its measurement using infra-red light radiated by the pellet surface. As such, surface porosity and surface separation from the core material may produce results that are slightly lower than the actual core pellet temperature. The reaction wave temperatures are shown in figure 8.1. The actual temperature profiles for selected pellets containing 3, 5 and 6 moles of titanium are shown in figures 8.2, 8.3 and 8.4 respectively.

8.3.1 Product Morphology

The morphology of the reaction products is seen to change with titanium and iron composition. Segregation between the metallic phase and the ceramic phase is seen in pellets that contain low quantities of titanium and iron. The optical micrographs in figure 8.5 and 8.6 are from a pellet of composition

$\text{Fe}_2\text{O}_3 + 2\text{Ti} + 10\text{wt}\% \text{ Fe}$. The metal (fig. 8.5) is seen to be quite free from ceramic inclusions whilst the ceramic phase (fig. 8.6) has metallic veins throughout it. The XRD analysis from table 8.3 show that the ceramic phase contains TiO , Ti_2O_3 and Fe_2Ti .

Increasing the iron diluent level to 40wt% changes the structure from a segregated one to a mixed metallic – ceramic, figure 8.7. The particles are fine and evenly dispersed. Increasing the diluent level to 50wt% in the same $\text{Fe}_2\text{O}_3 + 2\text{Ti}$ pellet brought the pellet to the limits of its ability to react if ignited via the SHS method, figure 8.8. The change in structure is easy to see. The reaction has occurred, but to a significantly lesser extent than the previous pellet. Areas of ceramic material (Ti_2O_3 and Ti_3O_5) are seen within the iron matrix. The typical morphology of the ceramic areas is one of a ceramic boundary containing within it, fine ceramic particulate. The boundary can be seen around a pore in the metallic matrix or completely surrounding the finer ceramic particles. The metallic matrix is quite porous. Increasing the iron diluent levels to 60% inhibits any SHS initiated reactions.

8.3.2 The $\text{Fe}_2\text{O}_3 + 3\text{Ti}$ Reaction

The stoichiometric composition to form a product of $2\text{Fe} + 3 \text{TiO}$ is $\text{Fe}_2\text{O}_3 + 3 \text{Ti}$. The product of this reaction is seen to consist of TiO and Fe_2Ti . Morphologically, there is gross segregation between the phases. Figure 8.9 shows this well. Adding 30wt% Fe to the composition dramatically changes the product morphology. The ceramic and metallic components are evenly mixed together, figure 8.10. The dark areas are porosity within the structure.

Adding a further 20wt% Fe diluent to produce a starting pellet composition of $\text{Fe}_2\text{O}_3 + 3 \text{ Ti} + 50\text{wt}\% \text{ Fe}$ produces equally dramatic results, as can be seen in figure 8.11. The pellet is on the limits of self sustaining reaction. Three areas are defined within the picture. The metallic area (mark X), the mixed area (mark Y) and the ceramic area (mark Z). Figure 8.12 shows the product formed by the reaction between $\text{Fe}_2\text{O}_3 + 6\text{Ti} + 20\text{t}\% \text{ Fe}$. This compositions product consists of discrete titanium oxides within a metallic matrix and is the best example of such a microstructure produced in this work.

8.3.3 Partial Reactions

The reaction mechanism between the Fe_2O_3 , titanium and diluent iron is revealed in figure 8.13. This is a sectioned pellet of composition $\text{Fe}_2\text{O}_3 + 4\text{Ti} + 50\text{wt}\% \text{ Fe}$ that has not fully reacted. The reaction did not have sufficient exothermic energy to proceed to the bottom of the sample. The reaction wave stopped halfway down the pellet, sintering the material below it. It shows the reaction between titanium, Fe_2O_3 and Fe that occurs as the combustion wave travels down the pellet. At the top of the figure is the limit of the melt (line X-X-X). Everything below this is due to the effect of sintering. The large particles are the titanium powders (for example, marks Y), the matrix in which they sit is a mixture of Fe and Fe_2O_3 (for example, marks Z). The Fe_2O_3 can be seen at the bottom of the figure as black areas around the Fe particles, figure 8.15.

Figure 8.14 is a close up of the reacted end; the titanium powders have reacted, forming titanium oxides within the boundaries of the particle (mark X). Some titanium powders have melted, forming porosity (mark Y). Figure 8.15 is a

close up of the cooler end. The titanium (marks X) has not reacted with the Fe_2O_3 to such an extent. There is a slight amount of surface reaction. The outline of the iron powders is clear to see (for example, marks Y).

Figure 8.16 details the reaction mechanism seen above. There were areas that still contained the initial reactant in powder form, and others in which the titanium powders had started to react. EDX analysis revealed the composition at the points, table 8.4.

<u>Mark</u>	<u>Composition</u>
1	100% Fe
2	100% Ti

A close up of a reaction interface, as seen at marks X, is shown in figure 8.17 and the related higher magnification image in figure 8.18. It is an interesting area of the sample in which a titanium powder has undergone a significant amount of reaction. Table 8.5 details the EDX analysis that was obtained from the points shown on figure 8.18. The probable phase is also noted.

Table 8.5 EDX Analysis at the Points Detailed in Figure 8.18

<u>Mark</u>	<u>Ti at%</u>	<u>Fe at%</u>	<u>O at%</u>	<u>Phase</u>
1	100	0	0	Ti
2	86	0	14	Ti with O in solid solution
3	49	37	14	~Fe ₂ Ti ₄ O
4	34	0	66	TiO ₂
5	34	66	0	Fe ₂ Ti
6	50	50	0	FeTi

The effect that the compact composition has on the limits of ignition and the product morphology is shown in figure 8.19. This figure is generated from the assessment of the product morphology and the ability of the pellet to ignite and react in the self-propagating mode.

8.4 Discussion

8.4.1 Product Oxide Composition

It is seen from table 8.3 that the products composition is influenced by the starting composition. In the undiluted compositions, there is a general tendency to form oxides that are near stoichiometric to the starting composition. This is the case for the 2, 3 and 4 moles of titanium series. The reason for the lack of TiO₂ formation in the 1.5 moles of titanium series is unknown. It is seen to form when titanium oxidises in air. It maybe that oxygen solution into the metallic iron and gaseous expulsion reduced the total oxide content of the

system to below that required to form TiO_2 . Ti_3O_5 has the same crystal structure as TiO_2 and can be described as an oxygen deficient TiO_2 .

The 4, 5 and 6 moles of titanium series can be described as a 3 moles of titanium composition with excess titanium. Taking the undiluted examples, we see that the complex iron-titanium oxide $\text{Fe}_2\text{Ti}_4\text{O}$ forms along side TiO in the 4 and 5 moles of titanium series and Ti_2O in the 6 moles of titanium series. Looking at just the titanium to oxygen ratio in the oxide, it is seen that the oxygen would have been in solution in the titanium if it were in pure form. The presence of iron in the metallic matrix promotes the formation of $\text{Fe}_2\text{Ti}_4\text{O}$. As such, without the iron, this phase would not exist. This work is in agreement with Wang *et al.* (1994a) who found that the phase distribution was dependant on the initial reactant composition and the combustion temperature.

8.4.2 Reaction Temperature

From figure 8.1 a general trend in the temperature profiles of the compacts is seen. Increasing the titanium or diluent iron content decreases the reaction wave temperature. The series of compositions that contain 3, 4, 5 and 6 moles of titanium decrease almost in parallel to one another as the amount of diluent is increased.

At 30wt% Fe the reaction temperature drops noticeably and continues to do so as more diluent is added. In contrast, the temperature of the reaction wave in the compositions that contain 1.5 and 2 moles of titanium shows a high degree

of sensitivity to the amount of iron diluent added to it. This effect can be explained by an analysis of the exothermicities of the reactions.

If we introduce the concept of 'energy release / mol' we can examine the real life exothermicities of these reactions. From table 8.2 we see the exothermic energy of the total reactions. If we divide this figure by the mass of reaction material that is required to make one mol of the product, we determine the 'energetics' of the mixture, table 8.6.

Compositions based on 5 and 6 moles of titanium will be less energetic than the 4 moles of titanium series as there is more titanium present (mass) in the compact.

Table 8.6 Calculated 'Energetics' of Various SHS Reactions Based on the $\text{Fe}_2\text{O}_3 + x\text{Ti}$ Scheme				
<u>Ti / mol</u>	<u>Stoichiometric Product</u>	<u>Exothermic Energy: kJ mol^{-1}</u>	<u>Mass of Reactants: g mol^{-1}</u>	<u>Energy Release: kJ g^{-1}</u>
1.5	TiO_2	125	232	0.54
2	Ti_2O_3	700	256	2.73
3	TiO	810	304	2.66
4	TiO	810	351	2.30

We would expect that the reaction with the highest energetics to have the highest reaction temperature, but that is not so. The 1.5 moles of titanium series has the lowest energetics of those calculated and has the highest reaction

temperature. However, the effect of the diluent on the combustion temperature is seen to be proportional to the energetics of the reactant materials. The 1.5 moles of titanium series is greatly effected, whilst the 2, 3 and 4 mol series are effected to similar, lesser amounts.

The 'energetics' of the system is therefore a measure of the sustainability of the reaction - the amount of extra energy generated by the reaction above that which is required to sustain it. A system with low 'energetics' (1.5 moles of titanium) is just managing to be self sustaining, the addition of a diluent drops the reaction temperature and causes incomplete reaction, figure 8.19. A system with high 'energetics' (3 moles of titanium) has sufficient excess energy to overcome the heatsink effect of the diluent and react completely, figure 8.19.

8.4.3 The Effect of Iron Diluent

The effect of dilution has been explored by Ranganath and Subrahmanyam (1995) who found in their analysis of the Ti + C combustion reaction, that having an excess number of moles of titanium in the composition reduces the adiabatic reaction temperature and the proportion of titanium that was molten during the reaction. In effect, not all the titanium melts during the reaction. This is demonstrated by analysis of the products of the 2 moles of titanium series in figures 8.1, 8.5 - 8.8 with the XRD analysis in table 8.3 and the figure 8.19. Initially the products are segregated (figures 8.5, 8.6). The reaction temperature is over 2100°C, thus the ceramic phase is molten. The high heat of the combustion reaction and the longer cooling times, allows the metallic phase to 'drop' out of the ceramic phase and coalesce. It should be noted that

titanium in solution with iron promotes the separation of titanium oxides from the metallic matrix (Gammal 1991).

Adding increasing amounts of diluent cools the reaction. At 40wt% Fe, figure 8.7, the reaction temperature is just under the melting point of the oxides. Here, there is no segregation, the ceramic is distributed within the metallic phase as fine particles. As the reaction temperature is below the melting point of the oxides they must form as solids or precipitate from the melt. Analysis of the Ti – O phase diagram shows that only Ti_2O and Ti_3O precipitate from titanium upon cooling, thus the oxides must form as solids in the molten matrix. Their formation as solids promotes solidification of the matrix (Hanumanth and Irons 1996), and inhibits coalescence. The rapid solidification of the matrix stops oxide growth producing the finely dispersed oxide product.

Increasing the diluent iron to 50wt%, figure 8.8, lowers the reaction temperature even further and stops complete melting of the constituents. The reaction is seen to be limited. Some titanium powders have internally oxidised without mixing with the iron matrix. The oxide dispersion is similar to that found in the 40wt% Fe sample, figure 8.7. Thus, the titanium powders have melted, oxidised but then been contained within the boundaries of the powder. This could be due to a solid oxide shell forming around the titanium powder or rapid solidification of the matrix stopping the reaction.

8.4.3.1 Reaction Temperature Profiles

Figure 8.2 shows that increasing the iron percentage in the reactions based on 3 moles of titanium, smoothes the pellet temperature profile. The sample with no iron features a large 'exotherm' at 3-11 seconds, and a smaller one – also featuring in the sample with 20wt% - at 15-20 seconds. The initial 'exotherm' detected in the sample with no added iron is at the same temperature as the solidification temperature of TiO. Chapter 5, figure 5.21, detailed the morphology of the product. With this morphology, the solidification temperature profile of the porous ceramic shell is captured. This effect is seen moderately in the sample with 20wt% Fe, but due to the lesser degree of segregation, it is not as marked. The effect is non-existent in the 40wt% Fe sample. The secondary 'exotherm' appears in all the samples, but does not relate temperature wise, to any product phase changes. The temperature is relatively low, below the melting point of titanium oxides and metallic iron, so it could be a Fe – Ti alloy, possibly the exothermic formation of FeTi or Fe₂Ti. However, due to the segregated physical structure it is not possible to deduce.

The low temperature 'exotherms' are seen in the 5 moles of titanium samples in figure 8.3. Again, these structures are relatively segregated and thus it is difficult to determine the individual process that is causing the reaction. However, the temperature is near the melting point of iron, and could be a Fe – Ti alloy. The mixed structure of the sample containing 40wt% iron contains no evidence of 'exotherms'. This is because the compact solidifies within seconds and is recorded as a solid cooling. This is the same for the 6 moles of titanium series of compacts.

8.4.4 The $\text{Fe}_2\text{O}_3 + 3\text{Ti}$ Reaction

The $\text{Fe}_2\text{O}_3 + 3\text{Ti}$ reaction is of interest as it forms the stoichiometric oxide TiO. It is the starting point in the analysis of the more dilute 4, 5 and 6 moles of titanium systems. The morphology of the products is seen to follow those described for the 2 moles of titanium system.

Figures 8.9 - 8.11 depict the transition across the morphologies with increasing iron diluent content. In figure 8.9 there is a definite boundary between the phases. In the metallic phase on the right hand side are spherical areas of TiO. To form an oxide sphere within the metal, both the metal and oxide must have been liquid. The reaction temperature is $\sim 2000^\circ\text{C}$ which is sufficient for this to be the case. On the left hand side of the metallic area, TiO is seen to be in a dendritic form. This is evidence that it must have grown as a solid within the molten iron-titanium-oxygen alloy during cooling. Thus the initial reaction products are liquid titanium oxide, the majority of which segregates from the metal, and a liquid Fe-Ti-O alloy. Oxygen has a very small solubility ($<0.002\text{at}\%$) in iron but a solubility in titanium of $\sim 30\text{at}\%$. Upon cooling of the alloy there is some titanium oxide and iron titanium oxide precipitation. Although no Fe-Ti-O phases were found in the ceramic shell it is possible that there are quantities in the metallic phase.

A mixed morphology is seen in the sample with 30wt% Fe. Here, the compact reaction temperature is just above the melting point of TiO. Thus it solidifies rapidly and traps the metal phase within it. An even, mixed, morphology is the

result. In effect, the excess metal is acting to fill the pores of the solid ceramic phase (Feng *et al.* 1994).

50wt% Fe puts the composition onto the limits of its self sustainability. The reaction temperature is below the melting point of TiO and oxides that form will be solid. There are areas of ceramic dispersed within the metallic region (mark X), bordered by large regions of ceramic phase (mark Z). In-between these regions is a thin area of phase that has the appearance of that in figure 8.10 (mark Y). The titanium oxides formed at mark X are the same as those in figure 8.7. Their angular morphology is evidence of their precipitation from the melt. The formation and composition of the ceramic under mark Z is not known.

8.4.5 Morphology Control and the 'Ideal' Morphology

In the series of compositions in table 8.1, it has been shown that titanium oxides mainly form as liquids, but can be precipitated from the metallic matrix. Iron can act to produce definable oxide phases that would not exist without its presence. It is seen that the cooling rate of the compact is a defining factor in enabling the phases to be trapped in place. Slow cooling from high temperatures enables gross segregation, whilst too low a temperature inhibits complete reaction. In general, the product microstructure is dependant on the different physiochemical properties of the reactants and the products (Feng *et al.* 1994) and the extent of liquid and gaseous species at the reaction front. As such, for this system, each case must be examined in its own right.

By analysing the morphology of the products a graph was constructed to describe the boundary conditions that are at work with these compositions, figure 8.19. It should be pointed out that due to the dependency of the product morphology on the cooling rate of the sample, the conditions only apply with samples of identical size, reacted under identical conditions. Explorative investigations into scaling up the reaction produced morphologies that bore no relation to the boundary conditions in this work.

The drive to produce an ideal material of discrete titanium oxides within a metallic matrix was realised in the composition $\text{Fe}_2\text{O}_3 + 6\text{Ti} + 20\text{wt}\% \text{Fe}$. Under the experimental conditions employed in this research the composition produced the morphology displayed in figure 8.12. The XRD analysis shows the oxides to be $\text{Fe}_2\text{Ti}_4\text{O}$ or Ti_2O . Both these phases are precipitates. Ti_2O precipitates when the solid solution $\text{TiO}_{2.35\%}$ cools below $\sim 600^\circ\text{C}$. The formation of $\text{Fe}_2\text{Ti}_4\text{O}$ is known to be promoted by the presence of the iron. The oxides have a globular appearance and most are not coherent with the matrix, suggesting that they formed as liquids in the liquid matrix. With a maximum reaction temperature of $\sim 1700^\circ\text{C}$, no literature on iron titanium oxides liquid at this temperature could be found.

8.4.6 Reaction Mechanism

Under limited heating there is a reaction between the titanium powders and the Fe_2O_3 . This is seen as the appearance of a black interface around the titanium particles, figure 8.15. Although the figure is not in colour, it was seen that the outer edge of the titanium powders had turned a light golden colour, evidence

of oxidation to TiO. When the compact temperature is significant enough to melt the matrix, figure 8.14, there is mass oxidation of the titanium powders. The oxide morphology is typical of solid oxide formation within a molten matrix. The oxides have not mixed with the molten matrix as the formed oxide shell is solid and confines them to within the titanium powder. Kanuary (1992) states that the $\text{Fe}_2\text{O}_3 + \text{Al}$ and $\text{Ti} + \text{C}$ reactions are based around the metal phase melting and forming a molten alloy complex around the non-metal. Diffusion of species across this alloy then controls the reaction. This is possibly true in the mentioned reactions as the metallic phase in both cases has a lower melting point than the non-metal phase. In this reaction, the Fe_2O_3 will melt first and no literature could be found on similar systems.

The actual reaction scheme is shown in detail in figures 8.16, 8.17 and 8.18. The reaction is only partial, as can be seen from the one element results of the powders in figure 8.16, table 8.4. However it is extensive, with a reaction layer, marked R, of about $5\mu\text{m}$ thick. This layer is thought to be the black layer observed in the optical micrographs. Its cracked morphology and brittleness would make it prone to removal during polishing, this would lower it below the metallic surface and give it the 'black' appearance. The morphology of the titanium particle is unlike the original powder. It has a crystalline appearance that could be due to it melting and solidifying again. This could be caused by the exothermic heat of the oxidation at the reaction layer, mark R. Under conditions of full melting, with a molten oxide shell, the titanium metal would mix with the molten iron based matrix. However, in this case the oxide shell was solid and the titanium was confined to within it.

The phase under mark 2, figure 8.18, is titanium, but has a 'sintered powder' appearance. A similar morphology was seen on the titanium and Fe_2O_3 sintered samples from chapter 5, figure 5.40. Its slightly darker colour on the BSE micrograph agrees with the EDX analysis of a higher oxygen content than the pure titanium. The structure could be explained as it is known that titanium significantly embrittles as it absorbs oxygen. This layer is probably a oxygen rich titanium solid solution that has cracked as it has formed, during processing or after melting and recrystallisation. As such the original boundary between the titanium powder and the Fe_2O_3 powder is under mark 3. Here we find the Fe - Ti - O phase that could be $\text{Fe}_2\text{Ti}_4\text{O}$. This phase forms from the reaction between the Fe_2O_3 and titanium and it could be the first liquid phase to form. If we ignore the oxygen content, the Ti - Fe ratio is 57% - 43% which is close to the low melting point eutectic composition of 70% - 30%. Later oxidation and iron migration could have altered the composition. Under conditions where significant quantities of this phase forms, the reaction would go to completion. In this case there is only a slight reaction (0.5 μm thick). Additional titanium cation diffusion through this layer forms the TiO_2 under mark 4. This then stops any additional iron diffusion into the titanium.

Around the outside of the titanium powder is an extensive, porous, metallic network of $\sim 10\mu\text{m}$ in width, figure 8.17. The EDX analysis, table 8.5 - marks 5 and 6, reveals this to be Fe_2Ti and FeTi . The network channel width of $\sim 1\mu\text{m}$ is similar to the diameter of the Fe_2O_3 powder. The possible method of formation for this phase is the sintering of the Fe_2O_3 powder, its reduction to a sintered Fe mass, and then the diffusion of titanium into the Fe to form the mixed phases.

Saidi (1995) thought that the Fe-Ti phases were involved in the iron – titanium - carbon reaction, whilst Fan *et al.* (1997) could not find any evidence for the phase. It is evident that they exist but it is impossible to determine what part they play in the reaction. The primary reaction appears to be at the interface, at marks 2, 3 and 4.

8.5 Conclusions

- Increasing the iron diluent content increases the complexity of the phases formed and reduces the combustion temperature.
- The product can take one of three morphologies; segregated, mixed or partially reacted.
- Titanium oxides that are liquid at the reaction temperatures and have to be trapped in position by a rapidly solidifying matrix to form even dispersions.
- Titanium oxides that are solid at the reaction temperatures are generally confined to the boundaries of the titanium powders, due to the formation of a solid titanium oxide layer.
- The oxidation and alloy formation reactions that occur in the compact are complex and related. It is impossible to deduce the reaction mechanism. However, it is possible to say the iron does play a part in it and is not inert.

Chapter 8

Figures

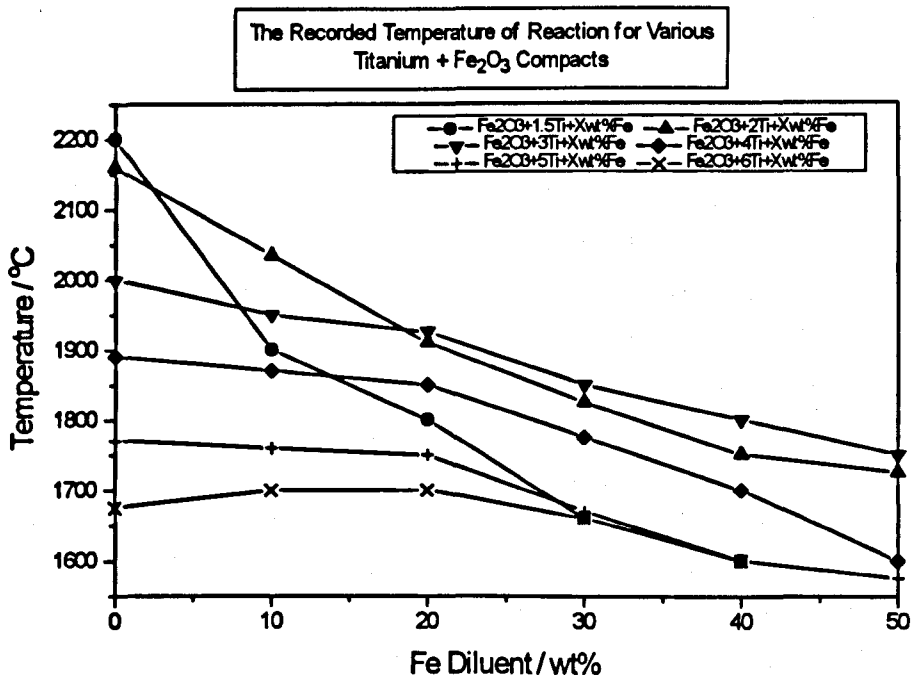


Figure 8.1

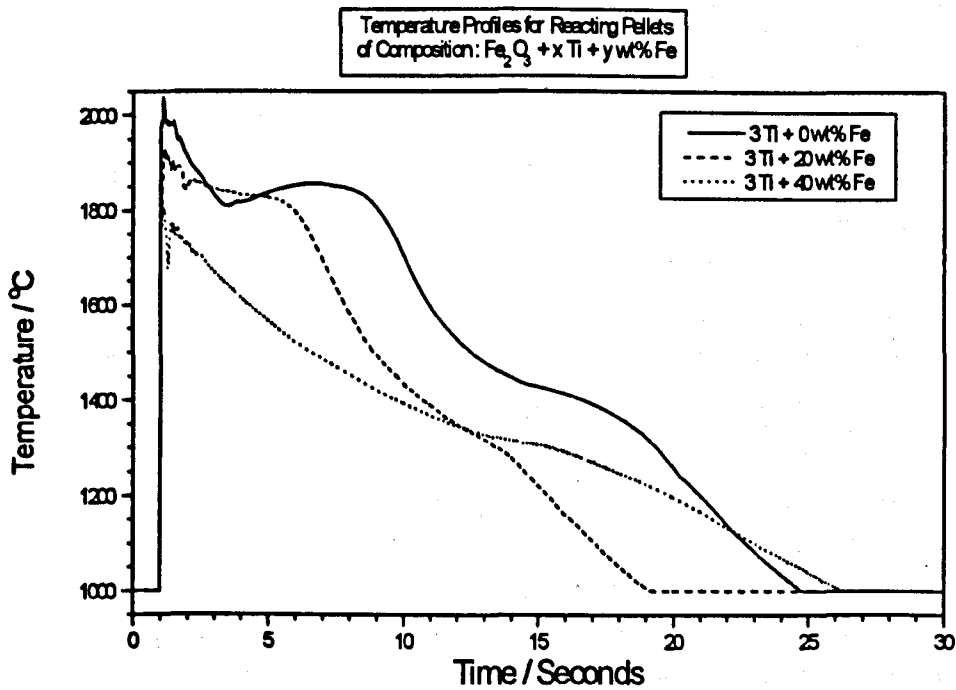


Figure 8.2

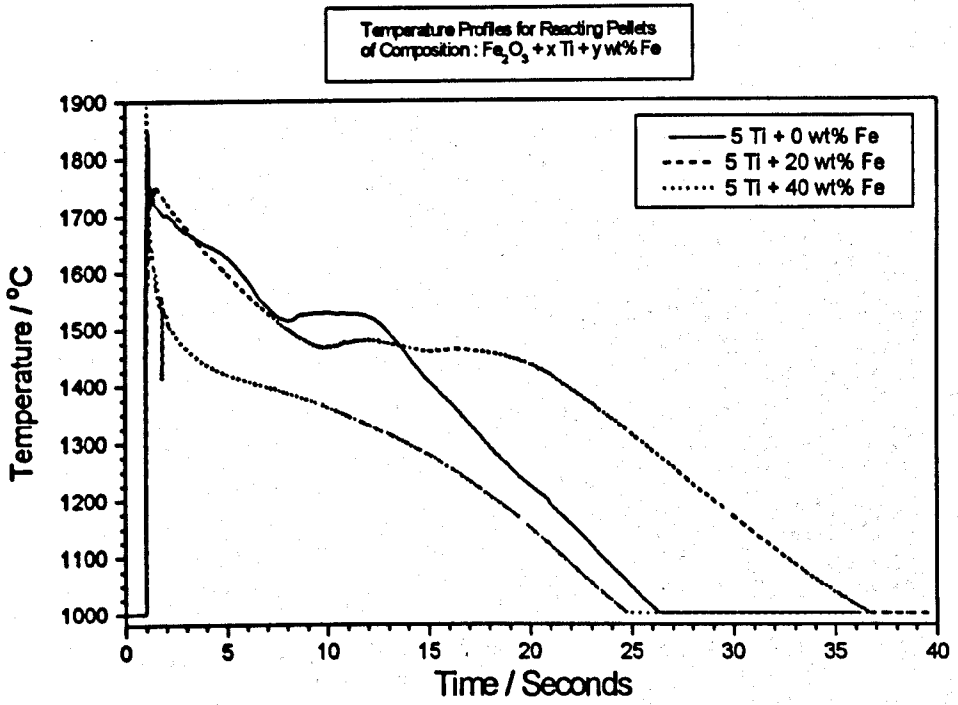


Figure 8.3

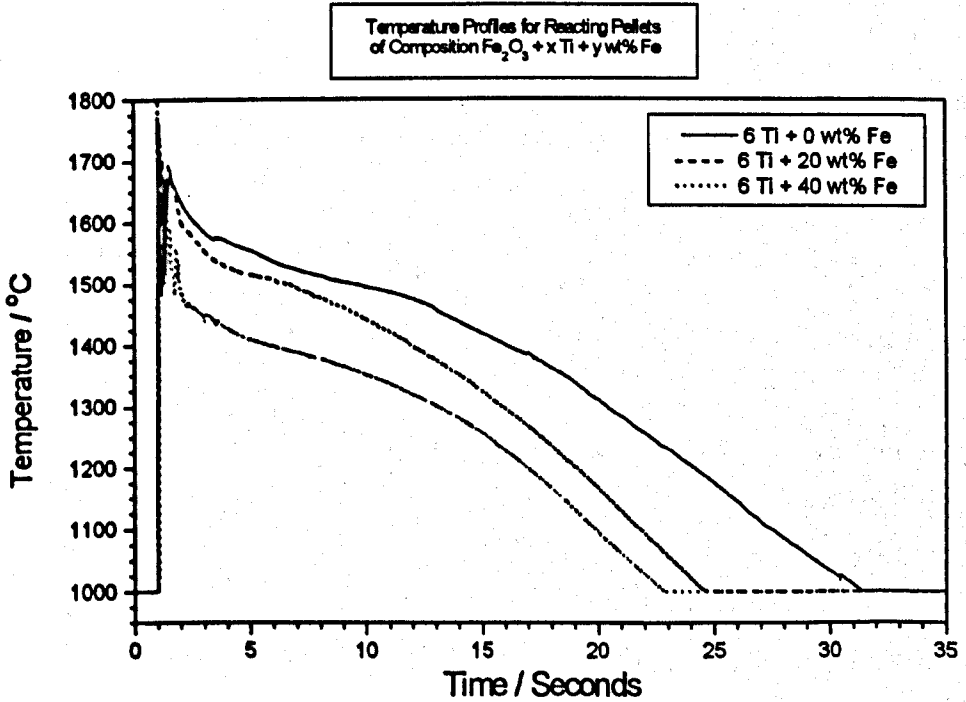


Figure 8.4

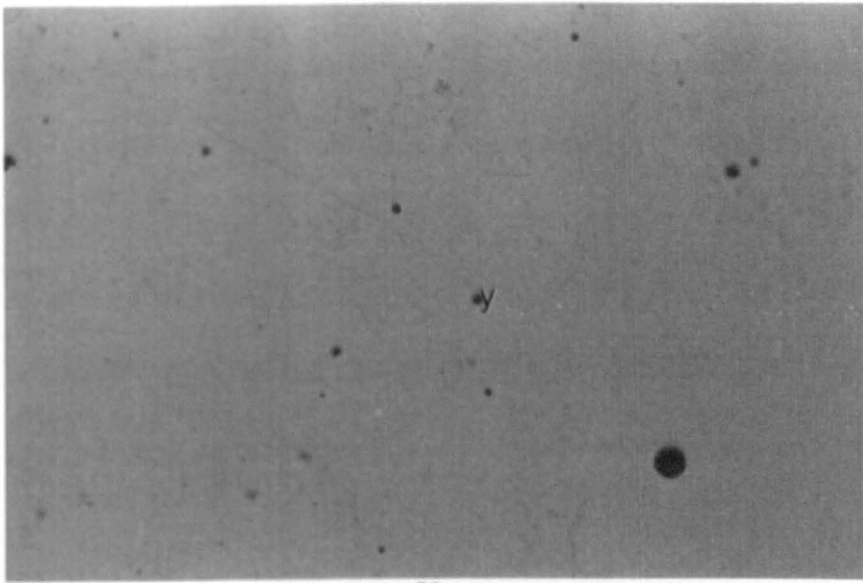


Figure 8.5 Optical Micrograph of the Metallic Product from a $\text{Fe}_2\text{O}_3 + 2\text{Ti} + 10\text{wt}\% \text{Fe}$ Compact. Dark areas (y) are ceramic product in the metallic matrix.

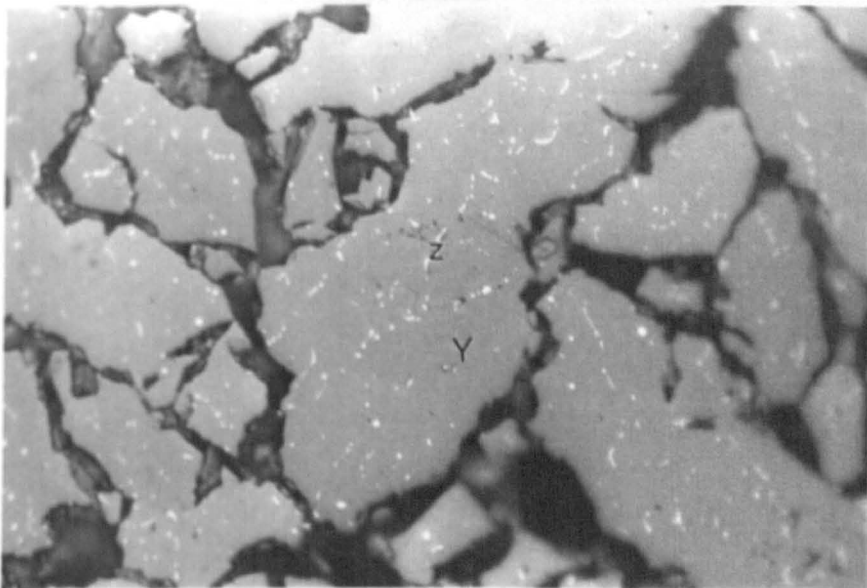
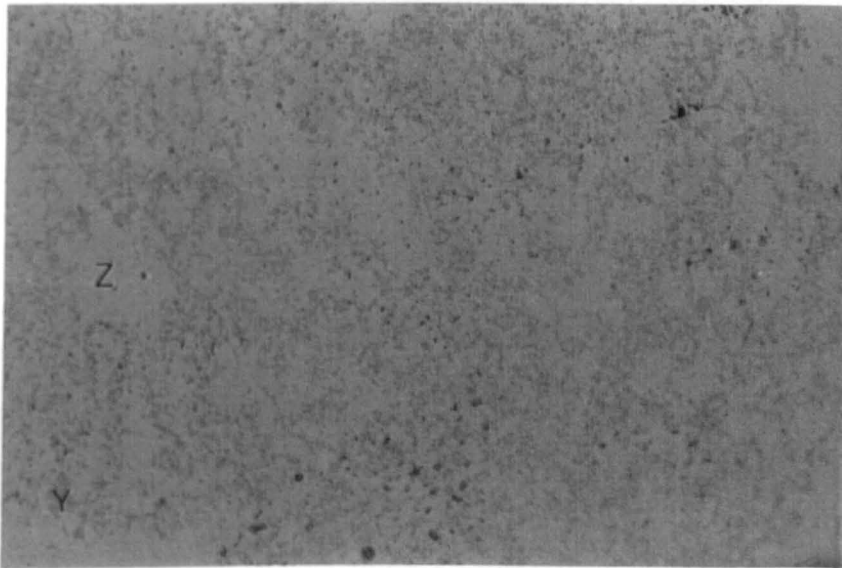
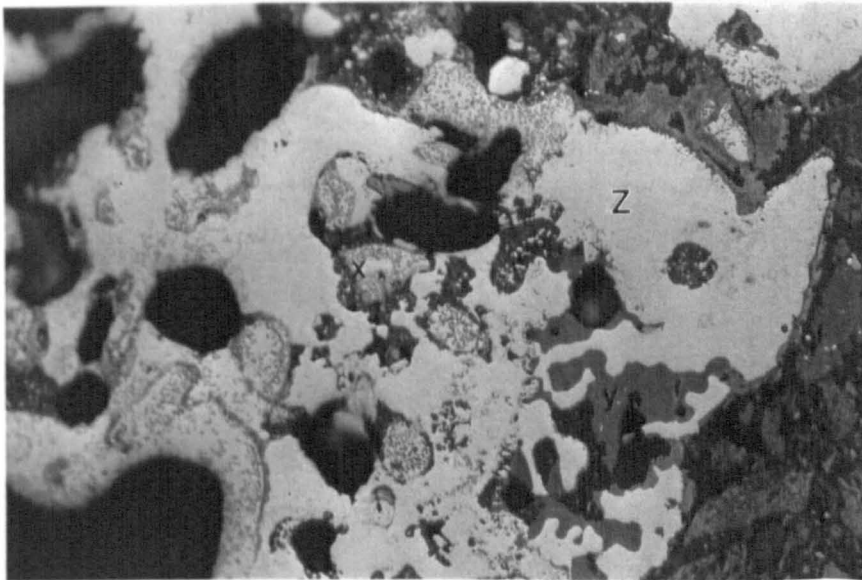


Figure 8.6 Optical Micrograph of the Ceramic Product from a $\text{Fe}_2\text{O}_3 + 2\text{Ti} + 10\text{wt}\% \text{Fe}$ Compact. Dark ceramic phase (Y) contains silver metallic particles (z).



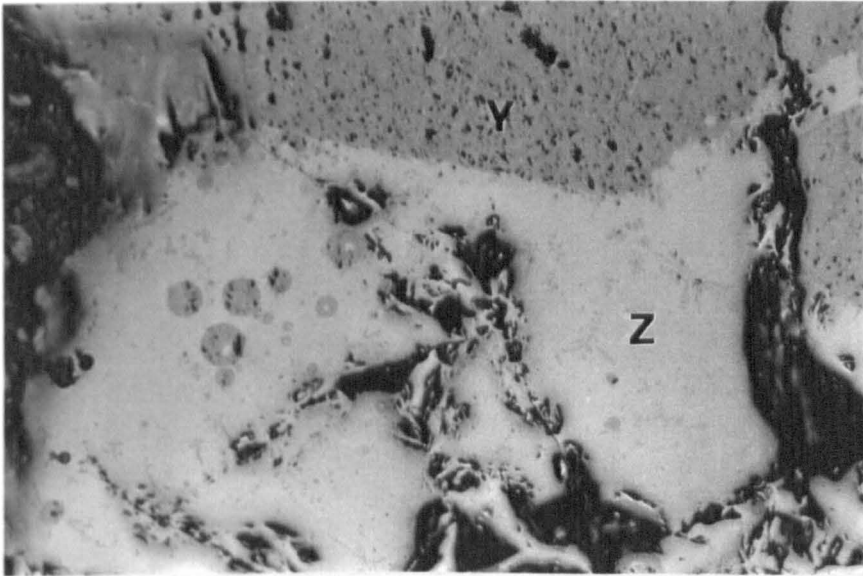
————— 50 μ m

Figure 8.7 Optical Micrograph of the Product from a $\text{Fe}_2\text{O}_3 + 2\text{Ti} + 40\text{wt}\%$ Fe Compact. Ceramic phase (Y) dispersed in metallic matrix (Z).



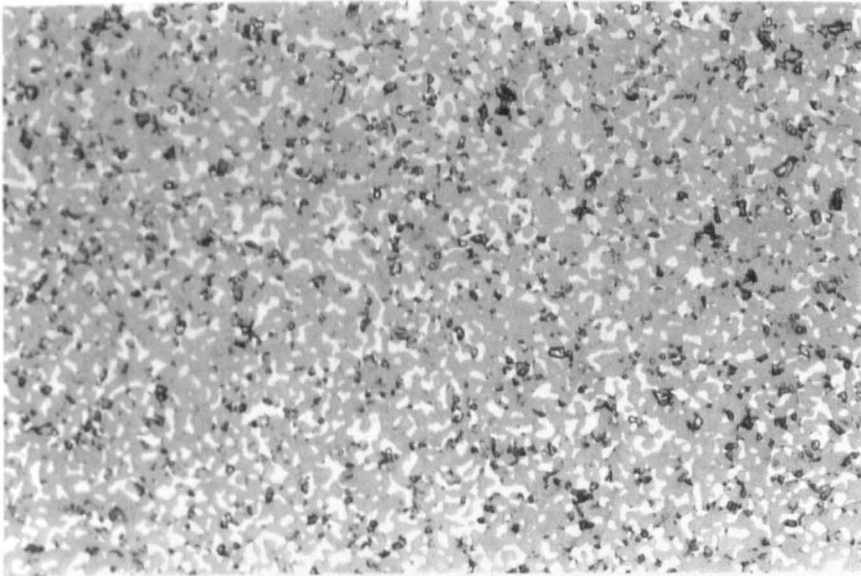
————— 50 μ m

Figure 8.8 Optical Micrograph of the Product from a $\text{Fe}_2\text{O}_3 + 2\text{Ti} + 50\text{wt}\%$ Fe Compact. Ceramic material (x and y) in iron based metallic matrix (Z).



—————100 μ m

Figure 8.9 Optical Micrograph of the Product from a $\text{Fe}_2\text{O}_3 + 3\text{Ti}$ Compact. Ceramic area (Y) segregated from metallic area (Z).



—————50 μ m

Figure 8.10 Optical Micrograph of the Product from a $\text{Fe}_2\text{O}_3 + 3\text{Ti} + 30\text{wt}\%$ Fe Compact. The Light Phase is the Metallic, the Dark the Ceramic.

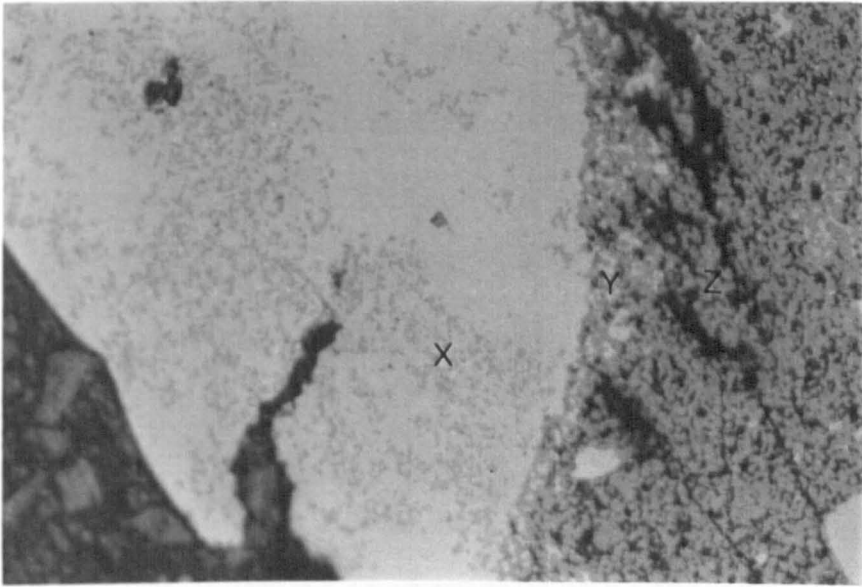


Figure 8.11 Optical Micrograph of the Product from a $\text{Fe}_2\text{O}_3 + 3\text{Ti} + 50\text{wt}\%$ Fe Compact.

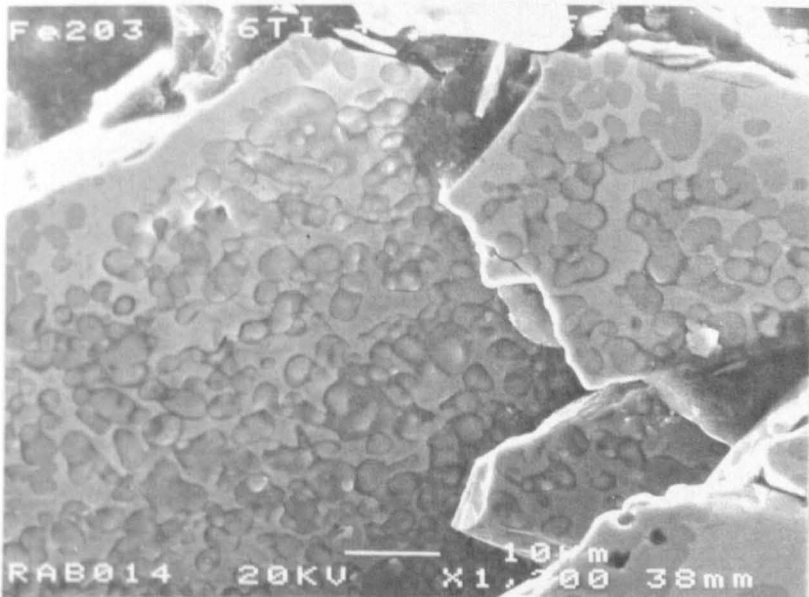


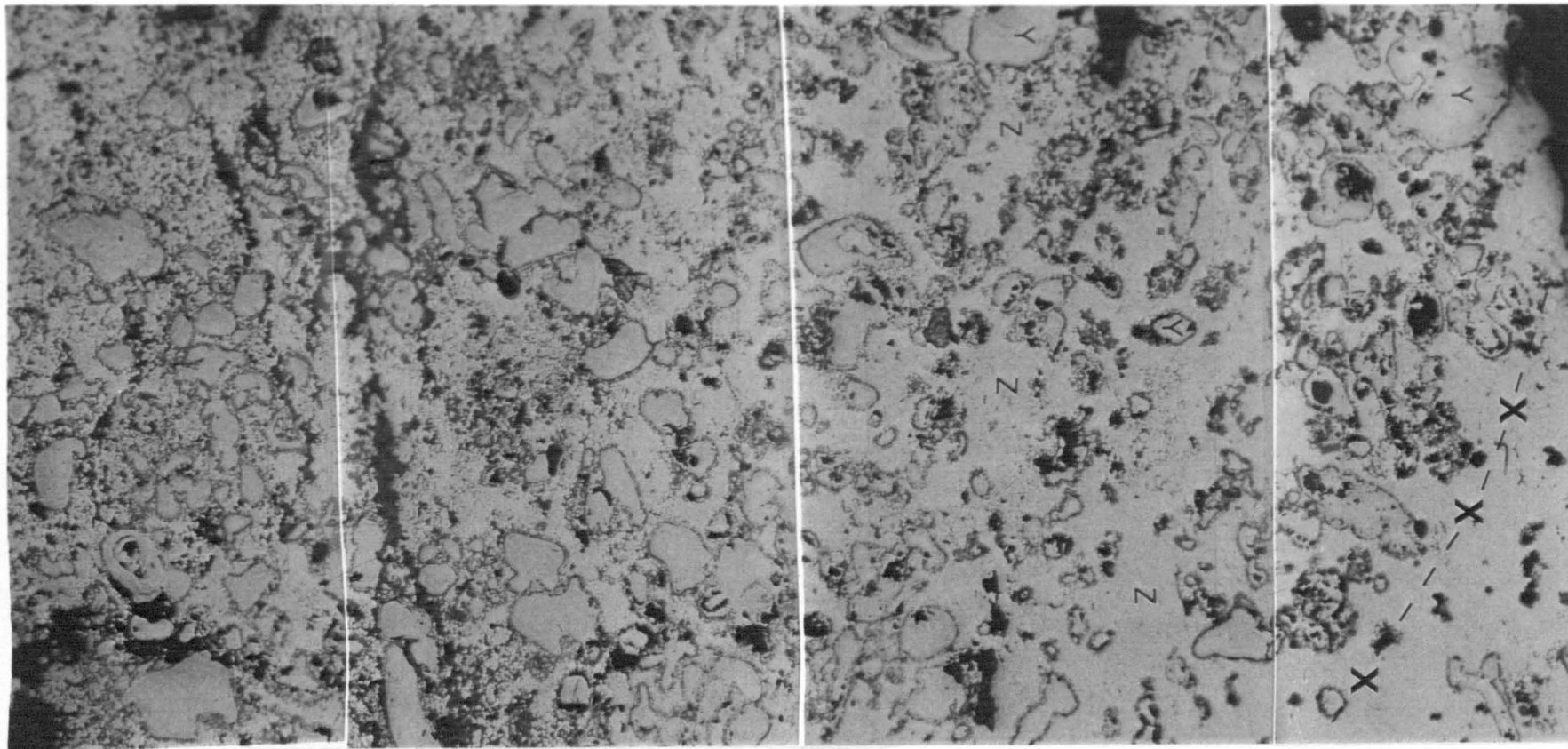
Figure 8.12 SEM Micrograph of the Product from a $\text{Fe}_2\text{O}_3 + 6\text{Ti} + 20\text{wt}\%$ Fe Compact.

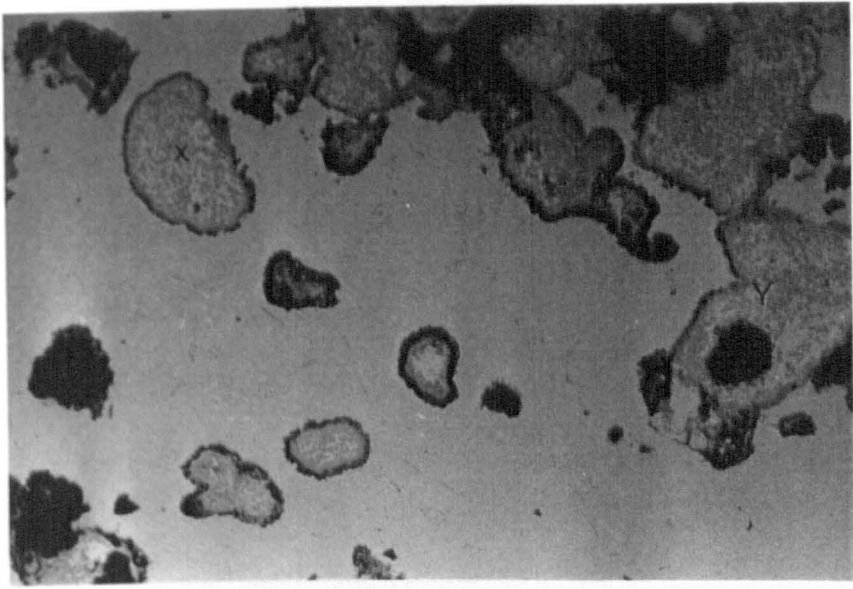
Figure 8.13 Optical Micrographs of a Part Reacted, Sectioned Compact of Composition $\text{Fe}_2\text{O}_3 + 4\text{Ti} + 50\text{wt}\% \text{Fe}$

100 μm

BOTTOM

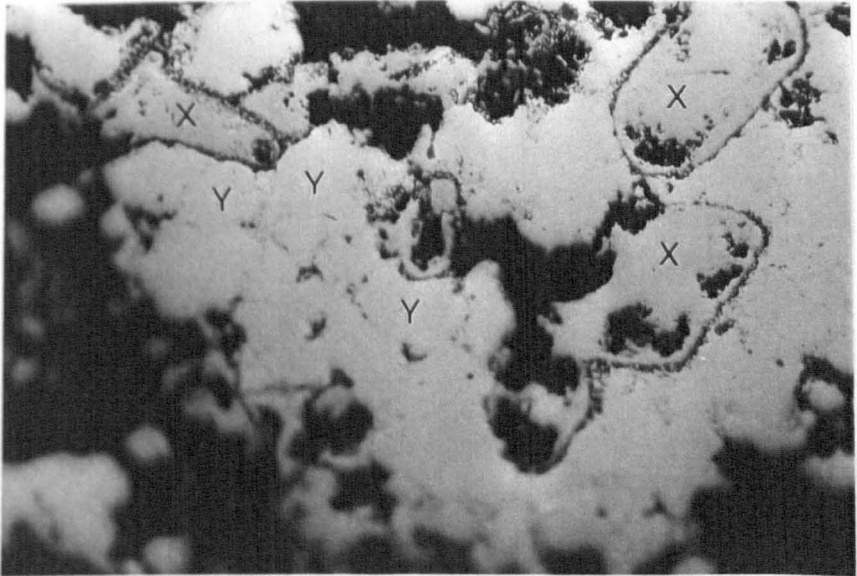
TOP





————— 50 μ m

Figure 8.14 Close Up Optical Micrograph of the Reacted End of the Part Reacted, Sectioned Sample seen in Figure 8.13



————— 50 μ m

Figure 8.15 Close Up Optical Micrograph of the Cooler, Unreacted End of the Part Reacted, Sectioned Sample seen in Figure 8.13

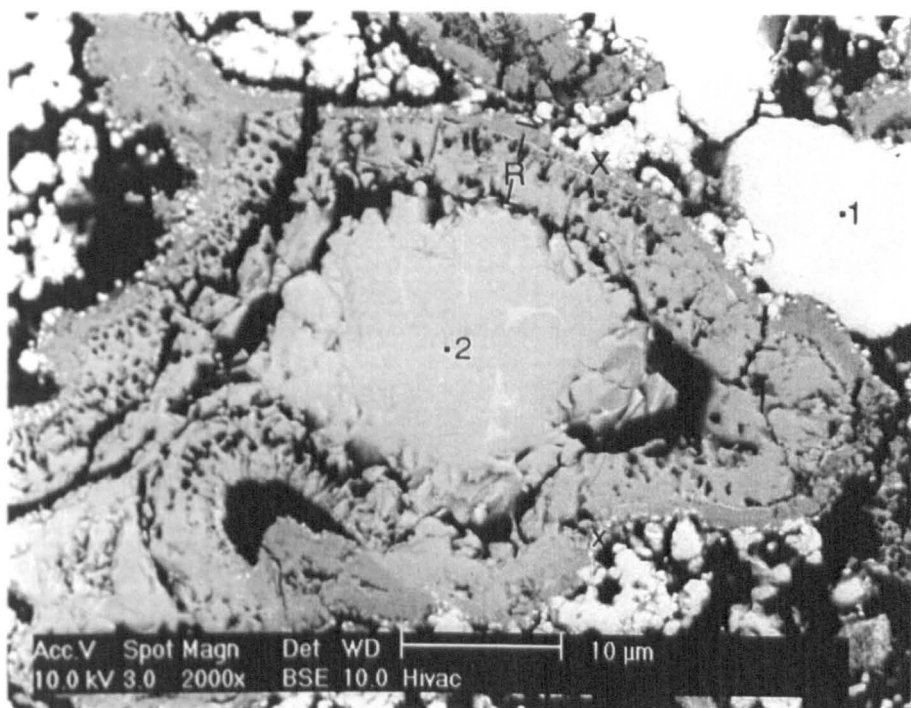


Figure 8.16 E-SEM Image of Powders Taken from the Part Reacted, Sectioned Sample seen in Figure 8.13

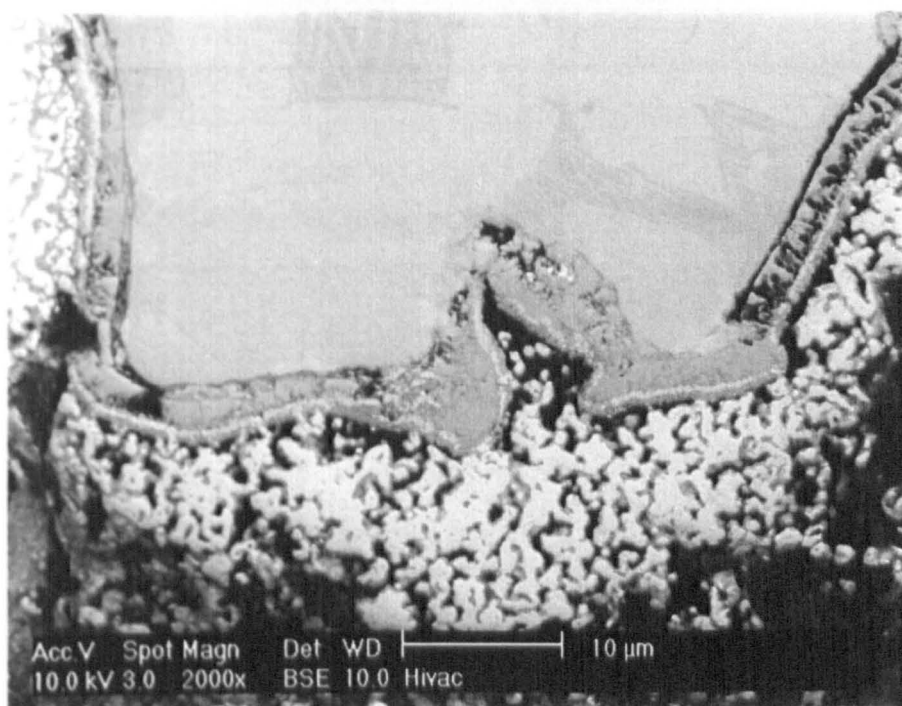


Figure 8.17 E-SEM Image of Powders Taken from the Part Reacted, Sectioned Sample seen in Figure 8.13

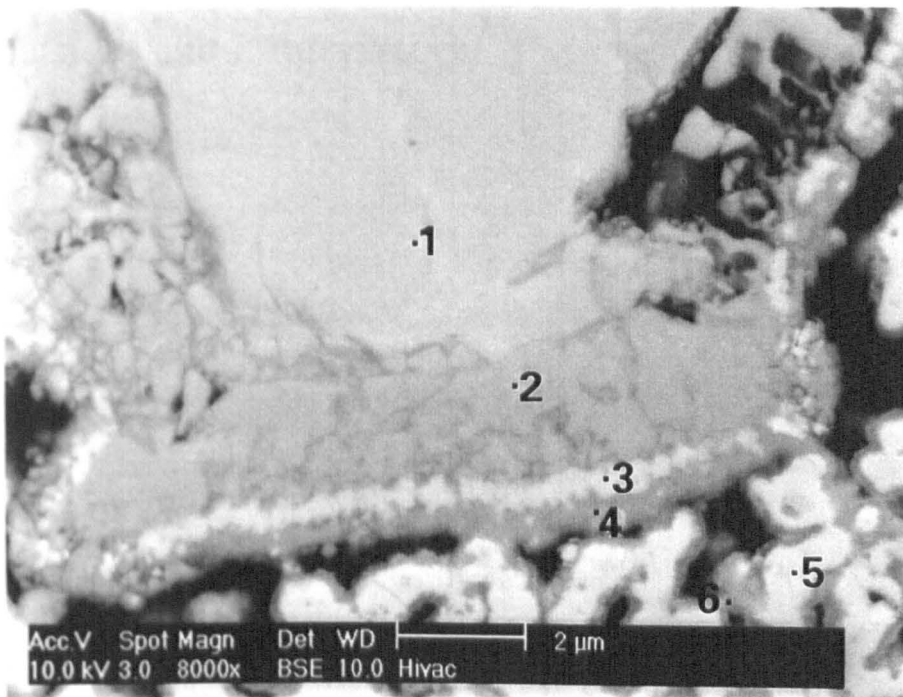


Figure 8.18 Detail of the E-SEM Image of Figure 8.17

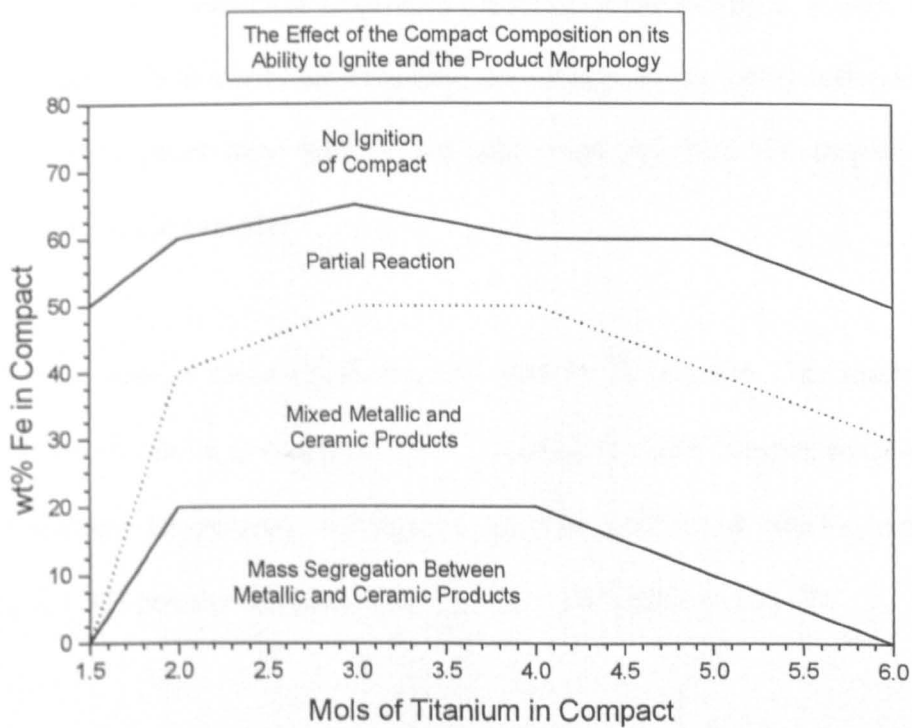


Figure 8.19

Chapter 9

Conclusions and Future Work

9.1. Conclusions

1. The oxidation of titanium powder compacts in air has been investigated. The exothermic oxidation of titanium in air can be sufficient to cause melting of the titanium. The formation of the liquid titanium phase signals the onset of combustion.
2. The ambient temperature required to promote ignition of the compact is determined by the titanium particle size. Temperatures as low as 550°C were seen to be sufficient to promote ignition of the compact. Within the experimental boundaries investigated, the density of the pellet influences the oxygen penetration into the compact, and therefore the degree of oxidation of the compact.
3. Titanium powder reacts exothermically with Fe_2O_3 powders. The reaction temperature can be in excess of 2200°C. Using $<150\mu\text{m}$ titanium powders, the ambient temperature required to promote ignition of stoichiometric $\text{Fe}_2\text{O}_3 + 3\text{Ti}$ powder compacts in air or argon atmospheres, is 600°C.
4. It was calculated that an oxide thickness of $\sim 1\mu\text{m}$ was sufficient to cause melting of the titanium powder particle. The oxide thickness was seen to agree with experimental findings.

5. A computer programme has been written that faithfully models the oxidation reaction between titanium powder compacts in air. Experimental evidence verifies the accuracy of the computer model.
6. Even dispersions of titanium oxides within a Fe-Ti matrix can be produced by the combustion reaction between Fe_2O_3 and titanium. The morphology and composition of the products of these reactions is dependant on the starting reactant composition and the reaction temperature.

9.2. *Future Work*

1. Investigation and development of the Fe_2O_3 and titanium reaction model. The effect of temperature, heating rates, atmosphere and time.
2. Further work to introduce more accurate methods of determining key compact characteristics such as heat flow, diffusion of species, density, the effect of melting etc. The production of a 3 dimensional model.
3. Further development of the mathematical model to include the Ti + C and Ti + C + Fe systems.
4. Introducing additional oxide stabilising elements to the Fe_2O_3 + titanium composition such as carbon and nitrogen. Are mixed oxycarbides / oxynitrides formed?

5. Investigating the addition of Fe-Ti alloys as diluents or use them as the source of reactant titanium.
6. Investigate the effect of using different iron oxides – FeO, Fe₃O₄ – to vary the reactant iron – oxygen ratio.
7. Add the SHS formed iron-titanium oxide composites to steels to investigate their effect, are they ferrite nucleating or grain refining ?

Chapter 10

Acknowledgements

I would like to thank Professor J. V. Wood for organising and supporting this research and Dr. P. H. Shipway for his help, guidance and daily support, without which this research and subsequent thesis would not have existed. Thanks also to the E.P.S.R.C. for funding the research and the London and Scandinavian Metallurgical Company Ltd. for sponsoring the work and helping with the supply of materials and manufacturing equipment.

Chapter 11

Bibliography

- 1) Abbud-Madrid A., Branch M.C. and Daily J.W. (1996); "Ignition and Combustion of Bulk Titanium and Magnesium at Normal and Reduced Gravity"; 26th Symposium (international) on Combustion / The Combustion Institute, pp 1929-1936.
- 2) Akhtar N., Janes R. and Parker M. J. (1996); "Solid-state Kinetics and Reaction Mechanisms for the Formation of $Y_2Cu_2O_5$ "; Journal of Materials Science, Vol. 36, pp 3053-3056.
- 3) Armstrong R. (1992); "Theoretical Models for the Combustion of Alloyable Materials"; Metallurgical Transactions A, Vol. 23A, pp 2339-2347.
- 4) Askeland D. R. (1992) ; "The Science and Engineering of Materials"; Second S.I. Edition, Chapman and Hall, London. ISBN 0-412-34260-X.
- 5) ASM Handbook (1992a); "Alloy Phase Diagrams"; Volume 3, ISBN 0-871707-377-7, pp199.
- 6) ASM Handbook (1992b); "Alloy Phase Diagrams"; Volume 3, ISBN 0-871707-377-7, pp1793.
- 7) Bakhman N.N , Kuznetsov G.P. and Puchkov V.M. (1998); "Critical Conditions of the Combustion of Compressed Titanium Specimen"; Combustion, Explosion and Shock Wave, vol 34, 3, pp292-297.
- 8) Barzykin V. V. (1992); "Initiation of SHS Processes"; Pure and Applied Chemistry, Vol. 64, No. 7, pp 909-918.
- 9) Bhattacharya A. K. (1992); "Modelling of the Effects of Porosity and Particle Size on the Steady-state Wave Velocity in Combustion Synthesis"; Journal of Materials Science, Vol. 27, pp 1521-1527.
- 10) Bickley R.I., Gozalez-Carreno T. and Palmisano L. (1991); "A Study of the Interaction Between Iron(III) oxide and Titanium(IV) oxide at Elevated Temperatures"; Materials Chemistry and Physics; 29, pp475-487.
- 11) Bloshenko V.N., Bokii V.A. and Borovinskaya I.P. (1984a); "Dissolution of a Metal Oxide Film During Titanium Carbide Synthesis"; Fizika Goreniya I Vzryva, vol 20, 6, pp 87-90.
- 12) Bloshenko V.N., Bokii V.A. and Borovinskaya I.P. (1985); "Oxidation of Metal Particles in the Heating Zone During the Combustion of SHS Systems"; Combustion, Explosion and Shockwaves. vol 21, pp88-92.
- 13) Bloshenko V.N., Bokii V.A. and Borovinskaya I.P. and A.G. Merzhanov (1984b); "Self-Cleaning of SHS Titanium Carbide from Impurity Oxygen"; Fizika Goreniya I Vzryva, vol 20, 6, pp 90-94.
- 14) Borovinskaya I.P. (1992); "Chemical classes of the SHS processes and materials"; Pure and Applied Chemistry. Vol 64, 7, pp 919-940.

- 15) Bowen C. R. and Derby B (1994); "Differential Thermal Analysis of Ignition Temperatures in a Self-Propagating High-Temperature Synthesis Reaction"; *Journal of Thermal Analysis*, Vol. 42, pp 731-719.
- 16) Bowen C. R., Hulsmann S. and Derby B. (1991); "Preliminary Studies on the Manufacture of Multiphase Ceramics by Self-Propagating High-Temperature Synthesis (SHS); Deutsche Keramische Gesellschaft, Koln, Germany, pp 631-635.
- 17) Bunin V. M., Borovinskaya I. P., Mikulinskaya L. F. and Sychev A. E. (1993); "Tungstenless Solid Alloys Based on Titanium Carbide Obtained by SHS with a Nickel-Molybdenum Binder"; *Inorganic Materials*, Vol. 29, No. 8, pp 1027-1029.
- 18) Cao G. and Varma A. (1994); "A New Expression for Velocity of the Combustion Front During Self-Propagating High-Temperature Synthesis"; *Combustion Science and Technology*, Vol. 102, pp 181-191.
- 19) Capaldi M. J. and Wood J. V. (1996); "Production and Characterization of TiC-Containing Materials by Self-Propagating High-Temperature Synthesis"; *Journal of Materials Synthesis and Processing*, Vol. 4, No. 4, pp 245-253.
- 20) Capaldi M. J., Saidi A. and Wood J.V (1997); "Reaction Synthesis of TiC and Fe-TiC Composites"; *ISIJ International*, Vol. 37, no. 2, pp 188-193.
- 21) Chandran R. G., Patil K. C. and Chandrappa G. T. (1995); "Combustion Synthesis, Characterisation, Sintering and Microstructure of Mullite-Cordierite Composites"; *Journal of Materials Science Letters*, Vol. 14, pp 548-551.
- 22) Chang D.K, Won C.W., Chun B.S. and Shim G.C. (1995); "Purifying Effects and Product Microstructure in the Formation of TiC Powder by the Self-Propagating High-Temperature Synthesis"; *Metallurgical and Materials Trans. B*, vol 26B, pp 176-179.
- 23) Chidambaram P. R., Meier A. and Edwards G. R. (1996); "The Nature of Interfacial Phenomena at Copper - Titanium / Alumina and Copper - Oxygen / Alumina Interfaces"; *Materials Science and Engineering*, A206, pp 249-258.
- 24) Choi Y. and Rhee S-W (1995); "Effect of Carbon Sources on the Combustion Synthesis of TiC"; *Journal of Materials Science*, Vol. 30, pp 4637-4644.
- 25) Choi Y. and Rhee S-W. (1994); "Equilibrium in the reaction of Ti and C to Form Substoichiometric TiC_x "; *Journal of Materials Science Letters*, Vol. 13, pp 323-325.
- 26) Choi Y., Mullins M. E. Wijayathilleke K. and Lee J. K. (1992); "Fabrication of Metal Matrix Composites of TiC-Al through Self-Propagating Synthesis Reaction"; *Metallurgical Transactions A*, Vol. 23A, pp 2387-2392.
- 27) Cismaru D. and Momirlan M. (1978); "X-Ray Investigations in Some Experiments of Titanium Oxidation in Air at Different Temperatures"; *Revue Roumaine De Physique*; vol 23, 6, pp607-611.

- 28) Dechamps M. and Lehr P. (1977); "Oxidation of Alpha Titanium in Oxygen Atmospheres"; The Journal of the Lesser Common Metals. Vol 56, 2, pp193-207.
- 29) Dechamps M., Feldman R. and Lehr P. (1976); "High Temperature Oxidation of Titanium: Physical and Mathematical Models"; Proceedings of the 3rd International Conference on Titanium. May 1976 Moscow. Plenum Press, New York. USA.
- 30) Dcevi S. C. (1994); "Differential Thermal Analysis of Exothermic Reactions in the Synthesis of MoSi₂"; Journal of Materials Science Letters, Vol. 13, pp 868-871.
- 31) Dcevi S.C. (1991); "Structure of the Combustion Wave in the Combustion Synthesis of Titanium Carbides"; Journal of Materials Science, Vol. 26, pp 2662-2670.
- 32) Degnan C. (1995); "The Processing and Wear Properties of a Fe (WTiC) MMC"; Thesis, Department of Materials Engineering and Materials Design, Nottingham University, Nottinghamshire, U.K.
- 33) Duan H-P., Sheng Y., Liu M. and Hoyi L. (1996); "Stainless Steel Lined Composite Steel Pipe Produced By Centrifugal SHS Process"; Journal of Materials Science Letters, Vol. 15, pp 1060-1061.
- 34) Dumez M. C., Marin-Aryal R. M. and Tedenac J. C. (1996); "Effects of Heating Rate and Pressure on the Reaction Mechanism of High-Pressure Combustion Synthesis of NiAl Compounds"; Journal of Materials Synthesis and Processing, Vol. 4, No. 2, pp 105-113.
- 35) Dunmead S. D. and Munir Z. A. (1992a); "Temperature Profile Analysis in Combustion Synthesis: 1, Theory and Background"; Journal of the American Ceramic Society, Vol. 75, No. 1, pp 175-179.
- 36) Dunmead S. D. and Munir Z. A. (1992b); "Temperature Profile Analysis in Combustion Synthesis: 2, Experimental Observations"; Journal of the American Ceramic Society, Vol. 75, No. 1, pp 180-188.
- 37) Dunmead S.D., Munir Z.A. and Holt J.B. (1989); "Gas-Solid Reactions under Self-Propagating Combustion Mode", Solid State Ionics, Vol. 32/33, pp 474-481.
- 38) Erogu S. and Gallois B. (1997); "Growth and Structure of TiC_xN_y Coatings Chemically Vapour Deposited on Graphite Substrates"; Journal of Materials Science, Vol. 32, pp 207-213.
- 39) Evans U.R. (1960); "The Corrosion and Oxidation of Metals", Edward Arnold, London, pp834.
- 40) Fan Q., Chai H. and Jin Z (1996); "Microstructural Evolution in the Combustion Synthesis of Titanium Carbide"; Journal of Materials Science, Vol. 31, pp 2573-2577.
- 41) Fan Q., Chai H. and Jin Z. (1997); "Role of Iron Addition in the Combustion Synthesis of TiC-Fe Cermet"; Journal of Materials Science, Vol. 32, pp 4319-4323.

- 42) Feng A. and Munir Z. A. (1994); "Field Assisted Self Propagation Synthesis of β -SiC"; Journal of Applied Physics, Vol. 76, No. 3, pp 1927-1928.
- 43) Feng A. and Munir Z. A. (1996); "Relationship Between Field Direction and Wave Propagation in Activated Combustion Synthesis"; Journal of the American Ceramics Society, Vol. 79, No. 8, pp 2049-2058.
- 44) Feng H. J., Hunter K. R. and Moore J. J (1994); "Combustion Synthesis of Ceramic and Metal-Matrix Composites"; Journal of Materials Synthesis and Processing, Vol. 2, No. 2, pp 71-86.
- 45) Filonenko A.K. and Barzykin V.V. (1996); "The Effect of Density on the Limits and Regularities of Spin Combustion of Titanium in Nitrogen"; Combustion, Explosion and Shockwaves, vol 32, 1.
- 46) Fischer E. (1997); "Thermodynamic Calculation of the O – Ti System"; Journal of Phase Equilibria, Section I: Basic and Applied Research, Vol. 18, No. 4, pp 338-343.
- 47) Gammal T. E. (1991); "Influence of Alloying Elements and Metalloids on the Emulsion and Separation Behaviour of Steel and Slag"; Steel research, Vol. 62, No.2, pp 152-156.
- 48) Garkol' D. A., Gulyaev P. Yu., Evstigneev V. V. and Mukhachev A. V. (1994); "A New High-Speed Brightness Pyrometry Method to Investigate Self-Propagating High-Temperature Synthesis"; Combustion, Explosion and Shock Waves, Vol. 30, No. 1, pp 72-76.
- 49) Gedevanishvili S. and Munir Z. A. (1994); "Field Assisted Combustion Synthesis of MoSi₂-SiC Composites"; Scripta Metallurgica et Materialia, Vol. 31, No. 6, pp 741-743.
- 50) Glassman I. and Papas P. (1994); "Determination of Enthalpies of Volatilization for Metal Oxides/Nitrides Using Chemical Equilibrium Combustion Temperature Calculations"; Journal of Materials Synthesis and Processing, Vol. 2, No. 3, pp 151-159.
- 51) Grabke H. J., Brumm M. and Steinhorst M. (1992); "Development of Oxidation Resistant High temperature Intermetallics"; Materials Science and Technology, Vol. 8, pp 339-340.
- 52) Gregg J. M. and Bhadeshia H. K. D. H. (1994a); "Bainite Nucleation from Mineral Surfaces"; Acta. Metall. Mater., Vol. 42, No. 10, pp 3321 – 3330.
- 53) Gregg J. M. and Bhadeshia H. K. D. H. (1994b); "Titanium-Rich Mineral Phases and the Nucleation of Bainite"; Metallurgical and Materials Transactions A, Vol. 25A, pp 1603-1610.
- 54) Gunaji V. and Sinclair S. (1995); "Ignition and Combustion of Titanium and Titanium Alloys"; ASTM Special Technical Publication. 1267, pp 81-85.
- 55) Halverson D. C., Edwald K. H. and Munir Z. A. (1995); "Improving the uniformity in Combustion Synthesized Titanium Carbide"; Journal of Material Science, Vol. 30, pp 3697-3703.
- 56) Halverson D.C., Edwald K.H. and Munir Z.A. (1993); "Influence of Reactant Characteristics on the Microstructures of Combustion

- Synthesised Titanium Carbide"; Journal of Materials Science, Vol. 28, pp 4583-4594.
- 57) Hanumanth G. S. and Irons G. A. (1996); "Solidification of Particle-Reinforced Metal-Matrix Composites"; Metallurgical and Materials Transactions B, Vol. 27B, pp 663-671.
 - 58) Javel J. F., Dirand M., Nassik F. Z. and Gachon J. C. (1996); "Real Time X-Ray Diffraction Study of the Formation by SHS of the Phases γ' and H in the Ternary System Al Ni Ti"; Journal De Physique IV, Colloque 2, supplement au Journal de Physique III, Vol 6, C2, pp 229-234.
 - 59) Kalpakjian S. (1992); "Manufacturing Engineering and Technology"; Second Edition, Addison-Wesley Publishing Company, ISBN 0-201-63093-1, Chapter 21.
 - 60) Kang Y-S., Miyamoto Y., Murakoa Y. and Yamaguchi O. (1995); "Fabrication and Characterization of $\text{MoSi}_2 / \text{Al}_2\text{O}_3 / \text{Ni} / \text{Al}_2\text{O}_3 / \text{MoSi}_2$ FGM's"; Journal of the Society of Materials Science Japan, Vol. 44, No. 501, pp 705-709.
 - 61) Kanuary A. M. (1992); "A Kinetic Model for Metal + Nonmetal Reactions"; Metallurgical Transactions A, Vol. 23A, pp 2349-2356.
 - 62) Kanury A. M. and Hernandez-Guerrero A. (1994); "Steady Planar Propagation of the Gasless SHS Reaction Producing Titanium Carbide"; Combustion Science and Technology, Vol. 102, pp 1-19.
 - 63) Kanury A. M. and Hernandez-Guerrero A. (1995); "Ignition of the Gasless SHS Reaction Producing Titanium Carbide"; Combustion Science and Technology, Vol. 104, pp 181-191.
 - 64) Kim H. S., Rogers P. S. and Rawlings R. D (1995); "Effect of Inert Diluent on Combustion Synthesis in the Aluminium Potassium Dichromate System"; Journal of Materials Science Letters, Vol. 14, pp 1587-1590.
 - 65) Kingsley J. J., Suresh K. and Patil K. C. (1990); "Combustion Sythesis of Fine-Particle Metal Aluminates"; Journal of Materials Science, Vol. 25, pp 1305-1312.
 - 66) Kivalo L. I., Grigorenko N. F. and Skorokhod V. V. (1988); "Contact Reaction Between a Liquid and a Soild Phase in a Finely Divided Titanium-Iron System"; Poroshokovaya Metalluriya, No. 9(309), pp 25-28.
 - 67) Ko S. G., Won C. W., Chun B. S. and Sohn H. Y. (1995); "The Self-Propagating High-Temperature Synthesis (SHS) of Ultrafine High-Purity TiC Powder from $\text{TiO}_2 + \text{Mg} + \text{C}$ "; Journal of Materials Science, Vol. 30, pp 2835-2837.
 - 68) Kofstad P. (1966); "High Temperature Oxidation of Metals". John Wiley and Sons, Inc. pp166-179.
 - 69) Kofstad P. (1972); "Non Stoichiometry, Diffusion and Electrical Conductivity in Binary Metal Oxides"; Wiley - Interscience, ISBN 0-471-49776-2, John Wiley and Sons Inc. London.

- 70) Kritsalis P, Coudurier L. and Eustathopoulos N. (1991); "Contribution to the Study of Reactive Wetting in the CuTi / Al₂O₃ System"; Journal of Materials Science, Vol. 26, pp 3400-3408.
- 71) Kubaschewski O. and C. B. Alcock (1983); "Metallurgical Thermochemistry"; 5th Edition, Oxford, New York, Pergamon Press.
- 72) Kubaschewski O. and Hopkins B. E. (1953); "Oxidation of Metals and Alloys"; Butterworths Scientific Publications, 2nd Edition, London.
- 73) Kudo H. and Odawara O. (1989); "Characteristics of Self-Propagating Reaction in TiN Combustion Synthesis"; Journal of Materials Science, Vol. 24, pp 4030-4033.
- 74) Kume M., Tanihata K., Takahashi A. and Miyamoto Y. (1992); "New Nitriding Process Using SHS"; International Journal Self-Propagating High-Temperature Synthesis; Vol. 1, No. 2, pp 265-270.
- 75) LaSalvia J. C. and Meyers M. A. (1992); "Combustion Synthesis in the Ti-C-Ni-Mo System: Part 2. Analysis"; Metallurgical and Materials Transactions A, Vol. 26A, pp 3011-3019.
- 76) LaSalvia J. C., Kim D. K., Lipsett R. A. and Meyers M. A. (1992); "Combustion Synthesis in the Ti-C-Ni-Mo System: Part 1. Micromechanisms"; Metallurgical and Materials Transactions A, Vol. 26A, pp 3001-3009.
- 77) LaSalvia J. C., Meyers M. A. and Kim D. K. (1994); "Combustion Synthesis / Dynamic Densification of TiC - Ni Cermets"; Journal of Materials Synthesis and Processing, Vol. 2, No. 4, pp 255-259.
- 78) Lee J-H., Thadhani N. N. and Grebe H. A. (1996); "Reaction Sintering of Shock Compressed Ti + C Powder Mixtures"; Metallurgical and Materials Transactions A, Vol. 27A, pp 1749-1759.
- 79) Lee M. L., Lee H. L. and Lee H. J. (1995); "Submicron Al₂O₃ / SiC Composite Powder Preparation by SHS Technique"; Journal of Materials Science Letters, Vol. 14, pp 1515-1517.
- 80) Lee W-C. and Chung S-L. (1995); "Ignition Phenomena and Reaction Mechanisms of the Self-propagating High-temperature Synthesis Reaction in the Ti + C System"; Journal of Materials Science, Vol. 30, pp 1487-1494.
- 81) Leung C., Weinert M., Allen P. B. and Wentzcovitch R. M. (1996); "First-Principles Study of Titanium Oxides"; Physical Review B, Vol 54., No. 11, pp 7857-7864.
- 82) Levashov E. A., Filonov M. R. and Borovinskaya I. P. (1995); "Some Properties of Novel Structural Ceramics, Produced by Combustion Synthesis Technology"; Journal of Materials Synthesis and Processing, Vol. 3, No. 2, pp 111-114.
- 83) Li H. P., Bhaduri S. B. and Sekhar J. A. (1992); "Metal-Ceramic Composites Based on the Ti-B-Cu Porosity System"; Metallurgical transactions A, Vol. 23A, pp 251-261.

- 84) Li J. T. and Ge C. C. (1996); "Investigation on the Microstructural Aspects of Si_3N_4 Produced by Self-Propagating High Temperature Synthesis"; *Journal of Materials Science Letters*, Vol. 15, pp 1051-1053.
- 85) Lihrmann J. M., Herve P. and Petitet J. P. (1991); *Processing of Titanium Carbide By Self-Propagating High-Temperature Synthesis (SHS)*; Deutsche Keramische Gesellschaft, Koln, Germany, pp 637-641.
- 86) Lihrmann J. M., Vrel D. and Petitet J. P. (1995); "Self-Propagating High Temperature Synthesis. The Example of Titanium Carbide"; *Sustained High temperature Synthesis – Ann. Chim. Fr*, Vol. 20, pp 111-121.
- 87) Liu Z. and Gao W. (1998a); "A Numerical Model to Predict the Kinetics of Anisothermal Oxidation of Metals"; *High Temperature Materials and Processes*, Vol. 17, No 4, pp 231-236.
- 88) Liu Z. and Gao W. (1998b); "Anisothermal Oxidation of Micro-Crystalline Ni-20Cr-5Al Alloy Coating at 850-1280°C"; *Scripta Materialia*, Vol. 38, No 7, pp 1057-1063.
- 89) Makino A., Araki N. and Kuwabara T. (1994); "Flammability Limits, Dilution Limits and Effect of Particle Size on Burning Velocity in Combustion Synthesis of TiC"; *JSME International Journal, Series B*, Vol. 37, No. 3, pp 576-582.
- 90) Maksimovich G. G., Fedirko V. N. and Lizun A.T. (1986); "The Question of the Mechanism of Titanium Oxidation"; *Soviet Materials Science*, Vol. 22, No 2, pp 190-194.
- 91) Mari D. and Dunand D. C. (1995); "NiTi and NiTi-TiC Composites: Part 1 Transformation and thermal Cycling Behaviour"; *Metallurgical and Materials Transactions A*, Vol. 26 A, pp 2833 - 2847.
- 92) Markworth A.J. (1977); "On the Kinetics of Anisothermal Oxidation"; *Metallurgical Transactions A*, Vol. 8A, December, pp 2014-2015.
- 93) Maupin H. E. and Rawers J. C. (1993); "Metal-Intermetallic Composites Formed by Reaction Sintering Elemental Powders"; *Journal of Materials Science Letters*, Vol. 12, pp 540-541.
- 94) McCauley J.W. (1990); "An Historical and Technical Perspective on SHS"; *Ceramic Engineering Sci. Proc.*; 11[9-10], pp 1137-1181.
- 95) Meier G. H. and Pettit F. S. (1992); "High Temperature Oxidation and Corrosion of Intermetallic Compounds"; *Materials Science and Technology*, Vol. 8, pp 331-338.
- 96) Merzhanov A. G. and Rogachev A. S. (1992); "Structural Macrokinetics of SHS Processes"; *Pure and Applied Chemistry*, Vol. 64, No. 7, pp 941-953.
- 97) Merzhanov A. G., Rogachev A. S., Mukas'yan A. S. and Khusid B. M. (1990); "Macrokinetics of Structural Transformation During the Gasless Combustion of a Titanium and Carbon Powder Mixture"; *Fizika Goreniya I Vzryva*, Vol. 26, No. 1, pp 104-114.
- 98) Merzhanov A.G (1983); *Fizik. Khim. Soverem. Problem.* 7

- 99) Merzhanov A.G., Borovinskaya I.P. and Shkiro V.M. (1995); "Dynamics of Phase Formation During SHS Processes"; *Annals de Chimie – Science des Materials*, Vol 20.
- 100) Mishra S. K., Das S., Goel R. P. and Ramachandrarao P. (1997); "Self-Propagating High Temperature Synthesis (SHS) of Titanium Carbide"; *Journal of Materials Science Letters*, Vol. 16, pp 965-967.
- 101) Misra A. K. (1990); "Identification of Thermodynamically Stable Ceramic Reinforcement Materials for Iron Aluminide Matrices"; *Metallurgical Transactions A*, Vol. 21A, pp 441-446.
- 102) Miyamoto Y. and Ohyanagi M. (1993); "Development of Functionality Ceramic Composites by SHS Routes"; *New Functionality Materials, Vol C – Synthetic Process and Control of Functionality Materials*, pp 145-152.
- 103) Miyamoto Y., Tanihata K., Li Z., Kang Y. S. and Murakawa H. (1995a); "Development of Symmetric Gradient Structures for Hyperfunctional Materials by SHS/HIP Compaction"; *Advances in Science and Technology*, Vol. 10, *Intelligent Materials and Systems*. editor: P.Vincenzini.
- 104) Miyamoto Y., Tanihata K., Li Z., Kang Y. S. and Nishida K. (1995b); "SHS/HIP Compaction of Functionally Gradient Materials"; *Advances in Science and Technology*, Vol. 4, *New Horizons for Materials*. editor: P.Vincenzini.
- 105) Moore J.J. and Feng H.J (1995a); "Combustion Synthesis of Advanced Materials: Part I. Reaction Parameters"; *Progress in Materials Science*, Vol. 39, pp 243-274.
- 106) Moore J.J. and Feng H.J (1995b); "Combustion Synthesis of Advanced Materials: Part II. Classification, Applications and Modelling"; *Progress in Materials Science*, Vol. 39, pp 275-316.
- 107) Mughal M. P. and Plumb O. A. (1993); "Thermal Densification of Metal-Ceramic Composites"; *Scripta Metallurgica et Materialia*, Vol. 29, pp 383-388.
- 108) Munir Z. A. (1992a); "Microstructural and Mechanistic Analyses of SHS Systems"; *The 1992 Powder Metallurgy World Conference*, keynote paper, ref ms\1992.06.
- 109) Munir Z. A. (1992b); "Reaction Synthesis Processes: Mechanism and Characteristics"; *Metallurgical Transactions A*, Vol. 23 A, pp 7-13.
- 110) Munir Z. A. (1996); "The Use of an Electric Field as a Processing Parameter in the Combustion Synthesis of Ceramics and Composites"; *Metallurgical and Materials Transactions*, Vol. 27A, pp 2080-2085.
- 111) Murry J. C. and German R. M. (1992); "Reactive Sintering and Hot Isostatic Compaction of Niobium Aluminide NbAl₃"; *Metallurgical Transactions A*, Vol. 23A, pp 2357-2362.
- 112) Odawara O. (1990); "Combustion and Plasma Synthesis of High Temperature Materials" Editors: Munir Z. A. and Holt J. B., VCH Publishers, New York, 1st Edition.

- 99) Merzhanov A.G., Borovinskaya I.P. and Shkiro V.M. (1995); "Dynamics of Phase Formation During SHS Processes"; *Annals de Chimie – Science des Materials*, Vol 20.
- 100) Mishra S. K., Das S., Goel R. P. and Ramachandrarao P. (1997); "Self-Propagating High Temperature Synthesis (SHS) of Titanium Carbide"; *Journal of Materials Science Letters*, Vol. 16, pp 965-967.
- 101) Misra A. K. (1990); "Identification of Thermodynamically Stable Ceramic Reinforcement Materials for Iron Aluminide Matrices"; *Metallurgical Transactions A*, Vol. 21A, pp 441-446.
- 102) Miyamoto Y. and Ohyanagi M. (1993); "Development of Functionality Ceramic Composites by SHS Routes"; *New Functionality Materials*, Vol C – Synthetic Process and Control of Functionality Materials, pp 145-152.
- 103) Miyamoto Y., Tanihata K., Li Z., Kang Y. S. and Murakawa H. (1995a); "Development of Symmetric Gradient Structures for Hyperfunctional Materials by SHS/HIP Compaction"; *Advances in Science and Technology*, Vol. 10, *Intelligent Materials and Systems*. editor: P.Vincenzini.
- 104) Miyamoto Y., Tanihata K., Li Z., Kang Y. S. and Nishida K. (1995b); *SHS/HIP Compaction of Functionally Gradient Materials*"; *Advances in Science and Technology*, Vol. 4, *New Horizons for Materials*. editor: P.Vincenzini.
- 105) Moore J.J. and Feng H.J (1995a); "Combustion Synthesis of Advanced Materials: Part I. Reaction Parameters"; *Progress in Materials Science*, Vol. 39, pp 243-274.
- 106) Moore J.J. and Feng H.J (1995b); "Combustion Synthesis of Advanced Materials: Part II. Classification, Applications and Modelling"; *Progress in Materials Science*, Vol. 39, pp 275-316.
- 107) Mughal M. P. and Plumb O. A. (1993); "Thermal Densification of Metal-Ceramic Composites"; *Scripta Metallurgica et Materialia*, Vol. 29, pp 383-388.
- 108) Munir Z. A. (1992a); "Microstructural and Mechanistic Analyses of SHS Systems"; *The 1992 Powder Metallurgy World Conference*, keynote paper, ref ms\1992.06.
- 109) Munir Z. A. (1992b); "Reaction Synthesis Processes: Mechanism and Characteristics"; *Metallurgical Transactions A*, Vol. 23 A, pp 7-13.
- 110) Munir Z. A. (1996); "The Use of an Electric Field as a Processing Parameter in the Combustion Synthesis of Ceramics and Composites"; *Metallurgical and Materials Transactions*, Vol. 27A, pp 2080-2085.
- 111) Murry J. C. and German R. M. (1992); "Reactive Sintering and Hot Isostatic Compaction of Niobium Aluminide NbAl₃"; *Metallurgical Transactions A*, Vol. 23A, pp 2357-2362.
- 112) Odawara O. (1990); "Combustion and Plasma Synthesis of High Temperature Materials" Editors: Munir Z. A. and Holt J. B., VCH Publishers, New York, 1st Edition.

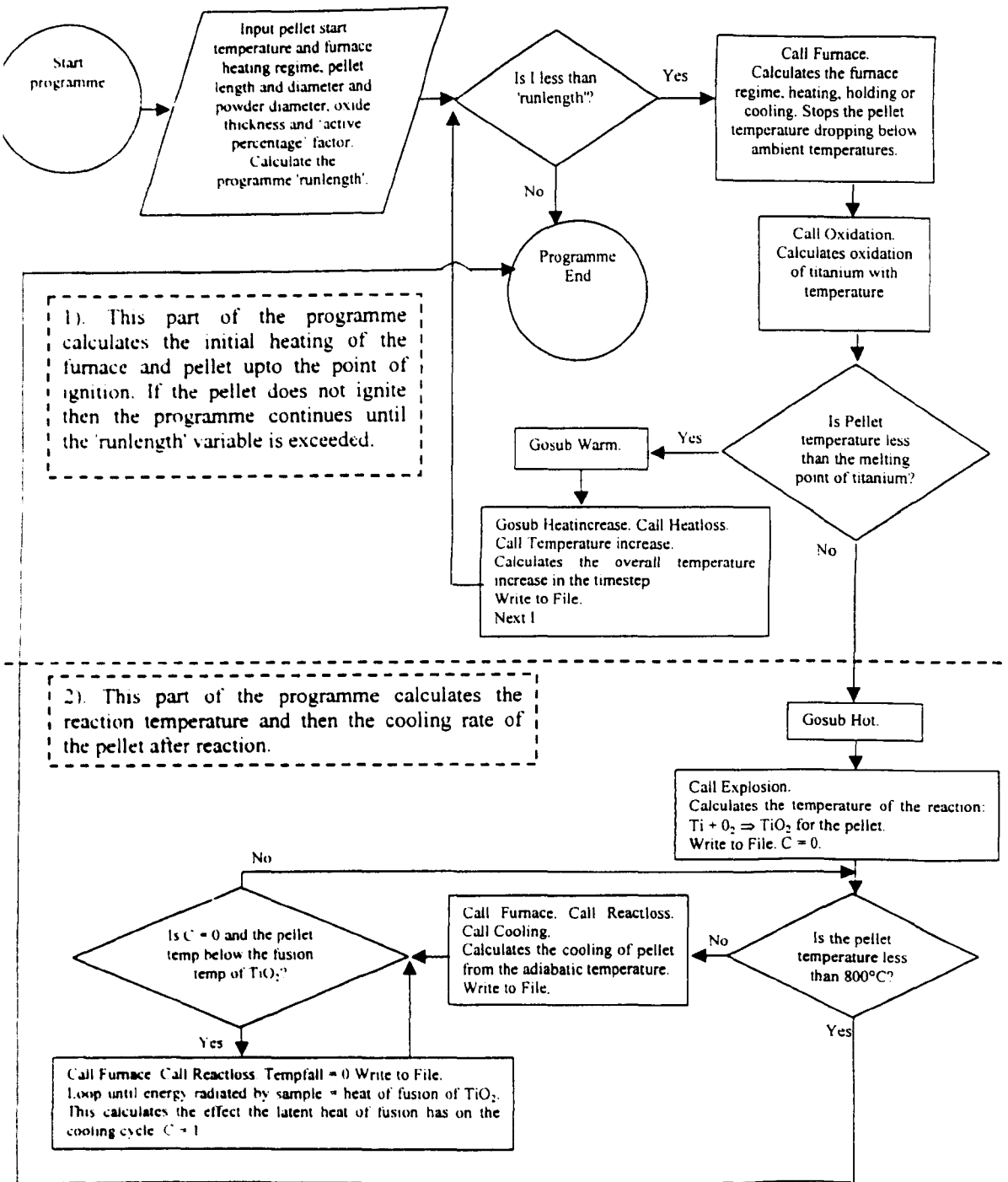
- 113) Okamoto H (1996); "Fe-Ti (Iron -Titanium)"; Journal of Phase Equilibria, Supplemental Literature Review: Section III, Vol. 17, No. 4, pp 369.
- 114) Olevsky F., Mogilevsky P., Gutmanas E. Y. and Gotman I. (1996); "Synthesis of In Situ TiB₂ / TiN Ceramic Matrix Composites from Dense BN-Ti and Bn-Ti-Ni Powder Blends"; Metallurgical and Materials Transactions A, Vol. 26A, pp 2071-2079.
- 115) Poyurovskaya I.E. and Ryabchuk L.I (1988); "Ignition of Titanium by the Radiation in Air Flow"; 7th All-Union Conference on the Interaction of Optical Radiation with Matter. March 1988, Leningrad, USSR. Vol 37, No. 3, pp 104-109.
- 116) Pribytkov G. A., Semonova A. A. and Itin V. I. (1983); "Combustion Synthesis of Intermetallides of the Iron-Titanium System"; Fizika Goreniya i Vzryva, Vol. 20, No. 5, pp 21-23.
- 117) Ranganath S. and Subrahmanyam J. (1995); "On the *In Situ* Formation of TiC and Ti₂C Reinforcements in Combustion Assisted Synthesis of Titanium Matrix Composites"; Metallurgical and Materials Transactions A, Vol. 27A, pp 237-240.
- 118) Rickerby D. S. (1982); "Lattice Parameters of Iron-Titanium Solid Solutions"; Metal Science, Vol. 16, pp 495-496.
- 119) Rode H. and Hlavcek V. (1994); "An Experimental Study of Titanium Powder Reactivity in Gaseous Environments. Part 1: Oxidation"; Combustion Science and Technology, Vol. 99, 1-3, pp 143-160.
- 120) Royal T. E., Namjoshi S. and Thadhani N. N. (1996); "Mechanistic Processes Influencing Shock Chemistry in Powder Mixtures of the Ti-Si, Ti-Al and Ti-B Systems"; Metallurgical and Materials Transactions A, Vol. 27A, pp 1761-1771.
- 121) Saidi A (1995); "Characterisation of Combustion Synthesis of Titanium Carbide Metal Matrix Composites" Post Doctorate Thesis, Department of Materials Engineering and Materials Design, Nottingham University, Nottingham, England.
- 122) Saidi A., Chrysanthou A., Wood J.V. and Kellie J.L.F. (1994); "Characteristics of the Combustion Synthesis of TiC and Fe-TiC Composites"; Journal of Material Science, Vol. 29, pp 4993-4998.
- 123) Shimada S and Kozeki M. (1992); "Oxidation of TiC at Low Temperatures"; Journal of Materials Science, Vol. 27, pp 1869-1875.
- 124) Shingu P. H., Ishihara K.N., Ghonome F., Hayakawa T., Abe M. and Taguchi K. (1990); "Solid State Synthesis of TiAl by Use of Pseudo HIP"; Proceedings of the First US-Japanese Workshop on Combustion Synthesis, January 11-12, 1990. pp 65-71.
- 125) Shon I. J. and Munir Z. A. (1995); "Synthesis of MoSi_{2-x}Nb and MoSi_{2-y}ZrO₂ Composites by Field Activated Combustion Method"; Materials Science and Engineering, A202, pp 256-261.

- 126) Shteinberg A. S. and Knyazik V. A. (1992); "Macrokinetics of High-Temperature Heterogenous Reactions: SHS Aspects"; Pure and Applied Chemistry, Vol. 64, No. 7, pp 965-976.
- 127) Shteinberg A. S., Shcherbakov V. A. and Ponomarev M. A. (1995); "Effect of Impurity Degassing on Solid Flame Structure: Critical Characteristics of Solid Flame Propagation"; Journal of Materials Synthesis and Processing, Vol. 3, No. 2, pp 83-91.
- 128) Singh M. (1996); "Thermodynamic Analysis for the Combustion Synthesis of SiC-B₄C Composites"; Scripta Materialia, Vol. 6, pp 923-927.
- 129) Sirca S., Gabel H., Stoltzfus J. and Benz F. (1991); "The Analysis of Metals Combustion Using a Real-Time Gravimetric Technique"; ASTM Special Technique Publication 'Flammability and Sensitivity of Materials' ; 1111, pp 313-325.
- 130) Skolianos S., Kattamis T. Z., Chen M. and Chambers B. V. (1994); "Cast Microstructure and Tribological Properties of Particulate TiC-Reinforced Ni-Base or Stainless Steel Matrix Composites"; Materials Science and Engineering, A183, pp 195-204.
- 131) Song T. H., Lee H. L., Pai C. H. and Mitsushashi T. (1995); "thermal Conductivity of Fe-Si Alloys Prepared by the SHS Process"; Journal of Materials Science Letters, Vol. 14, pp 1715-1717.
- 132) Sousa C. and Illas F. (1994); "Ionic-Covalent Transition in Titanium Oxides"; Physical Review B, Vol. 50, No. 19, pp13974-13980.
- 133) Stolin A. M., Stelmakh L. S., Zhilyaeva N. N. and Khusid B. M. (1995); "The Phenomenological Theory of High Temperature Deformation of Self-Propagating High-Temperature Synthesis (SHS) Products"; Journal of Materials Synthesis and Processing, Vol. 3, No. 1, pp 19-23.
- 134) Strangle G. C. and Miyamoto Y. (1995); "FGM Fabrication by Combustion Synthesis"; MRS Bulletin, January, pp 52-53.
- 135) Subrahmanyam J. and Mohan Rao R. (1994); "Combustion Synthesis of MoSi₂-WSi₂ Alloys"; Materials Science and Engineering, A138, pp 205-210.
- 136) Subrahmanyam J. and Vijayakumar M. (1992); "Review: Self-propagating high-temperature synthesis"; Journal of Materials Science, Vol. 27, pp 6249-6273.
- 137) Tanihata K., Miyamoto Y., Masushita K-I., Ma X., Kawasaki A. Watanabe R. and Hirano K. (1993); "Fabrication of Cr₃C₂ / Ni Functionally Gradient Materials by Gas-Pressure Combustion Sintering"; Ceramic Transactions, Vol. 34, pp 361-368.
- 138) Tavgen V.V., Shinkareva E.V., Karpinchik E.V. and Zonov Y.G. (1992); "Oxidation of Titanium with Heating in an Air Atmosphere"; Soviet Powder Metallurgy and Metal Ceramics, Vol. 31, No. 3, pp193-196.
- 139) Terry B. S. and Chinyamakobvu O. S. (1992a); "Dispersion and Reaction of TiC in Liquid Iron Alloys"; Materials Science and Technology, May, Vol. 8, pp 399-405.

- 140) Terry B. S. and Chinyamakobvu O. S. (1992*b*); "Assesment of Reactions Occuring During the Solid State Processing of Iron-Based Titanium Diboride Composites"; *Journal of Materials Science*, Vol. 27, pp 5661 –5665.
- 141) Tomoshige R. and Matsushita T. (1996); "Production of Titanium – Aluminium – Carbon Ternary Composites with Dispersed Fine TiC Particles by Combustion Synthesis and Their Microstructure Observations"; *Journal of the Ceramic Society of Japan*, Vol. 104, No. 2, pp 94-100.
- 142) Unnam J., Shenoy R.N. and Clark R.K. (1986); " Oxidation of Commercial Purity Titanium"; *Oxidation of Metals*, Vol. 26, 3-4, pp 231-252.
- 143) Ustundag E., Subramanian R., Vaia R., Dieckmann R and Sass S. L. (1993); "In Situ Formation of Metal-Ceramic Microstructures, Including Metal-Ceramic Composites, Using Reduction Reactions"; *Acta Metall. Mater.*, Vol. 41, No. 7, pp 2153 - 2161.
- 144) Venkatachari K. R., Huang D., Ostrander S. P. and Schulze W. A. (1995); " A Combustion Synthesis Process for Synthesising Nanocrystalline Zirconia Powders"; *Journal of Materials Research*, Vol 10, No. 3, pp 748-755.
- 145) Viljoen H. J. and Puszynski J. A. (1994); "Analysis of Propagation Charateristics During Nonadaibatic Condensed Phase Combustion"; *Journal of Materials Synthesis and Processing*, Vol. 2, No. 4, pp 247-253.
- 146) Vol'pe B. M. and Evstigneev V. V. (1993); "Features of Self-Propagating High_temperature Synthesis in Titanium Based System"; *Fizika Goreniya I Vzryva*, Vol. 29, No. 4, pp 37-42.
- 147) Vol'pe B. M., Garkol' D. A., Evstigneev V. V., Milyukova I. V. and Saigutin G. V. (1995); "Investigation of Reaction in an Ni-Al-Cr SHS System Based on High-Temperature Brightness Pyrometry"; *Combustion , Explosion and Shock Waves*, Vol. 31, No. 5, pp 550-554.
- 148) Vrel D., Lihrmann J. M. and Tobaly P. (1994); "Contribution of Solid-State Diffusion to the Formation of Titanium Carbide by Combustion Synthesis"; *Journal of Materials Synthesis and Processing*, Vol. 2, No. 3.
- 149) Vukhvid V. I. (1992); "Modifications of SHS Processes"; *Pure and Applied Chemistry*, Vol. 64, No. 7, pp 977-988.
- 150) Vukhvid V. I., Maklakov S. A., Zhirkov P. V., Gorshkov V. A., Timokhin N. I. and Dovzhenko A. Y. (1997); "Combustion Synthesis and Structure Formation in a Model Cr-CrO₃ Self –Propagating High-Temperature Synthesis System"; *Journal of Materials Science*, Vol. 32, pp 1915-1924.
- 151) Wang H. H., Luck R. and Predel B. (1993); "Heat Capacities of Intermetallic Compounds in the Iron – Titanium System"; *Z. Metallkd.*, Vol. 84, No.4, pp 230-236.

- 165) Yuranov I. A., Fomin A. A. Shiryaev A. A. and Kashireninov O. E. (1994); "A Chemical Model for Solid-Phase Gasless Combustion of the Self-Propagating High-Temperature Synthesis (SHS) System Mo + B"; *Journal of Materials Synthesis and Processing*, Vol. 2, No. 4, pp 239-246.
- 166) Zemansky M. W. and Dittman R. H. (1997); "Heat and Thermodynamics"; 7th Edition, The McGraw-Hill Companies, Inc., ISBN 0-07-017059-2, pp 94-100.
- 167) Zenin A. A., Merzhanov A. G. and Nersisyan G. A. (1981); "Thermal Wave Structure in SHS Processes (By the Example of Boride Synthesis)"; *Fizika Goreniya I Vzryva*, Vol. 17, No. 1, pp 79-90.
- 168) Zhirkov P. V., Maklakov S. V., Dovzhenko A. Yu., Yuhvid V. I. And Gorshkov V. A. (1995); "Microstructure Formation During Nonstationary Self-Propagating High-Temperature Synthesis (SHS) with Melting Products"; *Journal of Materials Synthesis and Processing*; Vol. 3, No. 3, pp 181-191.
- 169) Zhou Z. and Stangle G.C. (1995); "Kinetics of a Non-Catalytic Gas-Solid Chemical Reaction Under SHS like Conditions"; *Journal of Materials Science*; Vol. 30, pp 3256-3264.
- 170) Zhuravlev V.S. and Turchanin M.A. (1997); "Reasons for the Formation of Various Titanium Oxide Phases upon Wetting Aluminium Oxide with Titanium-Containing Metallic Solutions"; *Powder Met. And Metal Ceramics*; Vol. 34, No. 3-4, pp141-146.

Appendix A: Figure 7.2 Flowchart for the Titanium Oxidation Computer Programme.



Appendix B: Walk Through of the Computer Model - Ti_Burn.bas

1.1 Introduction

The computer programme has been designed to model the oxidation behaviour of a pellet made up of particles of spherical titanium, heated via a furnace in air. The model takes into account the exothermic nature of titanium oxidation in determining the pellet temperature and can predict whether the oxidation reaction becomes self propagating and if so, the adiabatic temperature of the reaction. The temperature profile during cooling is also modelled. In addition to this, the model allows the user to define most of the parameters that are involved in the experimental system.

To aid the user of the model the following commentary outlines the individual sections of the programme, relating the equations used, to one another. It is written to aid the user in understanding the written programme, not the numerical model behind the programme. All figures are in S.I. units. Inputs are converted into Metres, Joules and Kg.

1.2 Programme Breakdown

The breakdown will follow the order in which the programme runs.

1.2.1 Opening Statements

- **Programme information**
 1. **DECLARE SUB:** declares the sub programmes and the input and outputs required by and returned by the sub programmes.
- **SUB TEMPERATUREINCREASE:** determines the temperature change in K, in the pellet, due to the energy gained from oxidation and furnace heating / cooling.
 - **SUB HEATLOSS:** determines the energy lost or gained by the pellet via radiative and conductive means. If the pellet is cooler than the furnace, heat will be gained from the furnace by radiative and conductive means. If the pellet is hotter than the furnace it will lose heat in a like manner.
- **SUB OXIDATION:** determines the amount of oxide formed in 1 programme cycle.

- **SUB EXPLOSION:** determines the adiabatic temperature of the reaction. It assumes that the reaction is instantaneous, the whole of the pellet reacting at once.
 - **SUB REACTLOSS:** determines the heat energy lost or gained by the pellet after the exothermic reaction in SUB EXPLOSION. It is the same equation as SUB HEATLOSS with some different values.
 - **SUB COOLING:** determines the heat lost in K from the pellet after the exothermic reaction in SUB EXPLOSION.
 - **SUB FURNACE:** controls the furnace temperature during the programme run.
2. Printed introduction to the programme.
 3. **INPUT FILENAMESS;** Opens up a file for storage of the produced data, this can be user defined. The file is an ASCII text file.

1.2.2 GOSUB METALDATA

This sub routine holds the data for the metals and oxides used in the programme. It is used to load the data into memory prior to running the programme.

- **TIDENS:** titanium density.
- **OXDENS:** titanium oxide, TiO_2 , density.
- **TIMOLMAS:** titanium molar mass.
- **OXMOLMAS:** titanium oxide, TiO_2 , molar mass.
- **TIMELT:** melting temperature of titanium.
- **TIVAP:** vaporisation temperature of titanium.
- **TIO2MELT:** melting temperature of TiO_2 .
- **TIHEAT:** latent heat of fusion for titanium
- **TIVAPHEAT:** latent heat of titanium vaporisation.
- **TIO2HEAT:** latent heat of melting for TiO_2 .

1.2.3 GOSUB COMPACTDATA

This sub routine sets variables attributed to the size of pellet and the powder constants. It loads them into the memory prior to the programme execution. The programme is designed to model the temperature of an cylindrical pellet formed from spherical titanium powders at their

maximum packing density of 74%. The user defines the length and diameter of the pellet and the titanium powder diameter, pre-existing oxide thickness on the titanium powder and the percentage of titanium powder surface area that oxidises.

1.2.3.1 User Defined Parameters

1. **PELDIAM:** Pellet diameter, in mm.
2. **LENGTH:** Pellet length, in mm.
3. **PARTDIAM:** Titanium powder diameter, in microns.
4. **THICKNESS:** The thickness of oxide originally on the titanium powder.
5. **ACTIVEPERCENTAGE:** As the pellet heats during the reaction the outside surface can easily oxidise due to an abundance of oxygen, the centre is however starved of oxygen and cannot contribute to the exothermic heat increase of the pellet. This factor, which has to be derived from experiments, determines what percentage of the pellet will actually contribute to the exothermic heat increase. It does this by altering the percentage of surface area of titanium powder which is said to be active.

1.2.3.2 Constants

1. **PACKDENS:** The packing density of the titanium spheres, is set to 74%, the maximum packing density for spheres.

1.2.3.3 Calculations

Standard geometrical calculations are used to determine these parameters.

1. **PELDIAM:** Converted into PELRAD, the radius of the pellet.
2. **PELSURF:** The pellet surface area is calculated.
3. **PELVOL:** The pellet volume is calculated.
4. **PARTDIAM:** Converted into PARTRAD, the radius of a titanium powder.
5. **TIRAD:** The actual radius of titanium in the powder is calculated by taking away the oxide thickness from the titanium powder radius. This leaves the radius of just the titanium metal in the powder.

6. **TIVOL**: The actual volume of titanium in one powder particle.
7. **PARTVOL**: The volume of the powder particle.
8. **PARTNUM**: Calculates the number of particles in the pellet.
9. **PARTSURF**: The total surface area of the powder in the pellet is calculated. The value is linked to the radius of the actual powder, not the radius of the titanium, which is slightly less than that of the powder due to oxide. This value does not decrease with time, and is set as a constant. The model does not take into account the fact that the active surface, i.e. the surface area at which there is titanium / oxygen contact is less than the powder diameter or that it will decrease as the oxide thickness builds up. This has not been addressed as the model shows that ignition of titanium occurs at oxide thickness' below 5µm. As the powder size is in reality greater than 50µm the decreased surface area has a negligible effect on the result.
10. **PELMOLTI**: The actual mols of titanium in the pellet. This is related to the TIVOL.
11. **OXMAS**: The mass of TiO₂ formed. Here it is calculated from the initial thickness of oxide on the powder, and described the initial mass of oxide on the powder.
12. **MOLTIO2**: The mols of TiO₂ in the pellet. It is calculated from the OXMAS and PARTSURF. It is related here to the original thickness of oxide on the powder.

1.2.4 SETTING THE FURNACE PARAMETERS

The furnace modelling programme contains a start temperature, a ramp to a holding temperature, a hold time at the holding temperature and a cooling rate from the holding temperature to room temperature (20°C). These parameters are user designated. The furnace model is an ideal model and takes no account for actual furnace temperature lags. Inputted data is used directly to define the furnace temperature profile. The minimum holding time is 1 timestep.

1.2.4.1 *User Initialised or Defined Parameters*

1. **SURTEMP**: The furnace temperature. The input is the furnace starting temperature.
2. **PELTEMP**: The pellet temperature. The input is the pellet starting temperature.

3. **HEATRATE**: The heating rate of the furnace.
4. **HOLDTEMP**: The temperature at which the furnace can be set to hold at. The parameter has to be entered whether there is a heating rate or not. It tells the programme how hot the furnace has to get before the **HOLDTIME** parameter starts to work.
5. **HOLDTIME**: The length of time the furnace holds at the **HOLDTEMP**.
6. **COOLRATE**: The cooling rate of the furnace. This parameter is initiated when the **HOLDTIME** parameter has been exceeded in the furnace timer sub programme.
7. **TIMESTEP**: This determines the time interval at which the programme loops. Each time the programme loops it carries out a series of calculations; the main equations determine the oxide growth, cooling rate, heating rate and temperature increase. For accuracy it is therefore prudent to use as small a **TIMESTEP** as possible. This is governed by the hardware in use, time available and the graphical package that will be used to plot the outputted data. In the case of Origin, it can only store a maximum of 30,000 rows of data. A small timestep and long runlength may well exceed this and require a longer timestep to complete the model run. Tests have shown that a 1 second timestep is a good compromise between accuracy and runlength.

1.2.4.2 *Parameters Initialised to 0*

To aid the user in the understanding of the programme, parameters that are assigned a value later on in the programme are initially set to 0. This happens automatically in QBasic, however it is easier to visualise and track changes if these parameters are set to zero at the beginning of the programme. Parameters initialised are:

- **HTIMER**
- **HEATINCJ**
- **REACTLOSJ**
- **MOLTIO2**
- **TOTLOS**
- **TOTLOSTI**
- **TICHANGE**

- TIGAIN
- TILOSS

1.2.4.3 *Conditional Statement*

IF SURTEMP > HOLDTEMP...; this statement compares the initial furnace temperature to the holding temperature. If the initial temperature is higher than the holding temperature an error is produced at the computation of NO1, occurring later on in this section. To prevent this the programme exits.

1.2.4.4 *Calculations*

1. TEMPSTEP: The temperature rise of the furnace every time step.
2. RUNLENGTH: This parameter defines the number of cycles that the programme will have to go through to complete the heating, holding and cooling of the furnace. It is only accurate if the pellet does not ignite. Once the pellet has ignited the length the programme continues to run is controlled by the pellet temperature. The parameters NO1, NO2 and NO3 calculate the time, in seconds, it takes to complete the heating, holding and cooling steps of the furnace. The set minimum and maximum values for RUNLENGTH are there to aid the user of the system. Most RUNLENGTHs are below 1200 seconds, however, as the programme will exit when the furnace temperature reaches room temperature additional seconds may well be required to model the cooling of the pellet to room temperature. The maximum is set to 30000 as this is the largest number of rows (cycles) of data that the graphical plotting package 'ORIGIN' can import.

1.2.5 THE PROGRAMME CYCLER

1.2.5.1 *The Programme Cyler*

FOR I = 1...; ⇒ NEXT I; runs the programme written within its boundaries. The number of cycles is determined by the RUNLENGTH and TIMESTEP. All values and variables within

the programme cycles are recalculated each cycle of the programme. In this way values are dynamic and change according to these components.

1.2.5.2 *Calculated Values*

1. **MOLTIO2:** Recalculated each cycle by adding MOLTIO2INC, the amount of TiO₂ formed in a timestep, to the previous value.
2. **PELMOLTI:** Recalculated by negating MOLTIO2INC from the previous value.
3. **MAXENERGY:** The amount of energy available if the titanium oxidises to TiO₂. Determined by the available titanium, PELMOLTI, and the enthalpy of formation of TiO₂, OXENTH.

1.2.5.3 *GOSUB OXENTH CALC*

This sub programme calculates the enthalpy of formation of TiO₂, OXENTH, at the pellet temperature, PELTEMP. Kirchoff's Law is used to calculate this. There is roughly a 1.8% rise in the OXENTH from 298K to the melting point of titanium.

1.2.5.4 *CALL FURNACE*

Determines the heating schedule of the furnace. Returns the correct SURTEMP for the time period. Keeps a track on the hold time. There is also a parameter to stop the furnace cooling below room temperature.

1.2.5.5 *CALL OXIDATION*

Determines the mass of oxide formed in a time step. The programme uses the theory of a 'dummy time' to calculate the amount of oxide formed. The anisothermal oxidation is said to be made up of small steps of isothermal oxidation, of time period, TIMESTEP. This sub programme returns the total mass of oxide, OXMAS and the mass of oxide formed in the timestep, OXMASINC. The constants used in the oxidation rate equation are only accurate from 450 - 850°C.

1.2.5.6 *Conditional Statement*

IF PELTEMP < TIMELT...; this statement is the condition that determines when the pellet will ignite. It is said that this will happen at the melting point of titanium. If this occurs then the programme skips out of the loop and starts to run HOT, if PELTEMP is less than TIMELT the programme continues in the loop, running WARM.

1.2.6 GOSUB WARM

This sub routine contains the equations that govern the model up to the ignition point. After it has finished the programme returns to the programme cyler.

1.2.6.1 *GOSUB HEATINCREASE*

Sub programme to calculate the amount of heat energy formed in a time step.

1. OXIDEMAS: The mass in kg of oxide formed in a timestep is calculated, this is used to calculate MOLTIO2, the mols of TiO₂ formed in a timestep.
2. HEATINCJ: The energy liberated by the formation of MOLTIO2 mols of TiO₂.

1.2.6.2 *CALL HEATLOSS*

Sub programme to calculate the heat lost by radiative or conductive means.

1. HEATLOSJ: Heat lost from the surface of the pellet by radiative and conductive means.
H, the heat transfer coefficient and the emissivity are set to 10 and 0.5 respectively.

1.2.6.3 *Calculations*

1. TOTALHEATJ: The total amount of heat energy available after cooling of the sample
2. PELTEMP: The actual pellet temperature, calculated by adding on the TEMPRISE
3. TIMEREAL: The actual time, incremented by TIMESTEP.
4. OXOUT: The oxide thickness on the powder, in microns.

1.2.6.4 CALL TEMPERATUREINCREASE

A sub programme to change the energy gained or lost in the timestep into a temperature change.

1. TEMPRISE: The temperature change of the pellet in K. Changes in phase are taken into account.

1.2.6.5 Conditional Statement

IF PELTEMP >= 1155...; takes the latent heat of the $\alpha \Rightarrow \beta$ titanium transformation into account during the heating or cooling cycle. If the energy available for absorption by the transformation is less than the total amount required to transform the titanium then when the pellet cools below the transformation temperature only the energy that had been absorbed will be released exothermically.

1.2.7 GOSUB HOT

Once the programme has entered HOT it stays within it. HOT calculates the adiabatic temperature of the reaction and then models the cooling of the pellet. Once the pellet is below a threshold temperature the programme is exited.

1.2.7.1 GOSUB EXPLOSION

Calculates the adiabatic temperature of the reaction. Returns the adiabatic temperature in the term PELTEMP.

1. CONFAC: A percentage which describes the amount of titanium that will oxidise to form TiO_2 . This is included as experiments have shown that the outside surface reacts first, forming a solid layer and sealing the inner metal from the atmosphere. This has consequences for the total energy liberated, the adiabatic temperature and the cooling cycle of the pellet.
2. MOL: the total amount of Ti in the pellet.

3. MOLSOFOXIDE and MOLSOFMETAL: Using the CONFAC percentage the amounts of oxide and metal, respectively, can be determined.
4. FUSIONTiO2, FUSIONTi and VAPI: The latent heats of fusion or vaporisation of TiO₂ or Ti.
5. DH: The amount of exothermic energy available to raise the temperature of the pellet

1.2.7.1.1 The Adiabatic Temperature Cycler

This loop programme adds up the energy absorbed by the pellet materials as they heat up. Phase changes and fusion and vaporisation energies are included. When the energy absorbed is equal to or greater than the available energy the loop finishes. The PELTEMP is then returned.

1.2.7.2 Looping Cycle

The rest of SUB EXPLOSION is contained within a loop which cycles until the pellet temperature, PELTEMP, is less than 800°K.

1.2.7.3 Sub Programmes

1. CALL FURNACE: Returns the correct SURTEMP.
2. CALL REACTLOSS: Returns the amount of energy lost or gained in the timestep. Returns REACTLOSJ
3. SUB COOLING: Calculates the heat capacities of the materials in the pellet.

1.2.7.4 Calculations

1. TEMPFALL: The °K temperature change of the pellet.

1.2.7.5 Conditional Statements

1. IF PELTEMP < ...; statements which add on the latent heat of transformation or fusion of the pellet constituents to the cooling model.

Programme Ends

Appendix C: Computer Programme - Ti_Burn

```
REM ** Filename: Ti_Burn.BAS
REM ** This programme was written by Robert A Brown, Ph.D. student at the
REM ** Department of Materials Engineering, Nottingham University, 1998/9.

REM ** The programme models the reaction between pure titanium powder and
REM ** oxygen as the pellet is heated in a furnace. The oxygen supply is
REM ** said to be unlimited. The titanium is said to be spherical and packed
REM ** at a constant density of 74%, the maximum packing density for spheres.
REM ** The point of ignition is said to be the melting temperature of
REM ** titanium, the oxide formed in all cases is TiO2 (rutile).

REM: References:
REM 1: Thermodynamics of Materials, Kubachewski, 5th Edition 1986
REM 2: CRC Handbook of Chemistry and Physics, 54th Edition. 1973-74
REM ** All Heat Capacity Data is from Ref: 1 **

DECLARE SUB TEMPERATUREINCREASE (TOTHEATJ!, PELMOLTI!, TEMPRISE!, PELTEMP!,
MULTIO2!, CPTI!, CPTIO2!)
DECLARE SUB HEATLOSS (HEATLOSJ!, PELSURF!, PELTEMP!, SURTEMP!, TIMESTEP!)
DECLARE SUB OXIDATION (PELTEMP!, OXMAS!, TIMESTEP!, OXMASINC!, TIMEDUM!)
DECLARE SUB EXPLOSION (FUSIONTI!, TIVAP!, TIVAPHEAT!, TIHEAT!, FUSIONTIO2!,
TIMELT!, TIO2MELT!, MOL!, HEAT!, PELMOLTI!, MULTIO2!, PELTEMP!, MAXENERGY!,
OXMAS!)
DECLARE SUB REACTLOSS (REACTLOSJ!, PELSURF!, PELTEMP!, SURTEMP!, TIMESTEP!)
DECLARE SUB COOLING (PELTEMP!, MULTIO2!, CPTIO2!, CPTI!)
DECLARE SUB FURNACE (HTIMER!, HOLDTIME!, SURTEMP!, TIMESTEP!, TEMPSTEP!,
COOLRATE!, HOLDTEMP!)

REM **Printed introduction**
CLS
PRINT "          WELCOME TO THE 'TITANIUM - AIR' SHS MODELING PROGRAMME."
PRINT ""
PRINT "          Nottingham University, 1999"
PRINT ""
PRINT ""
PRINT "Please follow the instructions:"
PRINT ""

REM **Opens up the file for data storage**
PRINT "Input a filename for data output."
INPUT FILENAME$
PRINT ""
OPEN "C:\WINDOWS\ORIGIN\QB_DATA\TI_BURN\" + FILENAME$ + ".DAT" FOR OUTPUT AS #1

REM ** Loads Metal and Compact data**
GOSUB METALDATA
GOSUB COMPACTDATA

REM ***** FURNACE PARAMETERS ***** FURNACE PARAMETERS *****

REM **Sets the furnace starting temperature and converts it to K**
PRINT "Input the FURNACE STARTING TEMPERATURE in CELCIUS."
INPUT SURTEMP
PRINT ""
SURTEMP = SURTEMP + 273

REM **Sets the pellet starting temperature and converts it to K**
PRINT "Input the PELLET STARTING TEMPERATURE in CELCIUS."
INPUT PELTEMP
PRINT ""
PELTEMP = PELTEMP + 273

REM ** Sets the heating rate of the furnace up to the holding temperature**
PRINT "Input the desired HEATING RATE to the holding temperature in K/min."
INPUT HEATRATE
PRINT ""
HEATRATE = HEATRATE / 60

REM **Sets the furnace holding temperature**
PRINT "Input the desired HOLDING TEMPERATURE in CELCIUS."
INPUT HOLDTEMP
PRINT ""
HOLDTEMP = HOLDTEMP + 273
```

```

REM ** Conditional Statement for the furnace**
IF SURTEMP > HOLDTEMP THEN
PRINT "Your FURNACE TEMPERATURE is more than your HOLDING TEMPERATURE."
PRINT "This condition will create an error in the programme."
PRINT "Please start again."
GOTO 10
END IF

REM **Sets the holding time of the furnace at the holding temperature**
PRINT "Input, in MINUTES, the required HOLDING TIME"
PRINT "for the furnace at the holding temperature."
INPUT HOLDTIME
PRINT ""
HOLDTIME = HOLDTIME * 60

REM **Sets the cooling time of the furnace from the holding temperature**
PRINT "Input the COOLING RATE in R/min."
INPUT COOLRATE
PRINT ""
COOLRATE = COOLRATE / 60

PRINT "Input the required TIMESTEP in seconds."
PRINT "1 second give acceptable accuracy."
INPUT TIMESTEP
PRINT ""

REM ** The TEMPSTEP is the amount of temp rise per timestep**
TEMPSTEP = HEATRATE * TIMESTEP

REM **These set the variables to 0**
HTIMER = 0
HEATINCJ = 0
REACTLOSJ = 0
MOLTIO2INC = 0
TOTLOS = 0
TOTLOSTI = 0
TICHANGE = 0
TIGAIN = 0
TILOSS = 0

REM **Sets the number of cycles the programme has to run**
REM **to complete the heating cycle**
IF TEMPSTEP = 0 THEN
NO1 = 0
ELSE
NO1 = CINT((HOLDTEMP - SURTEMP) / TEMPSTEP)
END IF

NO2 = CINT(HOLDTIME)
NO3 = CINT(HOLDTEMP / COOLRATE)
RUNLENGTH = NO1 + NO2 + NO3
IF RUNLENGTH < 1200 THEN RUNLENGTH = 1200
IF RUNLENGTH > 30000 THEN RUNLENGTH = 30000
PRINT "Approximate programme RUNLENGTH = "; RUNLENGTH / TIMESTEP; "cycles"

REM*****

REM ** The programme cyler**
FOR I = 1 TO RUNLENGTH STEP TIMESTEP

REM **Total Mols of TiO2 in system**
MOLTIO2 = MOLTIO2 + MOLTIO2INC

REM ** Reduction in mols of Ti available due to oxidation of Ti**
PELMOLTI = PELMOLTI - MOLTIO2INC

REM**Calculates OXENTH at this PELTEMP
GOSUB OXENTHCALC

REM ** Calculation for MAXENERGY of system in J**
REM ** related to PELMOLTI, which decreases with oxidation**
REM ** and OXENTH which changes with PELTEMP
MAXENERGY = PELMOLTI * OXENTH

CALL FURNACE(HTIMER, HOLDTIME, SURTEMP, TIMESTEP, TEMPSTEP, COOLRATE, HOLDTEMP)
CALL OXIDATION(PELTEMP, OXMAS, TIMESTEP, OXMASINC, TIMEDUM)

```

```

IF PELTEMP < TIMELT THEN
  REM **TIMELT defines the point where the**
  REM ** combustion reaction starts**
  GOSUB WARM
ELSE
  GOSUB HOT
  END IF

NEXT I
10 PRINT ""
PRINT "The programme has finished."
PRINT "Data stored in file: "; FILENAME$
PRINT "Timestep = "; TIMESTEP; "seconds."
PRINT "Pellet Length "; LENGTH * 1000; "mm. Pellet Diameter "; PELDIAM;
"mm."
PRINT "Titanium Powder Diameter "; PARTDIAM; "microns."

CLOSE #1
END

REM*****

REM ** This calculates the heating and cooling of the**
REM ** pellet if there is no combustion**
WARM:

GOSUB HEATINCREASE
CALL HEATLOSS(HEATLOSJ, PELSURF, PELTEMP, SURTEMP, TIMESTEP)

TOTHEATJ = HEATINGCJ - HEATLOSJ

CALL TEMPERATUREINCREASE(TOTHEATJ, PELMOLTI, TEMPRISE, PELTEMP, MOLTIO2, CPTI,
CPTIO2)

REM** This statement applies the alpha to beta transition energy to the system
REM**3920 is the energy of transition in J/mol from alpha to beta in Ti.
REM** It is only accurate when PELTEMP is below SURTEMP
REM ** If PELTEMP is above SURTEMP the heat of fusion is likely to be
REM ** numerous times.
LATI = 3920 * PELMOLTI

IF PELTEMP > 1155 AND TOTHEATJ > 0 THEN
  TIGAIN = TIGAIN + TOTHEATJ
  IF TIGAIN > LATI THEN TIGAIN = LATI
  IF TIGAIN < LATI THEN TEMPRISE = 0
  TIMARK = 1
ELSEIF TIMARK = 1 AND PELTEMP < 1155 AND TOTHEATJ < 0 THEN
  TILOSS = TILOSS - TOTHEATJ
  IF TILOSS > LATI THEN TILOSS = TIGAIN
  IF TILOSS < TIGAIN THEN TEMPRISE = 0
END IF

PELTEMP = PELTEMP + TEMPRISE

TIMEREAL = TIMEREAL + TIMESTEP
REM **Writes data to file, real time, furnace temp, pellet temp, oxide
thickness**
OXOUT = (OXMAS / OXDENS)

WRITE #1, TIMEREAL, SURTEMP, PELTEMP, OXOUT
RETURN

REM*****

REM **Calculates the adiabatic temp of combustion and**
REM **cooling of the pellet after combustion**
HOT:

CALL EXPLOSION(FUSIONTI, TIVAP, TIVAPHEAT, TIHEAT, FUSIONTIO2, TIMELT,
TIO2MELT, MOL, TIO2HEAT, PELMOLTI, MOLTIO2, PELTEMP, MAXENERGY, OXMAS)
TIMEREAL = TIMEREAL + TIMESTEP
WRITE #1, TIMEREAL, SURTEMP, PELTEMP, PARTRAD

DO WHILE PELTEMP > 800
CALL FURNACE(HTIMER, HOLDTIME, SURTEMP, TIMESTEP, TEMPSTEP, COOLRATE, HOLDTEMP)
CALL REACTLOSS(REACTLOSJ, PELSURF, PELTEMP, SURTEMP, TIMESTEP)
CALL COOLING(PELTEMP, MOLTIO2, CPTIO2, CPTI)

```

```

TEMPFALL = REACTLOSJ / ((CPTI * PELMOLTI) + (CPTIO2 * MOLTIO2))

REM** Conditional Statements that apply the latent heat of fusion of
REM** TiO2 and Ti to the cooling model

IF PELTEMP < TIO2MELT AND TEMPFALL > 0 THEN
    TOTLOS = TOTLOS + REACTLOSJ
    IF TOTLOS < FUSIONTIO2 THEN TEMPFALL = 0
    END IF

IF PELTEMP < TIMELT AND TEMPFALL > 0 THEN
    TOTLOSTI = TOTLOSTI + REACTLOSJ
    IF TOTLOSTI < FUSIONTI THEN TEMPFALL = 0
    END IF

REM**3920 is the energy of transition from alpha to beta in Ti.
LATI = 3920 * PELMOLTI
IF PELTEMP < 1155 AND TEMPFALL > 0 THEN
    TICHANGE = TICHANGE + REACTLOSJ
    IF TICHANGE < LATI THEN TEMPFALL = 0
    END IF

PELTEMP = PELTEMP - TEMPFALL

TIMEREAL = TIMEREAL + TIMESTEP
REM **Writes data to file, real time, furnace temp, pellet temp, oxide
thickness**
OXOUT = (OXMAS / OXDENS)
WRITE #1, TIMEREAL, SURTEMP, PELTEMP, OXOUT, TICHANGE, REACTLOSJ, LATI
LOOP

GOTO 10
RETURN

REM*****

REM **DATA FOR TITANIUM AND TITANIUM OXIDE**
METALDATA:

REM: References:
REM 1: Thermodynamics of Materials, Kubachewski, 5th Edition 1980 ish
REM 2: CRC Handbook of Chemistry and Physics, 54th Edition. 1973-74

REM **Densities of Ti and TiO2 in kg m^-3. Both ref:2 **
TIDENS = 4510
OXDENS = 4260

REM **Molar masses in kg mol^-1. Both ref:2 **
TIMOLMAS = .0479
OXMOLMAS = .0799

REM **Melting or vapourisation point of Ti and TiO2 in K
TIMELT = 1943 'ref:1
TIVAP = 3550 'ref:2
TIO2MELT = 2133 'ref:1

REM ** Latent heat of fusion for Ti and TiO2 written in J / mol**
REM ** All ref:2
TIHEAT = 20928
TIVAPHEAT = 422736
TIO2HEAT = 66968

RETURN

REM*****

REM **INPUT DATA ON THE PELLET COMPACT**
COMPACTDATA:

PI = 3.1415926#

PRINT "Input the PELLET DIAMETER in mm."
INPUT PELDIAM
PRINT ""
PELRAD = PELDIAM / 2000

```

```

PRINT "Input the PELLETS LENGTH in mm."
INPUT LENGTH
PRINT ""
LENGTH = LENGTH / 1000

REM **Pellet surface area**
PELSURF = (2 * PI * PELRAD * LENGTH) + (2 * PI * PELRAD * PELRAD)

REM **Pellet volume**
PELVOL = PI * PELRAD * PELRAD * LENGTH

REM ** PARTDIAM in meters**
PRINT "Input the POWDER DIAMETER in microns."
INPUT PARTDIAM
PRINT ""
PARTRAD = PARTDIAM / 2000000

REM **Input of initial oxide thickness on particle**
PRINT "Input the INITIAL OXIDE THICKNESS on the powder in microns."
INPUT THICKNESS
PRINT ""

REM**Input of ACTIVEPERCENTAGE, the factor which determines the amount**
REM**of powder oxidised to produce heat, this is a factor which is **
REM**related to the situation that occurs in pellets in which only the**
REM**outside surface is actively oxidised during heating, the inside remains**
REM**unoxidised and thus produces no exothermic heat**
PRINT "Input your ACTIVEPERCENTAGE, a factor relating to the amount of"
PRINT "titanium exothermically oxidised during heating."
INPUT ACTIVEPERCENTAGE
PRINT ""
ACTIVEPERCENTAGE = ACTIVEPERCENTAGE / 100

REM **Calculates actual titanium powder diameter**
TIRAD = PARTRAD - (THICKNESS / 100000)

REM **Calculates actual titanium powder volume**
TIVOL = (4 * PI * (TIRAD ^ 3) / 3)

REM **Volume of particle of 'partrad' diameter**
PARTVOL = (4 * PI * (PARTRAD ^ 3) / 3)

REM **Packing density, 0.74 (74%) is the max for spheres**
PACKDENS = .74

REM** Number of particles of powder in pellet**
PARTNUM = PELVOL * PACKDENS / PARTVOL

REM ** Total surface area of powder in pellet**
PARTSURF = 4 * PI * (PARTRAD ^ 2) * PARTNUM

REM ** Mols of actual Ti in the pellet**
PELMOLTI = (PARTNUM * TIVOL * TIFENS) / TIMOLMAS

REM **Oxmas in kg/m^2**
OXMAS = (THICKNESS / 1000000) * PACKDENS

REM **MOLTIO2 in mol**
MOLTIO2 = (OXMAS / OXMOLMAS) * PARTSURF

RETURN

REM*****

REM **Heat produced in a time step**
HEATINCREASE:

REM **OXIDEMAS is now in kg**
OXIDEMAS = OXMASINC * (PARTSURF * ACTIVEPERCENTAGE)

REM **HEATINCREASE in J**
HEATINCJ = OXIDEMAS * OXENTH / OXMOLMAS

REM **mol of TiO2 produced in a timestep**
MOLTIO2INC = OXIDEMAS / OXMOLMAS

RETURN

```

```

REM*****

REM ** This sub routine calculates the Heat of Formation of TiO2 at PELTEMP
OXENTH-CALC:

REM** The calculation takes the form: int:PELTEMP/298 Cp X
REM** = integral of Heat Capacity of X between PELTEMP and 298

REM** EQ1) int:PELTEMP/1155 Cp (Hf:Ti)
REM** EQ2) int:PELTEMP/298 Cp (O)
REM** EQ3) Transformation Energy of alpha to beta titanium
REM** EQ4) int:1155/298 Cp (alpha Ti)
REM** EQ5) Heat of Formation of TiO2 @ 298K
REM** EQ6) int:298/PELTEMP Cp (TiO2)

REM** Total Equation = EQ1+EQ2+EQ3+EQ4+EQ5 = Heat of Formation of TiO2 at
PELTEMP
REM** EQ1, EQ2, EQ4A and EQ6 are variable with PELTEMP. EQ3, EQ4B and EQ5 are
constant.
REM** All figures in J

REM**Constants*****
EQ3 = 3976 'ref:2

EQ4.298 = (22.1 * 298) + ((10 / 2000) * 298 ^ 2)
EQ4.1155 = (22.1 * 1155) + ((10 / 2000) * 1155 ^ 2)
EQ4B = EQ4.1155 - EQ4.298

EQ5 = -912439 'ref:2

REM** Variables*****
EQ1.1155 = (19.8 * 1155) + ((7.95 / 2000) * 1155 ^ 2)
EQ1.PELTEMP = (19.8 * PELTEMP) + ((7.95 / 2000) * PELTEMP ^ 2)
EQ1 = EQ1.PELTEMP - EQ1.1155

EQ2.PELTEMP = (29.97 * PELTEMP) + ((4.186 / 2000) * PELTEMP ^ 2) - ((-1.67 *
100000) / PELTEMP)
EQ2.298 = (29.97 * 298) + ((4.186 / 2000) * 298 ^ 2) - ((-1.67 * 100000) / 298)
EQ2 = EQ2.PELTEMP - EQ2.298

EQ4.298 = (22.1 * 298) + ((10 / 2000) * 298 ^ 2)
EQ4.PELTEMP = (22.1 * PELTEMP) + ((10 / 2000) * PELTEMP ^ 2)
EQ4A = EQ4.PELTEMP - EQ4.298

EQ6.PELTEMP = (75.21 * PELTEMP) + ((1.17 / 2000) * PELTEMP ^ 2) - ((-18.2 *
10000) / PELTEMP)
EQ6.298 = (75.21 * 298) + ((1.17 / 2000) * 298 ^ 2) - ((-18.2 * 10000) / 298)
EQ6 = EQ6.298 - EQ6.PELTEMP
REM*****

REM** Final Equations in J/mol
OXENTHEQ = EQ2 + EQ4A + EQ5 + EQ6
OXENTHEQ1 = EQ1 + EQ2 + EQ3 + EQ4B + EQ5 + EQ6

REM**Conditional Statements to Organise the Equation
IF PELTEMP >= 1155 THEN OXENTHEQ = OXENTHEQ1
OXENTH = -OXENTHEQ

RETURN

SUB COOLING (PELTEMP, TIO2MELT, CP TiO2, CPTI)

REM **CP for solid Ti, in J K^-1 mol^-1**
ATI = 24.94
BTI = 6.57 / 1000
CTI = -1.63 * 100000
DTI = 1.34 / 1000000

REM **Titanium changes from hex to bcc at 1155K, in J**
ATII = 30.84
BTII = -8.87 / 1000
CTII = 0 * 100000
DTII = 6.44 / 1000000

IF PELTEMP > 1155 THEN ATI = ATII
IF PELTEMP > 1155 THEN BTI = BTII
IF PELTEMP > 1155 THEN CTI = CTII

```

```

IF PELTEMP > 1155 THEN DT1 = DT11

REM** Cp for liquid titanium. Titanium Melts at 1943K. In J
AT111 = 32.65
BT111 = 0
CT111 = 0
DT111 = 0

IF PELTEMP >= 1943 THEN AT1 = AT111
IF PELTEMP >= 1943 THEN BT1 = BT111
IF PELTEMP >= 1943 THEN CT1 = CT111
IF PELTEMP >= 1943 THEN DT1 = DT111

CPT1 = AT1 + (BT1 * PELTEMP) + (CT1 / PELTEMP ^ 2) + (DT1 * PELTEMP ^ 2)

REM*****

REM **CP for solid TiO2 in J K^-1 mol^-1**
A1 = 73.35
B1 = 3.05 / 1000
C1 = -17.03 * 100.00
D1 = 0

REM **CP for TiO2 LIQUID in J K^-1 mol^-1**
A2 = 89.57
B2 = 0
C2 = 0
D2 = 0

REM **This changes the CPs depending on the temperature**
IF PELTEMP < TIO2MELT THEN A2 = A1
IF PELTEMP < TIO2MELT THEN B2 = B1
IF PELTEMP < TIO2MELT THEN C2 = C1
IF PELTEMP < TIO2MELT THEN D2 = D1
CPTIO2 = A2 + (B2 * PELTEMP) + (C2 / PELTEMP ^ 2) + (D2 * PELTEMP ^ 2)

END SUB

SUB EXPLOSION (FUSIONTI, TIVAP, TIVAPHEAT, TIHEAT, FUSIONTIO2, TIMELT,
TIO2MELT, MOL, TIO2HEAT, PELMOLTI, MOLTIO2, PELTEMP, MAXENERGY, OXMAS)

PRINT ""
PRINT "          *** The pellet has combusted ****"
PRINT ""

PRINT " Please input a CONVERSION FACTOR. This determines";
PRINT " what percentage of the pellet will react. Input 0 to 100%"
INPUT CONFAC
CONFAC = CONFAC / 100

REM** Calculation of total mols in system**
MOL = PELMOLTI + MOLTIO2

REM**This section assigns the percentage of metal that oxidises**
MOLSOFOXIDE = PELMOLTI * CONFAC
MOLSOFMETAL = PELMOLTI * (1 - CONFAC)

REM ** FUSIONTIO2 is the latent heat of fusion of TiO2 in J.
REM ** FUSIONTI is the latent heat of fusion of Ti in J.
REM ** VAPTI is the vapourisation energy of the titanium that remains as metal.
FUSIONTIO2 = ((MOLSOFOXIDE + MOLTIO2) * TIO2HEAT)
FUSIONTI = (MOLSOFMETAL * TIHEAT)
VAPTI = (MOLSOFMETAL * TIVAPHEAT)

REM **Calculation of actual energy of system minus the heat of fusion for
REM **the amount of Titanium metal left unoxidised
DH = (MAXENERGY * CONFAC) - FUSIONTI

REM **Temperature step is temperature step of the programme**
REM **It is set to 1 for good accuracy**
DT = 1

REM **Energy absorbed**
EABSORB = 0

REM **Starting temperature = TIME1**

```

```

T = TIMELT
DO WHILE EABSORB < DH
T1 = T + DT
REM **CP for liquid Ti, in J K^-1 mol^-1**
TIA3 = 32.65
TIB3 = 0 / 1000
TIC3 = 0 * 100000
TID3 = 0 / 1000000
TIA = TIA3 * MOLSOFMETAL
TIB = TIB3 * MOLSOFMETAL
TIC = TIC3 * MOLSOFMETAL
TID = TID3 * MOLSOFMETAL
REM**CP for TiO2 SOLID in J K^-1 mol^-1**
TIO2A1 = 73.35
TIO2B1 = 3.05 / 1000
TIO2C1 = -17.03 * 100000
TIO2D1 = 0
REM **CP for TiO2 LIQUID in J K^-1 mol^-1**
TIO2A2 = 89.57
TIO2B2 = 0
TIO2C2 = 0
TIO2D2 = 0
IF T > TIO2MELT THEN TIO2A1 = TIO2A2
IF T > TIO2MELT THEN TIO2B1 = TIO2B2
IF T > TIO2MELT THEN TIO2C1 = TIO2C2
IF T > TIO2MELT THEN TIO2D1 = TIO2D2
TIO2A = TIO2A1 * (MOLSOFOXIDE + M * TIO2)
TIO2B = TIO2B1 * (MOLSOFOXIDE + M * TIO2)
TIO2C = TIO2C1 * (MOLSOFOXIDE + M * TIO2)
TIO2D = TIO2D1 * (MOLSOFOXIDE + M * TIO2)
REM **Energy Absorbed in Tempstep**
CP = (TIO2A + TIA) + ((TIO2B + TIB) * T) + ((TIO2C + TIC) / (T * T)) + ((TIO2D
+ TID) * T * T)
CP1 = (TIO2A + TIA) + ((TIO2B + TIB) * T1) + ((TIO2C + TIC) / (T1 * T1)) +
((TIO2D + TID) * T1 * T1)
IF CINT(T) = TIO2MELT THEN
EABSORB = EABSORB + (((CP + CP1) / 2) * DT) + FUSIONTIO2
ELSE
EABSORB = EABSORB + (((CP + CP1) / 2) * DT)
END IF
IF CINT(T) = TIVAP THEN
EABSORB = EABSORB + (((CP + CP1) / 2) * DT) + VAPTI
ELSE
EABSORB = EABSORB + (((CP + CP1) / 2) * DT)
END IF
T = T1
LOOP
PRINT "The calculated adiabatic temperature is ="; (T - 273); "deg.C"
PRINT ""
REM ** Explosive Peltemp**
PELTEMP = T
MOLTI02 = MOLSOFOXIDE + MOLTI02
REM ** In reality there is still some metal unoxidised (PELMOLTI = MOLSOFMETAL)
REM ** however, due to it being sealed off within the pellet and not in
REM ** powder form ( due to liquifying) the amount of titanium available
REM ** for oxidation is in effect 0.
PELMOLTI = MOLSOFMETAL
END SUB
SUB FURNACE (HTIMER, HOLDTIME, SURTEMP, TIMESTEP, TEMPSTEP, COOLRATE, HOLDTEMP)
REM **Determines what the heating schedule should be**
IF HTIMER >= HOLDTIME THEN
SURTEMP = SURTEMP - (COOLRATE * TIMESTEP)
ELSEIF SURTEMP < HOLDTEMP THEN

```

```

        SURTEMP = SURTEMP + TEMPISTEP
ELSE
    SURTEMP = HOLDTEMP
    REM** Holding temp time**
    HTIMER = HTIMER + TIMESTEP
END IF

REM **Stops the furnace temp going below room temperature**
IF SURTEMP < 293 THEN
    SURTEMP = 293
END IF

END SUB

SUB HEATLOSS (HEATLOSJ, PELSURF, PELTEMP, SURTEMP, TIMESTEP)
REM **Heat transfer coeff, H independant of T at the moment**
REM **HEATLOSJ in J**
REM ** Emivisity = 0.5 and STEFAN BOLTZMANN CONSTANT = 5.67*(10^-8)

H = 10
STEF = 5.67 * (10 ^ -8)
ESP = .5

HEATLOSJ = ((H * (PELTEMP - SURTEMP)) + ((STEF * ESP) * (PELTEMP ^ 4 - SURTEMP
^ 4))) * PELSURF * TIMESTEP

END SUB

SUB OXIDATION (PELTEMP, OXMAS, TIMESTEP, OXMASINC, TIMEDUM)
REM **Constants for the expression**

REM OXMAS has units of kg m^-2
REM m^2 = k * time
REM k = C exp (-Q/ RT)
REM C in units of kg^2 m^-4 s^-1 multiply by 100 from g^2 cm^-4 s^-1)
REM Q and R both in cal

REM ** Temp range, C, Q, type
REM ** 550-850, 0.16 g^2 cm^-4 s^-1, 45000 cal, parabolic
C = .16 * 100
Q = 45000
R = 1.986

REM **Expression for calculating the oxidation of titanium**
REM **w.r.t temperature**
k = C * EXP((-Q) / (R * PELTEMP))

REM **Calculation of dummy time**
REM **OXMAS and OXMASINC are in kg/m^2**
TIMEDUM = (OXMAS ^ 2) / k
OXMASINC = (k ^ .5) * (((TIMEDUM + TIMESTEP) ^ .5) - (TIMEDUM ^ .5))
OXMAS = (k ^ .5) * ((TIMEDUM + TIMESTEP) ^ .5)
END SUB

SUB REACTLOSS (REACTLOSJ, PELSURF, PELTEMP, SURTEMP, TIMESTEP)
REM** These are the heatloss constants for the reacted pellet**
H = 10
STEF = 5.67 * (10 ^ -8)
ESP = .9

REACTLOSJ = ((H * (PELTEMP - SURTEMP)) + ((STEF * ESP) * (PELTEMP ^ 4 - SURTEMP
^ 4))) * PELSURF * TIMESTEP

END SUB

SUB TEMPERATUREINCREASE (TOTHEAT, PELMOLTI, TEMPRISE, PELTEMP, MOLTIO2, CPTI,
CPTIO2)
REM **CP for solid Ti, in J K^-1 mol^-1**
ATI = 24.94
BTI = 6.57 / 1000
CTI = -1.63 * 100000
DTI = 1.34 / 1000000

REM **Titanium changes from hex to bcc at 1155K**
ATII = 30.84
BTII = -8.87 / 1000
CTII = 0 * 100000

```

```

DTII = 6.44 / 1000000

IF PELTEMP > 1155 THEN ATI = ATII
IF PELTEMP > 1155 THEN BTI = BTII
IF PELTEMP > 1155 THEN CTI = CTII
IF PELTEMP > 1155 THEN DTI = DTII

CPTI = ATI + (BTI * PELTEMP) + (CTI / PELTEMP ^ 2) + (DTI * PELTEMP ^ 2)

REM **CP for solid TiO2 in J K^-1 mol^-1**
ATIO2 = 73.35
BTIO2 = 3.05 / 1000
CTIO2 = -17.03 * 100000
DTIO2 = 0

CPTIO2 = ATIO2 + (BTIO2 * PELTEMP) + (CTIO2 / PELTEMP ^ 2) + (DTIO2 * PELTEMP ^ 2)

REM **TEMPRISE is the increase in pellet temp with PELTEMP**
TEMPRISE = TOTHEATJ / ((CPTI * PELMOLTI) + (CPTIO2 * MOLTI2))

END SUB

```

Appendix D: Computer Programme - Powder

```
'PROGRAMME TO FIND THE MASS AND THICKNESS OF OXIDE REQUIRED TO
'HEAT A POWDER OF D DIAMETER TO THE MELTING POINT OF TI (1943K)
'FROM 500 deg C, THE MINIMUM TEMP FOR REACTION
'
CLS

'SPECIFIC HEAT OF TI IN J kg^-1 K^-1
'TEMP RAISE FROM 500C TO MELTING POINT TO 1670 = 1170C
'cp = 523
SH = 611910

'DENSITY OF TITANIUM 4510KG
DT = 4510

'MOLAR MASS OF TI
MMTI = 47.9

'DENSITY OF TIO2 IN kg / M3
DOX = 4260

PI = 3.1415926#

PRINT "INPUT POWDER DIAMETER IN MICRONS"
INPUT DIAM
RAD = DIAM / 2000000

'VOLUME OF POWDER IN M^3
V = (4 * PI * (RAD ^ 3) / 3)
'MASS OF PARTICLE IN KG
MASS = DT * V

MOLSOFTI = MASS * 1000 * MMTI
'ENERGY REQUIRED TO HEAT PARTICLE
TIENERGY = MASS * SH

PRINT " DO THIS IN AIR OF FE2O3?, ENTER 1 FOR AIR, 2 FOR FE2O3"
INPUT ATMOSPH
IF ATMOSPH = 1 THEN TRANSENERGY = 945085.9 ELSE TRANSENERGY = 397343.5

'MOLS OF OXIDE REQUIRED TO MELT TI
AMOUNT = TIENERGY / TRANSENERGY
MOLSTIO2REQUIRED = AMOUNT
TIO2MASS = (MOLSTIO2REQUIRED * 79.9) / 1000 ' TO PUT IN KG
TIO2VOL = TIO2MASS / DOX

PRINT "POWDER RADIUS "; RAD
PRINT "VOLUME OF POWDER"; V
PRINT "MASS OF POWDER"; MASS
PRINT "ENERGY REQUIRED TO MELT PARTICLE"; TIENERGY
PRINT "MOLS OF OXIDE REQUIRED TO MELT PARTICLE"; MOLSTIO2REQUIRED
PRINT "MASS OF TIO2 REQUIRED TO MELT PARTICLE "; TIO2MASS
PRINT "VOLUME OF TIO2 REQUIRED TO MELT PARTICLE"; TIO2VOL

'IF THE MASS OF TIO2 FORMED IS TIO2MASS THEN TO CALCULATE THE THICKNESS
'OF THE OXIDE LAYER ON A DIAM BIG PARTICLE
THICK = .01 / 1000000
COUNT = 0
DO
TIO2V = (4 * PI * (RAD - THICK) ^ 3) / 3
SPAREVOLUME = V - TIO2V
THICK = THICK + (.01 / 1000000)
COUNT = COUNT + 1
LOOP UNTIL SPAREVOLUME >= TIO2VOL
PRINT "COUNT"; COUNT
PRINT "THICKNESS ="; THICK * 1000000; "IN MICRONS"
PRINT "SPAREVOLUME"; SPAREVOLUME
PRINT "TIO2V"; TIO2V
PRINT "V"; V
```